U. S. Department of Energy
1000 Independence Avenue, S.W.
Washington, D.C. 20585

Fiscal Year 2021: Second Quarter

Progress Reports:

Advanced Battery Materials Research (BMR) Program & Battery500 Consortium

Released June 2021
for the period of January – March 2021

Approved by

Tien Q. Duong
Manager, Advanced Battery Materials Research Program & Battery500 Consortium
Batteries & Electrification R&D
Office of Energy Efficiency and Renewable Energy – Vehicle Technologies Office
U.S. Department of Energy

ACKNOWLEDGMENTS

This report has been edited by the following team members:

- **T. A. Zachry,** Energy & Environmental Resources Group
- **Simon Thompson,** U. S. Department of Energy – Vehicle Technologies Office
- **Patricia H. Smith,** Naval Surface Warfare Center – Carderock

TABLE OF CONTENTS

TABLE OF FIGURES

TABLE OF TABLES

A MESSAGE FROM THE MANAGER: ADVANCED BATTERY MATERIALS RESEARCH PROGRAM AND BATTERY500 CONSORTIUM

The Vehicle Technologies Office (VTO) within the Office of Energy Efficiency and Renewable Energy (EERE) has two programs that perform cutting edge research to advance battery technology for electric vehicles. The Advanced Battery Materials Research (BMR) Program focuses on discovering high-performance materials, comprehensive modeling, and diagnostics analyses of materials and electrochemical cell behavior to address chemical, physical, and mechanical instabilities. It is composed of seven research task areas including: Liquid/Polymer Solid-State Electrolytes, Diagnostics, Modeling, Metallic Lithium, Sulfur Electrodes, Air-Electrodes/Electrolytes, and Sodium-Ion Batteries. The Battery500 program focuses on designing a cell that can achieve 500 Wh/Kg and 1000 cycles through novel cell architectures utilizing a lithium anode, a compatible electrolyte, and high-capacity cathodes. To accomplish this aggressive goal, the program is divided into 3 key areas: Materials and Interfaces, Electrode Architecture, and Cell Fabrication, Testing, and Diagnosis.

In this document, we report on the progress made on these projects from January 1, 2021 through March 31, 2021. A few notable achievements from the BMR investigators this quarter are summarized below:

- S. Martin's group at Iowa State University continued their investigations of developing low-cost, high performance mixed oxy-sulfide nitride (MOSN) glassy solid electrolytes (GSEs). Recent investigations have focused on the synthesis of new GSE materials using silicon and phosphorous based compounds. Electrochemical impedance spectroscopy measurements of coin cells using the newly formulated GSEs sandwiched between two Li-foil electrodes revealed a relatively constant interface over time with a bulk GSE impedance consistent with their project's ionic conductivity target values of ~ 1 mS/cm at 25°C and an electronic conductivity area specific resistance of >1 MΩ-cm^2.
- Oak Ridge National Laboratory (J. Nanda's team) is casting doubt on a common strategy of using $LiNbO_3$ to stabilize the interface between a sulfide solid electrolyte and Ni-rich oxide cathodes. The team observed that a 1 wt% $LiNbO_3$ coating on NMC-811 cathodes containing high surface-area carbon for enhanced electronic conductivity had little impact on cell capacity or cyclability.
- The team from University of Maryland (E. Wachsman and Y. Mo) conducted thermodynamic analysis based on first-principles computation to guide the discovery of coating materials to stabilize the interface between lithium and LLZO electrolyte. The entire Li-M-O ternary composition space, where M = B, C, N, Al, Si, P, Ti, V, Cr, Zr, Nb, Mo, Zn, Ga, Ge, Ta, or W, was investigated. Heat maps indicating the chemical stability of Li-M-O with LLZO were generated and could be a useful tool when identifying appropriate coating compositions.
- Argonne National Laboratory (ANL, Z. Chen's group) experimentally demonstrated that lithium dendrite can grow from the inside of dense LLZO pellets, suggesting that blocking electron conduction pathways is critical in solving the dendrite issue facing mixed conductors like LLZO.
- The V. Srinivasan group (ANL) developed a model to examine void formation in lithium metal taking into account the surface and bulk diffusion of lithium, effect of external pressure, and current density. Simulations suggest that as current density increases, the slow transport in the metal leads to formation of deep voids and delamination of the metal from the solid electrolyte when no external pressure is imposed.

Highlights from the Battery500 consortium team include the following:

Keystone Project 1: Materials and Interfaces

- The M. S. Whittingham team (Binghamton University) has shown that niobium can improve performance of nickel-rich NMC cathodes. A niobium oxide coating was found to reduce 1st cycle loss. Partial substitution of the manganese by niobium was able to stabilize the lattice, reduce heat evolution, and shift the onset of exothermic reaction to a higher temperature.

Keystone Project 2: Electrode Architecture

- The Brookhaven National Laboratory group (X. Yang and E. Hu) identified LiH as a significant component in the solid electrolyte interphase (SEI) on Li-metal anodes. Nanocrystalline LiF was also observed in SEI, but having a larger lattice parameter than the bulk LiF. This characteristic favors ion transport and may help to explain why the ionic insulator LiF can be beneficial for long-term cycling.

Keystone Project 3: Cell Fabrication, Testing, and Diagnosis

- Idaho National Laboratory (E. J. Dufek's team) found a direct correlation between the concentration of electrolyte aggregate clusters and Li||NMC-811 cycle life when localized high concentration electrolytes are used. Longer cycle life is achieved when such cluster concentration is increased.

Our next report, covering the third quarter of FY 2021, is expected to be available in September 2021.

Sincerely,

Tien Q. Duong

Tien Q. Duong
Manager, Advanced Battery Materials Research Program & Battery500 Consortium
Batteries & Electrification R&D
Office of Energy Efficiency and Renewable Energy – Vehicle Technologies Office
U.S. Department of Energy

TASK 1 – Liquid/Polymer Solid-State Electrolytes

Team Lead: Jihui Yang, University of Washington

Summary and Highlights

The BMR Program goal is to develop long-life batteries superior to commercial Li-ion systems in terms of cost, vehicle range, and safety. The BMR Program addresses the fundamental problems of electrode chemical and mechanical instabilities that have slowed development of affordable, high-performance, automotive batteries. The aim is to identify electrode/electrolyte materials that yield enhanced battery performance and lead to greater acceptance of electric vehicles (EVs). Currently, the U. S. Department of Energy (DOE) Vehicle Technologies Office (VTO) supports 14 projects in the BMR Program under this Task. These projects can be categorized into four general topics:

- **Liquid.** The projects for liquid electrolyte (LE) aim to develop electrolyte formulations, based on fluoro-chemistries, to achieve significantly improved operating voltage, increased durability, and increased energy density of Li-ion batteries at a reasonable cost. Nonaqueous polyelectrolyte solutions with high Li^+ transference numbers will be developed to achieve high rate capabilities at room temperature. In addition, electrolytes with new polymer binders bearing a pentafluorophenyl group on the backbone will be designed, synthesized, and tested.
- **Polymer.** The targets of polymer electrolyte (PE) projects include inorganic/polymer and polymer/gel hybrid electrolytes that have flexibility, mechanical strength, thermal stability, high ionic conductivity, stable interfaces against lithium metal, and polysulfide-trapping capability enabling energy density Li-S batteries, with comparable cycle life.
- **Self-Forming & Self-Healing.** The self-forming, self-healing electrolyte projects are focused on developing and implementing Li-metal-based metal fluorite and metal iodide batteries, capable of energy densities > 400-500 Wh/kg and 1000 Wh/L.
- **Solid-State.** The solid-state projects are to develop high conductivities solid electrolytes (SEs) / composite SEs that are scalable, are chemically and electrochemically stable, and will enable low-cost, high-energy-density solid-state lithium batteries (SSLBs).

Highlights. The highlights for this quarter are as follows:

- At Iowa State University of Science and Technology (ISU, S. Martin), symmetric cells were prepared to test the electrochemical behavior of the $58Li_2S + 32SiS_2 + 10[(1-x)Li_{0.67}PO_{2.83} + xLiPO_{2.5}N_{0.3}]$ glassy solid electrolyte (GSE) series. Coin cells were assembled using a disk of polished GSE between two Li-foil electrodes. Electrochemical impedance spectroscopy (EIS) measurements were collected every 30 minutes for the first 24 hours after the cell was assembled to evaluate possible reactions between the GSE and lithium metal. The team found that the area-specific bulk and interfacial resistances of the glasses rapidly stabilize and remain relatively constant over time, indicating that the interfacial layer is stable, and non-consuming. Furthermore, area-specific resistance (ASR) is linearly dependent on the thickness of the electrolyte. The thin-film mixed-oxy-sulfide-nitride (MOSN) GSEs are expected to show ASR values of roughly 10-25 Ω-cm^2. Ongoing efforts are focused on various methods to improve the interfacial contact, including through applied stack pressure, and interfacial chemistry modification.
- The University of Maryland (E. Wachsman, UMD) team conducted thermodynamic analysis based on first-principles computation to guide discovery of coating materials to stabilize the interface between lithium and $Li_7La_3Zr_2O_12$ (LLZO) electrolyte. The entire Li-M-O ternary composition space, where M = B, C, N. Al, Si, P, Ti, V, Cr, Zr, Nb, Mo, Zn, Ga, Ge, Ta, or W, was investigated. Heat maps of chemical stability of Li-M-O with LLZO were generated and could be a useful tool when identifying appropriate coating compositions.

Task 1.1 – Dual Function Solid-State Battery with Self-Forming, Self-Healing Electrolyte and Separator (Esther Takeuchi, Stony Brook University)

Project Objective. The project objective is to demonstrate a solid-state rechargeable battery based on a Li-metal anode and iodine cathode with a self-forming, self-healing electrolyte and separator with high gravimetric and volumetric energy density.

Project Impact. This program will enable demonstration of the proposed rechargeable battery with improved power capability, high energy density, and a self-forming, self-healing solid-state electrolyte (SSE) / separator. Technical insight will be gained regarding improved conductivity of the solid LiI based electrolyte, power capability of the proposed system, the self-healing nature of the LiI layer, the nature of the electrode-electrolyte interfaces, and feasibility of the system to reach the DOE targets.

Approach. The proposed concept is a dual function rechargeable solid-state battery (SSB) utilizing LiI combined with silver iodide (AgI) as the electrolyte, with lithium metal (and small quantities of silver metal) as the anode, with iodine as the cathode, and with a self-forming, self-healing separator/electrolyte. The battery will be assembled in the discharged state, where the anode and cathode will be created during the first formation (charge) step. Initially, silver ion (Ag^+) will diffuse toward the negative electrode and be reduced to silver metal (Ag^0), and iodine ion (I^-) will be oxidized to elemental iodine (I_2) at the cathode side. As the formation of the battery continues, lithium ion (Li^+) will form a Li-metal layer at the anode, with generation of iodine at the cathode. LiI will remain and serve as both the separator and electrolyte.

Out-Year Goals. This is a multi-year program where the effort is divided into three major tasks.

- Year 1 involves electrolyte preparation and characterization including preparation of SSEs and conductivity measurements.
- Year 2 focuses on cell construction and testing including both *in situ* and *ex situ* analysis.
- Year 3 focuses on cell characterization. Under the program, cycle life, efficiency, energy density, and the functional capacity of cells will be determined.

Collaborations. This project collaborates with A. Marschilok and K. Takeuchi of Stony Brook University.

Milestones

1. Conduct destructive analysis of tested cells. (Q1, FY 2021; Completed)
2. Perform extended cycle life testing. (Q2, FY 2021; Completed)

Progress Report

Extended cycle life testing was conducted on four cell configurations with varied interfaces at 40°C for 60 charge-discharge cycles of the LiI-LiI(HPN)$_2$ composite electrodes. (Figure 1a-d). The cells delivered smooth voltage profiles under the extended cell tests at 40°C. There was variation in Coulombic efficiency (CE) among the four cell types. Cell Type IV had consistent delivered capacity and CE, with nearly 100% CE for all 60 cycles. Cell Type II demonstrated stable delivered capacity with increasing CE over the initial cycles, where CE was initially at ~ 90% and increased to nearly 100% as cycling continued. Cell Type III showed ~ 40% CE. In contrast, the cell type with no interfacial modification is best represented by Cell Type I, where it was observed that CE decreased on successive cycles before reaching a plateau at ~ 20%.

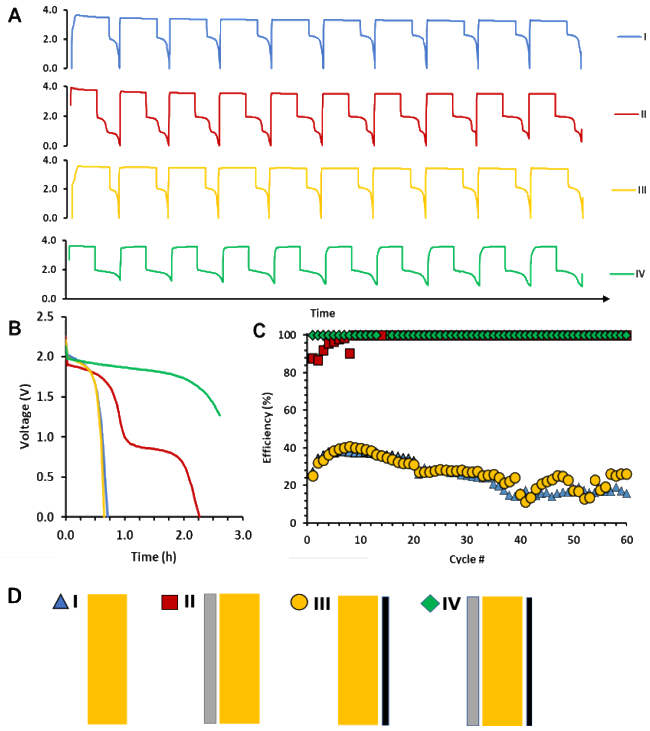

Figure 1. Cell designs I (blue), II (red), III (yellow), and IV (green). (a) 1st 10 cycle voltage profiles. (b) 1st cycle discharge. (c) Coulombic efficiencies over 60 cycles. (d) Schematics of 4 cell designs.

Of the four cell types, Cell Type IV was selected for the candidate deliverable cell with demonstrated improved cyclability and CE.

To determine additional parameters for comparison and benchmark testing, a series of current densities was tested with the cell construct with the highest CE (Cell Type IV). The improved SSE cells were able to successively undergo successive charge-discharge cycles at current densities up to 50 µA/cm^2 with no evidence of shorting, as shown in Figure 2.

Over the course of this program, the team has demonstrated an improved rechargeable Li/I$_2$ based battery with improved cyclability and CE compared to the benchmark cells from the beginning of the program. Multi-year efforts have led to development and improvements in synthesis methods, fabrication and preparation of the SSE, the function of the interface, and design of appropriate test conditions. The cell stack energy density of the final configuration is 390 Wh/kg.

One of the highlights of this system is its ability to self-form on charge, thus lending itself to long shelf life before use.

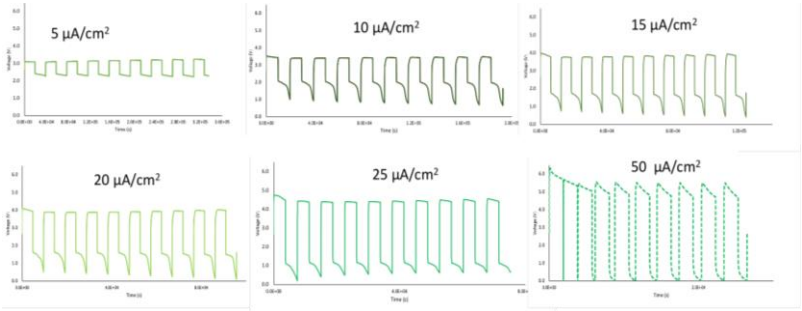

Figure 2. Cell design IV tested at different current densities.

Patents/Publications/Presentations

Publication

- Stackhouse, C. A., A. Abraham, S. Yan, L. Wang, N. Sadique, G. Singh, A. C. Marschilok, E. S. Takeuchi, and K. J. Takeuchi. "Self-Healing, Improved Efficiency Solid State Rechargeable Li/I_2 Based Battery." *Journal of The Electrochemical Society* 168 (2021): 010519.

Task 1.2 – Characterization and Modeling of Li-Metal Batteries: Characterization of Li^+ Transport in Polyelectrolytes
(Bryan D. McCloskey, University of California, Berkeley)

Project Objective. This task aims to understand lithium plating and stripping in non-traditional electrolyte systems (specifically, polyelectrolyte solutions and concentrated binary salt electrolytes) that have been proposed to reduce dendrite formation during lithium stripping and plating due to their high Li^+ transference numbers (t_+). The team will develop capabilities that allow them to understand how ion dynamics in these electrolytes impact macroscale transport properties and Li-metal plating and stripping.

Impact. Ultimately, this task will develop an understanding of how electrolyte composition and molecular interactions can be manipulated to positively impact ion transport of potential electrolytes for Li-metal batteries. This will provide a set of general design rules for novel electrolytes enabling stable, efficient high capacity Li-metal stripping and plating.

Approach. To understand various aspects of lithium plating and ion transport in these systems, the team will develop novel diagnostic and computational modeling techniques. Model polyelectrolytes, with pendant triflimide anions, will be used as polyanions, as their properties can be easily tuned via changes in the polymerization chemistry. Solution parameters that can be varied for both polyelectrolyte solutions and concentrated electrolytes include solvent and salt composition, additive inclusion, and the aforementioned polymer properties, all of which can have a profound impact on electrostatic interactions between charged species in solution, as well as interfacial stability and reaction kinetics of the lithium electrode. The team will develop capabilities that allow them to understand how molecular-level ion dynamics in these electrolytes impact macroscale transport properties and Li-metal plating and stripping. These computational simulations will be validated and refined by comparing results to experimentally measured transport properties of these electrolytes. They will optimize electrochemical methods for these electrolytes to evaluate relevant transport properties under the Newman concentrated solution theory framework, which has never been performed on these non-traditional electrolytes. ^1H and ^{19}F nuclear magnetic resonance (NMR) diffusometry will also be used to measure single-ion self-diffusion coefficients without an applied electric field; solution viscosity measurements using a state-of-the-art rotating sphere viscometer can be performed under entirely air-free and water-free conditions. The team will develop capabilities to quantitatively understand degradation mechanisms of various electrolytes during Li-metal stripping and plating. Specifically, differential electrochemical mass spectrometry (DEMS) will be used to study outgassing that occurs from electrolyte degradation processes.

Out-Year Goals. The ultimate goal of this project is to understand the influence of electrolytes with novel transport characteristics on the performance of Li-metal electrodes. Work will continue to build toward a complete understanding of Li-ion and counterion transport in polyelectrolyte solutions and concentrated electrolytes, as well as the impact of electrolyte transport properties on Li-metal uniformity during electrochemical stripping and plating. Outgassing measurements using DEMS will be developed to further probe the interfacial reactivity of lithium metal with electrolytes created in this project.

Collaborations. Collaborators on this project include K. Persson (atomistic and coarse-grained modeling) and N. Balsara (electrochemical characterization of PEs), both at Lawrence Berkeley National Laboratory (LBNL).

Milestones

1. Establish a simple method to measure activity coefficients and thermodynamic factors for a model electrolyte. (Q1, FY 2021; Completed)
2. Synthesize very low molecular weight oligomer triflimide-based polyions (pTFSI). (Q2, FY 2021; Completed).

3. Measure conductivity, self-diffusion, and concentration cells for model triflimide-based polyion (pTFSI) solutions. (Q3, FY 2021; In progress)
4. Establish electrophoretic NMR techniques for measuring the true Li^+ transference number of pTFSI solutions. (Q4, FY 2021; In progress)

Progress Report

This quarter, the team published a Perspective article, with collaborator K. Persson as the lead principal investigator (PI), entitled "Ion Correlations and Their Impact on Transport in Polymer-Based Electrolytes." The Perspective was published as an ACS Editors' Choice article. The aim of this article is to demonstrate the utility of the Onsager transport framework, which connects microscopic correlations in ion motion (which may be computed directly from molecular simulations) to macroscopic transport properties. The article discusses how various types of ion correlations (cation-anion, like-ion, and ion-solvent) manifest in common PEs, and the implications these correlations have on transference number, ionicity, and other bulk transport behavior. From this analysis, the team also suggests design rules for minimizing harmful ion correlations to develop improved electrolytes.

This quarter, the team also published a preprint article entitled "Interfacial Effects on Transport Coefficient Measurements in Li-ion Battery Electrolytes" in which they detail their work on understanding the reliability of electrochemical transport property measurement techniques. They had hoped to use these techniques to study ion transport in their polyelectrolyte systems; however, for electrolyte systems where the electrolyte resistance is smaller than the interfacial (solid electrolyte interface, or SEI) resistance, the team demonstrates that techniques that rely on lithium plating and stripping do not yield reliable transport properties (see Figure 3, which is the TOC Figure from the preprint). Instead, such measurements appear to probe both interfacial and transport phenomena that cannot easily be deconvoluted.

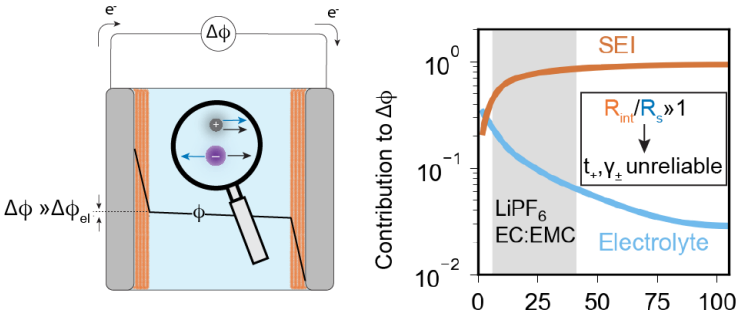

Figure 3. Lithium polarization experiments for electrolyte systems where interfacial resistance is larger than electrolyte resistance result in unreliable transference number and thermodynamic factor data because electrolyte potential contributions are orders of magnitude smaller than those from the SEI.

To measure transport properties of the project's polyelectrolyte solutions, the team is exploring new approaches for obtaining both the transference number and the total salt diffusion coefficient. They are beginning a collaboration with J. Urban's group at LBNL to measure salt diffusion coefficients using a microfluidic device and *in situ* confocal Raman microscopy. This method has previously been validated for measuring binary lithium salts in dimethyl carbonate (DMC) in both the dilute and concentrated regime. The team is using COMSOL multi-physics to model and design microfluidic device dimensions given the fluid properties and rough diffusion coefficients for their polyelectrolyte solutions. For transference number measurements, they are modeling and developing a low-volume Hittorf cell design. They will then use quantitative ^{7}Li and ^{19}F to measure salt concentrations on polarization, allowing them to extract transference numbers of the polyelectrolytes. The team plans to confirm the Hittorf transference number measurements using electrophoretic NMR when those capabilities become available in the fourth quarter of this fiscal year. In line with this quarter's goals, they now have a reliable synthesis methodology for synthesizing controlled molecular weight lithium bearing polymers and can reproducibly synthesize both styrene and methacrylate polyions (PS-LiTFSI, and PA-LiTFSI). They are

working with short-chain oligomeric polyions and comparing transport to the lithium-appended monomer. Next quarter, they will start gathering experimental transport data on the two polyelectrolyte systems using these methods.

Patents/Publications/Presentations

Publications

- Fong, K. D., J. Self, B. D. McCloskey, and K. A. Persson. "Ion Correlations and Their Impact on Transport in Polymer-Based Electrolytes." *Macromolecules* 54, No. 6 (2021): 2575–2591.
- Bergstrom, H. K., K. D. Fong, and B. D. McCloskey. "Interfacial Effects on Transport Coefficient Measurements in Li-ion Battery Electrolytes." *ECSarXiv* (2021). doi:10.1149/osf.io/b3yjm.

Presentation

- Women Excelling in Computational Modeling Engineering Seminar Series, Virtual (April 15, 2021): "Ion Correlations in Li-Ion Battery Electrolytes"; K. Fong.

Task 1.3 – Advanced Polymer Materials for Batteries (Zhenan Bao and Yi Cui, Stanford University)

Project Objective. This project will develop new polymer materials for batteries. The team will develop polymer coatings with specific mechanical properties that can accommodate the volume expansion and contraction of the Li-metal anode associated with deposition and stripping (charging and discharging).

Project Impact. The cycling stability and CE of Li-metal electrodes will be increased by implementation of a polymer-based protective layer that functions as an artificial SEI with desired properties. The improved performance will enable further development toward practical utilization of Li-metal anodes with higher cycling efficiency and less susceptibility to dendrite-based failure.

Approach. The project uses soft polymer coatings with dynamic crosslinking to give the resulting polymers liquid-like rheological properties and stretchable and self-healing properties. In previous work, the project has shown that such coatings resulted in uniform deposition/stripping of lithium metal and improved cycling stability of Li-metal electrodes. To understand the design rules for effective polymer coatings, the team chose a few representative polymers to systematically understand structure property relationships. Here, the team investigates the correlation between surface energy of the polymer and exchange current for lithium deposition.

Out-Year Goals. Work will progress toward the correlation between dielectric constant and exchange current. These findings will enable further understanding and development of various polymer coatings for protecting Li-metal anodes.

Collaborations. This quarter, the team is collaborating with J. Qin at Stanford University.

Milestones

1. New lithium anode coating design. Analyze the polymer chemistry and mechanical property using NMR, differential scanning calorimetry (DSC), and rheology. (Q1, FY 2021; Completed)
2. Analyze stability of the polymer in electrolyte and its ability to reduce the reaction in the Li-metal surface with EIS. (Q2, FY 2021; Completed)
3. Characterize the impact of the polymeric coating on lithium deposition morphology using scanning electron microscopy (SEM). (Q3, FY 2021)
4. Coat Li-metal electrodes with the polymeric coating and achieve stable lithium cycling for 150 cycles at 1 mA/cm^2 and 2 mA/cm^2 current density. (Q4, FY 2021)

Progress Report

Introduction

The team hypothesizes that an effective method to address the lithium anodic interfacial instability is to fundamentally alter the Li-ion deposition pathways by electrostatically blocking the heterogenous surface regions that concentrate lithium ions due to high electric field. This can be experimentally implemented using electro-inactive cations at the interface that can "shield" the inhomogeneous protrusion on the electrode surface to neutralize the electric field landscape. However, this strategy can be successful only when it is ensured that these electro-inactive cations do not undergo reduction during the lithium deposition process. In other words, their reduction potential needs to be even lower than that of Li^+ ions that already have the lowest intrinsic reduction potentials among metallic cations. Previously, Ding et al. pointed out that Cs^+ can achieve lower reduction potential than Li^+ by tuning its concentration based on Nernst Equation. Furthermore, it was shown that addition of Cs^+ ions in the electrolyte resulted in improved lithium deposition morphology and battery operation. However, the concentration dependent electrochemical stability of Cs^+ ions can be undermined by their localized aggregation at the electrode surface, resulting in the reduction of Cs^+.

Instead of using free cations, here the team proposes to tether the electroactive cations (Pyrrolidinium, or Py^+) onto a flexible and stable polymer backbone (polydimethylsiloxane, or PDMS) to form a PDMS-based poly (ionic liquid) (PDMS-Py) coating that would homogenize the electric field distribution on the electrode surface and promote uniform lithium deposition. Based on previous study, Py^+ was selected based on its lower reduction potential in comparison to Li^+, and its chemical stability with the Li-metal anode. Incorporation of Py^+ in a polymer coating on the lithium anode is a facile method that does not alter existing manufacturing capabilities and also limits their interaction with other battery components. Building on previous studies on anodic coating using polymers [polyethylene oxide (PEO), Nafion, polyvinylidene difluoride (PVDF)], and drawing on the team's previous knowledge on designing cation-tethered polymeric coating on anode surface, this work—the interfacial material in this work—is designed on economically viable chemistry and to be chemically and electrochemically inert with lithium metal, to possess a conducting pathway for lithium conduction, and to be mechanically robust for adapting to rapid volume changes.

Polymer Coating Design

Figure 4a illustrates lithium anode coated with PDMS-PyTFSI containing electro-inactive cations and its counter anion TFSI. In the absence of any coating, the concentrated electric field at the surface protrusion triggers a self-amplified surface roughening process of lithium deposition (Figure 4b). The presence of cations is hypothesized to neutralize the radiating electric field and helps to homogenize lithium deposition pathways. Figure 4c showcases the "cationic shielding" phenomenon where the presence of the PDMS-PyTFSI coating results in redistribution of Li^+ ions away from the surface protrusions, leading to a more uniform topology. The physiochemical prerequisites of the PDMS-Py polymer coating for the cationic shielding mechanism are as follows: (1) cations in the PDMS-PyTFSI backbone should have a lower reduction potential than that of Li^+, and (2) sufficient mobility of the polymer chains is essential for electric-field-based response of the cations.

In previous work, the team utilized a system of random co-polymer on poly(acrylic) backbone: one of the co-polymer side chains contains the Py^+ (pyrrolidinium) cation units, and the other side chain is perfluoroalkyl as an inert component that can also lower the glass transition of the final co-polymer and introduce mobility to the polymer chains.

Instead of using a relatively rigid poly(acrylic) backbone, the new design (Figure 4d) utilizes the flexible poly(dimethylsiloxane) (PDMS) backbone, which efficiently brings down the polymer's glass transition temperature (*T*g) so that they no longer need to introduce another fluorinated component, and all of the polymer side chains can be functionalized with the Py^+ cation units. Beyond the benefit of mechanical flexibility, PDMS-based polymer is economically viable compared to any fluorinated polymer, its mechanical property can be regulated via controlled crosslinking, and it is inert and electrochemically stable with lithium metal.

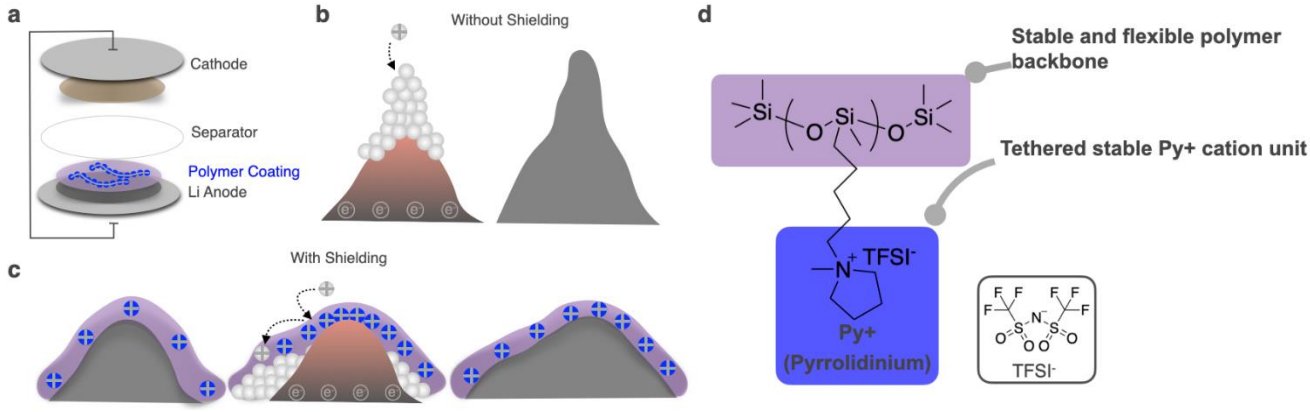

Figure 4. PDMS-Py as the anodic coating for Li-metal batteries. (a) Li-metal battery with polymer-coated anode. (b) Concentrated electric field at vicinity of surface protrusions causes the self-amplifying dendritic deposition of lithium ions. (c) Coating on Li-metal anode. During Li^+ deposition, cations in PIL coating remain electrochemically stable and can effectively shield the Li^+ ions, resulting in more flat and homogeneous deposition. (d) Chemical structure of the PDMS-PyTFSI coating.

Stability of the Polymer on Lithium Metal Anode

To examine the stability of the PDMS PyTFSI (not crosslinked) coating on the Li-metal anodes, a layer of polymeric coating was applied to the electrode surface via dip coating the Li-metal chip in a polymer THF solution (0.1 g/ml). The coated Li-metal chips were then assembled into Li||Li symmetric coin cell with 50 µl of electrolyte, and the EIS was measured over 100 hours. Two of the most commonly used ether-based [1 M lithium bis(trifluoromethane-sulfonyl)imide (LiTFSI) and 1 wt% $LiNO_3$ in 1,3-Dioxolane (DOL) / 1,2-Dimethoxyethane (DME)] and carbonate-based [1 M $LiPF_6$ in ethylene carbonate (EC) / diethyl carbonate (DEC) and 10% fluoroethylene carbonate (FEC)] electrolytes were used in the system. To understand the changes in the interfacial impedance, control experiments with lithium chips that were just dipped in THF solvent and then assembled into the coin cells with the two aforementioned electrolytes were also performed.

Based on the interfacial impedance data shown in Figure 5 a-d, the team can see that the interfacial impedance increased overtime in both ether- and carbonate-based electrolytes. For the case of carbonate electrolyte, a layer of PDMS PyTFSI coating on the Li-metal surface effectively reduced the increase of interfacial impedance. Over the 100 hours of measurement, the interfacial impedance of PDMS PyTFSI coated lithium increases from 300 ohm to 330 ohm, while the uncoated bare lithium's interfacial impedance increases from 190 ohm to 360 ohm. The stable interfacial impedance value of the coated lithium metal in carbonate electrolyte shows that this polymer can effectively protect the lithium metal from further carbonate electrolyte corrosion while remaining on the electrode surface.

For the case of ether-based electrolyte, the bare lithium metal's interfacial impedance increased to almost two times the starting value at the first 20 hours of measurements. By applying a layer of polymeric coating on the surface, the interfacial impedance increases much slower over the period of 100 hours, and eventually stabilizes at 1.5 times the value of the starting impedance. Overall, the application of a PDMS PyTFSI coating layer can limit the reaction between lithium metal and the electrolytes, and the coating is also stable on the electrode surface for long periods of time.

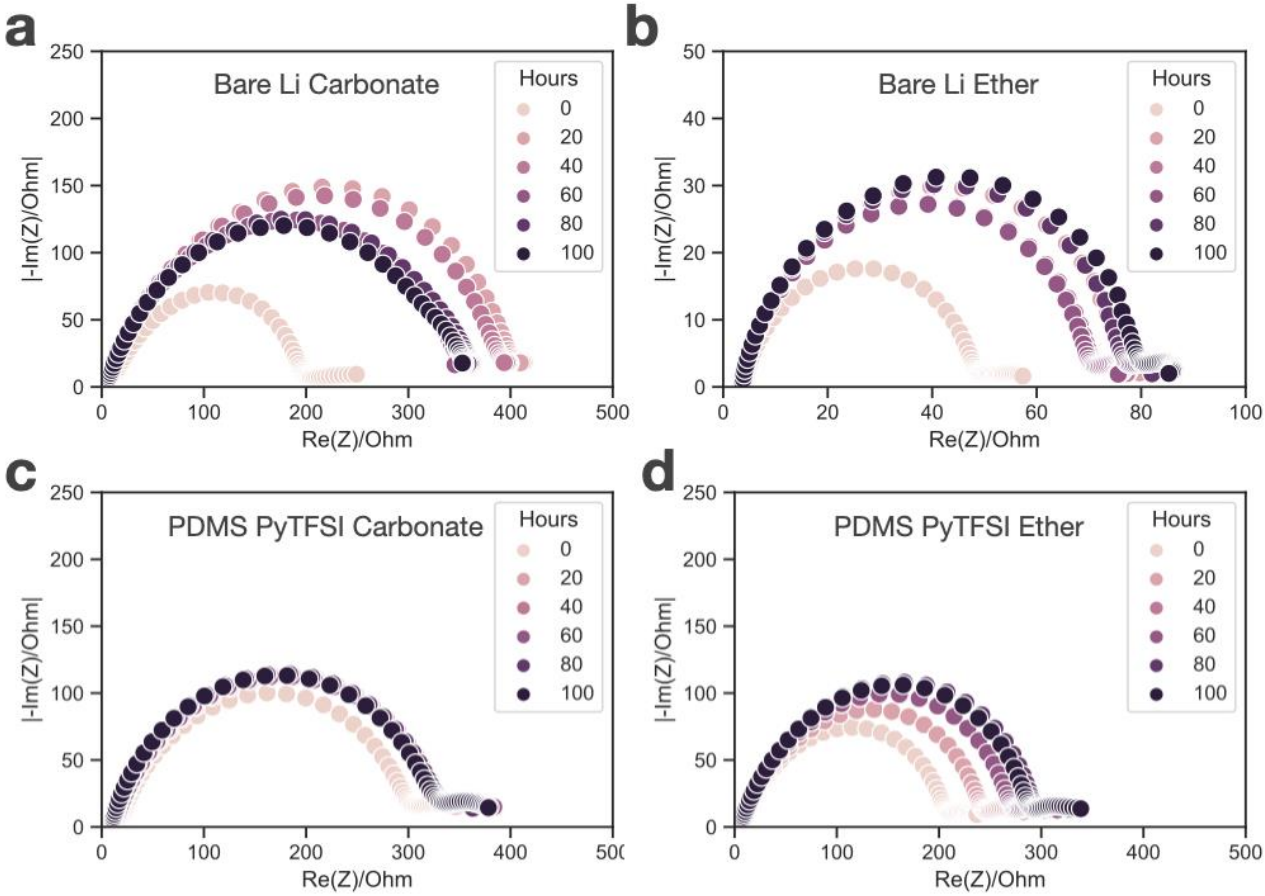

Figure 5. Interfacial impedance measured over 100 hours on Li||Li symmetric cell with 50 µl of electrolytes in between the two electrodes. The carbonate electrolyte is composed of 1 M $LiPF_6$ in EC/DEC and 10% FEC; the ether electrolyte is composed of 1 M LiTFSI and 1 wt% $LiNO_3$ in DOL/DME. The absolute value of the imaginary part of the interfacial impedance (Z) and the real part of the Z was measured through electrochemical impedance spectroscopy and plotted: bare lithium with (a) carbonate electrolyte and (b) ether electrolyte; and PDMS PyTFSI coated lithium with (c) carbonate electrolyte and (d) ether electrolyte.

Patents/Publications/Presentations

Publications

- Boyle, D. T., W. Huang, H. Wang, Y. Li, H. Chen, Z. Yu, W. Zhang, Z. Bao, and Y. Cui. "Corrosion of Lithium Metal Anodes during Calendar Ageing and its Microscopic Origins." *Nature Energy* 6 (March 22, 2021): 487–494.
- Wang, H., W. Huang, Z. Yu, W. Huang, R. Xu, Z. Zhang, Z. Bao, and Y. Cui. "Efficient Lithium Metal Cycling over a Wide Range of Pressures from an Anion-Derived Solid-Electrolyte Interphase Framework." *ACS Energy Letters* 6, No. 2 (2021): 816–825.
- Li, J., Y. Cai, H. Wu, Z. Yu, X. Yan, Q. Zhang, T. Z. Gao, K. Liu, X. Jia, and Z. Bao. "Polymers in Lithium-Ion and Lithium Metal Batteries." *Advanced Energy Materials.* doi: 10.1002/aenm.202003239; Publication Date (Web): January 25, 2021.

Task 1.4 – Improving the Stability of Lithium-Metal Anodes and Inorganic-Organic Solid Electrolytes (Nitash Balsara, Lawrence Berkeley National Laboratory)

Project Objective. The project objective is to establish a new hybrid electrolyte that will be stable against cells with a Li-metal anode.

Project Impact. PEs offer increased stability in lithium batteries in comparison to more widely used LEs. Nanostructured electrolytes containing both soft, ion-conducting domains and rigid, nonconducting domains offer the opportunity to tune both mechanical and electrical properties separately. Such electrolytes are conveniently made by block copolymer self-assembly. Most of the block copolymer electrolytes studied thus far comprise organic polymer chains for both the conducting and rigid domains. The team hopes to synthesize new electrolytes that simulataneously have high transport properties and have greater stability against lithium in comparison to organic diblock copolymers.

Approach. First, the team synthesizes hybrid diblock copolymers by incorporating monomers that contain an inorganic component. Then, electrolytes are prepared by mixing these diblock copolymers with salt. Electrochemical and mechanical characterization of these materials is performed before carrying out cycling X-ray tomography (XRT) experiments and *in situ* small angle X-ray scattering (SAXS) experiments. The combination of these approaches enables rational design of materials that exhibit improved stability against lithium metal.

Out-Year Goals. The project will synthesize a new hybrid electrolyte that is designed to be stable against lithium metal. The material is a block copolymer in which one block contains acryloisobutyl polyhedral oligomeric silsesquioxane (POSS). The second block is a conventional PE (PEO). Electrochemical characterization of this polymer will include measurement of all transport properties including conductivity, diffusion coefficient, and transference number. The stability against lithium metal will be evaluated by cyclic voltammetry (CV), while its applications as an electrolyte will be evaluated and visualized using cycling XRT experiments on symmetric Li-hybrid-Li cells.

Collaborations. There are no active collaborations this quarter.

Milestones

1. Synthesize at least 2 POSS-containing single ion conductors (SICs). (Q1, FY 2021; Completed)
2. Develop the relationship between non-linear mechanical properties and ion transport in solid block copolymer electrolytes. (Q2, FY 2021; Completed)
3. Conduct *in situ* X-ray scattering experiments on Li-polymer-Li symmetric cells to quantify polymer morphology in the presence of an applied field. (Q3, FY 2021)
4. Conduct XRT experiments on Li-polymer-Li symmetric cells to quantify dendrite growth in block copolymer electrolytes. (Q4, FY 2021)

Progress Report

Milestone Status. The team determined the non-linear mechanical property of two block copolymers by creep experiments.

Understanding the factors affecting the lithium dendrite growth could enable successful implication of Li-metal anodes. One approach in mitigating dendrite growth is to use electrolytes with increased mechanical rigidity.[1] In this context, polymer-based electrolytes have been shown to provide mechanical rigidity against lithium dendrite growth during electrochemical lithium deposition.[2] In the present work, the rigidity of the copolymer is quantified in terms of storage modulus and yield stress.

The polymers used in this study are hybrid organic-inorganic diblock (PEO-POSS) and triblock (POSS-PEO-POSS) copolymers where the PEO is the ion conducting soft segment and the POSS is the mechanically rigid segment. The compositions of the copolymers are shown in Table 1. Both copolymers have similar volume fraction of the conductive block (f_{EO}) and molecular weights.

Table 1. Comparison of PEO-POSS and POSS-PEO-POSS diblock and triblock copolymers.

PEO-POSS/ POSS-PEO-POSS	Structure	MW of PEO (kg mol^{-1})	MW of POSS (kg mol^{-1})	f_{EO}
10-4	Diblock	10	3.8	0.76
2-10-2	Triblock	10	3.8	0.76

Figure 6a shows the storage modulus of the neat copolymers measured at 90°C. Both diblock and triblock copolymers exhibit similar storage modulus. The nonlinear mechanical properties of the copolymers were determined by creep experiments. In Figure 6b, the creep compliance curves are shown for the triblock copolymer at various applied stress. The triblock copolymer exhibits linear viscoelastic properties at lower values of applied stress. At 14000 Pa, the slope of the compliance curve increases exponentially, indicating the onset of plastic deformation. The yield stress was calculated by plotting the slope of the creep compliance curve as a function of the applied stress (Figure 6c). Figure 6c demonstrates that the yield stress of the triblock copolymer is higher (13000 ± 1000 Pa) than the diblock copolymer (4500 ± 500 Pa), although both copolymers have comparable storage moduli.

Diblock and triblock copolymer electrolytes were prepared by mixing LiTFSI salt with the copolymers. The salt concentration of the electrolytes was [Li]/[EO] = 0.1. Lithium symmetric cells were fabricated by sandwiching the electrolytes between two lithium electrodes. All experiments were performed at 90°C. Cells were preconditioned for multiple cycles at low current density (0.02 mA cm^{-2}) in the positive and negative directions to stabilize the SEI at each lithium electrode. The cells were then polarized at a current density of 0.15 mA cm^{-2}. Figure 6d shows that while the triblock copolymer electrolytes were able to sustain the current density, the diblock copolymer electrolyte showed signs of dendrite growth after 1 hour. The observation of stable deposition in the triblock copolymer electrolyte while lithium dendrites short circuit the diblock copolymer electrolyte is attributed to the lower yield stress of the diblock copolymer.

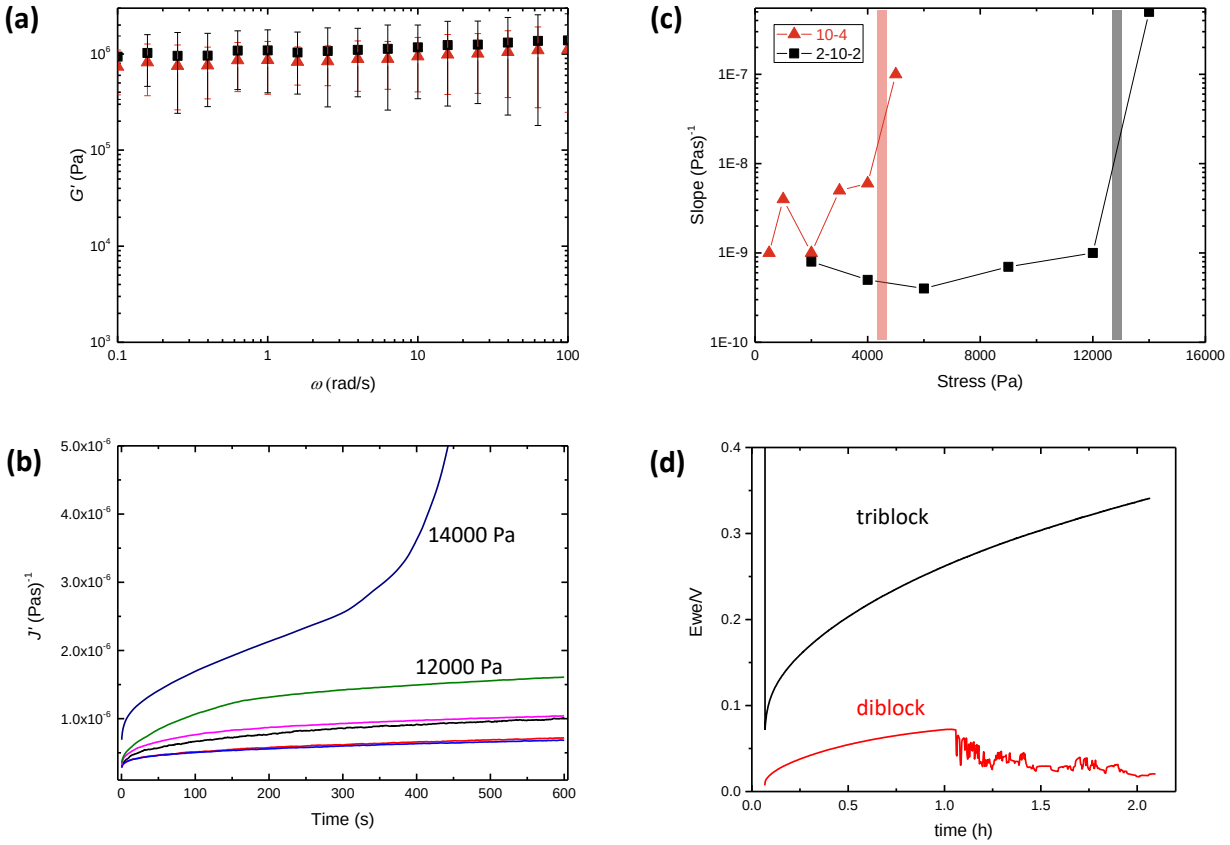

Figure 6. (a) Storage modulus of the diblock (red triangle) and triblock (black square) copolymer. (b) Creep compliance of the triblock at difference applied stress. Below 12000 Pa, the polymers exhibit viscoelastic behavior. At 14000 Pa, the slope of compliance increases sharply. (c) Yield stress of the copolymers measured from the slope of the creep compliance curve. (d) The electrolyte was subjected to 0.15 mA cm^{-2} current, and the potential response was observed with time. The cells with diblock copolymer electrolytes failed within 1 hour, but the cells with triblock copolymer electrolyte were able to sustain the current. All data were collected at 90°C.

References

[1] Monroe, C., and J. Newman. *Journal of the Electrochemical Society* 152, No. 2 (2005): A396.

[2] Frenck, L., G. K. Sethi, J. A. Maslyn, and N. P. Balsara. *Frontiers in Energy Research* 7, 115 (2019).

Patents/Publications/Presentations

Publication

- Sethi, G. K., S. Chakraborty, C. Zhu, E. Schaible, I. Villaluenga, and N. P. Balsara. "Effect of Crystallization of the Polyhedral Oligomeric Silsesquioxane Block on Self-Assembly in Hybrid Organic-Inorganic Block Copolymers with Salt." *Giant* 6 (2021). doi: 10.1016/j.giant.2021.100055.

Presentations

- University of California, Berkeley (UCB), Department of Chemical Engineering Colloquium, Virtual (March 3, 2021): "Transient Structure of Block Copolymer Electrolytes under Dc Polarization"; M. Galluzzo.
- American Physical Society Meeting, Virtual (March 17, 2021): "Impact of Frictional Interactions on Conductivity and Transference Number in Ether- and Perfluoroether-Based Electrolytes"; L. Grundy.
- American Physical Society Meeting, Virtual (March 19, 2021): "Effect of Crystallization of the Polyhedral Oligomeric Silsesquioxane Block on Self-Assembly in Hybrid Organic-Inorganic Block Copolymers with Salt"; G. K. Sethi.

Task 1.5 – Development of Thin, Robust, Lithium-Impenetrable, High-Conductivity, Electrochemically Stable, Scalable, and Low-Cost Glassy Solid Electrolytes for Solid-State Lithium Batteries (Steve Martin, Iowa State University of Science and Technology)

Project Objective. The objective of this project is to develop new Li^+-conducting MOSN GSEs that are impermeable to lithium dendrites, have high conductivities, are scalable through low-cost glass manufacturing, are chemically and electrochemically stable, and will enable low-cost, high-energy-density SSLBs. The SSLBs constructed from these new GSEs will meet and exceed all program objectives: usable specific energy @ C/3 ≥ 350 Wh/kg, calendar life 15 years, cycle life (C/3 deep discharge with < 20% energy fade) 1000, and cost ≤ $100/kWh.

Project Impact. This project will enable the team to demonstrate the following: (1) thin MOSN GSE films yield superior performance in a much safer, lower-cost, and Li-dendrite impenetrable form, and (2) high rate and long cycle life can be achieved in SSLBs using thin-film MOSN GSEs. The new GSEs in SSLBs are anticipated to increase energy density (anode basis) from ~ 300 mAhr/g to ~ 4,000 mAhr/g, enabling replacement of internal combustion engines in both light-duty and heavy-duty vehicles. Each 20% reduction in the ~ 1.6 billion liters of gasoline used per day in the United States would reduce CO_2 emissions by ~ 4 billion kg or 2 x 10^{12} l of CO_2 per day. The team will also increase scientific and engineering knowledge of thin-film GSEs in SSLBs.

Approach. The MOSN mixed glass former (MGF) glasses used for the GSEs in this project have been developed in previous work to have the necessary thermal stability and high ionic conductivity for successful use as a drawn-film electrolyte. In this project, the glass chemistry will be tuned for even more desirable properties, by investigating structure-property relationships and testing variations in glass chemistry.

Out-Year Goals. Work will progress toward developing a glass capable of being drawn to 100-µm thickness, while having high conductivity and electrochemical stability and good cycling ability.

Collaborations. There are no active collaborations this quarter.

Milestones

1. Accomplish: 100 cycles against lithium metal with no cell shorting and < 20% degradation of other properties. (Q4, FY 2021; Completed)
2. Accomplish: Optimize draw conditions for MOSN GSE to achieve 5 m × 5 cm x < 100-µm thin films. (Q4, FY 2021; In progress)
3. Accomplish: Fabricate MOSN MGF Li|GSE|Li cells in small area format, ~ 1 cm^2. (Q4, FY 2021; Completed)
4. *Go/No Go Decision*: Micro-sheet glass ribbon processing facility optimized / design capable of meeting the following performance requirements: glove box enclosing preform redraw facility reaches 10 ppm O_2 and H_2O, and 3 samples of MOSN MGF GSE ribbons have been drawn at 5 m × 5 cm × 100 µm. Analysis indicates technical approach capable of achieving performance targets. (Q4, FY 2021; In progress)

Progress Report

Task 1 - Development of New MOSN MGF GSEs

Development of MOSN MGF GSEs with Target Properties Capable of Cycling Lithium against LM

Table 2. Compositions of typical mixed oxy sulfide (MOS) and mixed oxy-sulfide nitride (MOSN) glassy solid electrolytes (GSEs) being studied at Iowa State University and their sample IDs used throughout the report.

Sample ID	Compositional Formula
ISU-6	$0.58Li_2S + 0.32SiS_2 + 0.1LiPO_3$
ISU-7	$0.58Li_2S + 0.32\ SiS_2 + 0.1[(1\text{-}x)Li_{0.67}PO_{2.87} + xLiPO_{3\text{-}3y/2}N_y]$, y = 0.314, x = 0, 0.1, 0.2, 0.3, 0.4, and 0.5

It was previously reported that a MOS glass with a composition of $0.58Li_2S + 0.32\ SiS_2 + 0.1\ LiPO_3$ was found to have an ionic conductivity of 0.7 mS/cm at 25°C and a working range of 110°C. Additionally, it was found that glasses in the ISU-7 series exhibit improved thermal stability with the addition of LiPON, reaching a working range ($\Delta T = T_C\text{-}Tg$) = ~ 120°C in the x = 0 .3 composition.

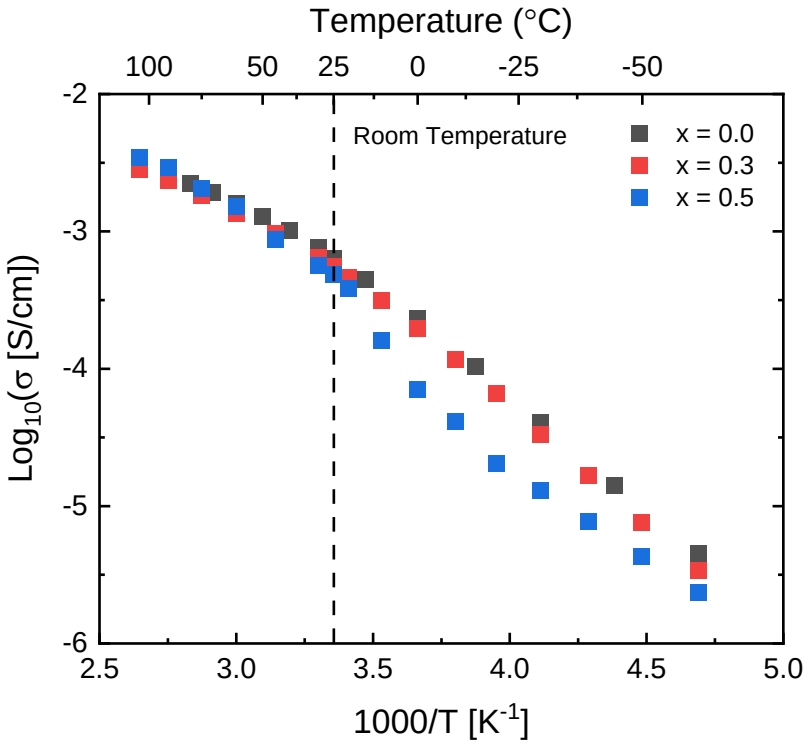

Figure 7. Arrhenius plots of the conductivities of ISU-7 series of glasses $0.58Li_2S + 0.32SiS_2 + 0.1[(1\text{-}x)Li_{0.67}PO_{2.87} + xLiPO_{3\text{-}3y/2}N_y]$ for glasses with x = 0, 0.3, and 0.5. In this series, y is held constant at 0.314.

This quarter, further characterization and testing of the newly developed ISU-7 series of GSEs were completed to further understand the effect of nitrogen on the ionic conductivity and underlying material structure. EIS was used to measure the temperature-dependent ionic conductivity of the ISU-7 GSEs from -60°C to 105°C, as shown in Figure 7. On incorporation of LiPON, the ionic conductivity of the MOS base-composition appears

relatively unaffected for glasses with $x < 0.3$, decreasing from 0.7 mS/cm ($x = 0$) to 0.33 mS/cm in the $x = 0.3$ composition. Further additions of LiPON were found to decrease the ionic conductivity as the result of the high field strength oxygen anions trapping lithium. Future work aims to optimize the thermal, chemical, and electrochemical properties of the ISU GSE through further compositional development and structural modification.

Development of these GSEs requires a detailed understanding of the underlying material structure and its effect on the GSE performance. Solid-state NMR was used to identify the short range order (SRO) structures present in the GSEs. The ^{29}Si NMR was used to identify the primary structural units in the GSE series and is given in Figure 8a. The most prominent NMR absorption peaks in the series are centered at 7 ppm and -10 ppm, which have been assigned to the SiS_4^{4-} and SiS_3^{2-} anions, respectively. Additional peaks are observed beyond -10 ppm to more negative chemical shifts that have been assigned to oxygen-containing silicon structures. Deconvolution of the spectra reveals that the glass structure is comprised of 15% SiS_4^{4-}, 30% SiS_3^{2-}, and 25% $SiS_{2-z}O_{1+z}^{2-}$ anions, with $0 \leq z \leq 2$. With the addition of LiPON, the concentration of non-networking SiS_4^{4-} species increases, while the concentration of the oxy-sulfide SRO species, $SiS_{2-z}O_{1+z}^{2-}$, appears to be unaffected. The ^{31}P NMR spectra (Figure 8b) were likewise collected and spectrally deconvoluted in the same manner as the ^{29}Si NMR spectra, and they reveal that nearly all of the phosphorus atoms in this GSE glass series occupy non-networking PS_4^{3-} or $PS_{4-w}O_w^{3-}$, $0 \leq w \leq 4$, units versus polymeric oxy-nitride SRO species and are predominately rich in sulfur. The lack of oxygen present in the ^{31}P NMR suggests the $LiPO_3$ and LiPON precursor materials undergo an anion exchange reaction with Li_2S and SiS_2 to produce MOS silicon species.

Initiate Development of Preforms of MOSN MGF GSEs that Do Not Crystallize

Various compositions have been previously identified as viable candidates for large-scale preparation via preform synthesis and film drawing. The MOS glass, of $0.58Li_2S + 0.32\ SiS_2 + 0.1\ LiPO_3$, possesses a large working range of 107°C, making it an ideal candidate to avoid crystallization. As detailed in this report, numerous parameters, including annealing conditions and precursor mixing, have been identified that can suppress crystallization and improve preform production.

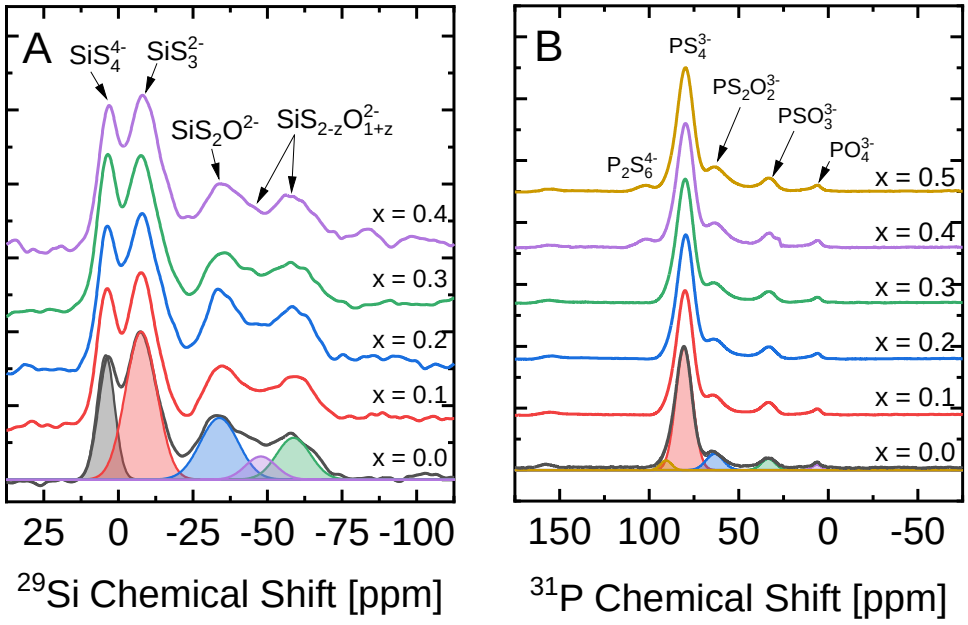

Figure 8. 29Si (a) and 31P (b) magic-angle spinning nuclear magnetic resonance spectra of $0.58Li_2S + 0.32\ SiS_2 + 0.1[(1\text{-}x)Li_{0.67}PO_{2.87} + xLiPO_{3\text{-}3y/2}N_y]$; y = 0.314 series ranging from $0.0 \leq x \leq 0.5$ collected on a 400-MHz (1H) spectrometer.

Task 2 - Develop Micro-Sheet Glass Ribbon Processing Facility for GSEs: Continue to Develop and Optimize the GSE Micro-Sheet Glass Ribbon Processing Facility

Work continued to develop optimal conditions for both preform preparation and thin-film glass drawing. Using the large-scale glass processing facility, 200-g MOS preforms can be prepared from large glass melts. Slow annealing has been found to greatly improve the quality of preforms by reducing thermal stress. In addition to preparing preforms directly from precursors, the team has found that glass from previously drawn preforms can be recycled, remelted, and recast multiple times. Assuming the glovebox and furnace atmosphere is maintained correctly, the MOS glass can be recycled indefinitely, leading to large reductions in materials cost. The recyclability of MOS glasses allows for an iterative approach to be used to optimize film preparation conditions.

During the film drawing process testing, MOS glass preforms were found to be more susceptible to thermal shock than the previously tested oxide glasses. Thus, various conditions must be improved to draw thin-films. The team has worked to develop protocols for MOS thin-film preparation, including slow heating profiles, preheating of all tools used to handle GSE preforms, and a lower film draw speed. This approach has steadily improved MOS film preparation.

Task 3 - Develop Processing Conditions Micro-Sheet Ribbons of MOSN MGF GSEs

Complete Optimization of Draw Conditions for Optimized Oxide GSEs < 500 µm

This task was completed previously with preparation of thin-film $LiPO_3$. A 250-g preform of $LiPO_3$ glass was prepared and drawn into thin-film with a thickness of 20-50 µm. The optimized oxide film preparation conditions now serve as the basis for preparation of MOS thin-films.

Complete Optimization of Draw Conditions for Optimized MOS MGF GSEs < 200 µm

A target glass chemistry of $58Li_2S + 32SiS_2 + 10LiPO_3$ was selected for large-scale preparation based on previously determined thermal properties. This MOS glass has a large working range of 107°C, $\Delta T \equiv Tc - Tg$, where *T*c is the onset temperature for crystallization of the GSE and *T*g is the glass transition temperature of the GSE, which is essential for thin-film preparation. Using the large-scale processing facility described previously, a 200-g preform of MOS glass was prepared, as shown in Figure 9a. It was found that heating the precursor Li_2S and SiS_2 starting materials to 700°C and holding for 10 minutes removed sulfur impurities, leading to a cleaner final product GSE. After this heating, the precursors were mechanically mixed in a Spex ball mill in small batches before being combined for melting. Using a custom drop furnace attached to the top of a N_2 glovebox, precursors were melted in a large vitreous carbon crucible and poured onto a heated brass

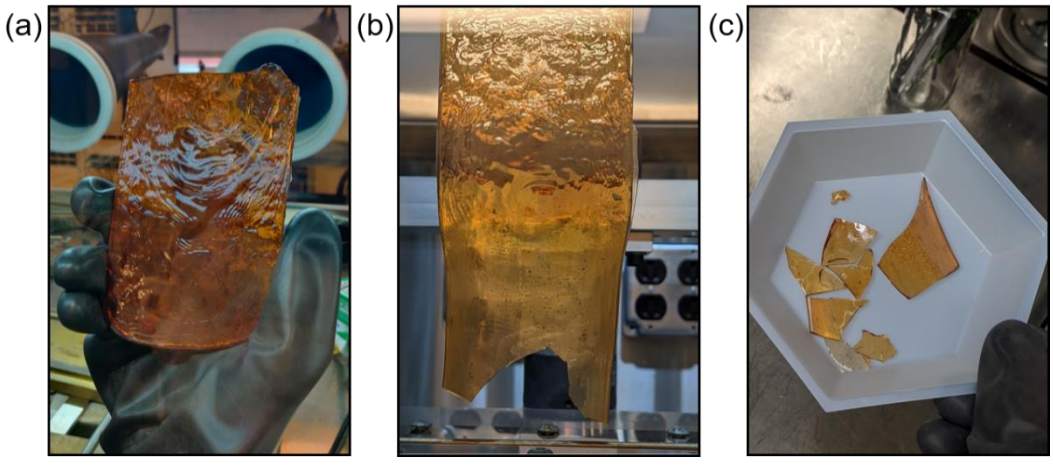

Figure 9. (a) Large preforms of mixed oxy sulfide (MOS) glass are created as precursors for film drawing. (b) MOS glass can be drawn into a thin film; however, pieces are prone to cracking and breaking. (c) MOS glassy solid electrolyte thin-films have been prepared with a thickness of 500 µm.

annealing plate. It was found that proper annealing conditions were crucial in reducing stress in the final preform. Systematic optimization of precursor treatment, melt times, and annealing conditions greatly improved the quality and consistency of MOS preforms.

Using a custom glass draw tower, MOS preforms can be softened and drawn into thin films, with conditions developed by working with $LiPO_3$ oxide glass as a starting point. Interestingly, MOS glass has been found to be extremely sensitive to the heating profile. For example, too fast of a heating rate up to the draw temperature causes the preform to crack. The MOS glass requires significantly slower heating rates than oxide glass, experiencing thermal shock when heated faster than 0.5°C/minute. Once heated above the *T*g, MOS glass became less viscous compared to $LiPO_3$ oxide glass at a similar temperature, ~ 300°C. The lower viscosity makes it more challenging to pull thin-film of MOS glass and has required careful control and optimization of drawing conditions. Currently, small amounts of film have been produced, and work is progressing well to create a thin-film ribbon of the target thickness of < 200 µm. As shown in Figure 9b, several centimeters of film can be prepared, although cracking remains an issue.

As shown in Figure 9c, MOS glass film was prepared by drawing of a preform. So far, films have been produced that are roughly 500-µm thick, and work is continuing to produce thinner films. The team has found that the waste MOS from preform drawing can be recycled and remelted multiple times, greatly reducing batch costs for thin-film development.

Complete Optimization of Draw Conditions for Optimized MOS MGF GSEs < 100 µm

While significant progress has been made in melting and casting GSE preforms and on optimization of draw conditions for MOS MGF GSEs into thin films and while the team is very optimistic that in the coming months they will be able to draw thin, < 100-µm thin films of GSEs, the films at this point are short: a few centimeters, thick ~ 500-µm pieces.

Task 4 - Fabricate and Test Lithium All-Solid-State Battery (ASSB) GSEs in Large Area Planar Formats

Complete Testing of Optimized MOSN MGF GSE in Small-Cell-Format Lithium ASSBs

Symmetric cells were prepared to test the electrochemical behavior of the $58Li_2S + 32SiS_2 + 10[(1\text{-}x)Li_{0.67}PO_{2.83} + xLiPO_{2.5}N_{0.3}]$ GSE series. Coin cells were assembled using a disk of polished GSE between two Li-foil electrodes. EIS measurements were collected every 30 minutes for the first 24 hours after the cell was assembled to evaluate possible reactions between the GSE and lithium metal. As shown in Figure 10a, the EIS spectra change over time, indicative of development of an interfacial layer due to reaction of lithium metal with the GSE. These Nyquist plots were fitted using a two RC circuit model to determine resistance values for both the Li|GSE interface and the bulk GSE. As shown in Figure 10b-e, the calculated resistance values were normalized by the area of the Li-metal electrodes and are plotted as a function of time for the entire MOSN glass series. Area-specific bulk and interfacial resistances of the glasses are seen to rapidly stabilize and remain relatively constant over time, indicating the interfacial layer is stable, and non-consuming. Furthermore, as ASR is linearly dependent on thickness of the electrolyte, the team expects that by decreasing thickness of the electrolyte from the current 1-mm to the target 50-µm thin film, they will see a corresponding drop in ASR by a factor of 20. Therefore, thin-film MOSN GSEs are expected to show ASR values of roughly 10-25 Ω-cm^2. It is important to note that variations in ASR values reported in Figure 10 are likely due to experimental variations in cell preparation rather than intrinsic properties of the MOSN electrolyte. Ongoing efforts focus on methods to improve interfacial contact, including through applied stack pressure, and interfacial chemistry modification.

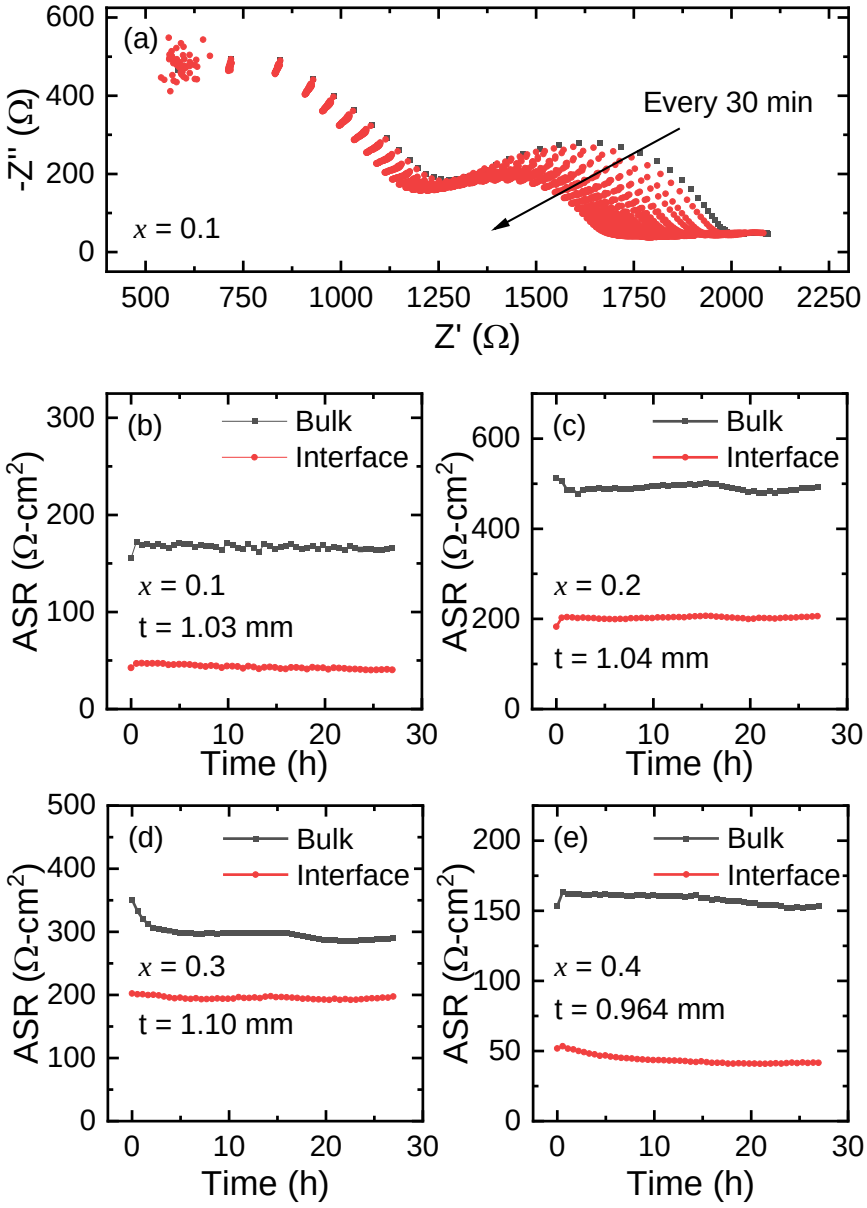

Figure 10. Electrochemical impedance spectroscopy of $58Li_2S + 32SiS_2 + 10[(1-x)Li_{0.67}PO_{2.83} + xLiPO_{2.5}N_{0.3}]$ glassy solid electrolytes in lithium symmetric cells. A Nyquist plot (a) demonstrates changes in impedance of the x = 0.1 glass while (b-e) show the changes in the calculated bulk and interfacial resistance of the x = 0.1, 0.2, 0.3, and 0.4 glasses, respectively.

To evaluate rate performance of prepared MOSN GSEs, critical current density (CCD) experiments were performed on both the $58Li_2S + 32SiS_2 + 10LiPO_3$ and the $58Li_2S + 32SiS_2 + 10[(1-x)Li_{0.67}PO_{2.83} + xLiPO_{2.5}N_{0.3}]$ (x = 0.2, 0.3) glasses. Symmetric cells were assembled and cycled for 80 cycles at 0.05 mA/cm^2 prior to CCD tests in which a fixed capacity of lithium was reversibly cycled for three cycles prior to a stepwise increase in current. An example of the CCD test is shown in Figure 11 for the x = 0.3 MOSN glass, which demonstrated a stable CCD of 0.25 mA/cm^2 prior to cell failure via shorting.

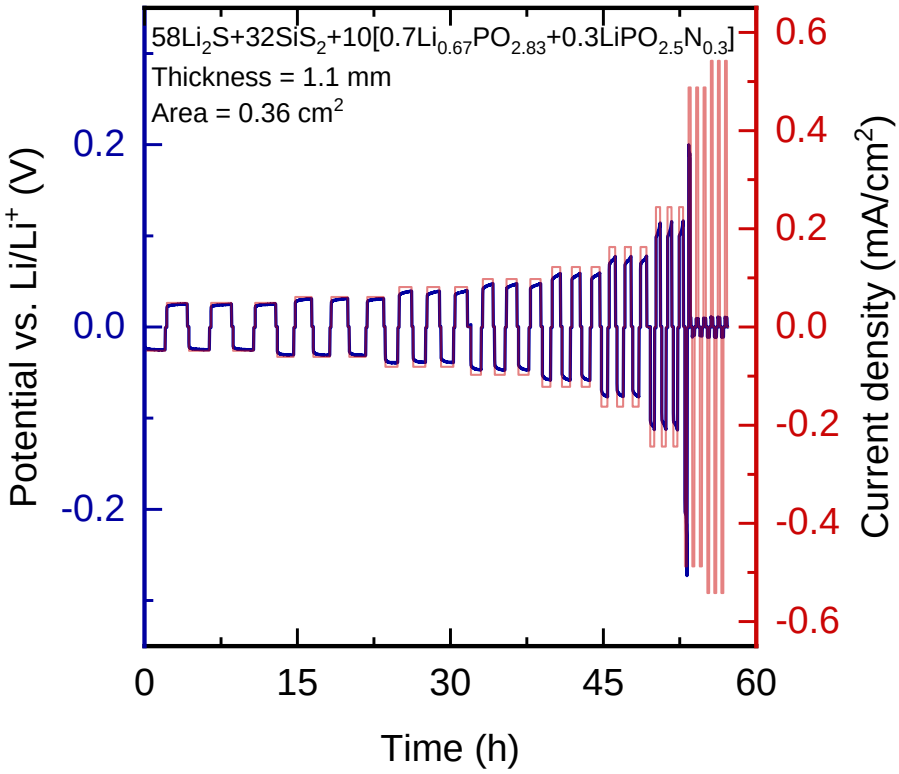

Figure 11. Critical current density test of $58Li_2S + 32SiS_2 + 10[(1-x)Li_{0.67}PO_{2.83} + xLiPO_{2.5}N_{0.3}]$ (x = 0.3) glass demonstrated 3 cycles at 0.25 mA/cm^{-2} before shorting when the current density was increased to 0.5 mA/cm^{-2}.

In addition to electrochemical testing of small batch GSEs, the first symmetric cells utilizing a MOS drawn thin-film were fabricated this quarter, using the $58Li_2S + 32SiS_2 + 10LiPO_3$ GSE. As described previously, 24 hours of EIS measurements were conducted on the cells to evaluate formation of an interfacial layer. As can be seen in Figure 12, three semi-circles are present in the Nyquist plot, indicating presence of three separate circuit elements in the Li|GSE|Li cell. While two of the semi-circles are expected to be associated with the bulk glass resistance and the Li-metal|GSE electrolyte interface, identification of the third process is still uncertain. Potential sources may include a nanocrystalline phase that precipitated during the thin-film drawing process, or an additional interfacial layer that is present due to the glass film being unpolished before cell assembly. Further testing is being done to better characterize and identify this feature. As the MOS thin-film drawing and preparation process is improved, more cells are being assembled for electrochemical characterization.

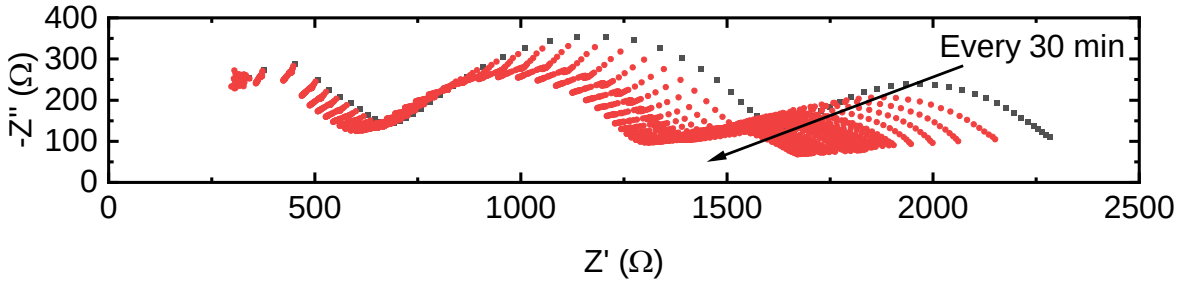

Figure 12. Nyquist plot of a symmetric Li|GSE|Li cell prepared using a drawn thin film of $58Li_2S + 32SiS_2 + 10LiPO_3$ GSE showing three distinct semi-circles.

In new research this quarter, preliminary efforts focused on preparation and optimization of cathode films to be used for testing of full-cell lithium ASSBs. Cathode films are being prepared using $LiFePO_4$ active material, which was chosen for initial method validation due to its highly reversible cycling and low chemical reactivity. Commercially available $LiFePO_4$ was combined with $58Li_2S + 32SiS_2 + 10LiPO_3$ glass powder by mechanical mixing in a Spex ball mill sealed in an inert N_2 atmosphere. The sample was milled for 5 minutes to promote an even dispersion of GSE and active material. Subsequently, a small amount of carbon black was added, followed by additional milling, to ensure good electrical conductivity. Electrode films were prepared by isostatic pressing of the powder to yield free-standing disks.

Full cells were assembled using a Li-foil anode, a MOS GSE, and a free-standing $LiFePO_4$ film cathode. The free-standing film cathode was layered directly on top of the film of glass electrolyte within a CR2032 coin cell case for electrochemical testing. Various electrochemical tests have been initiated, including CV to probe cell stability as well as galvanostatic cycling to investigate long-term cycling performance.

Initiate Testing of Optimized MOSN MGF GSE in Intermediate-Cell Format Lithium ASSBs

No significant progress has been made on intermediate-cell format testing.

Initiate Testing of Optimized MOSN MGF GSE in Large-Cell Format Lithium ASSBs

No significant progress has been made on large-cell format testing.

Patents/Publications/Presentations

The project has no patents, publications, or presentations to report this quarter.

Task 1.6 – Composite Solid Ion Conductor with Engineered Lithium Interface (Kyler Carroll and Cam Peebles, Wildcat Discovery Technologies)

Project Objective. In this project, Wildcat seeks to perform focused, fundamental research and development on composite polymer/ceramic electrolytes and for the protection of Li-metal anodes to develop a Li-metal ASSB that achieves DOE requirements for performance to enable potential commercialization of this technology. Wildcat will leverage its high-throughput (HT) battery platform to explore a broad composite electrolyte compositional space. Additionally, the HT platform will allow the team to screen hundreds of inorganic and organic coatings for Li-metal protection and translate the best results to all solid cells.

Project Impact. Successful widespread commercialization of EVs is contingent on developing safe high-energy-density batteries capable of long cycle life. Lithium metal affords the highest theoretical capacity (3,860 mAh/g) and lowest electrochemical potential (-3.04 V versus self-healing electrolyte), which offers the highest specific energy density of anode materials today. However, significant progress toward the passivation of lithium metal must occur before the energy density benefit can be realized. The intrinsic high reactivity between lithium metal with conventional Li-ion electrolytes (organic carbonate-based solvents) makes it extremely difficult to overcome these problems. The proposed composite polymer/ceramic electrolyte and a protected Li-metal anode will enable a Li-metal ASSB. It is expected that the outcomes from this effort will deliver a safe all-solid-state Li-metal pouch cell with over 350 Wh/kg and over 1,000 cycles (C/3) with the cost estimate below $100/kWh.

Approach. The project approach involves (1) identifying a suitable combination of solid ion conductor, polymer, and additive that minimizes overall interfacial impedance between the PE and solid ion conductor, and (2) identifying stable Li-metal protection agent or combination of agents that shows enhanced cycling performance (relative to a non-protected system) using the down-selected cell architectures.

Out-Year Goals. The out-year goals involve the screening of cathode composites to minimize interfacial resistance, the down selection of the best SSE, and the down selection of the best passivation approach for lithium metal. Following these developments, the final tasks will be to integrate these three components into a full SSB with improved cycle life.

Collaborations. All project tasks will be performed at Wildcat Discovery Technologies.

Milestones

1. Down select passivation approaches. (Q1, FY 2021; Completed)
2. Optimize SE. (Q2, FY 2021; In progress)
3. Integrate SE with cathode. (Q2, FY 2021; In progress)
4. Final Testing. (Q4, FY 2021; In progress)

Progress Report

This quarter, Wildcat utilized its HT platform to investigate further improvements in the protection of a Li-metal anode for use with SSE. Various types of protection materials were applied to the lithium metal with the goal of finding a system that showed reduced resistance compared to a baseline (non-protected) system. Systems with reduced resistances have been shown before at Wildcat to have better cycling performance when current is passed through the system. Once systems with minimal resistance were found, the system was further optimized and then tested in combination with various SSEs that have been developed in another part of this project.

Optimization of Composite Electrolyte

In previous quarters, the team optimized the composite ceramic-polymer electrolyte by introducing a PVDF polymer to replace the previously optimized PEO polymer to introduce higher voltage stability. Last quarter, they also found that in the full-cell integration, they can improve charge performance by switching the PVDF type (for example, chain length, functionality, and branching). Based on those results, this quarter they further investigated the PVDF type and tested the composite ceramic-polymer electrolyte conductivity as well as full-cell performance integration.

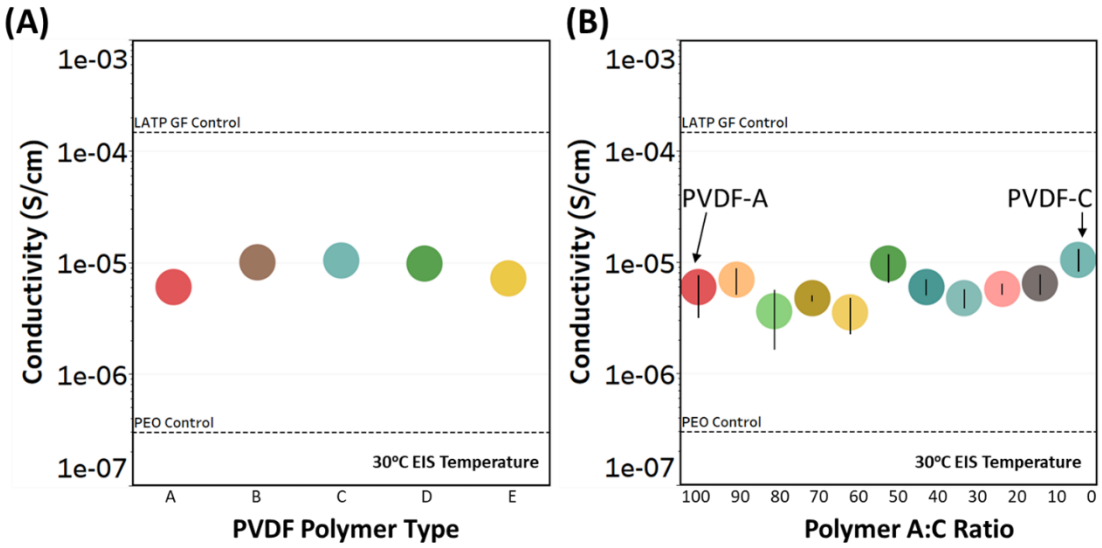

Figure 13. (a) Electrochemical impedance spectroscopy (EIS) data for different PVDF polymer types in the composite ceramic-polymer electrolyte. (b) EIS data for various ratios for blended PVDF types A and C.

Figure 13a shows room-temperature ionic conductivity for five PVDF polymer types, varying in chain length and functionality. While the results do not show significant improvement in ionic conductivity, the composite polymer-ceramic electrolytes processibility and performance in full-cell performance varied greatly, which is shown in Figure 16a. For the full-cell test, composite electrolyte containing PVDF-A had better initial charge rate performance, while composite electrolyte PVDF-C had better initial cycling performance. Based on processibility as well as their initial full-cell performance, the team decided to take two of the polymer types (A and C) and varied the weight percent ratio to see if they could further improve full-cell performance. They also checked the ionic conductivity, which is shown in Figure 13b, and selected the one with best ionic conductivity for the full-cell test. The hypothesis as to why these polymers affect full-cell performance is being investigated, but initial results suggest that the polymer type can significantly affect both the cathode/electrolyte and anode/electrolyte interfacial impedance. The team is continuing impedance spectroscopy investigation on these interfaces to gain a more detailed understanding.

Protected Li-Metal Anode Development

In a Li/Li symmetric cell format, Li-metal protection treatments are first screened using EIS immediately after a cell is built (analysis and interpretation of the collected EIS were shown in an earlier quarterly report). Figure 14 shows the initial resistance of Li/Li cells using various families of protection additives (such as salts and organics) represented in different colors and various types of SSE (PVDF, etc.) represented in different shapes (the legends for these are not included). The baseline system (labeled as "None") shows a range of resistance from ~ 250-1250 ohm depending on the SSE used in the cell. The relatively wider range of cell resistances suggests that the untreated lithium surface presents great challenges in batteries due to its inhomogeneous nature. Depending on the protection method, the repeatability of the interfacial resistance varies (look at the size of the black error bar)—for the better performing protection additives (see those with lower initial resistances), the repeatability of the system is good, while it is worse for higher resistance systems. In the past, the team has evaluated over 500 different conditions of lithium surface treatment by introducing various reactive additives onto the lithium surface. The protection additives in the green family showed significantly reduced resistances compared to other systems and the baseline system. This system was further explored (ratio of additives changed, etc.) to optimize its performance. Using an optimized additive system, the initial resistance of this system was measured at ~ 50 Ω, compared to the baseline system with an average of ~ 700 ohm using the same SSE. This reduced resistance should directly translate to systems where current is passed between the Li-metal electrodes.

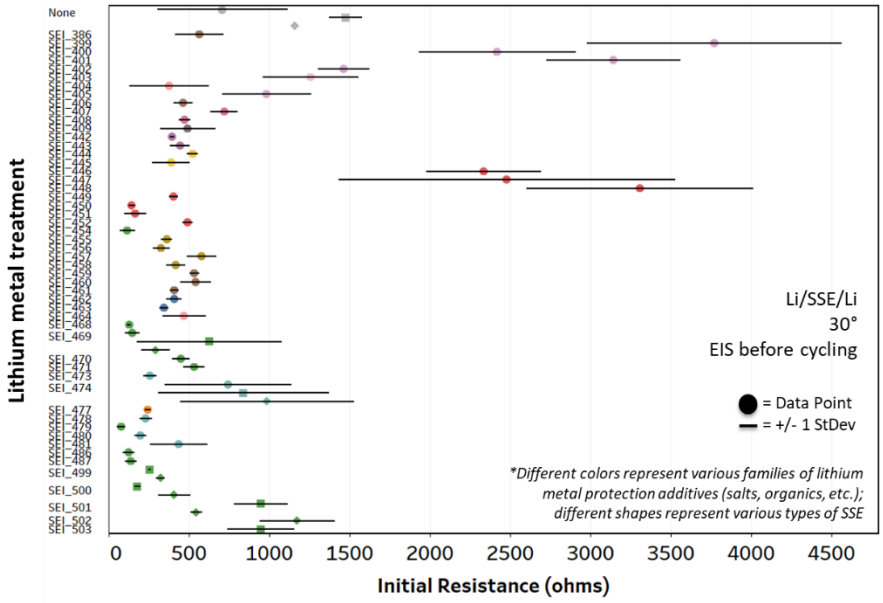

Figure 14. Screening of protected Li-metal anodes using Li/Li symmetric cells. The different colors represent various families of Li-metal protection additives (such as salts and organics), and the different shapes represent various types of solid-state electrolytes used in the cell.

After initial resistance is collected in the cells, they are subjected to cycling at 25°C using a plating/stripping current density of 1.0 mA/cm^2 for one hour. Figure 15 shows the plating/stripping voltage profile for a representative protected Li-metal anode (SEI_469 from Figure 14) and the baseline system using the same SSE. The protected Li-metal anode shows flat voltage profiles and relatively low overpotentials (~ 10-20 mV) even after cycling for 300 hours. In contrast, the baseline system shows dramatic and sporadic increases in voltage that occur throughout the cycling. These are likely indicative of Li-metal dendrite formation, which causes hard/soft shorts to occur in the Li/Li symmetric cell system.

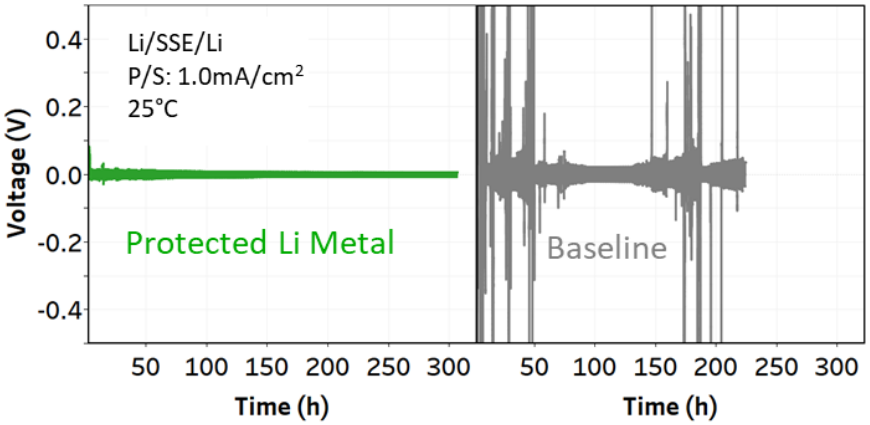

Figure 15. Long-term Li/Li symmetric cell cycling. The protected Li-metal anode (green) shows minimal overpotential with no indication of dendrite formation or soft/hard shorts. The baseline (non-protected) system shows consistent voltage spikes indicative of soft/hard shorts caused by dendrite growth.

Future work in this thrust includes optimizing the lower resistance systems and continuing to test their cycling at 1.0 mA/cm^2 current density and increasing current densities. In parallel, these systems are being tested in Li/NMC full cells to see how cycling correlates between symmetric cells and full cells.

Catholyte Development

Last quarter, Wildcat demonstrated the importance of incorporating SSE components within the cathode. The resultant electrode with the SSE components integrated into it was being referred to as the *catholyte*. This quarter, Wildcat continued evaluating catholyte compositions using its HT platform and integrating them with the state-of-the-art SSE and the protected lithium metal from Thrust 1 and Thrust 2, respectively. The SSE compositions that showed the highest ionic conductivities in Thrust 1 and the lithium protection that showed the lowest resistances in Thrust 2 were identified and chosen for this task. After evaluating several SSE/catholyte compositions using protected Li-metal from Thrust 2, Wildcat has successfully developed all-solid-state full cells that are capable of fully charging up to 4.3 V versus Li^+/Li. Figure 16a shows the Cycle-1 voltage traces of the all-solid-state full cells with different composite SSEs each featuring a different PVDF. For comparison, the voltage trace of a control cell with an identical catholyte and LE (1 M $LiPF_6$ in 1:1 EC:DMC) is also shown. The voltage traces of the LE cell and the all-solid-state cells with PVDF A, C, and D look similar, indicating that the all-solid-state cells work as well as conventional Li-ion cells with LE. Out of the several SSE compositions that Wildcat evaluated in this preliminary screening effort, one of the SSE types—with PVDF A—showed a promising cycling performance of about 84.2% capacity retention at the end of 20 cycles running at a rate of 0.1C (Figure 16b). With the successful development of a working all-solid-state full-cell, the focus now shifts toward improving cycling performance. In upcoming quarters, Wildcat aims to adopt a three-pronged approach for improving full-cell performance. First, they will screen for more catholyte compositions using the HT platform while simultaneously trying to minimize the amount of SSE content (≤ 30%) in the catholyte. Secondly, they will further investigate the role of PVDF types and ceramic types in composite SSEs in the context of full-cell performance. Thirdly, on optimizing the SSE composition and the catholyte in full cells at 60°C (which is the current testing temperature), they will then try to achieve a comparable full-cell cycling at lower temperatures.

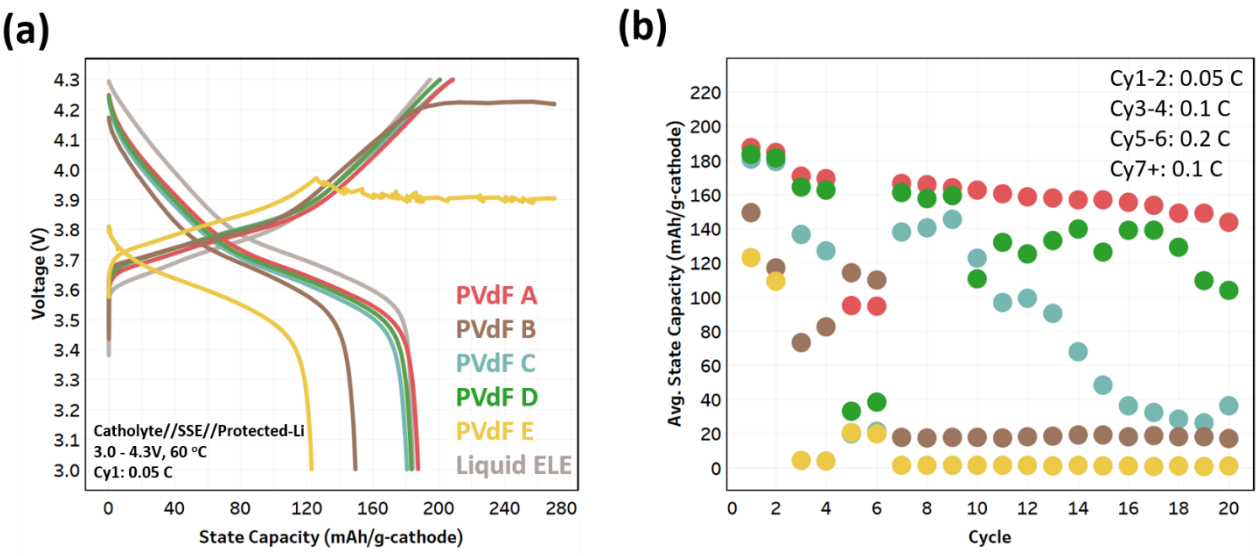

Figure 16. Performance of all-solid-state full cells. (a) Cycle-1 voltage traces of all-solid-state Li//NMC full cells with different PVDF types in the composite solid-state electrolyte. A control cell with an identical catholyte and a liquid electrolyte ("Liquid ELE": $LiPF_6$ in EC/DMC) is also shown. (b) Specific capacities of the all-solid-state full cells with different PVDFs in SSE for up to 20 cycles.

Patents/Publications/Presentations

The project has no patents, publications, or presentations to report this quarter.

Task 1.7 – Physical and Mechano-Electrochemical Phenomena of Thin-Film Lithium-Ceramic Electrolyte Constructs
(Jeff Sakamoto, University of Michigan)

Project Objective. While a small number of SEs exhibit high ionic conductivity (~ 1 mS cm at 298 K), few are stable against lithium metal. The garnet-type SE, based on the nominal formula $Li_7La_3Zr_2O_12$ (LLZO), is unique in that it is a fast ion conductor and—as demonstrated in the team's recent project (DE-EE-00006821)—is stable against lithium. Moreover, the team's former project successfully demonstrated a decrease in Li-LLZO interface resistance from 12,000 ohm cm^2 to 2 ohm cm^2 and stable cycling at 1 mA cm^2 for 100 cycles (± 15 µm of lithium per cycle). Although the past project demonstrated that LLZO is a viable SE for enabling batteries using metallic lithium, the studies used thick pellets (1 mm) and thick anodes (~ 500 µm). The goal of this project is to acquire a deep fundamental understanding of the physical and mechano-electrochemical phenomena that control the performance of cells consisting of thin LLZO (~ 10 µm), thin lithium anodes (~ 20 µm), and thin solid-state composite cathodes.

Project Impact. If successful, the project will gain knowledge to guide closely related commercialization efforts to scale the production of LLZO-based SSBs.

Approach. The team believes that to achieve a step increase in technology readiness level (TRL), the same performance characteristics previously shown should be demonstrated in technologically relevant cells, for example, thin LLZO and thin lithium.

Out-Year Goals. The out-year goals involve the following: custom thin-film composite (TFC) development, preliminary cycling studies, Vis cell development, lithium cycling, and polymer gel electrolyte (PGE) screening.

Collaborations. This project collaborates with Professors N. Dasgupta and D. Siegel of University of Michigan (UM), Mechanical Engineering.

Milestones

1. Initial design, fabrication, testing, and optimization of custom *operando* optical visualization cell. (Q1, FY 2021; Completed)

2. Initial integration of precision micro reference electrodes with thin lithium and TFC for 100 cycle tests. (Q2, FY 2021; Completed)

3. In thin lithium and thin LLZO TFC, determine the max cycling rates versus lithium thickness ranging between 2-17 µm. (Q2, FY 2021; Completed)

4. Refinement of custom *operando* optical visualization cell to quantify topographic lithium plating homogeneity versus cycle number. (Q4, FY 2021; In progress)

Progress Report

Initial Integration of Precision Micro Reference Electrodes with Thin Lithium and TFC for 100 Cycle Tests (Q2 Milestone; Completed). The team is carrying out extended cycling tests using hybrid TFC cells. The knowledge gained throughout this quarter enabled stable cycling. In hybrid cells, where the anode is 10-µm-thick lithium, representative DC polarization curves confirm that cycling follows ohmic behavior and is thus stable (Figure 17).

In Thin Lithium and Thin LLZO TFC, Determine Max Cycling Rates Versus Lithium Thickness from 2-17 µm (Q2 Milestone; Completed). Under more aggressive cycling conditions (discharge), deviation from ohmic behavior is observed. The behavior is dependent on lithium anode thickness. This quarter, *operando* analysis elucidated salient features in DC polarization data (Figure 18, symbols). Understanding the phenomena that control the behavior will help guide efforts to prevent severe polarization.

A Perspective article on the status and future of SSB research and development was accepted in *Joule*. The success in overcoming key challenges related to the electrochemo-mechanical behavior of solid-solid interfaces (SSIs) will determine the extent to which SSBs supplant Li-ion batteries. This Perspective provides an overview of the electrochemical, mechanical, and thermal properties of SSB components and how they dictate the design, manufacturing, and performance of the device. Based on solicited input from three global automakers, the article provides specific insights into the design criteria of SSBs for EVs and suggestions for future research.

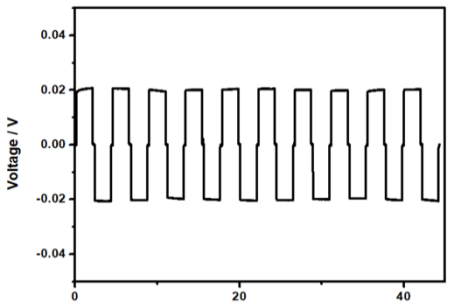

Figure 17. DC cycling of thin lithium (10 µm) LLZO cells: representative DC polarization curves.

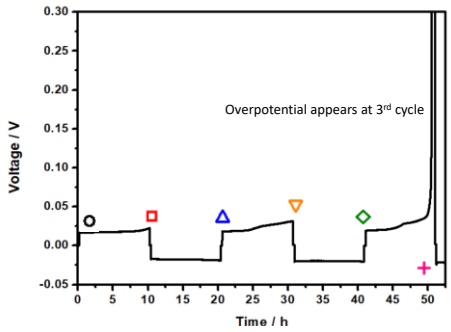

Figure 18. DC cycling of thin lithium (10 µm) LLZO cells: *operando* analysis of DC polarization data.

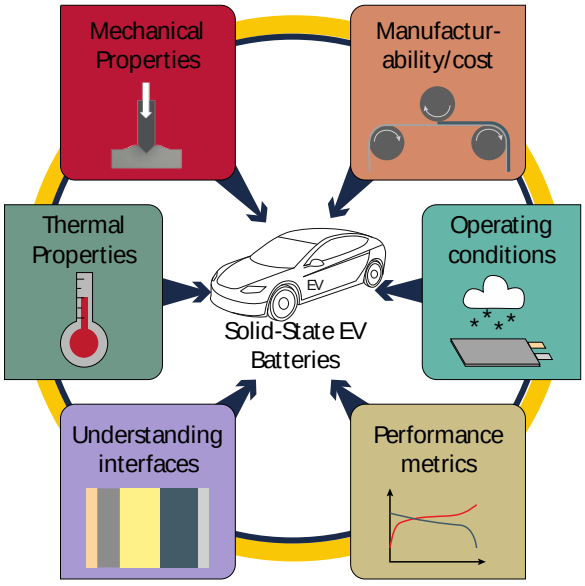

Figure 19. The team has had an invited Perspective accepted by *Joule*: Wang, M. J., E. Kazyak, N. P. Dasgupta, and J. Sakamoto. "Transitioning Solid-State Batteries from Lab to Market: Linking Electro-Chemo-Mechanics with Practical Considerations."

Patents/Publications/Presentations

The project has no patents, publications, or presentations to report this quarter.

Task 1.8 – Lithium Dendrite-Free Li_7N_2I-LiOH Solid Electrolytes for High-Energy Lithium Batteries (Chunsheng Wang, University of Maryland)

Project Objective. The objective of this project is to research, develop, and test Li-metal-based batteries that implement solid Li-ion conductors (LICs) equipped with Li_7N_2I-LiOH SE capable of achieving cell performance of 350 Wh/Kg energy density for 1000 cycle life with a cost of ≤ $100/kWh.

Project Impact. Lithium dendrite growth during charge/discharge cycles limits the use of ASSBs. A criterion for lithium dendrite suppression that is developed through systematical investigation on thermodynamics and kinetics of lithium dendrite growth will guide the electrolyte design. Li_7N_2I-LiOH and Li_3YCl_6 SE with high ionic conductivity and low electronic conductivity will be used to validate the criterion for lithium dendrite suppression, to achieve the project objective.

Approach. The team will establish the relationship among interface energy, lithium plating/stripping overpotential, interface resistance, SE stability with lithium, and CCD. The dendrite suppression criterion will be developed based on the relationship. The dendrite suppression capability for the Li_7N_2I-LiOH pellet will be evaluated by testing the CCD.

Out-Year Goals. The project will study the thermodynamics and kinetics of lithium dendrite growth in SSEs and develop lithium dendrite suppression criterion in SSEs. The Li_7N_2I-LiOH electrolytes and Li_7N2I-LiOH/Li_3YCl_6 bi-layer electrolytes will be used to validate the developed dendrite suppression criterion and support NCM cathodes.

Collaborations. There are no reported collaborations this quarter.

Milestones

1. Determine critical overpotential of Li_7N_2I-LiOH, LPS, and LLZO electrolytes. (Q1, FY 2021; Completed)
2. Develop lithium dendrite suppression criterion for SEs. (Q2, FY 2021; In progress)
3. Develop a kinetics model of SSEs. (Q3, FY 2021; In progress)
4. Critical current of Li_7N_2I-LiOH electrolytes should be > 4 mA/cm^2 at 3 mA/cm^2 of current. (Q4, FY 2021)

Progress Report

Li_3YCl_6 Electrolytes for Solid-State Li/NMC Batteries

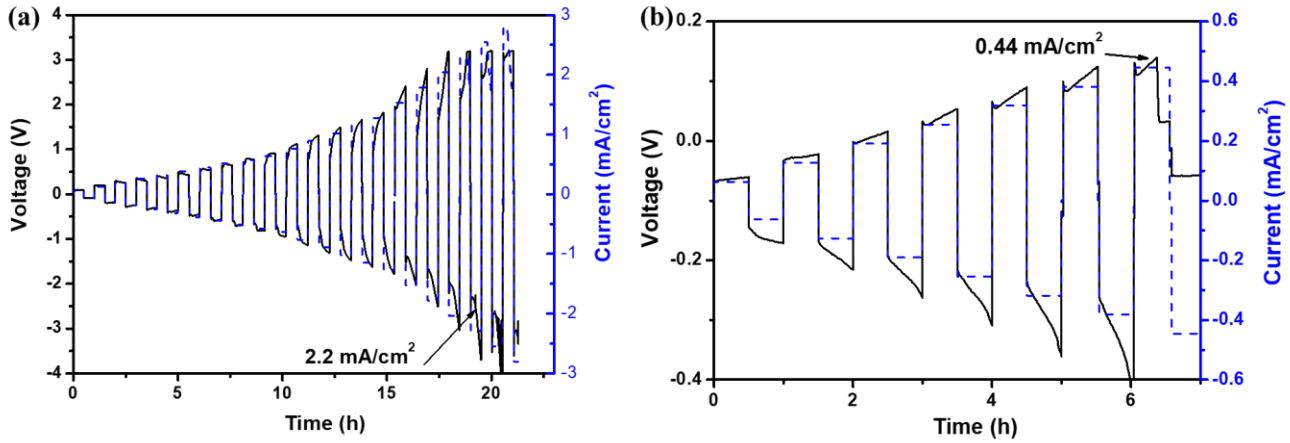

Figure 20. The lithium plating/stripping behavior for (a) the Li_7N_2I-LiOH|Li_3YCl_6|Li_7N_2I-LiOH cells. (b) Li-In|Li_3YCl_6|Li-In cells at a step-increase current for 0.5 hours.

Lithium halide SE materials Li_3YCl_6 exhibit high Li-ion conductivity of 0.3 mS cm^{-1} and high anodic stability (> 4.5 V) at room temperature by cold-pressing. However, inadequate chemical and electrochemical stability with lithium metal hinders its applications in Li-metal ASSBs. Here, the team protected Li_3YCl_6 using a thin layer of lithium stable Li_7N_2I-LiOH layer. They evaluated stability of Li_7N_2I-LiOH sandwiched Li_3YCl_6 to lithium anodes. The Li_7N_2I-LiOH|Li_3YCl_6|Li_7N_2I-LiOH cells were fabricated by cold-press. Due to the intrinsic stability and high interfacial energy of Li_7N_2I-LiOH toward lithium metal, as well as its low electronic conductivity, this layer can prevent the side reaction of lithium with Li_3YCl_6, and thus block electron injection and lithium dendrite penetration. By charging/discharging for a fixed 0.5 hour with the step-increase current density, the CCD for the Li_7N_2I-LiOH|Li_3YCl_6 sandwiched SSE is determined to be 2.2 mA/cm^2 with a capacity of 1.1 mAh/cm^2. In contrast, the CCD for the Li-In|Li_3YCl_6|Li-In cell is only a fifth that of Li_7N_2I-LiOH sandwiched Li_3YCl_6 electrolyte. These results demonstrate the Li_7N_2I-LiOH|Li_3YCl_6 bi-layer electrolyte can be used for Li-dendrite-free all-solid-state Li/NMC batteries.

Lithium Anode with Significant Different Ductility and Malleability

To avoid dendrite formation and propagation inside SSEs, the team modified the Li-metal anodes by adding "A" element to form Li-A alloy. The Li-A alloy can reduce interfacial resistance and also maintain close contact between lithium and SEs during lithium plating/stripping cycles. Four Li-A alloy anodes with different A concentrations of 1%, 5%, 10%, and 20% were synthesized. As demonstrated in Figure 21, these electrodes show significantly different behavior after pressing under 2 MPa. The electrode demonstrates well ductility and forms a thin foil with a smooth surface and metallic luster for the Li-A-1% alloy. With increasing A content, the pressed electrodes render wrinkles, cracks, gaps, and even fracture. As shown in Figure 21d-e, the pressed 20% A in lithium has a sharp fracture, and part of it even shattered into small pieces.

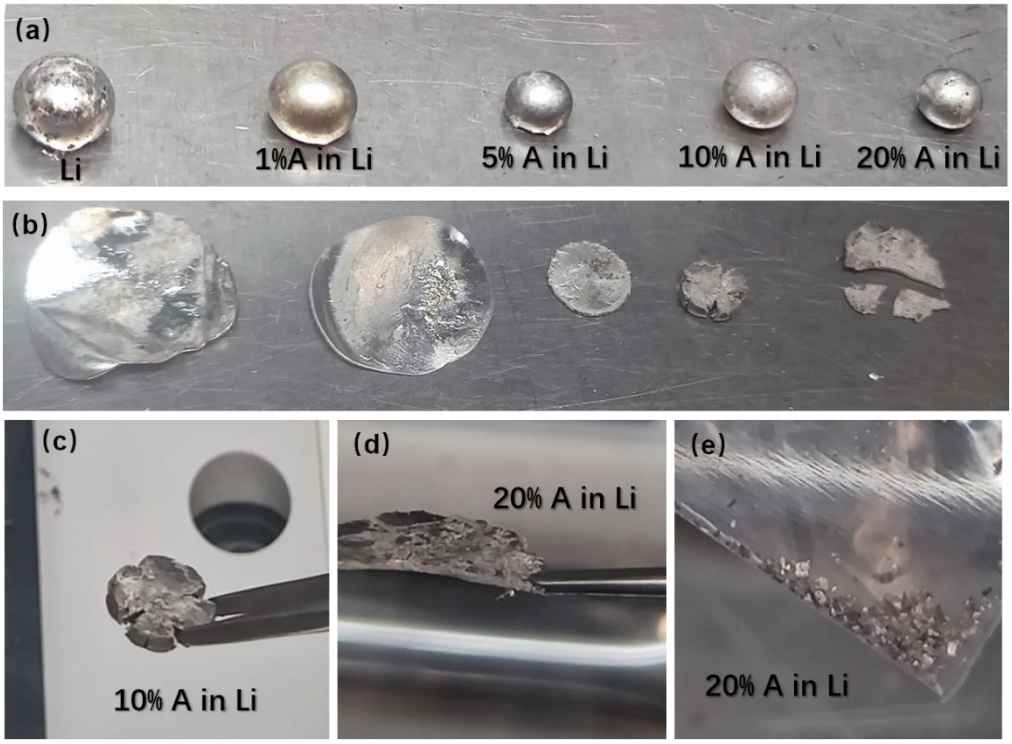

Figure 21. Digital pictures of lithium anode with significantly different ductility and malleability. (a) Electrodes before pressing. (b) Electrodes after pressing. (c) Magnification of the 10% "A" element in lithium. (d) Fracture of 20% A in lithium. (e) Shattered small pieces of the 20% A in lithium.

Performance of Li-A Alloy Anodes Evaluated Using Standard Ta-doped LLZO (LLZTO) Electrolytes

The LLTZO pellets were polished and immersed into the molten Li-A alloys at 300°C for 3 minutes. The Li-A alloys show high wettability with the LLZTO pellets, which makes Li-A alloys to easily attach on both sides of the LLZO pellet, forming a Li-A|LLZTO|Li-A symmetrical cell. The lithium plating/stripping behavior for these cells was evaluated at a step-increase current for a fixed one hour per cycle. As shown in Figure 22a, a high CCD of 1.3 mA/cm^2 was achieved for the Li-A-1%|LLZO|Li-A-1% symmetric cell, which is one of the highest among all surface-engineered solid-sate Li-metal batteries. Meanwhile, the cells with Li-A-5%, Li-A-10%, and Li-A-20% show much lower CCD ~ 0.3 mA/cm^2. The Li-A-20%|LLZO|Li-A-20% cell even showed a rapidly increasing overpotential at 0.2 mA/cm^2, and a drastically increasing overpotential exceeded the 5 V measuring limitation of the battery test equipment.

Galvanostatic lithium plating and stripping testing was used to evaluate the impedance of Li-A|SSE|Li-A cells. As shown in the magnified first 5 cycles curves (Figure 22b), at the current density of 0.1 mA cm^2, the voltage profiles of four cells using different Li-A anodes are almost the same, with a similar overvoltage of ~ 20 mV. The similar interface impedance between LLZO and four Li-A anodes demonstrates that all four Li-A anodes can contact well with LLZO electrolytes with similar interface impedance. The significant difference in CCD here is not caused by interface wettability or interface resistance, which people usually focus on when designing the anode part for the solid-state Li-metal battery.

Figure 22c shows that the Li-A-1%|LLZO|Li-A-1% symmetric cell is stable for 500 cycles at 0.5 mA cm^2. However, the symmetric Li-A|LLZO|Li-A cells with the other three Li-A anodes cannot even reach 0.5 mA cm^2 in the CCD test, although they have similar resistances with Li-A-1%|LLZO|Li-A-1% cell. This may result from the significant difference in the ductility and malleability of the electrode. The ductility of the electrode is addressed here for anode design in solid-state Li-metal batteries.

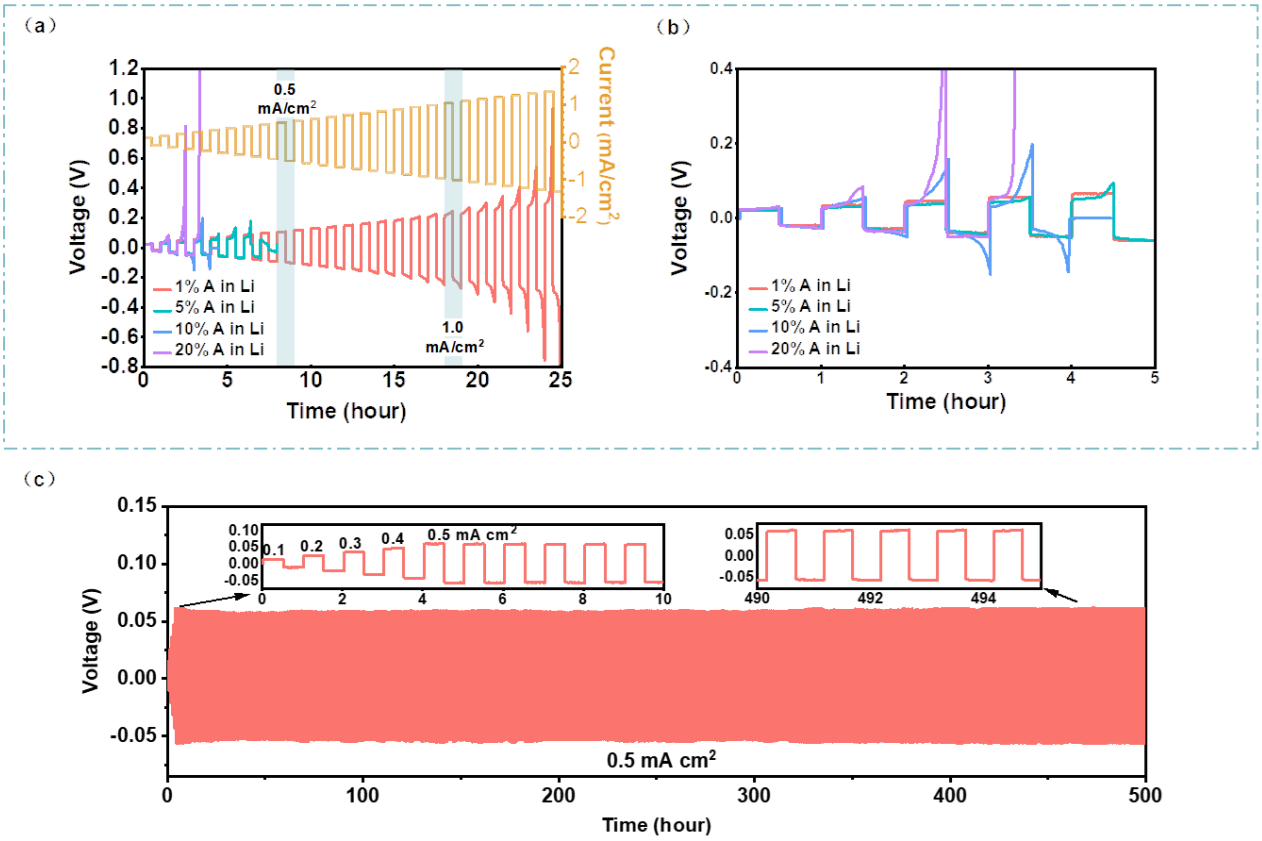

Figure 22 Electrochemical performance of Li-A|LLZO|Li-A symmetric cells with different A contents in the lithium anodes. (a) Lithium plating/stripping behavior for four Li-A|LLZO|Li-A cells at a step-increase current for 0.5 hours. (b) Magnified lithium plating/stripping profiles in the first 5 cycles of four Li-A|LLZO|Li-A cells (a, left). (c) Long-term cycling performance of Li-A-1%|LLZO|Li-A-1% symmetric cell at 0.5 mA/cm² with a magnification of the voltage profile of 1-10 cycles and 490-495 cycles.

Proof-of-Concept Full Cell

Li-A-1%|LLZTO|NMC-811 full cells (Figure 23a) are assembled. The NMC-811 with loading of ~ 0.8 mAh/cm² was selected as the cathode for the solid-state Li-metal battery. A small amount of LE (10 µL) was used to wet the NMC-811|LLZTO interface. Figure 23b demonstrates the EIS plot before (black circle) and after (red circle)100 cycles. The EIS plots indicate a small reduction of the resistance of the electrolyte after 100 cycles without short circuit. Figure 23c shows the typical charge/discharge curve of the Li|NMC-811 cell at 0.2 C. The cell maintains 82% of initial capacity after 100 cycles, indicating a stable Li-A-1%|LLZTO interface (Figure 23d).

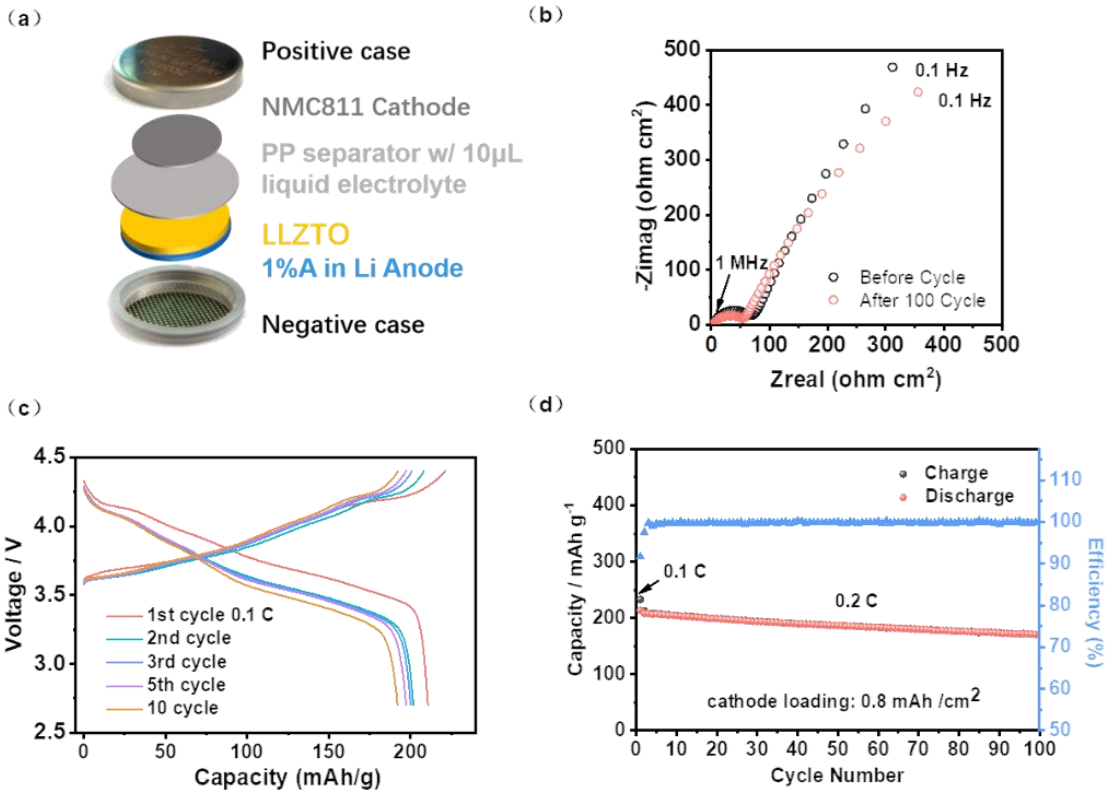

Figure 23. Electrochemical performance of Li-A-1%|LLZTO|NMC-811 full cells with cathode loading of 0.8 mAh/cm² at a 0.2 C (0.1 C for the first cycle for activation). (a) Schematic diagram of a Li-A|LLZTO|NMC-811 full cell. (b) Impedance spectra of the cell before and after 100 cycles. (c) Charge/discharge profiles and (d) cycling stability of Li-A-1%| LLZTO|NMC-811 full cells.

Patents/Publications/Presentations

The project has no patents, publications, or presentations to report this quarter.

Task 1.9 – Low Impedance Cathode/Electrolyte Interfaces for High-Energy-Density Solid-State Batteries (Eric Wachsman and Yifei Mo, University of Maryland)

Project Objective. The project objective is to research, develop, and test Li-metal-based batteries that implement solid LICs equipped with NMC cathodes integrated into the Li-metal/LLZ tri-layer architecture. Specifically, the team will achieve the following: (1) identify and demonstrate interfacial layers to achieve low-impedance and stable NMC/LLZ interfaces; (2) develop novel processing techniques to fabricate NMC/LLZ composite cathodes with low interfacial resistance; and (3) enable high-performance ASSBs with an energy density of 450 Wh/kg and 1400 Wh/L and negligible degradation for 500 cycles.

Project Impact. Instability or high resistance at the interface of high-energy cathode materials with Li-garnet SEs limits the high-energy-density lithium ASSBs. This project will lead to a fundamental understanding of solid-electrolyte/solid-cathode interfaces and a unique and transformative LLZ framework to enable high-energy-density, safe Li-metal batteries approaching ~ 400 Wh/kg.

Approach. In this new project, the team will build on their demonstrated expertise with garnet electrolytes and ASSB cells to accomplish the following: (1) engineer interfaces to overcome high NMC/LLZ interfacial impedance and interfacial degradation; (2) develop processing and fabrication techniques to achieve high-loading NMC/LLZ composite cathodes with low resistance and high cyclability; and (3) integrate the NMC/LLZ cathodes into all-solid-state Li-metal/LLZ cells to achieve high-energy-density batteries.

Out-Year Goals. The project will solve the current challenges of integrating garnet SE with a cathode to achieve a high-performance ASSB using a high-energy-density Li-metal anode. The resultant high energy density and stability using both high-energy-density Li-metal anodes and NMC cathodes will open new applications in portable electronics, EVs, and beyond.

Collaborations. This project funds work at UMD. The PI, E. Wachsman, will have management responsibility and will lead experimental efforts including garnet synthesis, interface processing, cell fabrication, and testing. The Co-PI, Y. Mo, will lead computational efforts on understanding stability between garnet and cathode and on identifying promising coating materials. No collaborations are reported this quarter.

Milestones

1. Experimentally determine thermochemical stability between interface-coated LLZ and infiltrated NMC. (Q1, FY 2021; In Progress)
2. Computations of promising coating materials determine appropriate compositions to stabilize the LLZ-NMC interface. (Q2, FY 2021; Completed)
3. *Go/No-Go Decision*: Demonstrate a 10-times reduction in interfacial impedance between coated and uncoated LLZ/NMC interfaces. Design capable of meeting performance requirements. (Q4, FY 2021; In Progress)

Progress Report

Progress on experimental results was impacted by COVID-19, which closed labs for 3 months; labs are still only partially reopened. However, computational aspects are on track.

Using demonstrated thermodynamic analyses for interface stability based on first-principles computation, the team studied trends in stability with LLZO and NMC throughout the entire Li-M-O ternary composition space to identify all compositions that are stable with LLZO as promising coating. The decomposition energy E_d of each composition with LLZO is illustrated by a heatmap of Li-M-O Gibbs ternary diagram (Figure 24). Li-M-O systems with different cations M exhibit significantly different stability with LLZO. The team extended analysis to other Li-M-O systems for cations M = B, C, N, Al, Si, P, Ti, V, Cr, Zr, Nb, Mo, Zn, Ga, Ge, Ta, or W, which are commonly considered and used for coatings (Figure 24). Many systems with nonmetal M, such as B, Al, Si, or P, only have one or two ternary Li-M-O compositions (in addition to Li_2O and Li_2O_2) stable with LLZO, leading to a narrow compositional space with good LLZO stability. The transition metal (TM) elements V, Cr, Nb, Ta, Zn, Ga, Ge, and nonmetals C and N are stable with garnet, and a wider Li-M-O compositional space of ternary Li-M-O oxides has good stability with LLZO. For cations M = Ti and Zr, the M metal exhibits minor reactions with LLZO, but the binary oxides M-O are stable with LLZO, leading to a wide compositional space stable with LLZO. Notably, for the Li-Zn-O system, Zn metal, ZnO oxide, and LiZn alloy are stable with LLZO. Thus, this system has the widest composition space stable with LLZO, and so should be a promising system for garnet coatings, as has been demonstrated in experiments. In general, one should select within this stable compositional space for garnet coatings, as the compositions outside react exothermically with LLZO and may cause side reactions and interfacial degradation. The team's Li-M-O heatmaps of stability with LLZO provide guiding maps for selecting compositions for garnet coating layers.

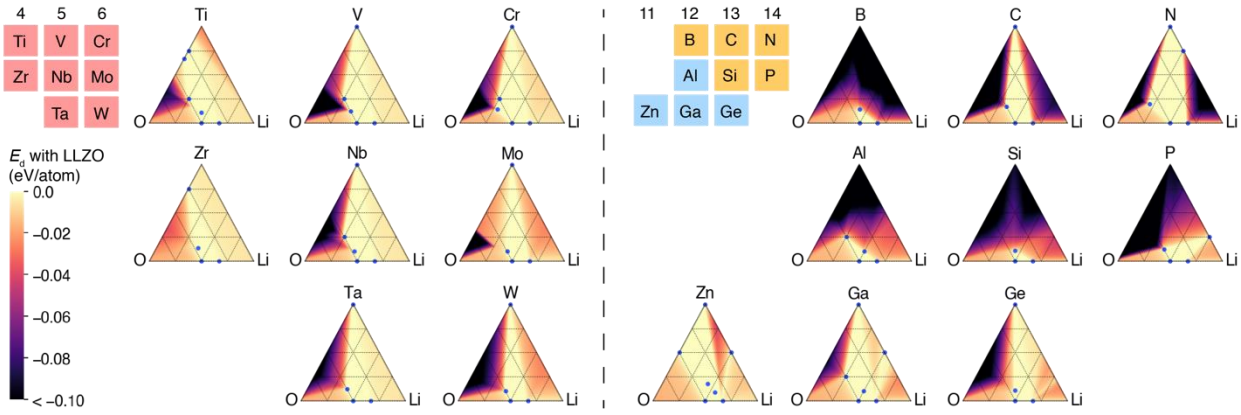

Figure 24. Heatmaps of chemical stability (Ed) of Li-M-O (M = B, C, N, Al, Si, P, Ti, V, Cr, Zr, Nb, Mo, Zn, Ga, Ge, Ta, or W) with LLZO. Known compounds that are stable with LLZO are marked with blue points.

In addition, the team also analyzed the stability of the entire Li-M-O composition space with NMC (Figure 25). Their analyses found that the only Li-M-O compositions stable with the cathode are along the tie-line of Li_2O and M-O metal oxides, and the cathode stability is generally good for O-rich compositions. They identify the coating layer stable with both SE and cathode by combining the heatmaps and stable regions of Li-M-O with LLZO and those with NMC cathode. The materials compositions along the tie-line of Li_2O to M-O oxides, including multiple ternary oxides, show decent stability with both LLZO and NMC. In summary, they have successfully achieved the milestone of identifying promising coating materials to determine appropriate compositions to stabilize the LLZO-NMC interface.

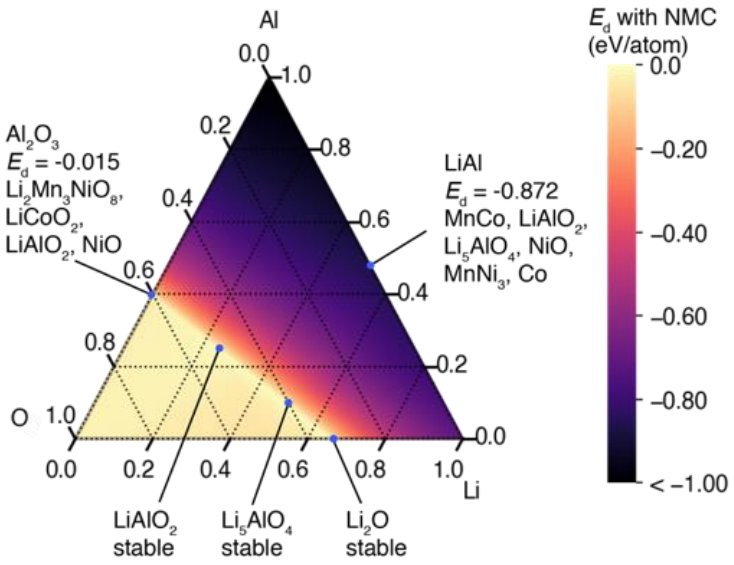

Figure 25. Heatmap of the decomposition energy of Li-Al-O compositions with NMC-111.

Patents/Publications/Presentations

Patent

- Ren, Y., and E. D. Wachsman. "Interlayer for Solid Cathode-Electrolyte Interface." Invention Disclosure.

Task 1.10 – Developing an *In Situ* Formed Dynamic Protection Layer to Mitigate Lithium Interface Shifting: Preventing Dendrite Formation on Metallic Lithium Surface to Facilitate Long Cycle Life of Lithium Solid-State Batteries
(Deyang Qu, University of Wisconsin, Milwaukee)

Project Objective. The objective of this project is to research, develop, and test Li-metal-based batteries that implement solid LICs equipped with a formed dynamic protection layer. The proposed project aims to enable safe, long-cycle lithium anodes to achieve cell performance targets of 400 Wh/Kg, over 100 cycles, with 15-year shelf life, and < $100/KWh cost.

Project Impact. Project efforts are to contribute an in-depth understanding of the lithium interface and dendrite growth prevention to the field of Li-metal batteries, which will pave the way for eventual development of high-energy-density, low-cost, and long-lasting lithium batteries. This advancement could be a crucial selling point for the greater adoption of EVs. This project will make possible the translation of fundamental research into practical implementation of high-energy lithium anodes, enabling eventual achievement of cell performance targets.

Approach. The novelty of this approach is that the team intends to mitigate the dendrite problem by creating a dynamic protection layer during the interface shift to prevent dendrite formation throughout battery operation.

Out-Year Goals. The project has three out-year goals: (1) *in situ* diagnostic tools are fully functional; (2) potential candidates for Li-anode modifications are identified; and (3) synthesis routes are designed.

Collaborations. The PI is the Johnson Control Endowed Chair Professor, who has close and frequent collaboration with Johnson Controls' scientists and engineers. The collaboration enables the team to validate the outcomes of fundamental research in pilot-scale cells. The PI also has been working closely with top scientists at Argonne National Laboratory (ANL), Brookhaven National Laboratory (BNL), LBNL, and Pacific Northwest National Laboratory (PNNL) and with U. S. industrial collaborators, for example, GM, Millipore Sigma, and Clarios. In addition, the team works with international collaborators in China, Japan, and South Korea. These collaborations will be strengthened and expanded to give this project a vision with both today's state-of-the-art technology and tomorrow's technology in development, while incorporating feedback from the material designers and synthesizers upstream, as well as from the industrial end users downstream.

Milestones

1. Lithium anode electrochemical performance evaluation. Synthesis n-type polymer materials and evaluation of the electrochemical performance. (Q1, FY 2021; Completed)

2. Roll-press coating development. Complete the process development of roll-press coating. (Q2, FY 2021; Completed)

3. Polycyclic aromatic hydrocarbon (PAH) derivative structure identified. Identification of the synergy of the parameters and their impact on dendrite growth. (Q3, FY 2021; In progress)

4. Synthesis and test of PE with PAHs. Synthesis of PE with various PAH functionalities, and test with lithium anode in a half cell. (Q4, FY 2021; In progress)

5. Dendrite suppression demonstrated; interim cell performance verified. Dendrite suppression on coated lithium anode demonstrated, and analysis indicates technical approach capable of achieving performance targets. (Q4, FY 2021; In progress)

Progress Report

This quarter, the team successfully synthesized halide (Li_3YCl_6) SSE, creating a dynamic and self-limiting protective layer between lithium anode and halide SSE. The performance of the technology was demonstrated in a NCM-811/halide/Li (with protective layer) full cell. The cell displayed high initial CE of 87% and stable cycle life over 100 cycles (so far; still cycling).

The high oxidation stability of halide SEs allows use of commercial 4V-class $LiMO_2$ (M=Ni, Co, Mn, Al) cathodes without any protective coating layer. To investigate the full-cell performance, cathode composite was made by hand grinding LYCl SE, bare $LiNi_{0.8}Co_{0.1}Mn_{0.1}O_2$ (NCM-811) powder, and vapor grown carbon fiber (VGCF) powder at a weight ratio of 6:3:1. The charge/discharge voltage profiles of NCM-811/LYCl/Li full cell and NCM-811/LYCl/LPSCl/Li full cell are compared in Figure 26a-b. The current density is 0.1 mA cm^{-2}, and the loading of NMC-811 is 6 mg cm^{-2}. At the initial cycle, NCM-811/LYCl/Li full cell exhibited a high charging capacity of 255 mAh g^{-1} and a low CE of 65%. In the following cycles, the electrochemical polarization continuously increased. At the 12th cycle, the charging curve showed a long voltage plateau at 4.05 V and failed to reach the upper cut-off voltage of 4.3 V. This could be caused by continuous reaction between freshly deposited lithium and LYCl during delithiation process. By contrast, the NMC-811/ LYCl/LPSCl/Li full cell delivered a capacity of 181 mAh g^{-1} and 183 mAh g^{-1} for the first two cycles, with a CE of 87% and 98%, respectively (Figure 26b). As marked in the blue circle, no additional slope occurs prior to reaching the charge plateau, indicating no formation of space charge layer at the NCM-811/LYCl interface. Typical curves representing the three-phase transition process of NCM-811 material can be clearly observed from dQ/dV curves (inset, Figure 26b) and CV profiles (Figure 26c). The EIS evolution of full cell during one charge/discharge cycle (Figure 1d) validates high interfacial stability of both LYCl/NCM-811 interface and LPSCl/Li interface. The full cell displayed stable cycling with a capacity retention of 91 % and a high CE of 99.7 % after 100 cycles (Figure 26e). This work displayed one of the highest initial CEs and capacity retentions to date. Figure 26f displays that the rate capability and a reversible discharge capacity of 90 mAh g^{-1} were achieved at 1C rate.

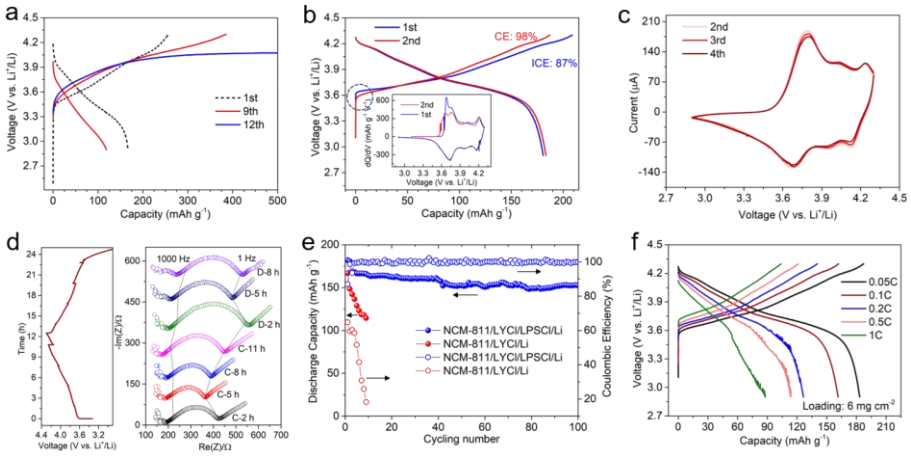

Figure 26. (a) Charge/discharge profiles of NCM-811/LYCl/Li cell at 0.1 mA cm^{-2}. Electrochemical performance of NCM-811/LYCl/LPSCl/Li cell: (b) initial two charge/discharge profiles at 0.1 mA cm^{-2} (corresponding dQ/dV curves shown in inset); (c) cyclic voltammetry profiles at 0.02 mV s^{-1}; (d) impedance evolution during one charge/discharge cycle, (e) cycling performance at 0.1 mA cm^{-2}, and (f) rate capability from 0.1 C to 1 C.

Patents/Publications/Presentations

The project has no patents, publications, or presentations to report this quarter.

Task 1.11 – Molecular Ionic Composites: A New Class of Polymer Electrolytes to Enable All-Solid-State and High-Voltage Lithium Batteries (Louis Madsen, Virginia Polytechnic Institute and State University)

Project Objective. Based on a newly discovered class of solid PE materials, that is, molecular ionic composites (MICs), the overall objective is to develop solid-state lithium conductors targeted for use in transportation applications. MICs form a mechanically stiff, electrochemically stable, and thermally stable matrix. Specific objectives include the following: (1) development of robust MIC electrolyte thin films (~ 20 µm) to serve as simultaneous nonflammable separators and dendrite-blocking Li^+ conductors, (2) electrochemical quantification of key performance metrics including electrolyte stability, interfacial reactions, and suitability/compatibility with a range of electrode materials, and (3) comprehensive investigation of ion transport mechanisms and electrode-electrolyte interfacial reactivity under practical operating conditions using NMR and synchrotron X-ray analyses.

Project Impact. Commercialization of Li-metal SSBs is hampered by lack of a functional nonflammable SE that can provide high ionic conductivity, wide electrochemical window, favorable mechanical properties to inhibit lithium dendritic growth, and low interfacial resistance. The tunable MIC materials platform has potential to fulfill these requirements with relatively simple fabrication techniques, and thus shows promise for enabling nonflammable SSBs that can be optimized for low cost and high energy density.

Approach. MICs rely on a unique polymer that is similar to Kevlar® in its strength, stiffness, and thermal stability, but with densely spaced ionic groups that serve to form an electrostatic network that permeates mobile ions in the MIC. The team can tailor the ion concentrations and types to yield MIC electrolyte films that are electrochemically compatible with Li-metal anode as well as a range of high-voltage layered cathodes. They are searching the composition space of lithium salts, electrochemically compatible ionic liquids (ILs), and polymer (PBDT) molecular weight to determine best composition windows for MIC electrolytes. The team is also investigating best methods for casting thin films in terms of temperature, solvent/evaporation conditions, and control over the initial liquid crystalline gel formation point. Concurrently, they are testing MIC films in various electrochemical cells, quantifying transport and structural/morphology parameters with NMR and X-ray techniques, and measuring key mechanical (dynamic mechanical thermal analysis, stress-strain) and thermal [DSC, thermal gravimetric analysis (TGA)] properties.

Out-Year Goals. This year, the team will further optimize the film casting process to obtain thin MIC electrolyte films, but will focus primarily on detailed electrochemical quantification of key performance metrics including electrolyte stability, interfacial reactions, and suitability/compatibility with a range of electrode materials (with the focus on lithium metal and layered oxides). The team will understand and optimize the oxidative stability and interfacial impedance properties of MIC electrolytes. The team will develop and characterize working battery cells incorporating MIC electrolyte films with various cathode and anode materials, and will work to understand fundamental material compositions and interfacial compatibilities to choose favorable combinations for safe SSBs with high energy density.

Collaborations. The team is collaborating with T. J. Dingemans' group at University of North Carolina, Chapel Hill, in which they are forming composites based on PBDT polymer and carbon materials such as graphene oxide, and are beginning to develop charged rigid-rod polymers building on the PBDT structure. The team is exploring shear rheology and broadband dielectric spectroscopy collaboration with R. H. Colby at Pennsylvania State University (PSU). They are collaborating with D. Nordlund at SLAC National Accelerator Laboratory (SLAC) to conduct synchrotron X-ray studies on MIC films.

Milestones

1. Determine optimal synthetic conditions, Li-ion loading, and chemical composition. (Q4, FY 2020 / Q1, FY 2021; In progress)
2. Determine parameter spaces for film formation, and develop design capable of meeting performance requirements for film casting process. (Q2, FY 2021; In progress)
3. Optimize oxidative stability by using NMC/MIC/NMC and Li/MIC/NMC cell platforms to determine the upper limit of cycling voltage. (Q3, FY 2021; In progress)
4. Optimize electrolyte chemistry to achieve minimal interfacial impedance. (Q4, FY 2021)
5. Initial full cell integration and performance evaluation with Li/MIC/NMC and cycling under high current density. (Q1, FY 2022)

Progress Report

This quarter, the team focused on (1) refining synthetic conditions and chemical compositions for fast Li^+ transport, (2) expanding parameter spaces for film formation, (3) developing advanced NMR characterizations to understand MIC film microstructure, and (4) exploring rigid-rod charge polymer (PBDT) as an electrode binder to possibly replace the ubiquitously used polymer PVDF.

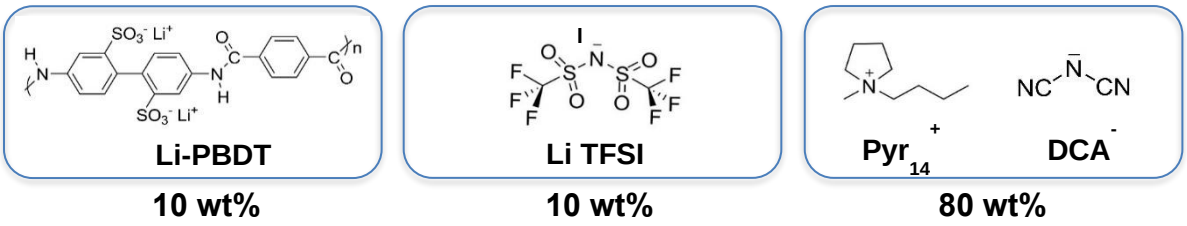

Figure 27. New example composition of molecular ionic composite electrolytes incorporating the DCA^- anion for faster Li^+ transport. The team is also working with the FSI^- anion and mixed systems to modulate morphology and phase segregation of different ions.

Figure 27 shows a new IL the team is incorporating into MIC electrolytes. This electrolyte composition forms a uniform film and exhibits an ionic conductivity of 1.0 mS/cm at room temperature, which is a factor of two higher than the previously optimized composition using 100% TFSI anions. Testing in Li|Li symmetric cells is ongoing. The team is also constructing membranes with $Pyr_{13}FSI$ IL and lithium bis(fluorosulfonyl) imide (LiFSI) salt, as discussed below.

The team has made another exciting discovery when attempting ion exchange after initial MIC formation. This ion exchange step provides an alternate to single-step film casting to enable a wider parameter space for ion type incorporation. When starting with MIC composed of PBDT and the IL C_2mimBF_4 and then ion exchanging by immersion in $Pyr_{13}FSI$ + LiFSI, a highly Li^+-dense nanocrystalline grain boundary (GB) phase condensed during the exchange process. The resulting materials, with structure depicted in Figure 28, show enhanced conductivity (> 1 mS/cm) and high Li^+ transference number (~ 0.5) while maintaining high elastic modulus (> 200 MPa) and non-flammability. The team has undertaken Li|Li symmetric cell cycling and a host of other tests, which are showing promising results for electrochemical stability and interfacial resistance.

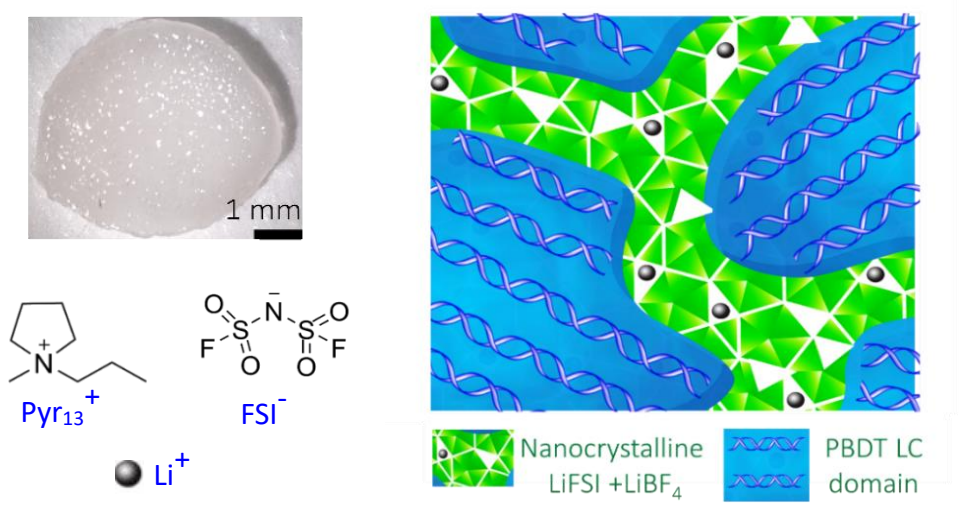

Figure 28. New molecular ionic composite membrane composition and internal structure. The image at upper left shows ion-exchanged electrolyte with iridescent appearance. At lower left are the chemical structures of new ions incorporated via ion exchange. The illustration at right shows liquid crystalline (LC) PBDT grains in blue, which provide a template for and scaffold to support the highly defective and conductive nanocrystalline phase containing LiFSI and $LiBF_4$. A publication has recently been accepted on this new material, with details of structure and transport characterized by solid-state nuclear magnetic resonance, X-ray diffraction, electrochemistry, electron microscopy, and Li|Li cell cycling.

Figure 29 shows two examples of the solid-state NMR (SSNMR) spectroscopy experiments employed to understand the new MIC/nanocrystal material presented in Figure 28. ^{7}Li SSNMR integration shows that all lithium is found in a single, locally anisotropic environment, in agreement with all Li^+ residing in the condensed nanocrystalline phase. ^{19}F SSNMR spectral integration and referencing with pure $LiBF_4^-$ and LiFSI spectra (not shown) allows assignment of anion environments/phases and quantification of relative abundances.

Beyond pure electrolyte development, the team has developed a protocol for incorporating PBDT as the polymeric binder for $LiFePO_4$ (LFP) cathodes. The team has found success with this system in that cycling efficiency and durability are comparable to the industry standard PVDF at comparable blend levels (3 wt%), and the PBDT system enables processing in water as opposed to using NMP, which is the solvent used for PVDF. Naturally, the water stability of a particular inorganic cathode type must be compatible with this, but some (as in the case below) will be. PBDT is simple to synthesize and should have a very low ultimate cost. The team is exploring this system by varying molecular weight and other polymer properties and processing parameters, and they are moving on to other cathode materials such as NMP- or LMO-based systems.

Figure 30 shows the electrochemical performance of the LFP electrodes examined using lithium metal as anode and a conventional LE (1 M LiBOB in EC-PC at 1:1 volume ratio) as electrolyte. When cycled at 0.2 C rate at room temperature, the specific discharge capacity of 3% PBDT-LFP closely approaches that of the 3% PVDF-LFP, reaching over 150 mAh/g at 22°C after a few initial cycles (Figure 30a). When cycled at 60°C and 0.2 C rate (Figure 30b), both 3% PBDT-LFP and 3% PVDF-LFP demonstrate a capacity of 160 mAh/g. This high capacity at low C rate suggests a high utilization efficiency of $LiFePO_4$ particles in the entire electrode, and thus a uniform and tight packing of the inorganic particles in the presence of binder.

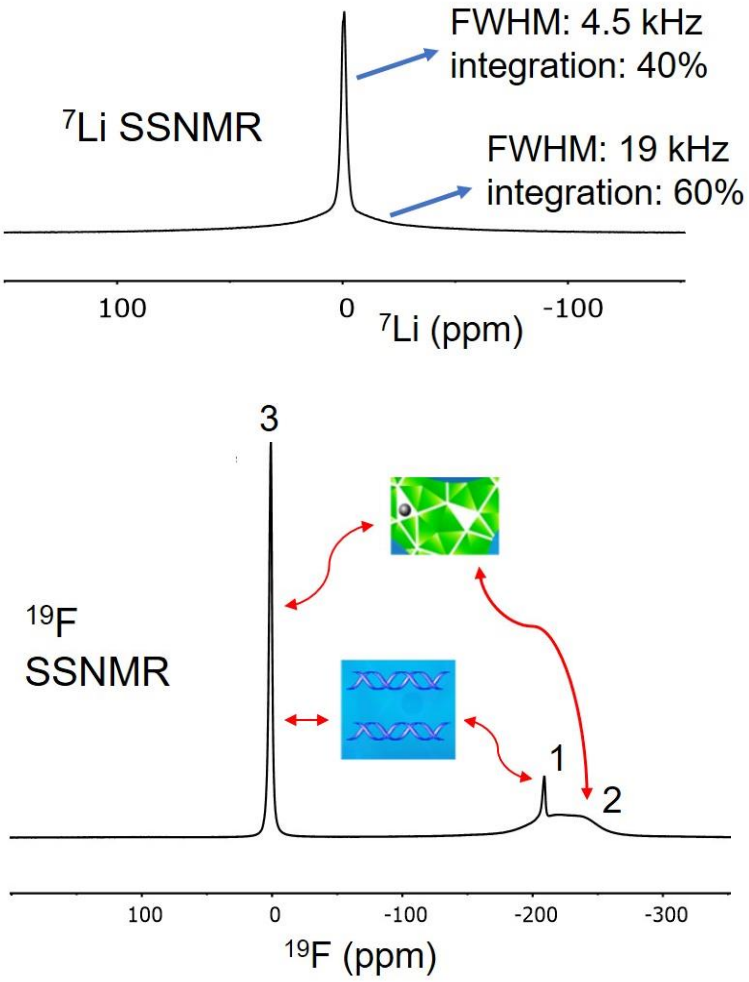

Figure 29. Solid-state ^{7}Li and ^{19}F nuclear magnetic resonance (NMR) of new molecular ionic composite (MIC)-nanocrystal system. (a) ^{7}Li solid-state NMR (SSNMR) showing that all lithium is found in a single, locally anisotropic environment. The narrow central peak arises from the central transition of the spin-3/2 ^{7}Li energy level structure. The broad peak originates from the NMR quadrupolar satellite transitions, and this peak shape arises from the superposition of an isotropic distribution of crystallite orientations. The 4:6 integration ratio of these two components confirms that only one type of environment for Li^{+} exists in this material, and the fact that the broad peak is observed confirms that the local environment is anisotropic, as expected for a nanocrystalline phase. (b) ^{19}F SSNMR identifying the different anions in the material (FSI^{-} and BF_4^{-}) and informing on their abundances and phase locations. Peak 1 is mobile BF_4^{-} found in the PBDT liquid crystalline (LC) phase. Peak 2 is solid-like BF_4^{-} found in the nanocrystalline grain boundary phase. Peak 3 is FSI- anion found in both phases, and is narrow due to the internal ^{19}F dynamics in this anion, even though ≈ 12% of each anion is in the LC phase and ≈ 88% in the nanocrystalline phase.

The specific capacity decreases with increasing cycling rate. At 22°C and 10 C rate, the specific discharge capacity of 3% PVDF-LFP and 3% PBDT-LFP is about 86 mAh/g and 73 mAh/g, respectively. The team attributes the modestly lower capacity retention of 3% PBDT-LFP as increasing C rate to the low electrolyte uptake of PBDT, which could potentially cause sluggish Li^{+} transport from the bulk electrolyte to the $LiFePO_4$ particle surface where it is covered by PBDT. As a result, during fast cell cycling the area of $LiFePO_4$ particles covered by PBDT is poorly lithiated/delithiated, which leads to the higher drop of reversible capacity. On the other hand, this suggests that the binding between PBDT and $LiFePO_4$ particles is tight. The team is exploring improved processing protocols and different molecular weight or other polymer modifications to improve this water-processable, mechanically strong, and ionically conductive PBDT binder.

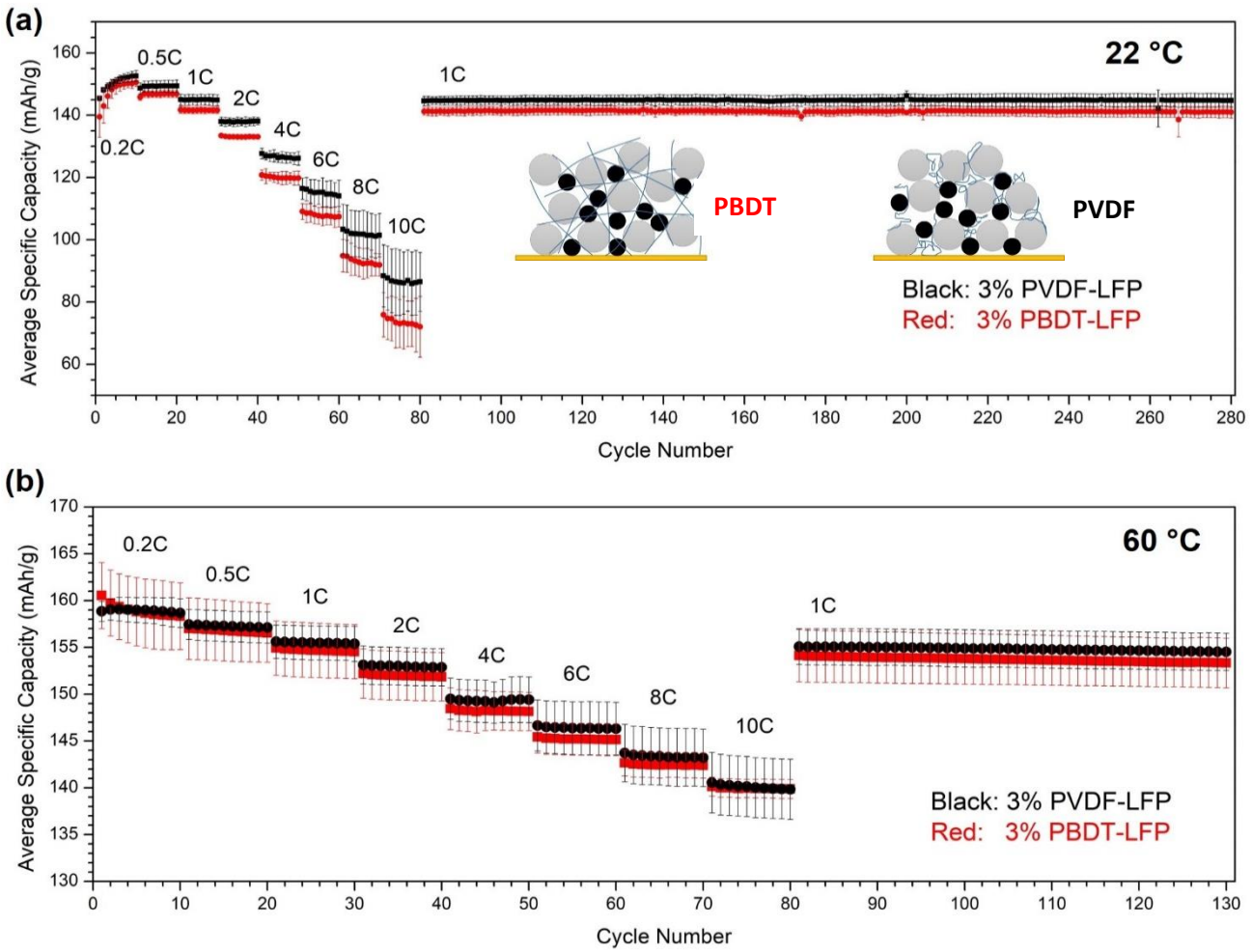

Figure 30. Specific discharge capacity of $LiFePO_4$ electrodes with PBDT and PVDF as binder at different C rates at 22°C (a) and 60°C (b). Each experiment is repeated 3 times, and error bars are shown for each cycle. The inset shows schematic illustrations of PBDT and PVDF conformations in electrodes. PBDT is a double helical rigid polymer with high aspect ratio enabling the possibility of combining multiple particles with the same double helix and more efficient utilization of the functional groups. PVDF is a soft-segmented polymer with a random coil conformation, which leads to low binding efficiency. PBDT can be processed in water, whereas PVDF is processed in NMP.

Patents/Publications/Presentations

Publication

- Yu, D., X. Pan, J. E. Bostwick, C. J. Zanelotti, L. Mu, R. H. Colby, F. Lin, and L. A. Madsen. "Room Temperature to 150°C Lithium Metal Batteries Enabled by a Rigid Molecular Ionic Composite Electrolyte." *Advanced Energy Materials* 11 (2021): 2003559.

Task 1.12 – All-Solid-State Batteries Enabled by Multifunctional Electrolyte Materials (Pu Zhang, Solid Power Inc.)

Project Objective. The project objective is to develop Li-metal SSBs enabled by multifunctional SSEs for EV application. The ultimate goal is scalable production of large-format ASSBs able to deliver ≥ 350 Wh/kg specific energy, ≥ 1000 cycle life, and ≤ $100/kWh cost.

Project Impact. The project impact is enabling scalable production of large format all-solid batteries required by the vehicle market and building domestic battery manufacturers as leaders in the global vehicle ASSB production. The proposed technology will address key limitations of state-of-the-art lithium batteries to meet DOE EV battery targets and accelerate their adoption as large-format EV batteries for sustainable transportation technology.

Approach. The project will develop a high-performance Li-metal solid-state cell enabled by a multifunctional SSE. The new SSE will (1) have high conductivity (up to 10 mS/cm), (2) be stable against lithium metal and high-voltage cathode (0-4.5 V), (3) promote uniform lithium plating (enabling > 2C charge rate), and (4) be compatible with large-scale manufacturing processes. The specific cell chemistry to be demonstrated will be the SSE with Li-metal anode and high-nickel-content Li-metal oxide cathode. The solid-state cell will be assembled by scalable roll-to-roll processes developed by Solid Power.

Out-Year Goals. In Year 1, multifunctional SSE will be developed with lithium ionic conductivity of ≥ 3 x 10^{-3} S/cm. CCD of ≥ 6 mA/cm^2 will be achieved in a symmetric lithium cell. The SSE design concept will be proven by demonstrating cycle life of ≥ 200 in a full cell. In Year 2, SSE material will be optimized with lithium ionic conductivity of ≥ 5 x 10^{-3} S/cm. Scalable cell assembly processes will be developed. Cycle life of ≥ 500 will be demonstrated in a full cell. In Year 3, large-format solid-state cells (> 2Ah) will be assembled/tested to meet the final goal: ≥ 350 Wh/kg, ≥ 1000 cycles, and ≤ $100/kWh cost.

Collaborations. The proposed team consists of Solid Power and a subcontractor, University of California, San Diego (UCSD). Solid Power (PI: P. Zhang) will develop the multifunctional SSE and other cell components, assemble cells, and conduct cell tests. UCSD (PI: Y. S. Meng) will carry out material characterization by using advanced techniques such as X-ray photoelectron spectroscopy (XPS), cryo – scanning transmission electron microscopy (cryo-STEM) imaging, cryo-STEM energy dispersive X-ray spectroscopy (EDX), electron energy loss spectroscopy (EELS), and cryo – focused ion beam (cryo-FIB) milling. The UCSD team seeks to quantify the kinetics and evolution of each contributing factor and its impact on battery performance.

Milestones

1. Charge rate ≥ 0.5C. (Q1, FY 2021; Completed)
2. Pouch cell capacity ≥ 200 mAh. (Q2, FY 2021; Completed)
3. SSE CCD ≥ 18 mA/cm^2. (Q3, FY 2021; In progress)

Progress Report

SSE Coating and 200-mAh Pouch Cell Assembly

The SSE separator coating process has been developed at pilot scale. A separator slurry was prepared by mixing the SSE powder, a binder, and a solvent by using an industrial mixer. The slurry was cast on a carrier film on a slot-die coater. The separator was then laminated to an NMC cathode to form a separator-cathode bi-layer, which was assembled into a solid-state cell by coupling a stand-alone Li-foil anode. In this quarter, large format double-layer-pouch cells at 200 mAh have been assembled and are being tested.

Figure 31 shows a coated separator by a roll-to-roll process (left) and a double-layer-pouch cell (right).

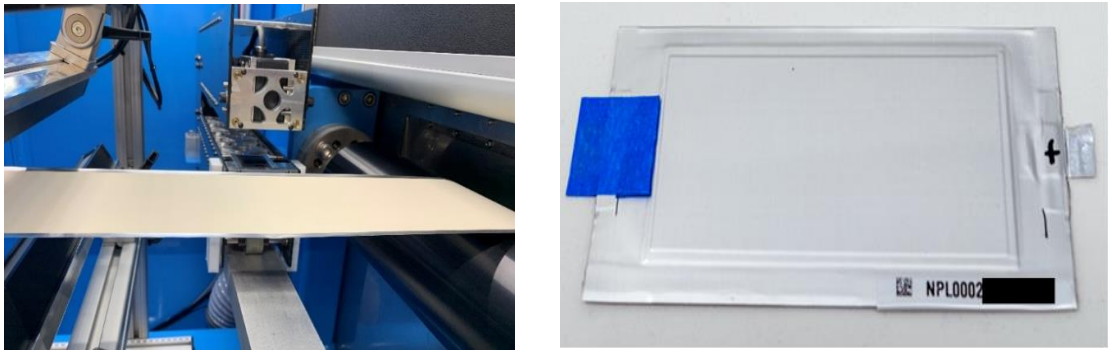

Figure 31. (left) Solid-state electrolyte separator coating on a slot die coater. (right) 200-mAh pouch cell.

Full Cell Demonstration

Having just started the 200-mAh cell evaluation, the team continued the cycle-life test of a lab-scale pouch cell. When tested at 2.8-4.2 V, C/5 – C/5, and ambient temperature (~ 25°C), the pouch cell showed 93% capacity retention after 220 cycles to date (Figure 32). It should be noted that capacity fluctuation was due to the ambient temperature change.

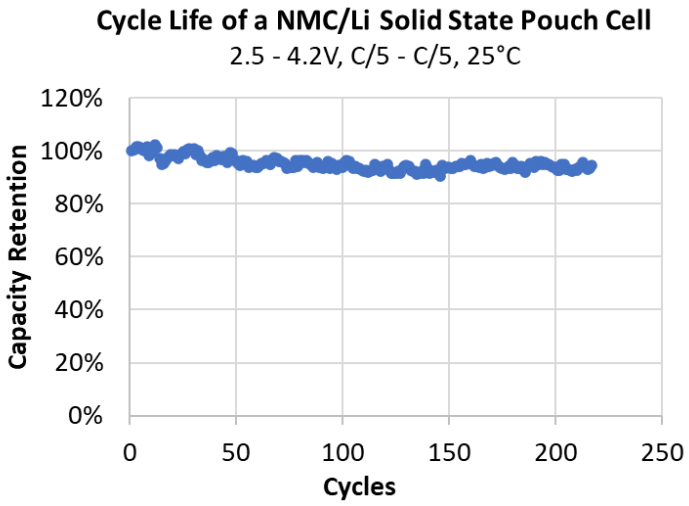

Figure 32. Cycle life of an NMC/Li-metal solid-state pouch cell with the multifunctional SSE at 25°C.

Patents/Publications/Presentations

The project has no patents, publications, or presentations to report this quarter.

Task 1.13 – Developing Materials for High-Energy-Density Solid-State Lithium-Sulfur Batteries (Donghai Wang, Pennsylvania State University)

Project Objective. The project objectives are to develop materials involving advanced S-C composite materials, solid additives, and sulfide-based SSEs, and to acquire knowledge for Li-S ASSBs. Li-S ASSBs with large areal sulfur loading (≥ 5 mg cm^{-2}) and high sulfur content (≥ 50 wt% in cathode), pairing with lithium or lithium alloy anode, will deliver a high initial specific capacity of over 1200 mAh g^{-1} at high charge/discharge rate (> 0.3 C) for 500 cycles with over 80% capacity retention.

Project Impact. This project aims to develop new materials to enable Li-S ASSBs with high energy density, excellent cycling stability, and good rate performance, and thus to build knowledge for fabrication of prototype Li-S ASSBs. Specifically, the developed new materials will greatly increase the specific capacity of sulfur and sulfur utilization at high areal sulfur loading, alleviate the interfacial problem between S-C composite and SSE within sulfur cathode, boost Li-ion conductivity, and improve moisture stability of glass and glass-ceramic sulfide-based SSE. Meeting the technical targets will potentially promote development of high-energy-density Li-S ASSBs and their practical application in EVs and plug-in hybrid EVs (PHEVs), and reduce petroleum consumption in the transportation sector by helping battery-powered vehicles become more accepted by consumers as a reliable source of transportation.

Approach. The project goal will be accomplished through developing new materials, together with in-depth characterization of sulfur cathode. Specifically, approaches to realize the project objectives include the following: (1) development of new carbon material with unique structure, high surface area, and large pore volume; (2) development of new S-C and S-C-M_xS_y materials (M = Li, Co, Ti, Mo, etc.) to facilitate electron/ion transport; (3) development of novel additives to tune interfacial behavior among components in the cathode; (4) development and optimization of new SSE through cation and anion doping with superior properties such as high ionic conductivity, good moisture, and stability; and (5) diagnostics, characterization, and cell tests on the developed new material or advanced sulfur cathode.

Out-Year Goals. The out-year goals are as follows: (1) develop new S-C-M_xS_y hybrid materials, new cathode additives, and anion-doped SEs (ionic conductivity above 3 mS cm^{-1} at room temperature), and (2) conduct characterization and performance tests on both material and electrode levels. The *Go/No-Go Decision* will be demonstration of all-solid-state sulfur cathode with over 1000 mAh g^{-1} discharge capacity at 0.1 C discharge rate and 50 wt% sulfur content for 100 cycles at room temperature.

Collaborations. There are no active collaborations.

Milestones

1. Demonstrate sulfur cathode with above 1000 mAh g^{-1} capacity at 0.2 C at 60°C. (Q1, FY 2021; Completed)
2. Demonstrate new anion-doped electrolyte with ionic conductivity > 2 mS cm^{-1} at 25°C, and sulfur cathode with > 1000 mAh g^{-1} using additives (≤ 3 wt%) at 0.3 C for 50 cycles. (Q2, FY 2021; Completed)
3. Demonstrate sulfur cathode with > 1000 mAh g^{-1} at 0.3 C for 50 cycles at 60°C using hybrid conductive materials. (Q3, FY 2021; In progress)
4. Demonstrate sulfur cathode with > 1000 mAh g^{-1} at 0.1 C for 100 cycles at room temperature, and anion-doped SEs with ionic conductivity > 3 mS cm^{-1} at 25°C. (Q4, FY 2021)

Progress Report

Synthesis of Anion-Doped SSE

Based on results collected last quarter, the Li_3PS_4-3$LiBH_4$ SSE has been successfully synthesized using a solution-based approach. This quarter, the team further optimized the molar ratios between Li_3PS_4 and $LiBH_4$ and the preparation conditions (time, procedures, etc.). To synthesize Li_3PS_4-x$LiBH_4$ SSEs, lithium sulfide (Li_2S), phosphorus pentasulfide (P_4S_{10}), and lithium borohydride ($LiBH_4$) were used as precursors. As a result, in addition to the previously synthesized Li_3PS_4-3$LiBH_4$, another two compositions (Composition 1 and Composition 2) were synthesized by varying the molar ratios of each precursor. A low annealing temperature of 160°C was employed. The ionic conductivities of the synthesized SSEs at different temperatures were measured by EIS using Al/SE/Al batteries (Figure 33a-b). The calculated ionic conductivities at different temperatures and corresponding EIS spectra are summarized in Figure 33c. At 25°C, the Composition 1, Composition 2, and Li_3PS_4-3$LiBH_4$ SSEs showed ionic conductivities of 1.22 mS cm^{-1}, 2.46 mS cm^{-1}, and 3.96 mS cm^{-1}, respectively. Among all compositions, Composition 2 SSE demonstrated the highest ionic conductivity with a low activation energy of 0.212 eV. The high ionic conductivities of Composition 1 and Composition 2 SSEs meet the targeted milestone for this quarter.

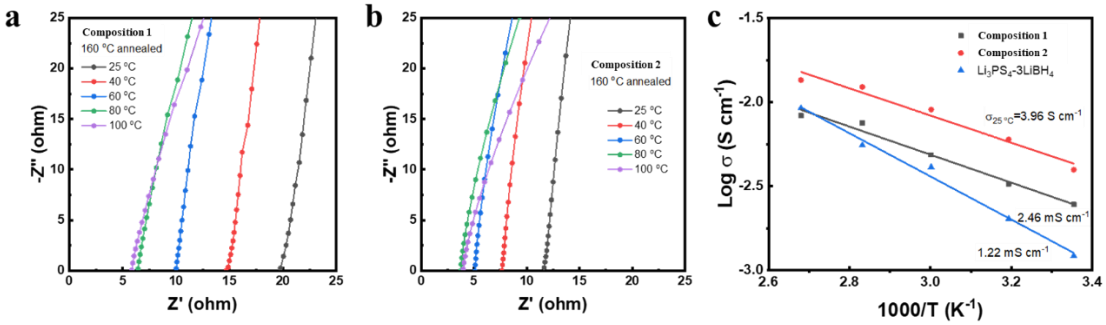

Figure 33. Electrochemical impedance spectra of the (a) Composition 1 and (b) Composition 2 solid-state electrolytes (SSEs). (c) Arrhenius conductivity plots for Composition 1, Composition 2, and Li_3PS_4-3$LiBH_4$ SSEs from 25°C to 100°C.

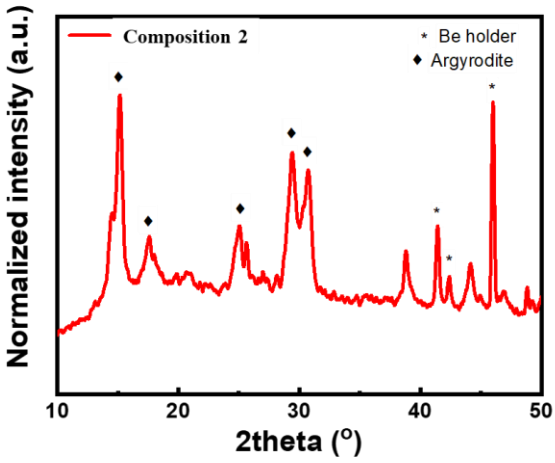

Figure 34. X-ray diffraction spectra of Composition 2 solid-state electrolyte.

Besides basic ionic conductivity measurement, the X-ray diffraction (XRD) pattern of Composition 2 SSE was examined, and the result is depicted in Figure 34. Characteristic peaks corresponding to Argyrodite structure were observed. Meanwhile, some unknown peaks with low intensity were noticed as well. These peaks probably represent impurities in the sample that are either residual precursors or side-reaction products. Further investigation and quantification are needed to determine the content and composition of the impurities. Additionally, SEM was employed to study the morphology of the Composition 2 SSE powders, as shown in Figure 35. Both a secondary electron image and a backscattered electron image were collected. Composition 2 SSE agglomerate with size of ~ 10 μm was observed. The orthorhombic morphology from β-Li_3PS_4 powders was partially maintained, while rod-like SSE particles aggregated and split the big particle. The team plans to further optimize the electrolyte compositions, preparation approach and conditions, annealing temperature, and other parameters. Meanwhile, other advanced characterization techniques like Raman and SSNMR spectroscopy will be used to obtain structural and morphological information of the prepared SSEs.

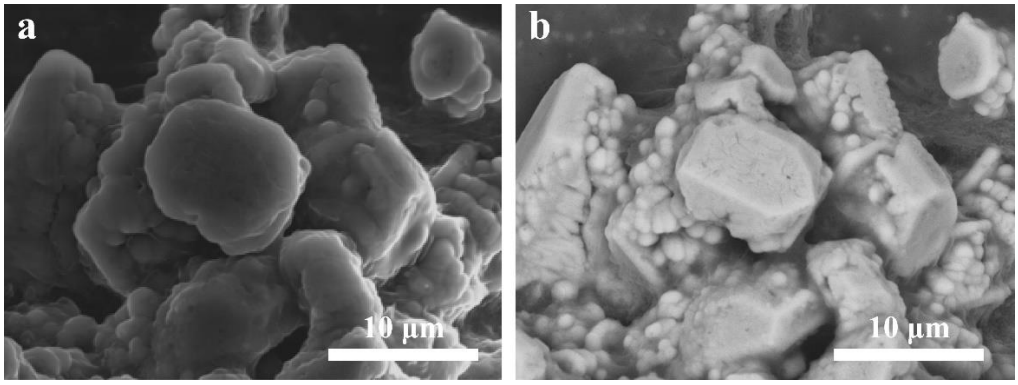

Figure 35. Scanning electron microscopy images of Composition 2 solid-state electrolyte powders. (a) Secondary electron image. (b) Backscattered electron image.

Synthesis of Anion-Doped SSE

This quarter, the team also continued research on electrochemically active molecules (EAMs) additives for Li-S ASSBs. Based on the sulfur cathode with high sulfur content of ~ 50 wt%, the team further decreased the additive amount to below 3 wt%, and cycling performance of the cell was tested at 0.3 C rate under CCCV mode at 60°C (Figure 36). The sulfur cathode with a sulfur loading of ~ 1.51 mg cm^{-2} demonstrated high initial discharge capacity of over 1400 mAh g^{-1}; after 50 cycles, the specific capacity still maintained above 1000 mAh g^{-1}. The superior cycling performance of sulfur cathode using EAM additives (< 3 wt%) met the targeted milestone for Q2. Moreover, to be noted, $75Li_2S{\cdot}25P_2S_5$ glass-type SSE with low ionic conductivity of ~ 0.4 mS cm^{-1} at 25°C was employed in both sulfur cathode and electrolyte membrane. Further improvement of cycling performance might be achieved by using another SSE with higher ionic conductivity. More work will be performed to further reduce the content of EAM additive as well as identify other types of EAM additives for Li-S ASSBs.

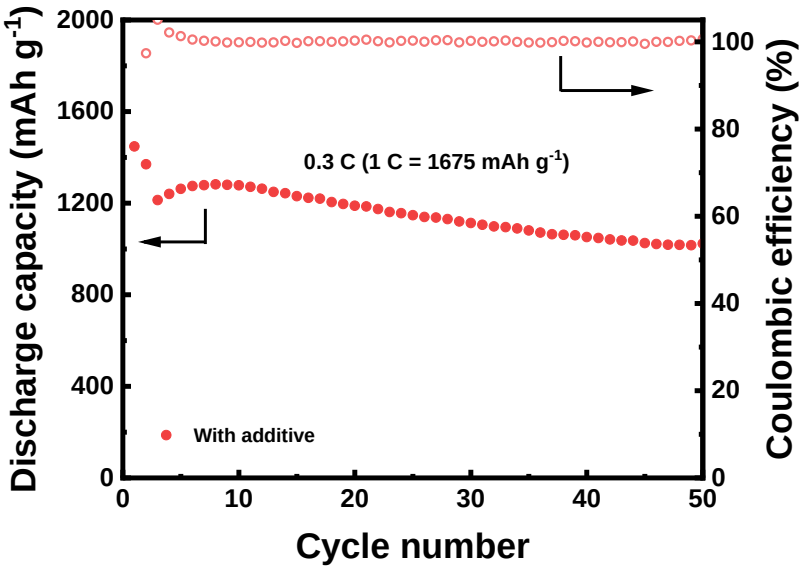

Figure 36. Cycling performance of Li-sulfur all-solid-state battery using electrochemically active molecules additive at 60°C.

Patents/Publications/Presentations

The project has no patents, publications, or presentations to report this quarter.

Task 1.14 – Hot Pressing of Reinforced Lithium-NMC All-Solid-State Batteries with Sulfide Glass Electrolyte
(Thomas Yersak, General Motors LLC)

Project Objective. The objective of this project is to research, develop, and test Li-NMC ASSBs capable of achieving program performance metrics by implementing sulfide glass SSEs and hot-press processing in a dry room environment. The performance of ASSBs with sulfide SSEs is limited because they are essentially green tapes with up to 20% porosity. In composite cathodes, the porosity limits energy density and power, while porosity in the separator acts as a conduit for Li-metal deposits if cycling conditions (that is, C-rate, operating temperature, and pressure) are not strictly controlled. The goal of the project is to demonstrate that the hot-pressing method and appropriately formulated sulfide glass SSEs can eliminate porosity to enable Li-NMC ASSBs with energy density of > 350 Wh/kg.

Project Impact. The hot-press processing method and appropriately formulated sulfide glass SSEs may enable Li-NMC ASSBs with improved energy density > 350 Wh/kg. The GM processing technology depends on heating a sulfide glass SSE above its glass transition temperature, T_g, at which point it can consolidate via viscoplastic flow. In the composite cathode, hot pressing provides liquid-like contact between the NMC cathode and SSE to increase energy density and power by enabling thick composite cathodes with high active material loading. Furthermore, cathode-supported sulfide glass separators can be made dense and thin by hot pressing. A dense separator enables the robust use of a Li-metal anode because lithium deposits may be more effectively blocked, preventing cell shorting.

Approach. The sulfide SSE used in the composite cathode, otherwise known as the catholyte, will dictate the processing specifications for ASSB hot pressing. Thermal stability can be achieved by NMC passivation and proper catholyte formulation. This project will systematically evaluate different NMC coatings, catholyte formulations, and hot-press processing specifications (that is, temperature, time, and pressure). The performance of hot-pressed ASSBs will be compared to green baseline ASSBs and hot-pressed control ASSBs consisting of the β-Li_3PS_4 and Li_6PS_5Cl model SSEs. Electron microscopy will be employed to understand interfacial phenomena and track composite cathode microstructure before and after hot pressing.

Out-Year Goals. In the second year of this project, a sulfide glass SSE will be formulated specifically for use as the separator. The separator glass SSE formulation will be designed to achieve full densification under the hot-press processing specifications determined for the catholyte. Separator glass formulation design will also consider cathodic stability, moisture stability, and ionic conductivity. Once a system of separator glass SSE and catholyte has been determined, the third year of the project will demonstrate hot-pressed full cells at the coin-cell and single-layer pouch-cell levels, which meets program target performance metrics.

Collaborations. GM will lead this project with no subrecipients.

Milestones

1. Establish protective coating on cathode: select best coating method and coating chemistry. Confirm conformality of coating using microscopy. (Q2, FY 2020; Completed)
2. Develop suitable baseline system with reversible capacity of ~ 120 mAh/g. (Q3, FY 2020; Completed)
3. Determine parameters required to prepare cathode samples via FIB/SEM lift-out and to analyze samples via high-resolution transmission electron microscopy (HRTEM). (Q2, FY 2021; Completed)
4. Demonstrate hot-pressed cathode with reversible capacity of 120 mAh/g. Analysis indicates technical approach capable of achieving performance targets. (Q3 FY 2021; In progress)

Progress Report

Work during this quarter and the preceding six-month, no-cost extension period focused on efforts to characterize the buried NCM/SSE interface in test cells assembled by hot pressing. The project's initial plan was to study this interface using HRTEM of samples prepared by the FIBSEM sample lift out technique as previously described.[1] However, SSE reactivity and beam damage slowed progress using this method. As an expedient alternative, the team implemented CV, DSC, and XPS to study the buried NCM/SSE interface. The resulting data show subtle differences between samples; however, the team suspects that electrode microstructure and changes in bulk SSE properties likely play larger roles in influencing performance of test cells assembled by hot pressing. Activities this quarter aimed to elucidate these principles.

To study the buried NCM/SSE interface, the team employed equipment at the UM Michigan Center for Materials Characterization, also known as $(MC)^2$. To study electrode microstructure, they used Xe ion plasma FIB (PFIB, Helios G4 UXe, Thermo Fisher Scientific). Figure 37a shows a picture of the PFIB at $(MC)^2$, and Figure 37b shows a micrograph of a composite cathode cross section, which can be processed using digital image analysis software to provide data on electrode microstructure (for example, porosity and heterogeneity). HRTEM samples were prepared (Figure 37d) by the lift out technique using a cryo-FIB (Helios 650, Thermo Fisher Scientific) and transferred to HRTEM using newly installed sample transfer hardware (Figure 37c). Cyro-HRTEM (Talos F200X, Thermo Fisher Scientific) was used to study the buried NCM/SSE interface. However, as shown in Figure 37e-f, the SSE was damaged by the electron beam despite cryogenic temperature (-170°C) and utilization of beam dose control (that is, modulating acceleration voltage between 200 kV and 80 kV).

In parallel with electron microscopy, the team also studied the buried NCM/SSE interface using DSC, CV, and XPS. Figure 38a shows the 1st cycle voltage profiles for cells with 7:3 (w/w) cathode composites of NCM85-10-5@$LiNbO_3$ and different SSE catholytes. These cells were assembled by hot pressing at 200°C for 10 minutes. The cell made with catholyte Candidate B delivered the best performance, with a discharge capacity of nearly 200 mAh/g, while the cell made with baseline β-Li_3PS_4 had a discharge capacity of only 55 mAh/g. The thermal stability of the cell made with catholyte Candidate B motivates work to characterize the buried NCM/SSE interface in search of principles that promote good thermal stability.

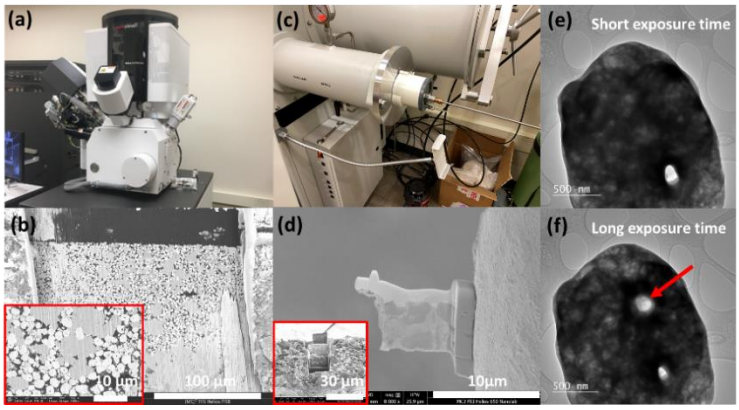

Figure 37. (a) Xe^+ plasma focused ion beam (PFIB) at the University of Michigan $(MC)^2$ user facility. (b) Composite cathode cross section successfully prepared with PFIB. (c) Sample transfer hardware installed at $(MC)^2$. (d) High-resolution transmission electron microscopy (HRTEM) sample prepared by cryo-FIB scanning electron microscopy lift-out technique. (e) HRTEM image of candidate B solid-state electrolyte after short exposure time. (f) HRTEM of candidate B after long exposure time.

DSC scans of the composites at a scan rate of 10 K/min do not yield appreciably different exothermic responses (Figure 38b). To learn more, the team used a variable heating rate approach to assess the energy of activation (E_a) for the reaction between the SSE and the NCM (full dataset not shown). They find from the Kissinger method that the E_a for β-Li_3PS_4/NCM is 242 kJ/mol, whereas for Candidate B/NCM it is closer to 260 kJ/mol and therefore anticipated to be marginally more stable at the 200°C pressing temperature. Partial integration of the reaction exotherm finds several slope changes in the % reaction completion versus temperature, which indicates that the full reaction between the SSEs and the NCM proceed through a complex reaction mechanism consisting of multiple steps, likely with intermediate phases.

Figure 38c presents CV data for different catholyte SSEs. Test cells were constructed with a working electrode consisting of a 9:1 (w/w) SSE and carbon black composite and a Li-metal counter electrode. Three metrics provide information on SSE stability, namely, onset voltage, peak anodic current, and the peak anodic voltage. The data suggest that catholyte Candidate B (red) has the best anodic stability among the SSEs tested since it has both the highest onset and peak anodic voltages. It is not clear that good anodic stability translates to good thermal stability. For this reason, XPS was used to study the buried NCM/SSE interface. In previous work, XPS was used to study the interface between charged NCM and sulfide SSE.[2] Here, the team shows that interfacial anodic SSE decomposition is similar to interfacial thermal SSE decomposition. They are the first to use XPS to study the thermal stability of the interface between NCM and sulfide SSE. In this experiment, composites of NCM and either β-Li_3PS_4, Candidate A, or Candidate B were fabricated by cold pressing or hot pressing at 200°C. Figure 39 depicts the S 2p transition for a composite of NCM and β-Li_3PS_4. The S 2p signal can be deconvoluted into two spin-orbit doublets corresponding to the P–S–Li (S 2p3 at binding energy of 161.1eV) and P=S (S 2p1 at binding energy of 162.3 eV); see Figure 39a. The deconvoluted peaks for the hot-pressed composite were slightly shifted by 0.5 eV toward higher binding energy (Figure 39b), which indicates that the β-Li_3PS_4 SSE was oxidized during the hot-pressing process. The spectra for the composites made with Candidate A and Candidate B catholyte (data not shown) are nearly identical to that of the β-Li_3PS_4 and previously reported data for charged NCM.[2]

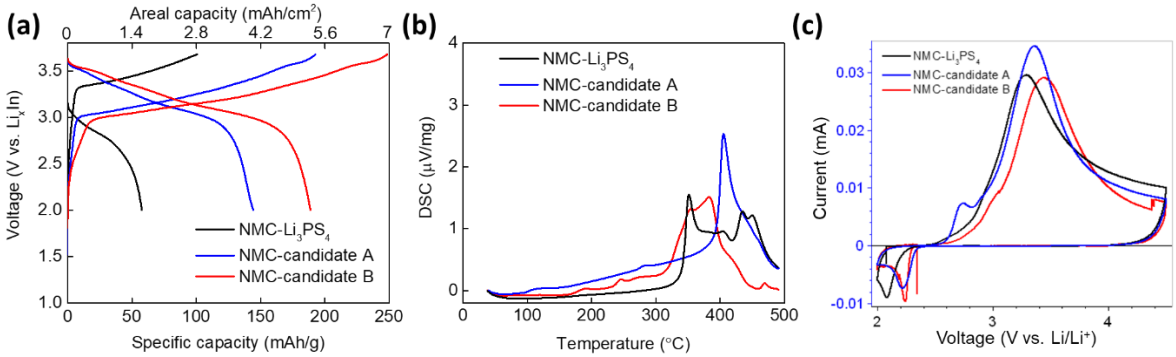

Figure 38. (a) 1st cycle voltage profiles for a variety of cells hot pressed at 200°C. In each case, the cathode is 40 mg of a 7:3 (w/w) composite of NCM@$LiNbO_3$ and solid-state electrolyte (SSE). (b) Differential scanning calorimetry scans for 7:3 (w/w) composites of NCM@$LiNbO_3$ and different SSEs. (c) Cyclic voltammetry scans for 9:1 (w/w) composites of catholyte candidates and carbon black.

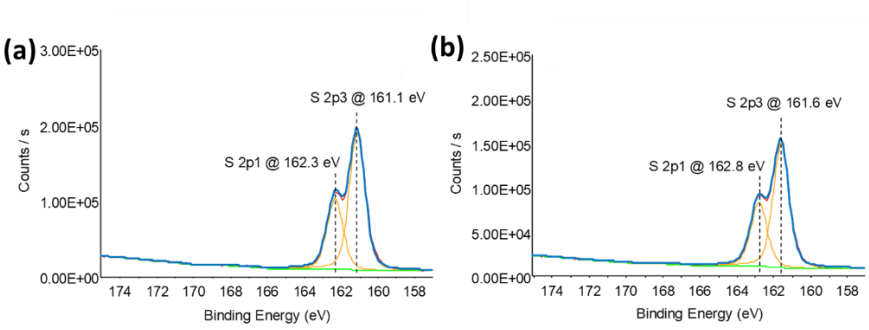

Figure 39. X-ray photoelectron spectra of the S 2p region and corresponding fits for composite NCM85-10-5/βLi_3PS_4 cathode fabricated by (a) cold pressing at 25°C and (b) hot pressing at 200°C.

References

[1] Woo, J. H., et al. *Journal of the Electrochemical Society* 159, No. 7 (2012): A1120–A1124.

[2] Tsukasaki, H., et al. *Journal of Power Sources* 367 (2017): 42–48.

Patents/Publications/Presentations

Patent

- Yersak, T. A., J. Salvador, C. Kang, and F. Hao. “Battery with Cathode-Supported Solid State Electrolyte Separator and Compliant Li Metal Interlayer.” P052492; U. S. patent application.

TASK 2 – DIAGNOSTICS

Team Lead: Guoying Chen, Lawrence Berkeley National Laboratory

Summary and Highlights

To meet the goals of the VTO programs on next-generation EVs, low-cost and abuse-tolerant batteries with higher energy density, higher power density, better safety, and longer lifetimes are needed. In pursuit of these goals, high cell operating voltages and demanding cycling conditions are used, which leads to unprecedented chemical and mechanical instabilities in cell components. Successful implementation of promising electrode materials (such as silicon anode and high-voltage cathodes) and new cell chemistry (such as high-energy Li-metal cells combined with SSEs) requires better understanding of fundamental processes, especially those at the interface/interphase of both anode and cathode. Identifying and understanding structure-property-electrochemical performance relationships in materials and various failure modes in cell chemistry are therefore more pressing than ever, not only in guiding battery development activities but also the scale-up efforts needed for commercialization.

Task 2 takes on these challenges by combining model systems, *ex situ*, *in situ*, and *operando* approaches, with an array of state-of-the-art analytical and computational tools. Numerous subtasks are tackling the chemical processes and reactions at the electrode/electrolyte interfaces in Li-metal batteries. Researchers at LBNL use surface- and bulk-sensitive techniques, including Fourier transform infrared (FTIR), attenuated total reflectance (ATR)-FTIR, near-field infrared (IR) and Raman spectroscopy/microscopy, and scanning probe microscopy (SPM) to characterize changes in materials and the physio-chemical phenomena occurring at the interface of Li-metal electrode. GM is developing *in situ* diagnostic techniques, including atomic force microscopy (AFM), nano-indentor, dilatometer, and stress-sensor, to be combined with atomic/continuum modeling schemes to investigate the coupled mechanical/chemical degradation of the SEI layer as well as the microstructural evolution at the interface/interphase of Li-metal anode. ANL aims to develop high-conductivity ceramic electrolytes through cation doping and to identify mechanistic barriers that limit chemical, mechanical, and electrochemical durability of solid/solid interfaces. University of Houston (UH) is developing multidimensional diagnostic tools, including FIB-SEM, time-of-flight secondary ion mass spectrometry (TOF-SIMS), and in-SEM nanoindentation, to probe structural, chemical, and mechanical evolution at the interfaces of SSLBs. At LBNL, model systems of electrode, SSE, and their interfaces with well-defined physical attributes are being developed and used for advanced diagnostic and mechanistic studies at both bulk and single-particle levels. These controlled studies remove the ambiguity in correlating a material's physical properties and reaction mechanisms to its performance and stability, which is critical for further optimization. Subtasks at BNL and PNNL focus on the understanding of fading mechanisms in electrode materials, with the help of synchrotron-based X-ray techniques (diffraction and hard/soft X-ray absorption) at BNL and HRTEM/STEM and related spectroscopy techniques at PNNL. The final subtask at Stanford/SLAC develops and utilizes an integrated X-ray characterization toolkit to investigate and generate insights on SSBs, by tracking the evolution of nanoscale chemistry as well as structure, microstructure, and transport properties. The diagnostics team not only produces a wealth of knowledge key to developing next-generation batteries, they also advance analytical techniques and instrumentation with a far-reaching effect on material and device development in various fields.

Highlights. The highlights for this quarter are as follows:

- The LBNL (R. Kostecki) group used *in situ* near-field FTIR nano-spectroscopy (nano-FTIR) to investigate the interfaces in a Li/LiTFSI-PEO/C (graphene) solid-state model cell. Their study revealed the amorphous mosaic structure of the SEI and established a new methodology in characterizing similar systems.

- The PNNL (C. Wang) group used cryo-HRTEM, EDX spectroscopy, and EELS techniques to characterize the structural and chemical distributions in the deposited lithium and SEI layer formed in different electrolytes. The correlations among nanostructure, chemistry of the SEI, and lithium morphology were established, providing guidance on the design of electrolyte chemistry toward dendrite-free Li-metal batteries.
- The ANL (Z. Chen) group experimentally demonstrated that lithium dendrite can grow from inside of dense LLZO pellets, suggesting that blocking electron conduction pathways is critical in solving the dendrite issue facing mixed conductors like LLZO.

Task 2.1 – Characterization and Modeling of Lithium-Metal Batteries: Model-System Synthesis and Advanced Characterization
(Guoying Chen, Lawrence Berkeley National Laboratory)

Project Objective. This project will use a rational, non-empirical approach to design and develop SSE materials and interfaces for next-generation Li-metal batteries. Combining a suite of advanced diagnostic techniques with carefully prepared model-system samples, the project will perform systematic studies to achieve the following goals: (1) obtain understanding on the role of SSE grain and GBs on ion conduction and dendrite formation, (2) obtain fundamental knowledge on rate- and stability-limiting properties and processes in SSEs when used in Li-metal batteries, (3) investigate the reactivities between SSE and electrodes, and gain insights on the dynamic evolution of the interfaces, and (4) design and synthesize improved SSE materials and interfaces for safer and more stable high-energy Li-metal batteries.

Impact. The project will focus on fundamental understanding of SSE and relevant interfaces to enable its use in Li-metal batteries. Knowledge gathered from model-system based studies will guide the design and engineering of advanced materials and interfaces. The use of the non-empirical, rational-design approach will develop high-energy battery systems with improved commercial viability.

Approach. The project will combine model-system synthesis and advanced diagnostic studies to investigate ion conduction and interfacial chemistry of SSE in Li-metal batteries. Single crystalline, polycrystalline, and amorphous model SSE samples with various grain and GB properties will be synthesized. Model interfaces between the SSE and electrodes with controlled properties will also be developed. Both bulk-level and single-grain level characterization will be performed. Global properties and performance of the samples will be established from the bulk analyses, while the single-grain-based studies will utilize time- and spatially-resolved analytical techniques to probe the intrinsic redox transformation processes and failure mechanisms under battery operating conditions.

Out-Year Goals. In the out-years, the project will deliver fundamental knowledge on the role of SSE microstructure in Li^+ conduction and lithium dendrite formation/propagation. Insights on performance-limiting physical properties and phase transition mechanisms as well as dynamic evolution of SSE/electrode interfaces will be obtained. Mitigating approaches, such as use of surface coating or "buffer layer" in stabilizing SSE/electrode interfaces, will be evaluated. Further, advanced SSE materials and interfaces for improved high-energy Li-metal batteries will be designed and synthesized.

Collaborations. This project collaborates with the following PIs: G. Ceder, K. Persson, M. Doeff, B. McCloskey, R. Kostecki, and R. Prasher (LBNL); W. Yang (Advanced Light Source, ALS); D. Nordlund and Y. Liu (Stanford Synchrotron Radiation Lightsource, SSRL); C. Wang (PNNL); and J. Nanda (Oak Ridge National Laboratory, ORNL).

`Milestones

1. Development of SSE/Li model interfaces for studying the reactivities and dendrite formation at the Li-metal anode interface. (Q1, FY 2021; Completed)
2. Synthesis of SSE model samples and model interfaces for studying reactivities and dendrite formation at Li-metal anode. (Q2, FY 2021; Completed)
3. Advanced diagnostic studies of SSE/Li-metal anode interfaces. (Q3, FY 2021; On schedule)
4. Obtain mechanistic understanding and deliver design strategies to mitigate reactivities at SSE/Li anode interface. (Q4, FY 2021; On schedule)

Progress Report

This quarter, the team prepared model interfaces of Li | Li_3InCl_6 (LIC) and Li | Li_3YCl_6 (LYC) to investigate the reactivities between lithium metal and halide SSEs. Figure 40a-b shows the SEM images of as-prepared LIC and LYC powder, respectively, synthesized after extensive ball milling at room temperature. The samples have a similar average particle size of several micrometers, although the LIC particles appear more fused than those of LYC. SSE pellets were prepared by cold sintering of ~ 80-100 mg of the halide powder, using an external pressure of 200 MPa at room temperature. Figure 40c-f shows SEM images of the planar (Figure 40c-d) and cross-sectional (Figure 40e-f) views of the pellets. The optical images are also shown in Figure 40c-d insets. Both pellets displayed an off-white color with relatively smooth and dense surfaces and cross sections. The overall thickness and dimeter were ~ 500 μm and 10 mm, respectively. The calculated densities were 2.22 and 2.44 g/cm^3, corresponding to a relative density of ~ 82% and 81% for LIC and LYC pellets, respectively. These values are similar to what was reported on other soft SSE pellets in the literature.

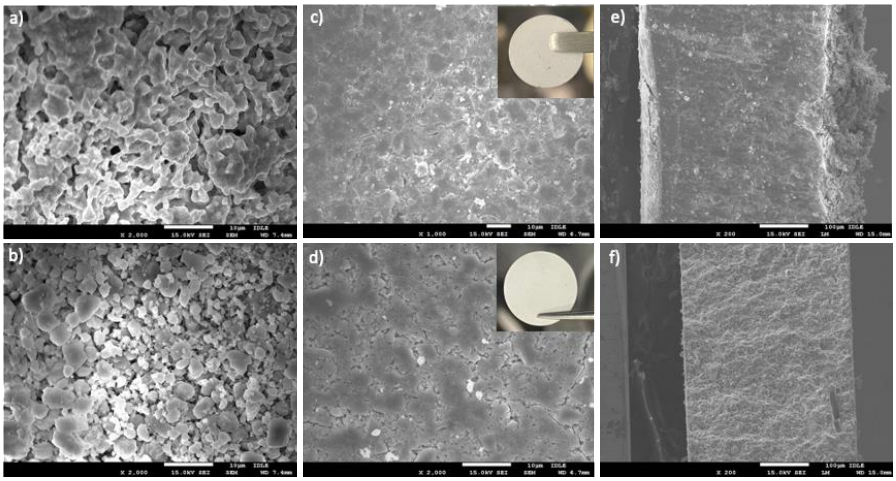

Figure 40. Scanning electron microscopy images of LIC (a/c/e) and LYC (b/d/f) solid electrolytes. (a/b) Powder samples. (c/d) Top-view and (e/f) cross-sectional view of the as-prepared pellets. Insets in (c/d) are optical images.

To investigate reactivities at the interface between lithium metal and the halide SSEs, intimate contact was achieved by pressing the prepared pellet together with a piece of lithium foil under an external pressure of 200 MPa. The assembly was then removed from the pressure jig and left inside the glovebox. After a varying amount of time, the SSE pellet was removed and analyzed by hard X-ray absorption spectroscopy (XAS). Figure 41 compares indium and yttrium K-edge X-ray absorption near-edge structure (XANES) spectra collected on the pristine and recovered LIC (Figure 41a) and LYC (Figure 41b) pellets after 2 and 30 days. The K-edge absorption energy, determined by the normalized intensity at 0.5, can be used to monitor the changes in metal chemical state. As shown in Figure 41a, the absorption edge energy for pristine LIC was at ~ 27.941 KeV, consistent with indium at 3^+ oxidation state. While the edge remained at the same energy after two days in

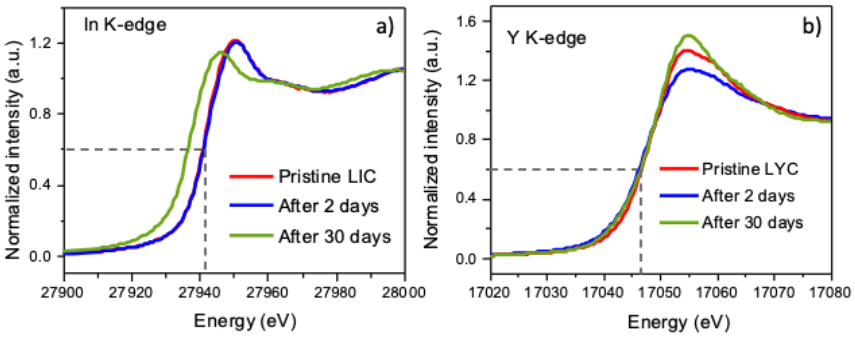

Figure 41. K-edge X-ray absorption near-edge structure spectra of (a) indium collected on LIC and (b) yttrium collected on LYC pellets.

contact with lithium metal, a significant low-energy shift occurred after 30 days, suggesting extensive reduction of indium after prolonged exposure to lithium metal. On the other hand, the yttrium *K*-edge energy in LYC remained unchanged at ~ 17.045 KeV, even after 30 days. These results confirm superior chemical stability of LYC against lithium metal. Future work will characterize cycling-induced chemical and structural changes at the SSE/Li-metal anode interface.

Patents/Publications/Presentations

Patent

- Ahn, J., D. Chen, and G. Chen. "A Method for Synthesizing High-Energy Lithium-Ion Battery Cathode Materials." U. S. Patent Application Serial No. 63/104,738.

Publications

- Chen, D., J. Ahn, and G. Chen. "An Overview of Cation-Disordered Lithium-Excess Rocksalt Cathodes." *ACS Energy Letters* 6 (2021): 1358–1376. doi: 10.1021/acsenergylett.1c00203.
- Chen, D., J. Ahn, E. Self, J. Nanda, and G. Chen. "Understanding Cation-Disordered Rocksalt Oxyfluoride Cathodes." *Journal of Materials Chemistry A* 9 (2021): 7826. doi: 10.1039/d0ta12179g.

Task 2.2 – Interfacial Processes – Diagnostics
(Robert Kostecki, Lawrence Berkeley National Laboratory)

Project Objective. The objective of the proposed research is to establish specific design rules toward the next generation of low impedance Li-metal rechargeable batteries that are capable of performing 1000 deep discharge cycles at CE > 99.9% and suppressing lithium dendrite formation at high current densities (> 2 mA/cm^2). This project aims at the following: (1) establishing general rules between Li^+ transport properties in novel liquid/solid electrolytes, and (2) determining the mechanism of the SEI layer (re)formation. The other goal is development and application of far- and near-field optical probes and synchrotron-based advanced X-ray techniques to obtain insight into the mechanism of Li^+ transport and interfacial reactions in lithium/liquid model systems. Through an integrated synthesis, characterization, and electrochemistry effort, this project aims to develop a better understanding of lithium/LE interface so that rational decisions can be made as to their further development into commercially viable Li-metal cells.

Project Impact. Chemical instability and high impedance at the interface of Li-metal electrodes limits electrochemical performance of high-energy-density batteries. A better understanding of the underlying principles that govern these phenomena is inextricably linked with successful implementation of high-energy-density materials in Li-metal-based cells for PHEVs and EVs. New state-of-the-art techniques to identify, characterize, and monitor changes in materials structure and composition that take place during battery operation and/or storage will be developed and made available to the Program participants. The proposed work constitutes an integral part of the concerted effort within the BMR Program, and it supports development of new electrode materials for high-energy, Li-metal-based rechargeable cells.

Approach. The pristine and cycled composite electrode and model thin-film electrodes will be probed using various surface- and bulk-sensitive techniques, including FTIR, ATR-FTIR, near-field IR and Raman spectroscopy/microscopy, and SPM to identify and characterize changes in materials structure and composition. Novel *in situ / ex situ* far- and near-field optical multi-functional probes in combination with standard electrochemical and analytical techniques are developed to unveil the structure and reactivity at interfaces and interphases that determine materials electrochemical performance and failure modes.

Out-Year Goals. In the out-years, the project aims to achieve the following: (1) understand factors that control performance and degradation processes, (2) unveil structure and reactivity at hidden or buried interfaces and interphases that determine electrochemical performance and failure modes, and (3) propose effective remedies to address inadequate Li-metal-based battery calendar/cycle lifetimes for PHEV and EV applications.

Collaborations. The diagnostic studies will be carried out in sync with other diagnosticians (G. Chen, B. McCloskey, R. Prasher, and L-W. Wang) and theory and computational scientists (G. Ceder and K. Persson).

Milestones

1. Acquire near-field spectra from graphene/SEI. (Q1, FY 2021; Completed)
2. Determine composition of SEI on lithium via *in situ* near field FTIR measurements. (Q2, FY 2021; Completed)
3. Complete preliminary near-field FTIR and XPS investigations of surface reactivity of lithium in LE and SE. (Q3, FY 2021; In progress)
4. Develop a valid mechanism for non-uniform current distribution on lithium/electrolyte interface. (Q4, FY 2021; In progress)

Progress Report

This quarter, the team continued to characterize *in situ* interfaces in a model Li/LiTFSI-PEO/C (graphene) solid-state model battery cell during electrochemical cycling by near-field nano-FTIR in a nitrogen-filled glovebox. As a reminder, a monolayer graphene sheet was used as a working electrode and optical window for nano-FTIR probe characterization. After the lithium plating process, morphological and chemical changes at the graphene/Li-electrolyte (SSE) interface were probed through the graphene window at nanoscale resolution. The dry nitrogen atmosphere prohibited any interference from oxygen and moisture and allowed the team to obtain high-quality nano-FTIR spectra.

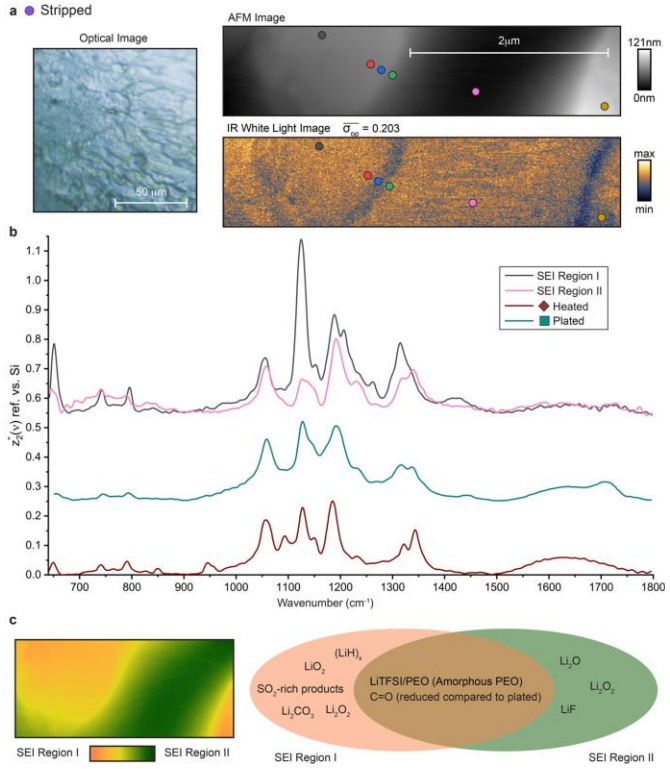

Figure 42. Characterization of the SEI at the graphene SEI post lithium stripping. (a) Optical microscopy (left), atomic force microscopy (top right), and s-SNOM WLI (bottom right) results. Overlaid circles indicate the spatial locations where nano Fourier transform infrared spectroscopy (nano-FTIR) spectra were acquired. (b) Nano-FTIR spectra of SEI region I (gray) and SEI region II (pink) post stripping. Also shown are the averaged nano-FTIR spectra collected at the graphene / solid-state electrolyte interface post heating (maroon) and post plating (green). (c) False color map qualitatively visualizing how the chemistry transitions in space from region I to region II (right hand side). (d) Venn diagram summarizing key similarities and differences between the two predominate SEI regions.

The optical image of the stripped interface shown in Figure 42a shows less variations in both color contrast and apparent topographic roughness when compared to the optical image of the plated interface. It is also apparent post stripping that spatial locations previously hosting tendril-like Li-metal deposits have become an interconnected collection of depressions. This is verified with the AFM results displayed in the top right of Figure 42a, where clear contrasts between depressed regions and higher regions are found. The nano-resolved IR WLI (Figure 42a, bottom right) is notably more uniform than the plated interface, possessing an optical roughness $\overline{\sigma_{op}}$ of 0.203, which is a reduction of 41.8% in comparison to the plated case. This indicates that although the two SEI regions are very different topographically, both still have somewhat similar infrared reflectivity / electronic conductivity. Additionally, from an empirical perspective, it is extremely relevant that electrochemical stripping protocols have removed all metallic lithium that had been plating at the interface.

The team finds that the SEI is an amorphous mosaic structure comprised of two predominate mesoscopic components/regions (while the bulk retains its original degree of crystallinity). The first region has inferior ionic conductivity and has a large amount of decomposition products such as Li_2CO_3, Li_2O_2, and SO_2-rich species, and, especially, lithium hydrides, which consume active components and contribute to lower CE and capacity fading. The second region supports reversible lithium transport and has quite similar absorption spectra to the pristine interface, apart from being amorphous, and possibly hosting slight amounts of LiF, LiO_2, and Li_2O. This region has a relatively high ionic conductivity that enables and influences the formation of electro-plated/stripped lithium micro morphologies, and may support Li-dendrite structures over many cycles. Ultimately this study unveils important basic scientific information about solid solid-electrolyte interfaces (and supported SEIs) that were previously inaccessible to the scientific community, and the methodologies used herein demonstrate a promising, pioneering pathway for the research community to investigate other systems comprised of other electrode materials, LEs, and metal batteries. This completes this quarter's milestone.

Patents/Publications/Presentations

The project has no patents, publications, or presentations to report this quarter.

Task 2.3 – Advanced *In Situ* Diagnostic Techniques for Battery Materials (Xiao-Qing Yang and Enyuan Hu, Brookhaven National Laboratory)

Project Objective. The primary objective of this project is to develop new advanced *in situ* material characterization techniques and to apply these techniques to support development of new cathode and anode materials with high energy and power density, low cost, good abuse tolerance, and long calendar and cycle life for beyond Li-ion battery systems to power PHEVs and battery electric vehicles (BEVs). The diagnostic studies will focus on issues relating to capacity retention, thermal stability, cycle life, and rate capability of beyond Li-ion battery systems.

Project Impact. The VTO Multi-Year Program Plan describes the goals for battery: "Specifically, lower-cost, abuse-tolerant batteries with higher energy density, higher power, better low-temperature operation, and longer lifetimes are needed for development of the next-generation of HEVs [hybrid electric vehicles], PHEVs, and EVs." The results of this project will be used for development of technologies that will significantly increase energy density and cycle life, and reduce cost. This will greatly accelerate deployment of EVs and reduce carbon emission associated with fossil fuel consumption.

Approach. This project will use a combination of synchrotron XRD and pair distribution function (x-PDF) and of neutron diffraction (ND) and pair distribution function (n-PDF); x-ray spectroscopies including hard/soft XAS, X-ray photon emission spectroscopy (PES); and imaging techniques including X-ray fluorescence (XRF) microscopy, transmission X-ray microscopy (TXM), and transmission electron microscopy (TEM).

Out-Year Goals. The out-year goals are to develop spectro-tomography, XRD, XAS, and PDF techniques and apply these techniques on Li-ion battery cathode, Na-ion battery cathode, and SSE.

Collaborations. The BNL team will work closely with material synthesis groups at ANL (Y. Shin and K. Amine) for the high-energy composite, at PNNL for the S-based cathode and Li-metal anode materials, and with ORNL on neutron scatterings. This project will also collaborate with industrial partners at GM and Johnson Controls, as well as with international collaborators.

Milestones

1. Complete 3D spectro-tomography studies of Li-rich layered material $Li_{1.2}Ni_{0.13}Mn_{0.54}Co_{0.13}O_2$ at various states of charge (SOC). (Q1, FY 2021; Completed)
2. Complete XRD, PDF analysis, and XAS studies of single-crystal sodium cathode material $Na_xNi_{0.76}Mn_{0.14}Co_{0.1}O_2$. (Q2, FY 2021; Completed)
3. Complete XRD/x-PDF/XAS studies of O3-type Na-cathode material $Na_xLi_{1.2-y}Mn_{0.54}Ni_{0.13}Co_{0.13}O_2$. (Q3, FY 2021; In progress)
4. Complete sulfur and phosphorus XAS studies of SSE $Li_{10}GeP_2S_{12}$ from various SOCs during the 1st cycle. (Q4, FY 2021; In progress)

Progress Report

This quarter, the second milestone was completed, and progress on other milestones was made. BNL has been focused on developing new diagnostic techniques to study and improve performance of high-energy-density Li-ion batteries. Developing single-crystal cathode material is one efficient strategy to suppress the anisotropic volume changes during ion extraction/insertion that make the materials intrinsically vulnerable to GB (inter-granular) fracture leading to rapid impedance increase and capacity decay. Scientists at PNNL led by P. Le used single crystal $LiNi_{0.76}Mn_{0.14}Co_{0.1}O_2$ (NMC-7611) to synthesize the analogue Na-ion cathode material $Na_zNi_{0.76}Mn_{0.24}Co_{0.1}O_2$ (Na_zNMC) by inserting sodium into delithiated phase of Li_yNMC. The micro-sized single-crystal Ni-rich sodium layered oxide Na_zNMC was obtained. In collaboration with PNNL scientists, the BNL team carried out characterization studies on the structural evolution of this material using synchrotron-based X-ray absorption techniques during the first sodiation and after multiple cycles. Results of *ex situ* XAS including XANES and extended X-ray absorption fine structure (EXAFS) for delithiated NMC-7611 and sodiation Na_xNMC-6711 after initial discharge (sodiation) and 10th cycle are shown in Figure 43. As shown in Figure 43a, Ni^{3+} is oxidized to Ni^{4+} after delithiation, and the 1st sodiation reduces nickel back to Ni^3; manganese and cobalt show little spectra changes. Figure 43b shows the *ex situ* EXAFS data of NMC-7611 cathode. In all cases, the EXAFS of nickel, manganese, and cobalt has shifts from delithiation state to sodiation state, suggesting the change of bond lengths between TM cation and their neighboring atoms. Quantitative local structural features are obtained through fitting the Fourier transformed EXAFS data against the layered model structure, with the results shown in Figure 43c indicating that the bond lengths between TMs and oxygen increase from delithiation to sodiation. Such change is obvious for nickel. The Debye-Waller (D W) factor for the TM—TM/Li/Na scattering path generally increases from delithiation to sodiation, suggesting that introducing sodium into an originally Li-based structure induces some local structural disorder. On cycling, such disorder may be relaxed, as seen from the decreased D-W factor from the 1st cycle to the 10th cycle.

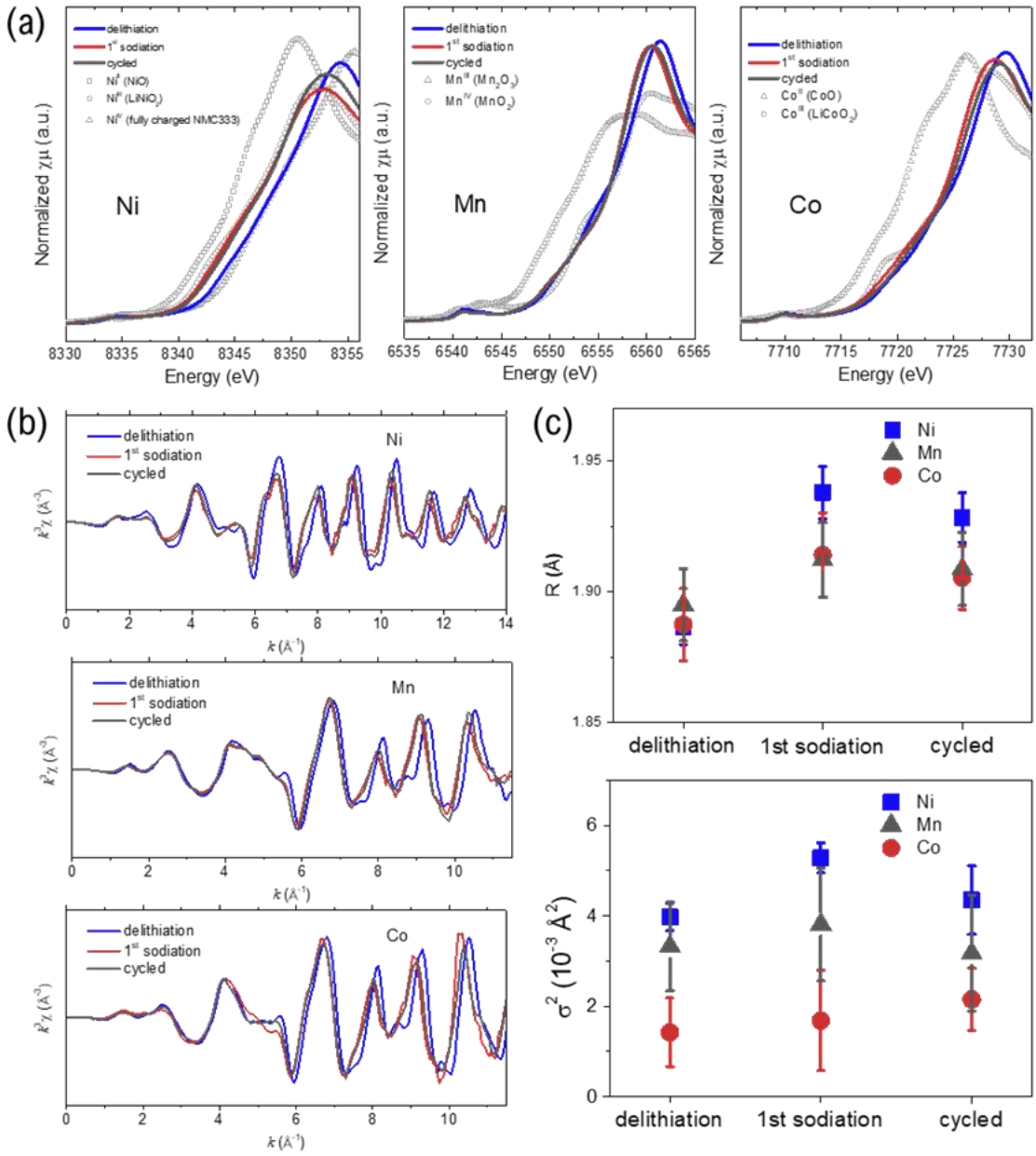

Figure 43. (a) X-ray absorption near-edge structure and (b) extended X-ray absorption fine structure spectra of delithiated NMC-7611 and sodiation Na_xNMC-6711 for initial discharge (sodiation) and 10th cycle. (c) Fitted local structural information including TM-O bond length (upper panel) and TM-TM/Li/Na disorder reflected by the Debye-Waller (D-W) factor (lower panel).

Patents/Publications/Presentations

Publications

- Zhang, J., Q. Wang, S. Li, Z. Jiang, S. Tan, X. Wang, K. Zhang, Q. Yuan, S-J. Lee, C. J. Titus, K. D. Irwin, D. Nordlund, J-S. Lee, P. Pianetta, X. Yu, X. Xiao, X-Q. Yang, E. Hu,* and Y. Liu.* "Depth-Dependent Valence Stratification Driven by Oxygen Redox in Lithium-Rich Layered Oxide." *Nature Communications* 11, No. 6342 (2020). doi: 10.1038/s41467-020-20198-w; Publication Date (Web): December 11, 2020. [Note: This paper was published in Q1 of FY 2021, but not included in that quarter's report.]
- Hu, J., Q. Wang, B. Wu, S. Tan, Z. Shadike, Y. Bi, M. S. Whittingham, J. Xiao,* X-Q. Yang,* and E. Hu.* "Fundamental Linkage Between Structure, Electrochemical Properties, and Chemical Compositions of $LiNi_{1-x-y}Mn_xCo_yO_2$ Cathode Materials." *ACS Applied Materials & Interfaces* 13, No. 2 (2021): 2622–2629. doi: 10.1021/acsami.0c18942; Publication Date (Web): January 7, 2021.
- Shadike, Z., H. Lee, O. Borodin, X. Cao, X. Fan, X. Wang, R. Lin, S-M. Bak, S. Ghose, K. Xu, C. Wang, J. Liu, J. Xiao,* X-Q. Yang,* and E. Hu.* "Identification of LiH and Nanocrystalline LiF in the Solid–Electrolyte Interphase of Lithium Metal Anodes." *Nature Nanotechnology* 16 (2021): 549–554. doi: 10.1038/s41565-020-00845-5; Publication Date (Web): January 28, 2021.
- Hu, E., Q. Li, X. Wang, F. Meng, J. Liu, J-N. Zhang, K. Page, W. Xu, L. Gu, R. Xiao, H. Li, X. Huang, L. Chen, W. Yang,* X. Yu,* and X-Q. Yang.* "Oxygen-Redox Reactions in $LiCoO_2$ Cathode without O-O Bonding during Charge-Discharge." *Joule* 5, No. 3 (2021): 720-736. doi: 10.1016/j.joule.2021.01.006; Publication Date (Web): March 17, 2021.

Task 2.4 – Probing Interfacial Processes Controlled Electrode Stability in Rechargeable Batteries (Chongmin Wang, Pacific Northwest National Laboratory)

Project Objective. The main objective is to explore interfacial phenomena in rechargeable Li-ion batteries of both solid-state and LE configuration, to identify the critical parameters that control the stability of interface and electrodes as well as SE. The outcome will be establishing correlations between structural-chemical evolution of active components of batteries and their properties. These correlations will provide insight and guidance to battery materials development groups for developing high-performance battery materials.

Project Impact. The proposed characterization work focuses on atomic-level structural and chemical analysis and direct correlation with battery fading properties. The work can be directly used to guide design of electrode materials with tailored microstructure and chemistry for enhanced properties of increasing the energy density of Li-ion batteries and to accelerate market acceptance of EVs, especially for PHEVs as required by the EV Everywhere Grand Challenge.

Approach. The project will use integrated advanced microscopic and spectroscopic techniques, including *in situ* S/TEM and *ex situ* S/TEM, environmental S/TEM, cryo-electron microscopy, and *in situ* liquid SIMS to directly probe the structural and chemical information during lithium deposition and stripping. Cryo-S/TEM with analytical tools, such as EDX and EELS, will be used to gain chemical and electronic structural information at the interface between lithium metal and electrolyte of both solid-state and liquid configuration, which will allow direct correlation between the morphology and chemistry. STEM – high-angle annular dark-field (HAADF) atomic-level imaging and EDX/EELS will be used to probe the interface and bulk lattice stability of cathode and SE in SSB. The work will be in close collaboration with the battery development group within the BMR and U. S.–Germany Collaboration on Energy Storage.

Out-Year-Goals. This project has the following out-year goals:

- Atomic-level multi-scale *ex situ* / *in situ* and *operando* S/TEM and cryo-S/TEM investigation on the fading mechanisms of energy-storage materials and devices in the system of both LE and SE; develop a fundamental understanding of electrochemical energy-storage processes and kinetics of electrodes.
- Develop new *in situ* and *ex situ* S/TEM capability for probing challenging questions related to energy storage technology for both solid-state and LE energy storage system.

Collaborations. This project collaborates with G. Chen (LBNL); J. Nanda (ORNL); Y. Yao (UH); K. Amine (ANL); D. Wang (PSU); A. Manthiram (University of Texas, or UT, Austin); W. Tong (LBNL); Y. Cui (Stanford University); J. Zhang (PNNL); J. Liu (PNNL); W. Xu (PNNL); X. Jie (PNNL); D. Lu (PNNL); X. Xiao (GM); Y. S. Meng (UCSD); and M. S. Whittingham (State University of New York, Binghamton].

Milestones

1. Measure the electronic properties of SEI layer and identify their dependence on the electrolyte chemistry. (Q1, FY 2021; Completed)
2. Identify the structure and chemistry of surface layer formed on lithium metal when it contacts with LE. (Q2, FY 2021; Completed)
3. Reveal the nature of reaction product and the fading mechanism of NMC cathode when in contact with SE. (Q3, FY 2021)
4. Identify the structural and chemical difference of SEI on lithium dendrite and spherical particle to gain the correlation between SEI and lithium morphology. (Q4, FY 2021)

Progress Report

Lithium metal is recognized as one of the most promising anode materials owing to its ultrahigh theoretical specific capacity and low electrochemical potential. Nonetheless, dendritic lithium growth has dramatically hindered the practical applications of Li-metal anodes. The dendritic lithium metal could penetrate through the separator, resulting in internal short-circuit of the battery. Further, the high surface area of lithium dendrite will significantly elevate the side reactions between metallic lithium and electrolyte, thus leading to fast capacity fading and short cycle life. Formation of spherical lithium morphology is an effective approach to avoid lithium dendrite growth. However, the mechanism governing the lithium deposition morphology is unknown. Here, the team explores the correlation of structural, chemical, and electronic composition of SEI on electrochemically deposited lithium metal (EDLi) with their morphologies.

The team uses cryo-HRTEM, EDX, and EELS techniques to systematically characterize the detailed structure and chemical distribution of EDLi and SEI layers formed in different electrolytes but with the same deposition conditions, intending to establish correlation between structure and chemical composition of SEI and lithium morphologies, as schematically shown in Figure 44.

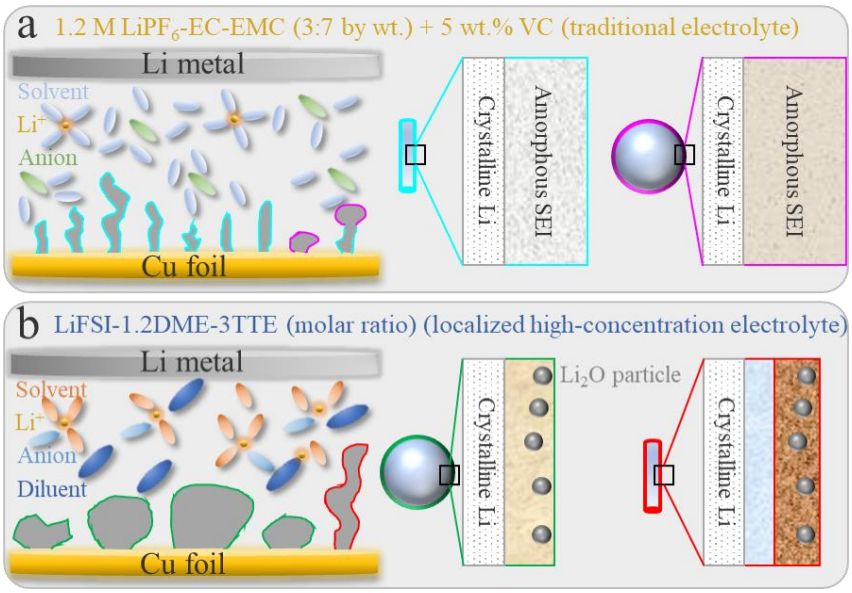

Figure 44. Schematic diagram of lithium deposits and SEI formed in traditional electrolyte (1.2 M $LiPF_6$-EC-EMC-5wt% VC) and localized high-concentration electrolyte (LiFSI-1.2DME-3TTE). (a) The morphology of lithium deposits formed in traditional carbonate-based electrolyte is dominated by whisker with very few particles. (b) The morphology of lithium deposits formed in the localized high-concentration electrolyte is dominated by particle with very few whiskers.

The team found that the morphology of lithium deposit strongly depends on the chemistry of electrolytes (Figure 45). In the traditional carbonated-based electrolyte, the deposited lithium metal is dominated by whisker morphology and with very few particles. In the ether-based electrolyte, the lithium deposits are dominated by particle morphology and with very few whiskers. Those two kinds of lithium morphology formed in the same electrolyte and under same deposition conditions give the team a perfect model to explore the underlying mechanism on formation of lithium particles and relationship with SEI.

Firstly, the lithium deposits of either particle or whisker formed in both carbonated-based and ether-based electrolytes are all unanimously single crystals shown by the HRTEM images and the selected area electron diffraction (SAED) patterns in Figure 45. Secondly, the SEIs formed in the carbonate-based electrolyte are monolithic amorphous structure, but show difference in thickness and chemical composition for the case of particle and whisker lithium deposit. The SEI on the whisker-shaped lithium deposits is ~ 20 nm in thickness and is mainly composed of oxygen, carbon, and trace amount of fluorine. The SEI on the particle-shaped lithium deposits is ~ 28 nm in thickness with a higher concentration of oxygen and lower concentration of carbon, as compared with the case of SEI on the lithium whisker (Table 3).

In marked contrast, SEIs formed in the ether-based electrolyte are much thinner. The SEI on the particle-shaped lithium deposits is ~ 7 nm in thickness and is amorphous with very few Li_2O nanoparticles embedded. The SEI on the whisker-shaped lithium deposits is ~ 13 nm in thickness and exhibits a bilayer structure: an inner layer of 4.5 nm monolithic amorphous, and an outer layer of 7.5 nm amorphous with few Li_2O nanoparticles embedded. The chemical compositions of those two SEIs are different as well. As shown in Table 3, the SEI on the particle-shaped lithium deposits is mainly composed of sulfur and a trace amount of oxygen, while SEI on the whisker-shaped lithium deposits is significantly rich in oxygen, but lean in sulfur.

These results establish a correlation among nanostructure, chemistry of the SEI, and lithium morphology, providing insights regarding the root cause for development of whisker-shaped lithium. The work can potentially serve to guide the design of electrolyte chemistry toward a dendrite-free Li-metal anode.

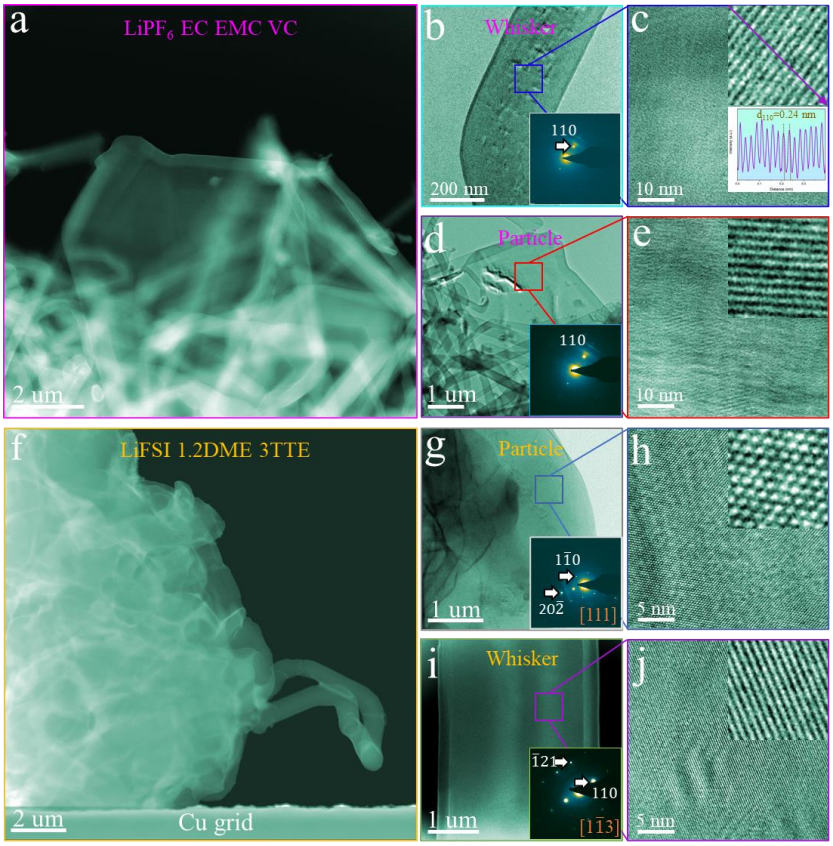

Figure 45. (a) Cryo – scanning transmission electron microscopy (Cryo-STEM) image of lithium deposits formed in traditional carbonate-based electrolyte. (b-c) Cryo-TEM images of whisker-shaped lithium deposit and (d-e) particle-shaped lithium deposit. (f) Cryo-STEM image of lithium deposits formed in localized high-concentration electrolyte (LHCE). (g-h) Cryo-TEM images of particle-shaped lithium deposit and (i-j) whisker-shaped lithium deposit. Lithium deposits formed in both traditional carbonate-based electrolyte and LHCE are single crystals with high crystallinity.

Table 3. Chemical composition of SEIs formed on different lithium deposits.

Composition / Electrolyte		O (wt.%)	C (wt.%)	F (wt.%)	P (wt.%)	S (wt.%)	N (wt.%)
Carbonated-based electrolyte	Whisker	53.6	43.6	2.3	0.6	\	\
	Particle	71.8	21.5	6.0	0.6	\	\
Ether-based electrolyte	Particle	22.7	0.0	4.4	\	71.1	1.7
	Whisker	63.9	3.5	9.4	\	18.7	4.6

Patents/Publications/Presentations

Publications

- Jia, H., Y. B. Xu, X. H. Zhang, S. D. Burton, P. Y. Gao, B. E. Matthews, M. H. Engelhard, K. S. Han, L. R. Zhong, C. M. Wang, and W. Xu. "Advanced Low-Flammable Electrolytes for Stable Operation of High-Voltage Lithium-Ion Batteries." *Angewandte Chemie International Edition* (2021): published online.
- Yang, H., M. Abdullah, J. Bright, W. Hu, K. Kittilstved, Y. Xu, C. Wang, X. Zhang, and N. Wu. " Polymer-Ceramic Composite Electrolytes for All-Solid-State Lithium Batteries: Ionic Conductivity and Chemical Interaction Enhanced by Oxygen Vacancy in Ceramic Nanofibers." *Journal of Power Sources* 495 (2021): 229796.
- Ren, X., P. Gao, L. Zou, S. Jiao, X. Cao, X. Zhang, H. Jia, M. H. Engelhard, B. E. Matthews, H. Wu, H. Lee, C. Niu, C. Wang, B. W. Arey, J. Xiao, J. Liu, J-G. Zhang, and W. Xu. "Role of Inner Solvation Sheath within Salt–Solvent Complexes in Tailoring Electrode/Electrolyte Interphases for Lithium Metal Batteries." *Proceedings of the National Academy of Sciences of the United States of America* (PNAS) 117 (2020): 28603–28613.

Task 2.5 – Integrated Atomic-, Meso-, and Micro-Scale Diagnostics of Solid-State Batteries (Yi Cui, William Chueh, and Michael Toney; Stanford University / SLAC National Accelerator Laboratory)

Project Objective. By developing a characterization toolkit that tackles length scales (Å to mm), cell pressure (1-100 bars), and dynamics (during synthesis, fabrication, and cycling), the project aims to generate insights to engineer SSBs for deployment in EVs. This interdisciplinary team aims to achieve this objective by merging a broad range of characterization approaches as well as modeling to track the evolution of nanoscale chemistry and structure, microstructure, and transport.

Project Impact. The project will have an impact in several areas: (1) accelerate rational design of coatings and artificial SEIs in SSBs; (2) inhibit the root causes leading to cell shorting, and enable high current cycling; (3) accelerate design of cathode coating and composite electrode architectures; and (4) reduce degradation and variability during SSB manufacturing via composition and surface engineering.

Approach. The project has a multi-fold approach that will encompass the following: (1) resolve nanoscale structure and chemistry of SEIs via cryo-TEM; (2) track SE and lithium microstructure evolution in 3D via X-ray micro and diffraction tomography; (3) visualize nanoscale ionic and electronic transport at GBs via conducting AFM; (4) map current distribution in cathodes via scanning transmission X-ray microscopy (STXM); and (5) monitor nanoscale SE evolution with gas impurity via *in situ* environmental TEM (E-TEM).

Out-Year Goals. The project will develop an integrated characterization toolkit to characterize SSBs within a single cycle and over hundreds of cycles, spanning a wide range of relevant length scales.

Collaborations. Project collaborations include work with SSRL, ALS, and Advanced Photon Source (APS) synchrotron light sources.

Milestones

1. Demonstrate *operando* X-ray microscopy to track lithium reactivity with LPS SE at open circuit as a function of pressure. (Q1, FY 2021; Completed)
2. Achieve 20-nm resolution for electrochemical impedance AFM for recording ionic and electronic conductivity. (Q2, FY 2021)
3. Determine composition of reacted phase between LPS and NMC cathodes after 10 cycles using various microscopy methods. (Q3, FY 2021)
4. Demonstrate *operando* SEM and FIB to record sub-surface microstructure in LLZO during lithium plating. (Q4, FY 2021)

Progress Report

This quarter, the team focused on lithium plating and short-circuiting behavior on LLZO SE. Inspired by the recent work in literature, they developed a microprobe experimental setup inside an Ar-filled glovebox to perform localized lithium plating on LLZO half cells with a thick Li-metal counter electrode. The metal probe, which can be as small as a few tens of micrometers, allows localized lithium plating between the probe tip and LLZO. Importantly, the setup makes it possible to investigate the microstructure of the LLZO before and after plating. Current constriction through the SE makes it difficult to subtract the ohmic resistance when significant current is present; nonetheless, it can be used to estimate the overpotential before the onset of lithium plating.

The as-received LLZO exhibited a several-hundred-nanometer-thick surface layer that could not be removed by heat treatment, contrary to recommendations from the manufacturer. Only with polishing can this layer be removed. This layer is not entirely dense and could contribute to additional surface area at the electrode/electrolyte interface. Even though polishing removes this layer, defects remain after achieving a mirror-like surface. Microprobe experiments at these defect sites indicate a significantly different plating behavior compared to flat areas. Systematic investigation is under way to understand the surface microstructure and the plating and short-circuiting behavior.

During the course of the experiment, the team discovered that LLZO surface is unstable in the Ar-filled glovebox, which does not house any organic liquids (that is, it is a glovebox dedicated to LLZO work). They developed a baseline experiment in which a freshly cleaved LLZO surface is used to determine the electrochemistry of the pristine electrode/electrolyte interface, with negligible exposure to the glovebox environment. For additional verification, they also developed a transfer mechanism to transfer the sample to a vacuum environment whereby atmospheric interaction can be eliminated altogether. In both cases, the team observed that the pristine surface exhibits much higher CCD as well as lower lithium plating overpotential. A closer examination by SEM revealed that exposure to the glovebox argon results in substantial roughening of the surface, indicating the formation of a surface phase. They hypothesize that this surface face is linked to the formation of Li_2CO_3; additional verification is under way. This finding has significant implication on the sensitivity of LLZO to even trace amounts of CO_2 that might be present in an Ar-filled glovebox.

Patents/Publications/Presentations

Presentation

- Argonne National Laboratory, Materials Science Division, Virtual (January 15, 2021); W. C. Chueh.

Task 2.6 – Investigating the Stability of Solid/Solid Interface (Zonghai Chen, Argonne National Laboratory)

Project Objective. The project objective is to characterize the physical/chemical properties of species at the solid/solid interfaces and to fundamentally understand the critical issues that limit the mechanical, chemical, and electrochemical stability of solid/solid interfaces at the cathode and the anode.

Project Impact. The project will lead to several areas of impact: (1) to generate knowledge that supports the rational design of materials and process development; (2) to establish structure-properties relationship of the interface; and (3) to understand the formation mechanism of lithium dendrite and to predict potential solutions.

Approach. The project approach is multi-fold: (1) understanding the physics behind the transformation between the low conductivity phase and the high conductivity phase; (2) investigating the bonding strength of the cathode electrolyte interface (CEI) using model systems; and (3) developing electrolytes with high ionic conductivity and good bonding to cathodes through cation doping.

Out-Year Goals. The project has the following out-year goals:

- Developing synchrotron-based diagnosis tools to investigate physical/chemical properties of solid/solid interface.
- Identifying mechanistic barriers that limit the chemical/mechanical/electrochemical durability of solid/solid interface.
- Developing model systems to validate the failure mechanism of solid/solid interface.

Collaborations. The project works with ANL collaborators A. Ngo, L. A. Curtiss, V. Srinivasan, Y. Ren, J. Libera, and Y. Z. Liu, and with BNL collaborators F. Wang and X. H. Xiao.

Milestones

1. *In situ* electron microscopic characterization of the dendrite formation on LLZO. (Q1, FY 2021; Completed)
2. Investigation of electronic conducting path in LLZO pellet. (Q2, FY 2021; Completed)
3. Investigation of the mechanical stability of cathode/LLZO interface using model system (Q3, FY 20201; On schedule)
4. Microscopic study of the mechanical stability of cathode/LLZO interface. (Q4, FY 2021; On schedule)

Progress Report

In last quarter's report, the team preliminarily demonstrated through *in situ* SEM experiments that a small fraction of lithium dendrite could be growing from the inside out of LLZO single particles, causing a crack of the LLZO particle. This observation is against the common belief that lithium dendrites grow from the outside into SSEs, causing penetration of lithium dendrites from the lithium side toward the cathode side. The team's observation implies a new lithium dendrite formation mechanism that can account for the failure mechanism of mechanically strong electrolytes like LLZO. This quarter, the same *in situ* experiments were conducted on hot-pressed LLZO pellets to validate this new dendrite formation mechanism.

Figure 46 shows a sequence of SEM images collected during the *in situ* experiment. The sample is a LLZO pellet prepared through hot press and shows a plate surface at the scale of micrometer level (Figure 46a). When a negative potential was applied on the tungsten tip, the lithium started to plate in between the LLZO surface and the tungsten tip (Figure 46b), as widely expected based on common knowledge. After applying a negative potential for about 10 minutes, two satellite spots clearly showed evidence of lithium dendrites more than 10 micrometers away from the tungsten tip (Figure 46c-d). The growth of these satellite lithium dendrites supports a new mechanism that lithium dendrite can also be grown from inside out of an LLZO pellet, even though a dense pellet was prepared using a hot press. When the experiment continued, the growth of satellite lithium dendrites continued, and dramatically at about 15 minutes, the accumulation of metallic lithium inside the LLZO pellet reached a critical limit and resulted in a big crack on the pellet for lithium dendrite to grow out (Figure 46e). This observation strongly confirms the new lithium dendrite formation that lithium can grow from inside out of LLZO. Blocking the electron conducting path is a MUST to resolve the dendrite growth issue of mixed conductors, like LLZO.

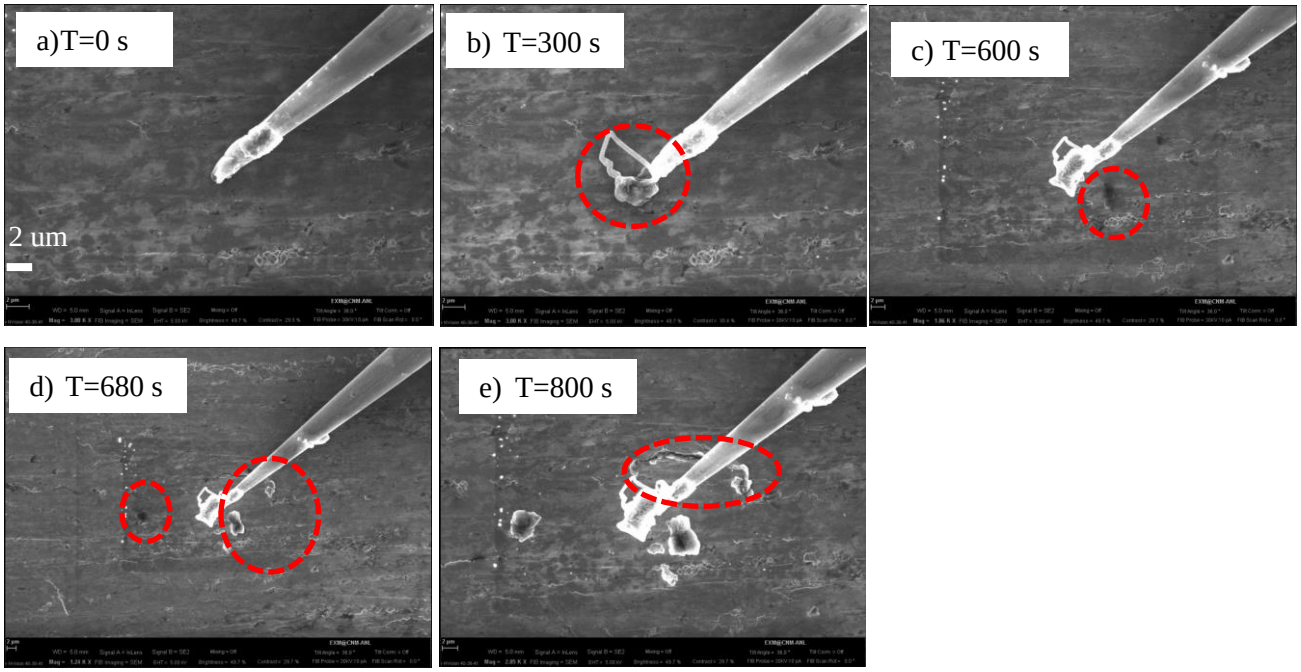

Figure 46. Snapshots of *in situ* scanning electron microscopy (SEM) experiment to stimulate lithium plating by applying negative potential on a tungsten tip. (a) SEM image at T = 0 s showing the smoothing LLZO surface. (b) SEM image at T = 300 s showing the plating of lithium metal under the tungsten tip. (c) SEM image at T = 600 s and (d) SEM image at T = 680 s showing the formation of lithium dendrites about 10+ µm away from the tungsten tip. (e) SEM image at T = 800 s showing formation of a crack on LZZO due to growth of lithium dendrite from inside out of LLZO.

Patents/Publications/Presentations

Publication

- Cai, J. Y., B. Polzin, L. L. Fan, L. Yin, Y. J. Liang, X. Li, Q. Liu, S. Trask, Y. Z. Liu, Y. Ren, X. B. Meng, and Z. H. Chen. "Stoichiometric Irreversibility of Aged Garnet Electrolytes." *Materials Today Energy* 20 (2021): 1006692.

Presentation

- American Ceramics Society, Florida (January 2021): "Chemical Stability of Garnet Electrolytes, Electronic Materials and Applications"; J. Y. Cai and Z. H. Chen.

Task 2.7 – Fundamental Understanding of Interfacial Phenomena in Solid-State Batteries (Xingcheng Xiao, General Motors)

Project Objective. The project objective is to develop a comprehensive set of *in situ* diagnostic techniques combined with atomic/continuum modeling schemes to investigate and understand the coupled mechanical/chemical degradation associated with dynamic interfacial phenomena in SSBs. Specifically, *in situ* observations and characterizations of lithium plating-stripping processes, lithium dendrite formation, interphase formation, and the induced interfacial stresses, as well as the mechanical and electrochemical properties of interfaces and interphases, are paramount. The study will provide useful guidelines for optimizing cell structure design and engineering interfaces and interphases to enable SSBs.

Project Impact. The project will provide fundamental understanding of the dynamic interfacial phenomena and the coupled mechanical and chemical degradation. In addition, it will establish a critical guideline to design safe and durable SSBs with energy density > 500 wh/kg for EV applications.

Approach. The multi-scale *in situ* diagnostic tools, including AFM, nanoindentation, dilatometer, stress sensors, and pressure cells, will be used to investigate mechanical behavior and microstructure evolution at interface/interphase during lithium plating and stripping. The information (along with Li-ion transport properties and microstructure evolution obtained using the advanced spectroscopic ellipsometry, and *in situ* TEM) will be correlated with electrochemical performance toward high cycle efficiency and dendrite-free SSBs. The goal of this understanding is to develop strategies for surface and interface engineering, apply them to commercially available SEs (including powder, pellets, and foils), and assemble SSBs for further validation and optimization, eventually extending cycle life for EV application.

Out-Year Goals. The project seeks to develop SSB model systems to capture critical mechanical properties and probe the coupled mechanical-chemical degradation by further developing comprehensive *in situ* diagnostic tools. All results obtained from these *in situ* studies, combined with advanced *postmortem* analysis and modeling, will be correlated with the cycling stability of SSBs. The *in situ* tools developed will be applied to the following two periods to deeply understand the coupled mechanical and chemical degradation of interface/interphase.

Collaborations. The co-PIs involved in experiments and simulation will be as follows: B. W. Sheldon and Y. Qi (Brown University), Y-T. Cheng and A. Seo (University of Kentucky), and Q. Zhang (GM).

Milestones

1. Correlation between interfacial mechanical failure mechanisms and current density and pressure. (Q1, FY 2021; Completed)
2. Summary of the thickness, chemical bonding, and structural information of the interphases between anode and SE, and cathode and SE. (Q2, FY 2021; Completed)
3. Identified mechanisms of ionic transport through the interface/interphase. (Q3, FY 2021)
4. Multi-scale modeling framework to describe the coupled mechanical/chemical degradation. (Q4, FY 2021)

Progress Report

Extending Density Functional Theory (DFT) – Kinetic Monte Carlo (KMC) Model to Other Interfaces

Two important interfaces are under investigation, namely Li/Li_2S, Li/Li_3N, and Li/LLZO. Li_2S and Li_3N are electrolyte decomposed products found at Li/GPS and Li/LiPON interfaces. LLZO is one of the important SEs being tested in experiments. The team's previously developed multiscale simulation framework has shown that interfacial properties (such as lithiophobic Li/LiF and lithiophilic Li/Li_2O) play an important role in maintaining a smooth lithium surface during delithiation. First, the interface work of adhesion and wetting angles is computed using DFT and ranked for these interfaces (as shown in Table 4).

The lithium vacancy formation energy was calculated at the Li/Li_3N and Li/LLZO interfaces. Compared to previously computed Li/Li_2O and Li/LiF interfaces, where the vacancy formation energy converges to the bulk values within three layers from the interface, the Li/Li_3N and Li/LLZO interfaces have a longer range to influence the vacancy formation energy. Both interfaces trap lithium vacancies. The Li/Li_3N interface is consistent with the team's previous hypothesis that the non-wetting, lithiophilic Li/Li_3N interface attracts lithium vacancies near the interface. While the Li/LLZO interface is wetting with a reasonably high work of adhesion, it still traps lithium vacancies. This may be related to the surface termination of the Li_3N and LLZO interfaces; both have higher cation concentrations and thus positive charge on the surface, while previously computed Li_2O and LiF surfaces are anions terminated. The positively charged surfaces can repel lithium, as the surface lithium atoms are slightly positively charged, lowering the lithium vacancy formation energy. Thus, the team hypothesizes that it is harder to maintain a flat lithium surface at Li/Li_3N and Li/LLZO interfaces.

Table 4. Li/SEI and Li/SE interfacial properties.

		W_{ad}h (J/m^2)	Wetting angle Θ (°)
Wetting	Li(001)/Li_2O(110)	1.11	~ 0
	Li(001)/Li_2S(110)	0.68	50
	Li(001)/Li_2PO_2N(010	0.64	55.9
	Li(001)/LLZO Zr rich (001)	0.63	60.2
Non-wetting	Li(111)/Li_3N(001)	0.39	103.1
	Li(001)/Li_2CO_3(001)	0.30	105.7
	Li(001)/LiF(001)	0.28	108.7

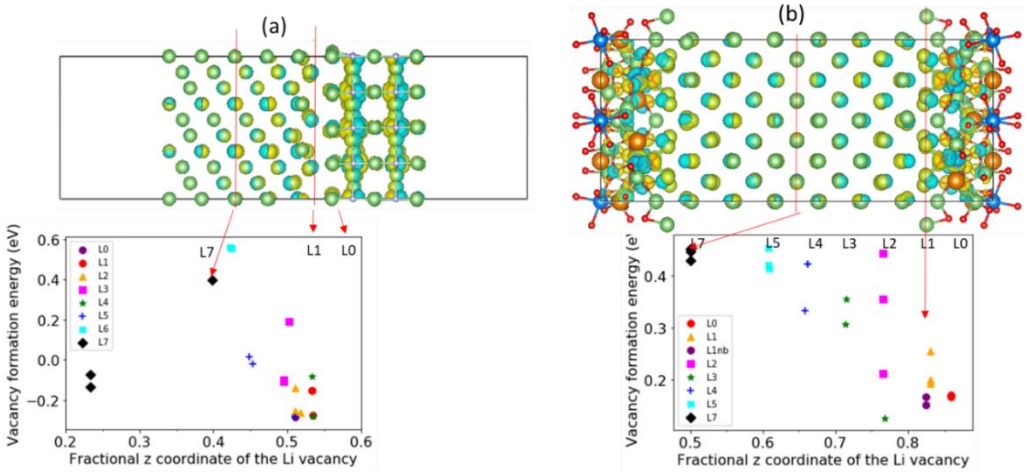

Figure 47. Vacancy formation energy near interfaces of (a) Li(111)/Li_3N(001) and Li(001)/LLZO Zr rich (001).

Micro – Computerized Tomography (CT) to Understand Interface Reaction between SE and Lithium Metal

LAGP is short for $Li_{1.5}Al_{0.5}Ge_{1.5}(PO_4)_3$, and it possesses a Li-ion conductivity of 5×10^{-4} S/cm at room temperature. However, the germanium is easily reduced by lithium metal, and this reaction is not self-limiting since the side-reaction product is a mixed electronic and ionic conductive phase. A CT scan can construct a 3D image of the object nondestructively. Without air exposure, the interfacial property of the solid-state cell is revealed. As shown in Figure 48, the coated sample shows a much more stable interphase. The control lithium electrode shows a bumpy structure, while the coated lithium electrode is flat. In addition, the control lithium has a thickness ~ 0.15 mm, which is a three-time increase compared with pristine lithium metal (0.05 mm). In contrast, the coated lithium maintains the same thickness as before. The increased thickness of control lithium electrode can be caused either by the unintimate solid-solid contact or the side reaction occurring within the lithium foil. An interphase with a distinct dark color is formed between SSE (LAGP) and lithium electrode, and this thickness can directly represent the side reaction level. In the control lithium electrode, the interphase layer caused by the side reaction is 0.07 mm, which is 2.33 times higher than the coated sample (0.03 mm). As a result, with coating, the side reaction between lithium electrode and LAGP is largely depressed, and a good cycle life is reached.

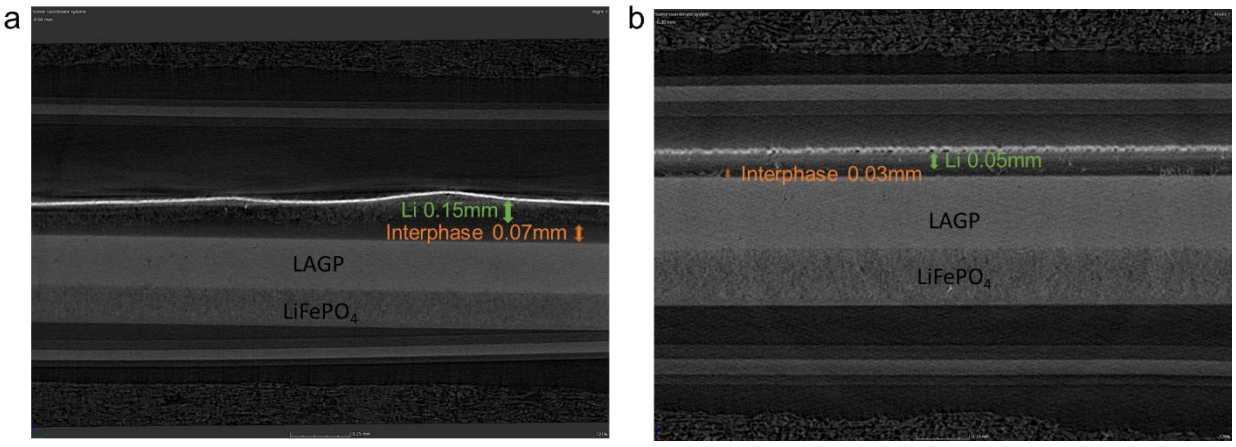

Figure 48. Computerized tomography scan of the cross-section of Li/LAGP/$LiFePO_4$ cell. (a) Li/LAGP/$LiFePO_4$ cell with control lithium electrode. (b) Li/LAGP/$LiFePO_4$ cell with coated lithium electrode.

Patents/Publications/Presentations

Patents

- Xiao, X., and M. Chen. "Methods for Forming Ionically Conductive Polymer Composite Polymer Interlayers in Solid-State Batteries." GM Ref. No. P054138-US-NP.
- Chen, M., and X. Xiao. "Composite Interlayers for Solid State Batteries and the Method of Making Same." GM Ref. No. P054203-US-NP.

Publications

- Yang, C. T., and Y. Qi. "Maintaining a Flat Li Surface during the Li Stripping Process via Interface Design." *Chemistry of Materials* (2021). In press. doi: 10.1021/acs.chemmater.0c04814.
- Swift, M. W., J. W. Swift, and Y. Qi. "Modeling the Electrical Double Layer at Solid-State Electrochemical Interfaces." *Nature Computational Science* 1 (2021): 212–220. doi: 10.1038/s43588-021-00041-y.

Task 2.8 – Multidimensional Diagnostics of the Interface Evolutions in Solid-State Lithium Batteries (Yan Yao, University of Houston)

Project Objective. The project objective is to develop a platform combining FIB-SEM tomography, TOF-SIMS, and in-SEM nanoindentation-based stiffness mapping for structural, chemical, and mechanical characterizations in SSLBs. Assessment of the influence of cell design and testing conditions (external pressure, current density, temperature) on the evolutions of interfaces will be performed.

Project Impact. The consolidated *in situ* structural–chemical–mechanical diagnostic platform established in this project will provide unprecedented insights into the failure mechanisms of SSLBs.

Approach. Space- and time-resolved structural, chemical, and mechanical characterizations of the cathode–electrolyte and anode–electrolyte interfaces will be performed on lithium ASSBs using FIB-SEM, TOF-SIMS, and in-SEM nanoindentation. Tasks include the following: (1) development of solid-state cell thin stacks and test-cell configurations that are suitable for *in situ* characterizations; (2) quantitative characterization and *in situ* tracking of interfacial voids formation within composite cathode and electrolyte layer; (3) identification and *in situ* tracking of the chemical composition, spatial distribution, and mechanical properties of electrolyte decomposition products at the lithium- and cathode-electrolyte interfaces; and (4) visualization, chemo-mechanical properties detection, and *in situ* tracking of lithium dendrites grown within the SE layer.

Out-Year Goals. In the out years, the project will develop thin-stack solid-state cells, micro-cells, in-SEM nanoindentation, and testing protocols. The correlation between structural evolution, electrolyte decomposition, and interfacial resistance increase will be investigated.

Collaborations. The UH team (Y. Yao, Z. Fan, and Y. Liang) works closely with the Rice University team (J. Lou and H. Guo).

Milestones

1. Nano-cell development. (Q4, FY 2021; In progress)
2. Cell optimization and electrochemical benchmarking. (Q2, FY 2021; Completed)
3. Multiscale structural investigations. (Q1, FY 2022; Initiated)
4. Composition and spatial distribution study. (Q2, FY 2022; Initiated)
5. Selected region mechanical property probing. (Q3, FY 2022; Initiated)

Progress Report

The team has optimized the fabrication process of nano-cells and improved yield. They can now fabricate nano-cells with various configurations and carry out selected *in situ* measurement and characterization on them. Figure 49 shows examples of the capability they developed. Characterization of a LPSCl electrolyte in the nano-cells is done on a strip of LPSCl connected to gold electrodes via platinum contacts (Figure 49a). EIS measurement of the Pt|LPSCl|Pt symmetrical cell shows an ionic conductivity of 1.7×10^{-3} S/cm. This result is in line with the value of the same electrolyte obtained from bulk cells (1.6×10^{-3} S/cm), indicating chemical integrity of the electrolyte, good contact between cell components, and overall successful demonstration of cell configuration. An NMC|LPSCl|$Li_4Ti_5O_{12}$ full cell was similarly fabricated (Figure 49c). CV shows noisy current response, and redox waves are not clearly isolated from the background (Figure 49d). This is not necessarily a flaw of the fabricated cell, but due to the extremely small current reaching the detection limit of the potentiostat. An incoming potentiostat with ultralow-current detection capability will be used in future electrochemical measurements. That the current was not properly recorded did not prevent cell operation and structural characterization.

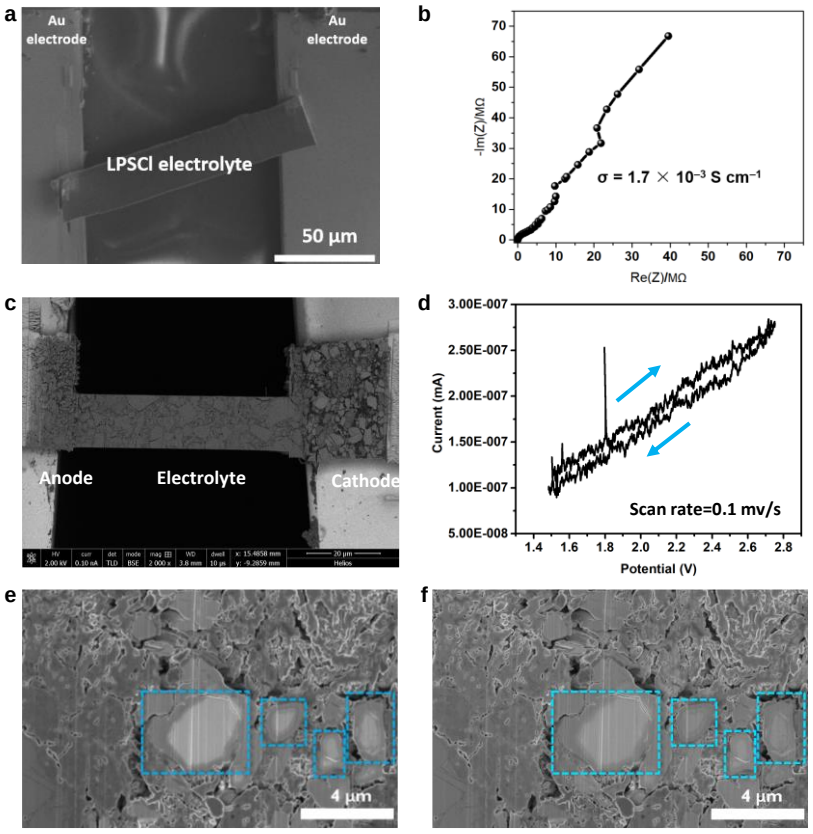

Figure 49. Electrochemical and structural characterization of nano-cells. (a-b) Structure (a) and impedance measurement (b) of a Pt|LPSCl|Pt symmetrical cell. (c-d) Structure (c) and cyclic voltammogram (d) of an NMC|LPSCl|LTO full cell. (e-f) *In situ* observation of the full cell before (e) and after (f) cycling.

An example of *in situ* SEM observation of the nano-cell electrodes is shown in Figure 49e-f. Highlighted in squares are NMC particles that show contrast gradients within the particle. The different greyscale could be reflective of local composition and/or crystallinity differences. Before cycling, the brighter and darker regions are distinctively separated by sharp lines (Figure 49e). The distinction was gradually lost on cycling, with some smaller particles appearing almost uniform (Figure 49f). Interpretation of such transformation will be made possible once current response information is obtained from CV. Other chemical and structural characterization methods are also being implemented to the nano-cell platform.

Performance optimization of the thin solid-state cells in general continued. The previous thin cells were most successful when Li-In anodes were used. For example, the team has reported on a Li-In|NMC|LPSCl full cell with a combined 100-µm thickness and stable capacity over 50 cycles (Figure 50a). Their original goal for the project, however, is to use lithium as the anode for practical higher-energy cells. Direct use of lithium metal in the project's thin cells leads to fast short-circuiting, probably the result of both lithium creeping and dendrite formation.

Several methods have been attempted to adapt lithium metal to the cells. One of them is to use an interlayer (≤ 10-μm thick) between the electrolyte and the lithium anode, a physical barrier that prevents any creeping lithium or dendrite to penetrate the thin electrolyte layer. A cell based on lithium anode and interlayer is shown in Figure 50b, which indicates an increased cell voltage versus a Li-In based cell. The suppression of lithium is quite successful in that the cell has survived 200 cycles without shorting, even though the electrolyte layer is 50-μm thick. The lower specific capacity than that shown in Figure 50a was due to the difference in cathode preparation methods. Other methods are also being developed and will be used in conjunction with the interlayer.

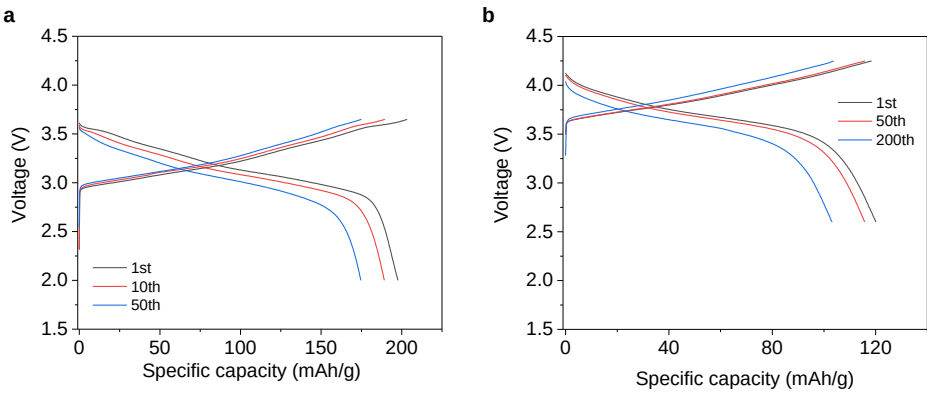

Figure 50. Charge–discharge profiles of (a) Li-In|LPSCl|NMC and (b) Li|interlayer|LPSCl|NMC thin cells.

Patents/Publications/Presentations

Publication

- Emley, B., Y. Liang, R. Chen, C. Wu, M. Pan, Z. Fan, and Y. Yao. "On the Quality of Tape-Cast Thin Films of Sulfide Electrolytes for Solid-State Batteries." *Materials Today Physics* 18 (2021): 100397.

Presentations (Invited)

- Nissan North America Battery Group, Virtual (March 25, 2021): "Cobalt-Free Solid-State Lithium Batteries"; Y. Yao.
- International Battery Seminar & Exhibit, Virtual (March 9–11, 2021): "Next-Generation Batteries for Electric Vehicles and Stationary Storage"; Y. Yao.
- The Electrochemical Society (ECS) Webinar, Virtual (February 24, 2021): "Next-Generation Batteries for Electric Vehicles and Stationary Storage"; Y. Yao.
- Yonsei University, Department of Chemical Engineering, Seoul, Korea, Virtual (January 18, 2021): "Organic Electrode Materials Design for Emerging Rechargeable Batteries"; Y. Yao.
- University of Freiburg, Germany, Virtual (January 13, 2021): "Next-Generation Batteries for Electric Vehicles and Stationary Storage"; Y. Yao.

TASK 3 – MODELING

Team Lead: Venkat Srinivasan, Argonne National Laboratory

Summary and Highlights

Achieving the performance, life, and cost targets outlined by VTO will require moving to next-generation chemistries, such as higher capacity Li-ion intercalation cathodes, silicon and other alloy-based anodes, Li-metal anode, and sulfur cathodes. However, numerous problems plague development of these systems, from material-level challenges in ensuring reversibility to electrode-level issues in accommodating volume changes, to cell-level challenges in preventing cross talk between the electrodes. In this task, a mathematical perspective is applied to these challenges to provide an understanding of the underlying phenomenon and to suggest solutions that can be implemented by the material synthesis and electrode architecture groups.

The effort spans multiple length scales, from *ab initio* methods to continuum-scale techniques. Models are combined with experiments, and extensive collaborations are established with experimental groups to ensure that the predictions match reality. Efforts also focus on obtaining parameters needed for the models, either from lower-length scale methods or from experiments. Projects also emphasize pushing the boundaries of the modeling techniques used to ensure that the task stays at the cutting edge.

A major focus of the effort is around Li-metal-based SSBs. While these chemistries hold promise, numerous challenges such as reactivity, conductivity, and mechanical stability prevent their commercialization. Mathematical models are ideal to provide the guidance and insights needed to solve these issues.

In the area of Li-metal anodes, the focus is on understanding how materials can be designed to prevent dendrite growth using continuum modeling approaches, combined with calculations on mobility in solid conductors. The results are used to guide materials development by providing the properties needed to prevent dendrites, while also achieving the energy and power goals. Models examine the role of the SEI on the morphology of the dendrite and describe the mechanical-electrochemical coupled effects that are critical for dendrite formation. Finally, efforts are focused on discovery of new solid ion conductors with properties that far exceed existing materials. The focus is on using these models as a guide before embarking on extensive experimentation.

Lithium metal with SEs will be paired with cathode materials, often intercalative in nature. Models are being developed to examine the solid-cathode interface in Li-metal based systems, where side reactions and interface debonding issues are known to limit cycling. These models are being used to understand how to prevent chemo-mechanical failure at the interface. Coatings, an effective strategy for high-voltage operation, are being explored with the aim of providing a rational design approach for new coating materials. In addition, focus is paid to porous electrodes with cathode particles to predict the impact of heterogeneities on electrode behavior.

Highlight. The highlight for this quarter is as follows:

- While most efforts on modeling lithium metal have focused on effects at the electrolyte region of the metal-electrode interface, experimental evidence has shown the importance of surface and bulk diffusion of lithium metal in determining the morphology during dissolution (or discharge). The V. Srinivasan group has now developed a model to examine void formation in lithium metal taking into account the surface and bulk diffusion of lithium, effect of external pressure, current density, etc., and has compared the model to recent experimental results. Simulations suggest that as current density increases, the slow transport in the metal leads to formation of deep voids and delamination of the metal from the SE when no external pressure is imposed.

Task 3.1 – Characterization and Modeling of Lithium-Metal Batteries: First-Principles Modeling and Machine Learning
(Kristin Persson, Lawrence Berkeley National Laboratory)

Project Objective. This project supports VTO programmatic goals by developing next-generation, high-energy cathode materials and enabling stable cathode operation at high voltages through target particle morphology design, functional coatings, and rational design of electrolytes. The end-of-project goals include the following: (1) understanding of the factors that govern charge transport in nonaqueous, superconcentrated LEs, (2) critical surface and coating design and optimization strategies that will improve cycling of Li-ion battery cathodes by reducing cathode degradation from oxygen loss, and (3) simulation and machine learning (ML) of the early formation of the SEI on Li-metal electrodes.

Project Impact. This project is aimed at providing fundamental insights into the atomistic mechanisms underlying surface reactivity and performance of Li-ion cathode materials and electrolytes with the ultimate goal to suggest improvement strategies, such as coatings, surface protection, novel electrolyte formulations, and particle morphology design. Transport modes as a function of solvent and salt concentrations will be clarified, and a data-driven reaction network framework will be designed and implemented to predict early SEI formation on lithium metal.

Approach. First-principles calculations, both static and dynamic approaches, are used to model SSE material thermodynamics and kinetics. LEs are modeled through coupled classical molecular dynamics (MD) and first-principles methods to accurately capture solvation structure as well as reactivity of the liquid system. The reaction network is built on large-scale first-principles data, using graph theory and ML models.

Out-Year Goals. Electrolyte work will be aimed toward understanding the atomistic interactions underlying performance of lithium electrolytes, specifically elucidating conductivity (as a function of salt concentration) and impact on the charge transport mechanisms at play. Amorphous coatings will be evaluated based on ionic transport metrics and thermodynamic stability. The reaction network will be tested against known interfacial species forming on lithium metal in $LiPF_6$/EC electrolytes.

Collaborations. This project is highly collaborative between BMR PIs G. Chen (LBNL), G. Ceder (UCB), and R. Kostecki (ANL). Improved coating formulations will be examined by Chen and Ceder, and interfacial reactivity insights will be corroborated by Kostecki.

Milestones

1. Preliminary insights into the SEI composition and reaction pathways for baseline electrolytes. First approximative reaction scheme proposed. (Q3, FY 2020; Completed)
2. Develop a valid model for amorphous structure as compared to experimental radial distribution function data. (Q3, FY 2021; In progress)
3. Quantify the effect of co-solvents to at least one superconcentrated electrolyte. (Q4, FY 2021; In progress)
4. Correlation of electrolyte chemistry and Li/SEI compositional structure determined. (Q1, FY 2022; In progress)

Progress Report

The Li-metal SEI project is aimed toward using a data-driven reaction network approach to identify reaction pathways responsible for the formation of important SEI component species. One goal of interest is identifying the formation mechanisms of lithium ethylene monocarbonate (LEMC), which has recently been proposed to be the major component of the Li-anode SEI rather than lithium ethylene di-carbonate (LEDC).

To that end, the team first improved the following two aspects of the reaction network. The entire workflow is shown in Figure 51. They proposed a systematic way of sampling the relevant molecular species to be included, for example, a fragmentation and ML-assisted recombination procedure. They generated the fragments of the starting materials (Li^+, EC, and water) and recombinant molecules through connecting one bond between any two fragments. Subsequently, all the recombinant molecules that are predicted to be exergonic on recombination by ML model BonDNet were included in the reaction network. The team utilized a mixed-integer linear programming (MILP) scheme to incorporate concerted reactions (reactions involving multiple bond changes at the same time) with up to five bond changes to account for complicated hydrolysis mechanisms. Following this procedure, they constructed a reaction network with 570 species and close to nine million reactions.

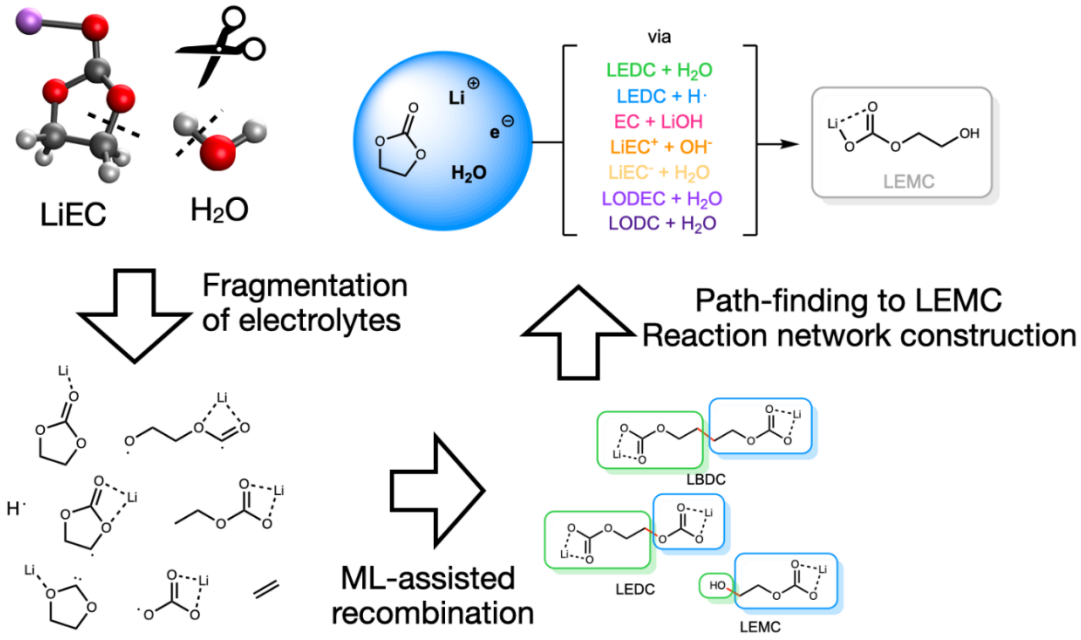

Figure 51. The workflow for constructing a reaction network for the Li^+/EC/H_2O system and pathfinding to LEMC.

Analyzing 30,000 top-ranking LEMC formation pathways as identified by the reaction network, the team (1) successfully recovered, automatically, two literature-proposed mechanisms, namely EC hydrolysis and LEDC hydrolysis pathways, and (2) found that nearly all feasible routes to LEMC involve water and/or LEDC participation. This condition severely limits the amount of LEMC that can form in the first cycles, as compared to LEDC, in well-dried commercial Li-ion electrolytes.

Patents/Publications/Presentations

The project has no patents, publications, or presentations to report this quarter.

Task 3.2 – Electrode Materials Design and Failure Prediction (Venkat Srinivasan, Argonne National Laboratory)

Project Objective. The main project objective is to develop computational models for understanding the various degradation mechanisms for next-generation Li-ion batteries. This year's goal is to use the continuum-based mathematical model to investigate interfacial stability between Li-metal electrodes and SEs during deposition and dissolution of lithium under externally applied currents. Both soft polymer and hard ceramic type electrolytes will be investigated. The team also aims to develop a computational model for understanding the interdiffusion of ions and its impact on other degradation mechanisms at the CEI. Ceramic-based SEs are expected to enable high-energy-density and liquid-free, safe, next-generation Li-ion batteries. Li-metal anodes should be incorporated due to their substantially larger volumetric and specific capacity, as compared to present day graphite-based anodes. During charge, lithium dendrites are observed through the SEs, which are supposed to occur because of the non-uniform current distribution at the Li/electrolyte interface. Interfacial detachment between the lithium electrode and SE has been observed during electrochemical dissolution of lithium (or, the stripping process), which can lead to nonhomogeneous contact and substantially higher charge transfer resistance between the electrode and electrolytes. Similar issues have also been observed at the Li/PE interface during lithium stripping, which will be investigated thoroughly. On the cathode side, diffusion of TMs into the SEs, along with delamination between cathode and SE, leads to increased interfacial resistance. The side reaction between cathodes and SEs is a bigger issue for the sulfides as compared to the oxide-based ceramics, whereas the delamination is supposed to be more dominant within the oxides. The developed computational model will be used to investigate the impact of physicochemical and transport properties of the SE on the overall interfacial degradation observed at both the cathode and anode sides. The main focus will be to elucidate interfacial issues and devise strategies to enable successful implementation of SE in next-generation Li-ion batteries.

Project Impact. Findings from this research will give a better understanding of the factors, at the electrode/SE interface, limiting the cycle life of SE-based Li-ion batteries. These results will help to enable all-solid-state Li-ion batteries.

Project Approach. The approach used here is to develop mesoscale models based on governing principles at the continuum level to describe the critical processes occurring in the materials. Electrochemical, microscopic, and spectroscopic data from experiments are combined with theories for parameter estimation and model validation. The model is then used to provide insights and guidance for design of new materials.

Out-Year Goals. At the end of this project, a computational framework will be presented that is capable of estimating lithium stripping and interdiffusion of ions at electrode/electrolyte interface.

Collaborations. This project collaborates with L. A. Curtiss, A. T. Ngo, and C. M. Phatak at ANL.

Milestones

1. Develop a mesoscale model to capture the void formation at the Li/LLZO interface during dissolution. (Q1, FY 2021; Completed)

2. Compare the lithium dissolution results as predicted by the mesoscale computations (conducted at ANL) with the experimental results obtained from the German (J. Janek, Giessen) group. (Q2, FY 2021; Completed)

3. Understand current distribution around a dendritic protrusion during lithium dissolution. (Q3, FY 2021; Initiated)

Progress Report

Compare Lithium Dissolution Results as Predicted by the Mesoscale Computations (Conducted at ANL) with Experimental Results Obtained from the German Group (J. Janek, Giessen). A mesoscale-level computational model was developed last quarter that is capable of capturing the formation of voids within the lithium electrode at the Li/LLZO interface. Surface diffusion of atoms is a key factor controlling the evolution of pores at the interface between lithium electrode and the SE, which eventually leads to delamination and significant impedance rise. Experiments conducted by the group of J. Janek (Giessen, Germany) clearly show the evolution of surface voids at the Li/LLZO interface. The German research group looked at the pore morphology using cryo-SEM techniques, and investigated the influence of applied current density, external pressure, etc. on the overall void formation process. This quarter, the team tried to compare the experimental results with those obtained from the mesoscale-level computational models. To obtain a better understanding of the pore morphology that evolves during the lithium stripping process, cryo-SEM imaging of the electrode/electrolyte cross section is conducted by the group of J. Janek. These results are shown in Figure 52a, which clearly depicts that the pores can be 5-10 µm in width and 1-2 µm in depth. These imaged voids are generated under an applied current density of 1 A/m^2. Computational simulations with a lithum surface diffusivity 2000 times larger than the lithium volume diffusivity lead to generation of similar void microstructures under equivalent current densities, which is shown in Figure 52b. A comparison between the depth of voids obtained at different current densities using the computational simulations is shown in Figure 52c, which compares well with the experimental observations.

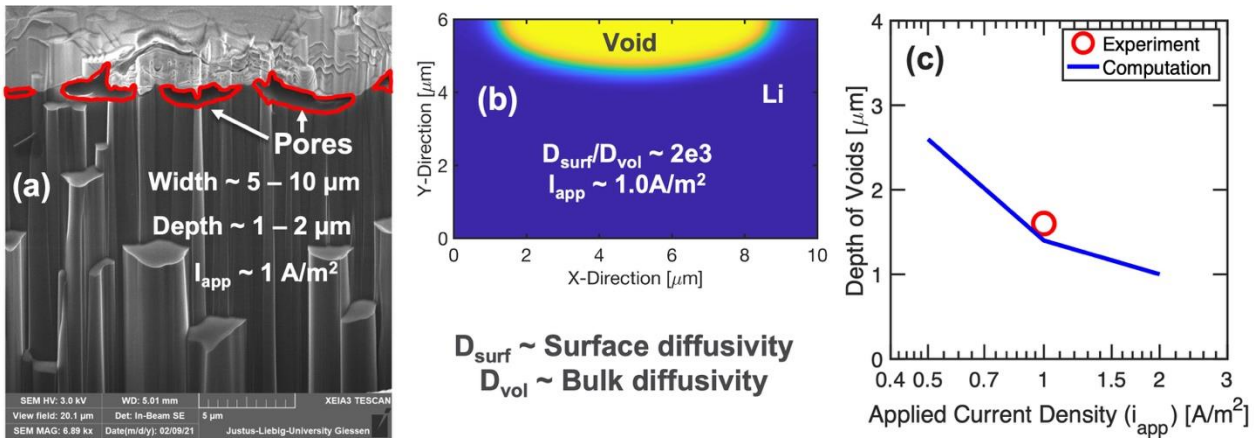

Figure 52. (a) Visualization of voids at the Li/LLZO interface using cryo – scanning electron microscopy techniques. (b) Computational simulation of void formation within lithium metal. The solid electrolyte is located at the top. Lithium is being stripped at an applied current density of 1 A/m^2. (c) Comparison between experimentally observed (red circle) and computationally predicted (blue solid line) depth of voids. It is evident that increasing the current density results in a decrease in pore depth.

The time required to completely delaminate the lithium electrode from the LLZO SE under different applied current densities is shown in Figure 53a. A comparison with experimental results regarding "time for failure" obtained by the group of J. Janek is shown in Figure 53b. A good comparison between computational models and experimental observations successfully completes the milestone for this quarter.

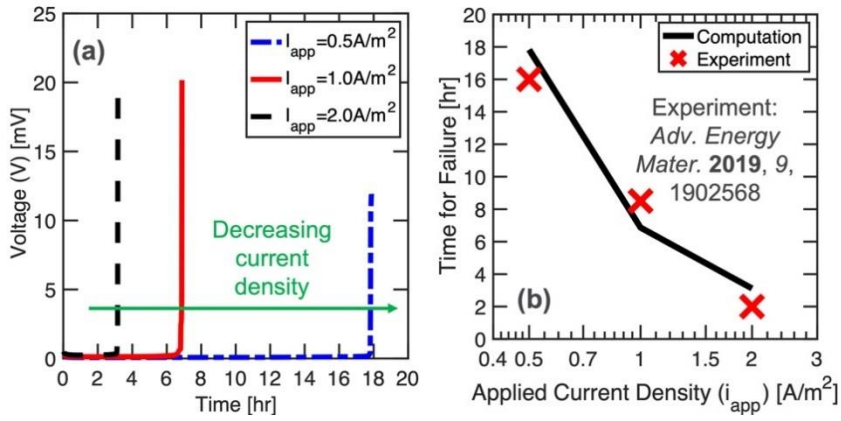

Figure 53. (a) Voltage versus time curves obtained at different lithium stripping current densities, which show rapid increase in overpotential when the electrode experiences complete delamination from the solid electrolyte. (b) Comparison between experimentally observed (red squares) and computationally predicted (black solid line) time for failure under different applied current densities. The experimental results are obtained from an article published by the group of J. Janek [*Advanced Energy Materials* (2019): 1902568].

Patents/Publications/Presentations

The project has no patents, publications, or presentations to report this quarter.

Task 3.3 – Modeling of Amorphous Solid-State Conductors (Gerbrand Ceder, University of California, Berkeley)

Project Objective. SSBs are promising to achieve high energy density. The project objective is to determine the design principles needed to create SSEs with high Li-ion conductivity, while also achieving stability against common Li-ion cathodes and Li-metal anodes.

Project Impact. The project will lead to understanding the factors that control Li-ion motion in crystalline and amorphous solids and will develop strategies to create stable interfaces against lithium metal and high-voltage cathode materials. The understanding of such processes is necessary to determine design principles to develop reliable ASSBs.

Approach. HT computation is used to screen suitable SE with high electrochemical stability and high ionic conductivity, by incorporating nudged elastic band (NEB) and an *ab initio* molecular dynamics (AIMD) method. Meanwhile, DFT is used to calculate bulk elastic constants of materials, surface energies, and interface decohesion energies of GBs. Thermodynamic interface stability is assessed from *ab initio* computed grand potential phase diagrams in which the lithium voltage can be controlled. Kinetic limits for SE decomposition are assessed by topotactic lithium insertion and removal from the SE.

Out-Year Goals. Future goals include the following: (1) gain insight into what creates high Li-ion conduction in sulfide and oxide solids, and (2) develop stable, processable solid-state conductors that can be applied in ASSBs.

Collaborations. There are no collaborative activities this quarter.

Milestones

1. Finite T phase diagram of L-P-S system. (Q1, FY 2021; Completed)
2. Develop model for electronic conductivity in SEs. (Q2, FY 2021; Completed)
3. Evaluate effect of ionic and electronic conductivity on lithium plating in SE. (Q3, FY 2021)
4. Develop a valid model for amorphous structure, and compare to spectroscopy data. (Q4, FY 2021)

Progress Report

Vulnerable Region for Lithium Deposition Inside Voids in the SE

The existence of electronic conductivity in SEs is believed to be one reason for metal penetration in SSB cells. The key issue to prevent Li-metal propagation through the electrolyte is to prohibit initiation of metal plating in the vulnerable region near the anode, as illustrated schematically in Figure 54. The team has built a transport model for a solid-state cell that includes both electronic and ionic currents in the SE. From this model, they can determine that the fraction of the SE that sees a negative plating potential (a_0/L), and is therefore susceptible to lithium deposition, is approximately the ratio of the anode surface overpotential (η_A) and the cell voltage $V_C - V_A$:

$$\frac{a_0}{L} \approx \frac{\eta_A - V_A}{\eta_A + \eta_C + (V_C - V_A)}$$

Here, η_A and η_C are the Butler-Volmer (BV) overpotentials at the anode/SE and cathode/SE interfaces, and V_A and V_C are the equilibrium voltage in the anode and cathode, respectively. The susceptible zone, a_0, reaches a maximum ($a_0 = 0.5L$) for a symmetric cell. This can be understood as a symmetric metal cell keeping the electronic chemical potential high everywhere in the SE. In a real cell, the raising of the cathode voltage reduces the fraction of the SE that is exposed to a negative plating potential. Even increasing the cathode potential to only $0.1\,V$ decreases a_0 to $0.04L$. This decrease is also reflected in the plating potential, which is pulled down at the cathode side by an amount that is equal to the cathode voltage. This analysis shows that a symmetric Li/Li cell is not realistic for studying Li-metal growth in SE. It is possible to fully prevent M metal deposition by increasing the anode voltage (for example, by using an alloying anode). The increase in anode voltage needs to be just enough to offset the anode overpotential, $V_A \geq \eta_A$. For example, when $\mu_M^A \leq -4.0\,meV$, no M deposition occurs regardless of the position of the void in the SE. This indicates that even minor voltage changes in the anode can modify the lithium penetration behavior in the SE. Indeed, many demonstrations of SSB in which no Li-metal penetration occurs use a nonmetal anode. The results indicate that cells that use a graphite or indium metal anode are not representative of Li-metal solid-state cells, as they underestimate the problem of Li-metal growth through the electrolyte.

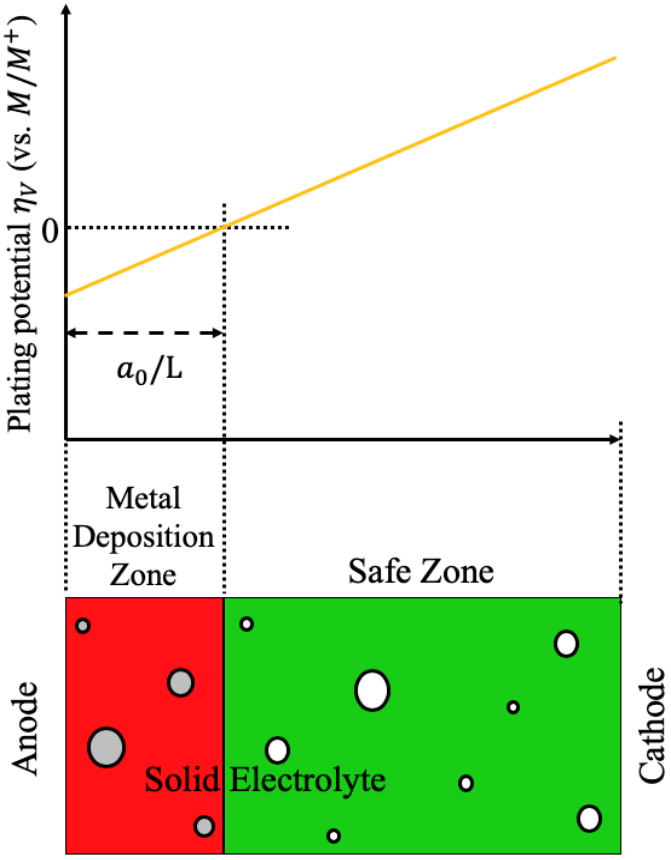

Figure 54. Schematic illustration of the metal deposition in voids of the solid electrolyte.

Patents/Publications/Presentations

The project has no patents, publications, or presentations to report this quarter.

Task 3.4 – Characterization and Modeling of Li-Metal Batteries: Force Field Theory and Lithium-Sulfur Battery Simulations
(Lin-Wang Wang, Lawrence Berkeley National Laboratory)

Project Objective. The project objective is to develop force field (FF) based on *ab initio* calculations to study Li-S cathode and lithium LE. It also includes designs for Li-S cathode systems for high gravimetric and volumetric capacities. Lithium diffusion in both LE in a confined space and in Li-S cathode systems is a main focus of this project. To enable calculation of large systems, ML-FF trained on *ab initio* calculation data will also be developed. The success of this new approach will greatly expand the capability of theoretical simulation for battery systems. ML-FF can also be used in combination with traditional classical FF to deal with the nonreactive parts of the system.

Project Impact. Making the Li-S battery a commercial reality will have a major impact on society and also help to realize the VTO goal of 500 km per charge for EV. However, the nature of chemical reaction makes it different from the traditional intercalation-based Li-ion battery. The molecular nature of Li_2S_n also allows solvation in the electrolyte. To address these problems, it is essential to have fundamental studies and understandings of the underlying mechanisms. Theoretical simulations can play an important role in discovering and designing new cathode materials. However, traditional *ab initio* calculations are limited by their computational size, while the classical FF simulations are limited by their accuracy and the lack of adequate FF. The development of ML-FF can overcome these problems by bridging the size gap between the *ab initio* simulation and the real systems that need to be studied.

Approach. ML-FF will be developed by first running *ab initio* simulations, which can generate hundreds of thousands of datasets. The project has a unique capability of decomposing the total energy of a DFT calculation into the energy of each atom. Compared to conventional DFT calculations, this increases the number of data by hundreds of times, an important requirement for ML model training. The dependence of the atomic energy to the local atomic bonding environment will be captured using ML methods. Three ML approaches will be: linear fitting; neural network (NN) model; and Gaussian process regression (GPR) model. The team will compare the efficacies of these models. Meanwhile, they will also deal with the long-range Coulomb interactions existing in the electrolyte system and the ionic species in LE. The idea is to first fit the charge density of the system and also remove the long-range electrostatic energy before the fitting of the local energy on each atom. The team will design new Li-S and Na-S cathode materials. In particular, they will design an amorphous Li-S mixture, with other materials such as carbon nanotube (CNT), black carbon, or electric conductive 2D materials.

Out-Year Goals. In outgoing years, the project will further develop computational methods for more accurate entropy and interaction energy calculations for the electrolyte, as well as for Li-S cathode systems.

Collaborations. The project will collaborate with G. Liu and Y. Cui for cathode design. It has also collaborated with F. Pan of Beijing University for lithium battery research in general.

Milestones

1. Lithium charge density fitting in electrolyte, to fit the long-range Coulomb interaction. (Q1, FY 2021; Initiated)
2. Study of electrolyte behaviors, including their stability problems. (Q2, FY 2021; In progress)
3. Incorporation of Coulomb interaction in the local energy calculation; ML-FF fitting. (Q3, FY 2021; In progress)
4. Further study of Li-S cathode with polymer, to study electric conductivity in such a system. (Q4, FY 2021; In progress)

Progress Report

The team has developed a special ML-FF for lithium electrolyte: EC and DEC molecules. The challenge is to describe the non-bonding interactions between the molecules. The non-bonding interactions include electrostatic potential interaction, exchange interaction due to charge overlap, repulsing due to Pauli exclusion principle, as well as van der Waals (vdW) interactions. The conventional ML-FF is good in terms of describing the valence bonding system, but it is difficult to describe the nonbonding interaction that could be long range. The team has thus developed a method that fits the electron charge density explicitly. They call this density-based ML-FF. The idea is to use this explicit charge density to describe the inter-molecule nonbonding interaction, while using ML-FF to describe the force and energy within one molecule. Figure 55 shows the fitted charge density for the DEC molecule. Spherical charges around each atom are used to fit the DFT-calculated charge density. As seen, accurate charge density can be obtained, for both the regions with small charge density (important to exchange interaction) and the regions with large charge density (important for Pauli exclusion principle repulsion). Figure 56 shows the ML-FF fitted intra-molecule force and energy, which is also rather accurate. Lastly, to describe the intermolecular nonbonding interaction, the team has summed the charge densities from the molecules to form the charge density of the whole system, and then uses Poisson equation to describe the electrostatic interaction, DFT functional to describe the exchange correlation energy, and Thomas Fermi approximation to describe the kinetic energy. One of the resulting nonbonding interactions is shown in Figure 57. This shows that the density-based ML-FF can describe the nonbonding interaction accurately. In subsequent study, they plan to carry out MD simulations for the density-based ML-FF model to see how accurately it can be used to describe the binding energies, as well as the molecule diffusion. They would also like to add the Li^+ and PF_6^- ions in the system. They plan to develop a polarization model to describe the response of the charge density under external electric field.

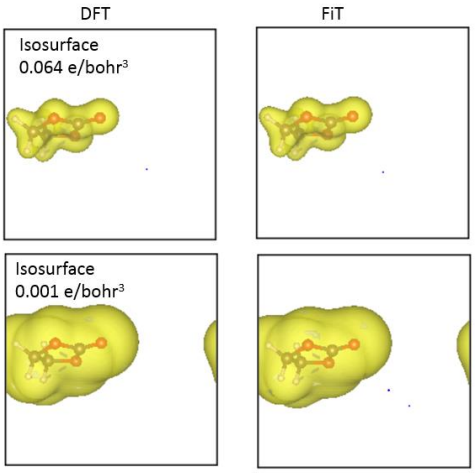

Figure 55. Comparison between the density functional theory calculated electron charge density and the fit charge density at different isosurface values.

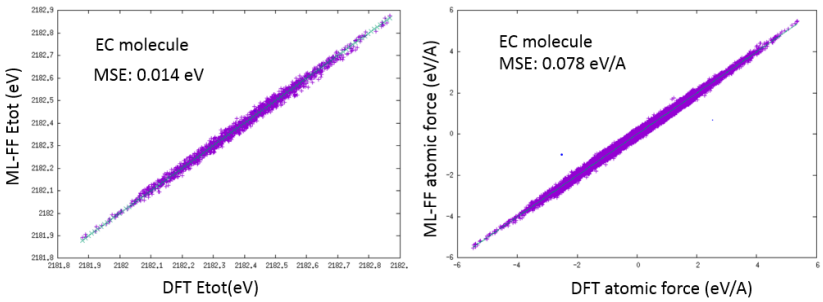

Figure 56. The intra-molecule total energy (left) and force (right) for an EC molecule using a linear fitting machine learning – force field model.

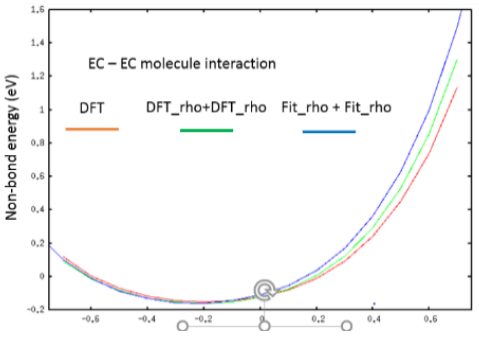

Figure 57. The nonbonding interaction energy between two EC molecules moving past each other, calculated directly with density functional theory (red), modeled with density functional theory molecular charge density (green), and the fit charge density (blue).

Patents/Publications/Presentations

The project has no patents, publications, or presentations to report this quarter.

Task 3.5 – *In Situ* and *Operando* Thermal Diagnostics of Buried Interfaces in Beyond Lithium-Ion Cells
(Ravi Prasher, Lawrence Berkeley National Laboratory)

Project Objective. Transport at various interfaces in *beyond lithium ion* cells will play a major role in electrochemical performance and reliability. It has not yet been possible to thermally profile a Li-metal cell during operation to provide a spatially resolved map of thermal transport properties throughout the cell. The objective of this research is to create a metrology capable of spatially resolved *in operando* thermal property profiling, and then to relate thermal property to the quality of electrodes and interfaces, and to use the developed thermal metrology to understand electrochemical processes in Li-metal batteries, such as dendrite growth, interface kinetics, and ionic transport.

Project Impact. Characterizing electrochemical processes in Li-metal cells such as lithium deposition and dendrite growth at interfaces is of great significance for understanding and enhancing their electrochemical performance and reliability. *In situ* and *operando* micro electrothermal sensors can provide significant information regarding the impact of buried interfaces as a function of time, material, voltage, current, temperature, etc. Therefore, it is important to develop *operando* micro electrothermal sensors and develop models relating those signals to electrochemical performance for *beyond lithium ion* cells. The physics-based model relating thermal and electrochemical properties based on these measurements can facilitate future design of Li-metal batteries.

Approach. To accomplish project goals, the team will utilize an in-house adapted 3-omega (3ω) technique to probe thermal properties of a Li-metal cell while it is in operation, without affecting the operation of the cell. The 3ω sensors will be deposited and fabricated on Li-metal cells based on previous learning on 3ω sensor fabrication. The characteristic depth of the thermally probed region is defined by the wave's "thermal penetration depth," $\delta_p = \sqrt{D/2\omega}$, where D is the sample's thermal diffusivity, and 2ω is the heating frequency of the thermal wave. By depositing the project's 3ω sensors on the battery's outer surface and adjusting ω, the team controls δ_p to span the full range from the top to the bottom layer, thereby noninvasively probing the thermal transport in subsurface layers and interfaces within the bulk of the battery. Thermal transport can be related to quality of the interfaces. By doing concurrent thermal transport and electrochemical performance measurements, the team plans to relate thermal transport to electrochemical performance. As frequency-based thermal measurement techniques provide excellent spatial resolution within the cell, the team also plans to study heat generation at the electrolyte – Li-metal interface and to relate the thermal signals to the interface kinetics and ionic transport. The frequency dependence of heat generated due to transport resistance is different from that due to kinetic resistance. The team plans to utilize this difference to separate the contributions of kinetic and transport resistance at the interface, which will enable understanding of interface kinetics and transport at the Li-metal – SSE interface.

Out-Year Goals. The project will design, build, and implement the adapted 3ω metrology to examine thermal properties and a general frequency-dependent thermal metrology to examine heat generation. This will involve developing and testing the metrology itself along with accompanying theory, designing compatible battery samples, and applying the technique to live cells. The team will measure thermal transport properties of battery materials provided by collaborators. Combined with the electrochemical performance measurement, this will provide significant information relating the thermal signal to the electrochemical process.

Collaborations. This project collaborates with two LBNL groups: V. Battaglia's for cell assembly for 3ω studies, and R. Kostecki's for pristine battery active material growths for studies of thermal signals related to electrochemical process.

Milestones

1. Completed iteration of electrothermal sensor design. (Q1, FY 2021; Completed)
2. Fabrication of Li-symmetric test cells with incorporated electrothermal sensors. (Q2, FY 2021; Completed)
3. Sensitivity analysis and sample design optimization to maximize measurement sensitivity to target electrochemical properties. (Q3, FY 2021; In progress)
4. Baseline impedance spectroscopy of cells for ion and electron mobility. (Q4, FY 2021)

Progress Report

This quarter, the team started assembling Li-symmetric cells with 3ω sensors and has carried out 3ω measurements to isolate the thermal interface resistance, which can then be related to the lithium morphology at the lithium-SSE interface. The symmetric cell consists of LLZO electrolyte with 100 µm of lithium foil on both sides, followed by 50-µm thick current collectors. One of the current collectors is coated with an electrical insulation layer consisting of 500 nm of alumina, 400 nm of parylene, and 200 nm of alumina; a 3ω sensor is deposited on top of the alumina layer. The schematic and the actual symmetric cell consisting of the 3ω sensor are shown in Figure 58.

(a) (b)

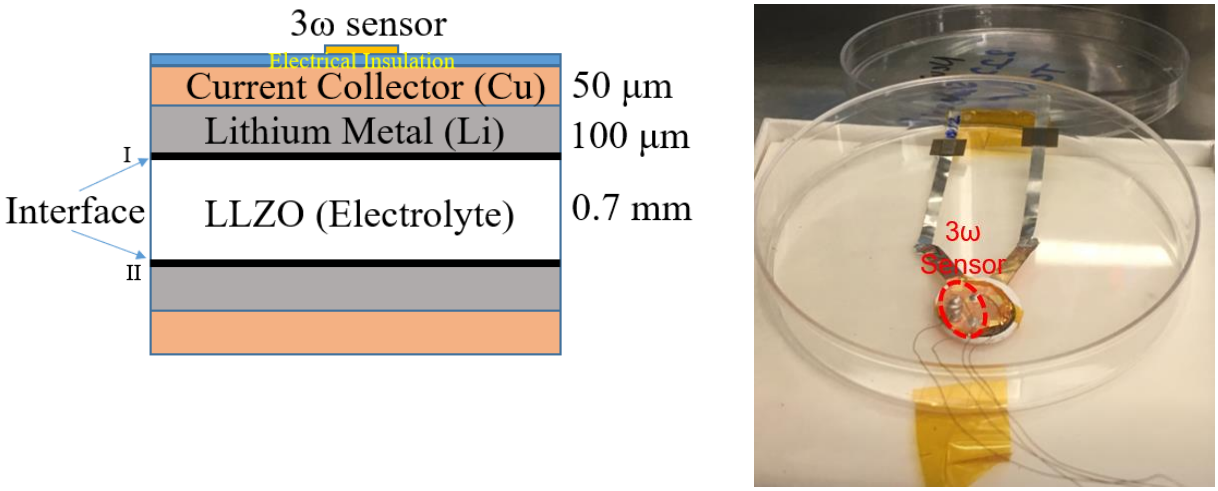

Figure 58. (a) Schematic of the lithium symmetric cell with 3ω sensor. (b) An actual symmetric cell assembled with an integrated 3ω sensor.

The raw 3ω signal for a symmetric cell and corresponding EIS for the same cell are shown in Figure 59a-b, respectively. From EIS, the electrical interface resistance for the cell is determined to be 6.05 kΩ, and from 3ω, the thermal interface resistance is determined to be 10^{-4} m^2K/W. The team plans to cycle this cell and perform subsequent EIS and 3ω measurements to track how interface resistance (both electrical and thermal) changes with the number of cycles.

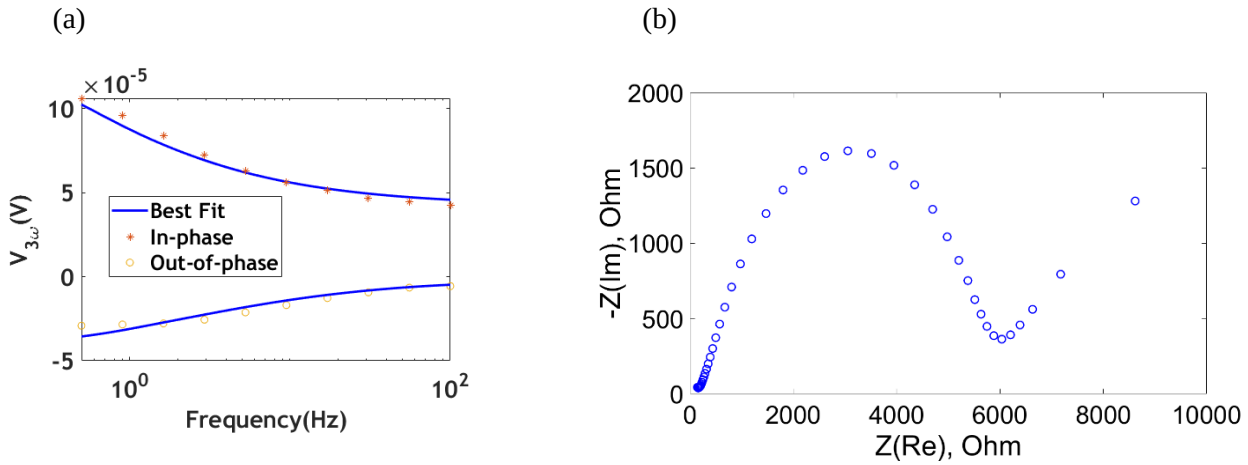

Figure 59. (a) Raw 3ω data and the best fit curve obtained for thermal interface resistance of 10^{-4} m^2K/W for the Li-LLZO interface. (b) Nyquist plot obtained from electrochemical impedance spectroscopy.

This quarter, the team also completed fabricating and characterizing the temperature coefficient of resistance (TCR) of 20 3ω sensors on the current collectors. A representative Resistance versus Temperature plot for a 3ω sensor is shown in Figure 60. These calibrated sensors will be used for making 20 cells, all of which will either have different electrolyte surface roughness or will be cycled at a different C-rate. The comparative study of thermal interface resistance change in these 20 cells will be used to correlate the effect of the electrolyte surface roughness or the charge/discharge condition on the evolution of the lithium-SSE interface.

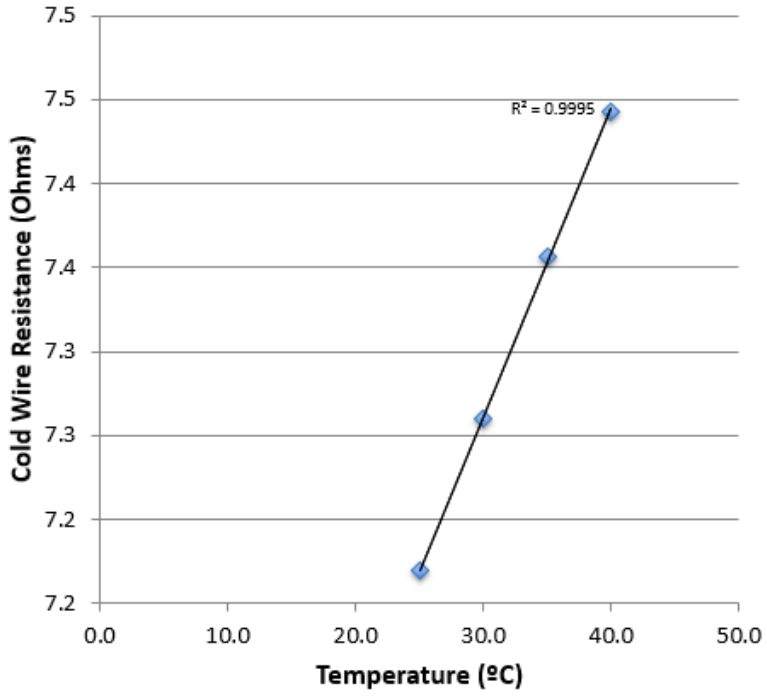

Figure 60. Resistance versus Temperature plot for a 3ω sensor. From the measurement, the cold wire resistance for the particular sensor was determined to be 7.2 Ω, and the temperature coefficient of resistance (TCR) was determined to be 0.018 Ω/K.

Patents/Publications/Presentations

The project has no patents, publications, or presentations to report this quarter.

Task 3.6 – Multi-Scale Modeling of Solid-State Electrolytes for Next-Generation Lithium Batteries (Anh Ngo, Larry A. Curtiss, and Venkat Srinivasan, Argonne National Laboratory)

Project Objective. This project is part of a multi-scale modeling effort to obtain an in-depth understanding of the interaction of the electrode and the SE aimed at developing highly efficient SSE batteries for vehicle applications. Input parameters needed for mesoscale (continuum) level calculations are being obtained from atomistic calculations including DFT and classical MD simulations. This atomistic input will enable a multi-scale computational procedure for SSEs that is capable of successfully capturing the physicochemical aspects during charge and discharge process, including lithium transport mechanisms, interfacial phenomena during the insertion and extraction of lithium ions, and mechanical deformation of SSE.

Project Impact. A major safety concern experienced with commercially available Li-ion batteries under some scenarios is leakage of the LE, which can potentially catch fire. Replacement of the LE is necessary to decrease the fire hazard and improve safety associated with present-day Li-ion batteries. In addition, use of SEs provides a path to prevent dendrites in Li-metal anodes, thereby leading to batteries with significantly higher energy density. The impact of this project will be to help in development of good SSEs as a replacement for the commercially used organic LEs to improve safety and energy density in Li-ion batteries.

Approach. Parameters needed for mesoscale modeling of grain interior (GI), GB, and electrode-electrolyte interface will be calculated by DFT-based calculations along with Monte Carlo (MC) and MD simulations. The calculations will be used to determine properties of the electrode with the SE as well as in GB regions of the SE. This will include calculations of structure, stability, ionic conductivity, Young's modulus, fracture toughness, exchange current density, and other properties.

Out-Year Goals. The out-year goals of this work are to calculate other properties such as fracture toughness and include other SSEs and coatings in the multi-scale modeling.

Collaborations. This project collaborates with Y. Cui at Stanford University.

Milestones

1. Determine stable surface of the Li_6PS_5Cl SSE and the NMC-811/Li_6PS_5Cl interface. (Q1, FY 2021; Completed)
2. Conduct AIMD study of electrochemical interface between NMC-811/Li_6PS_5Cl. (Q2, FY 2021; Completed)
3. Investigate Li-ion transport of the NMC-811/Li_6PS_5Cl interface, and calculate exchange current density. (Q3, FY 2021; Initiated)
4. Incorporate information obtained from the atomistic calculations into the mesoscale model, and predict the impact of performance. (Q4, FY 2021; Initiated)

Progress Report

SEs are expected to stabilize Li-metal anodes due to higher stiffness than lithium, which can effectively suppress propagation of dendrites. A combination of SEs with Li-metal anodes can also improve the volumetric energy density of commercially used Li-ion batteries, as well as improve the safety issues associated with them. Oxide SEs with garnet (LLZO) or NASICON (LATP) structure show extremely high elastic modulus (~ 150 GPa), which makes these solid ionic conductors non-conformable and decreases the electrochemically active surface area associated with the non-uniform Li-metal anode. On the other hand, sulfide-based SEs (LGPS, LPS) are mechanically softer (~ 20 GPa) and can potentially maintain better contact with the metal anode. These sulfide electrolytes also demonstrate better ionic conductivities (~ 1mS/cm or higher) than the oxides (~ 0.1 mS/cm). In this research, the team will investigate the sulfide-based SE Li_6PS_5Cl, which has an argyrodite type crystal structure. Being a sulfide, it shows significantly enhanced ionic conductivities (~ 2.5 mS/cm) under room temperature conditions, and the elastic modulus of this material is ~ 22 GPa. The inherent softness of Li_6PS_5Cl enables the cold sintering of these materials with layered oxide cathodes, which effectively avoids many cathode/electrolyte side reactions. During processing, cathode/electrolyte side reactions at elevated temperatures are a major issue for several oxide-based SEs (such as NMC/LLZO).

In spite of these advantages, sulfide SEs demonstrate poor interfacial stability with both Li-metal anode and layered oxide cathodes, which leads to continuous capacity fade and performance decay with cycles. The major problems faced by the Li_6PS_5Cl electrolyte located adjacent to the cathode active materials are as follows:

- Interdiffusion of TM (nickel, cobalt, and manganese), phosphorus and sulfur ions, and formation of a highly resistive CEI layer. Some experimental studies reveal possible formation of phosphates (PO_4^{3-}) and sulfates (SO_4^{2-}), which can potentially increase interfacial resistance.
- Formation of a space charge near the CEI due to strong attraction between lithium from electrolytes and oxygen from the cathode materials. Such a space charge layer can effectively increase interfacial resistance at the CEI.
- Oxidation and reduction of Li_6PS_5Cl itself during charge and discharge processes can substantially minimize effectiveness of the SE. For example, during charge, the SE can oxidize to LiCl, P_2S_5, and elemental sulfur. These side reactions can occur wherever there is a flow of electron.

  $$2Li_6PS_5Cl \rightarrow 2LiCl + P_2S_5 + 5S + 10Li^+ + 10e^- \quad (1)$$

  Such side reactions are usually irreversible in nature because the conventional cathode cells are never operated at potentials where reduction of these side products occur (sulfur and phosphorus reduce at 2 V and 1 V, respectively). Such undesired side reactions may lead to very high first-charge capacities with Li_6PS_5Cl SEs, but are never achieved later, not even the first discharge.

The first two phenomena mentioned above work to enhance the interfacial charge transfer resistance, which in turn aggravates the delamination-induced capacity fade. The third phenomena alters the bulk structure of the Li_6PS_5Cl electrolyte, which can substantially minimize the bulk conductivity of the SE. The influence of these side reactions at the cathode/solid electrolyte interface on overall cell performance is investigated in this study. Strategies to mitigate these issues through application of interphase layers will be studied using multi-scale modeling. Multi-scale modeling can provide insight into the mechanism for dendrite growth and other instabilities for guidance into how to prevent them. Mesoscale (continuum) modeling requires atomistic level input from theory or experiment to accurately capture physicochemical aspects during charge and discharge processes.

The team has carried out *ab initio* density functional calculations on Li_6PS_5Cl (LPSCl) interfaces with an NMC-811 cathode to determine its interfacial structure. They investigated the (10-14) surface of NMC-811, which is known to be the most stable surface. In addition, in previous literature this surface was reported to provide apparent Li-ion conduction paths, an important aspect in understanding the interface conduction with SSE.

They have also studied the dynamics of the NMC/LPSCl interface by carrying out AIMD simulations. From these simulations, they calculated the lithium mean square displacements (MSD) in LPSCl and NMC, as well as the corresponding diffusion coefficients (D) of lithium in these two materials at T = 500 K. The results of the simulations reveal that the diffusion coefficients of lithium atom in LPSCl and NMC are 2.87 x 10^{-5} cm^2/s and 0.77 x 10^{-5} cm^2/s, respectively. This suggests that there will be a significantly smaller migration barrier of the lithium within the LPSCL than NMC. A summary of the MSD results is shown in Figure 61. The team is performing AIMD at different temperatures to determine the effect on the results. The calculated structure of the interface and the Li-ion migration barrier will be used for calculation of exchange current density. The exchange current densities obtained from these first-principles calculations will be used as input for continuum-level modeling of the LPSCl/NMC-811 interface. The continuum-level modeling will provide insight into the interfacial resistance at the CEI.

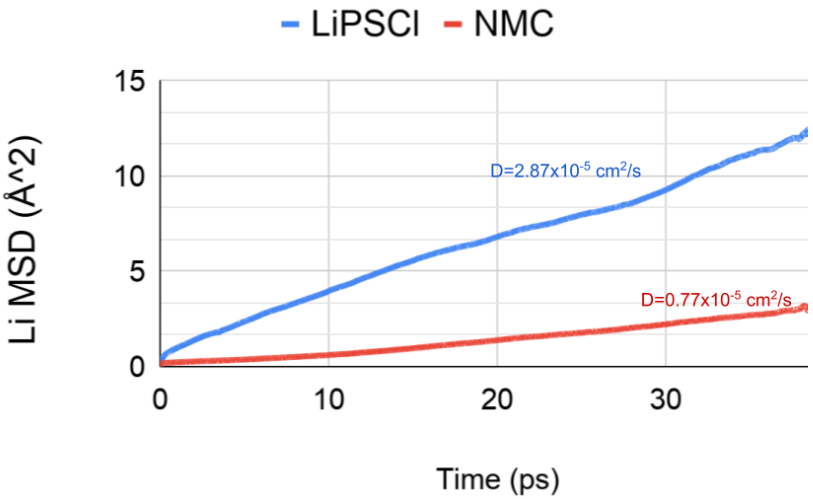

Figure 61. Lithium mean squared displacement (MSD) and diffusion coefficients (D) at T = 500 K obtained from the project's *ab initio* molecular dynamics simulations in NMC and Li_6PS_5Cl.

Patents/Publications/Presentations

The project has no patents, publications, or presentations to report this quarter.

Task 3.7 – Integrated Multi-Scale Modeling for Design of Robust 3D Solid-State Lithium Batteries (Brandon Wood, Lawence Livermore National Laboratory)

Project Objective. This project will develop a multi-scale, multi-physics modeling framework for probing the effects of materials microstructure and device architecture on ion transport within 3D ceramic SSB materials, with the goal of enhancing performance and reliability. The project has three primary objectives: (1) integrate multi-physics and multi-scale model components; (2) understand interface- and microstructure-derived limitations on ion transport; and (3) derive key structure-performance relations for enabling future optimization.

Project Impact. This project will lead to understanding interfacial losses and instabilities that impede performance and promote failure of SSBs. The multi-scale and multi-physics modeling framework developed in this work will address shortcomings of existing modeling strategies that either lack coupling of the multi-physics nature of various processes active in 3D batteries or fail to incorporate processes at different length scales to understand function. Ultimately, the tools and understanding generated by this project can be utilized to realize optimization of interface-dominated 3D batteries.

Approach. The project approach integrates simulations at three scales to predict ion transport limitations within the ceramic SSE LLZO, as well as across the interface between LLZO and $LiCoO_2$ (LCO) cathodes. A particular focus is on understanding the effects of microstructures and architectures resulting from processing of 3D SSBs as well as their mechanical and chemical evolution at different stages of cycling. First-principles and classical MD simulations are used to compute fundamental Li-ion diffusion within bulk SE and cathode materials, along/across GBs of the electrolyte, and along/across electrolyte/cathode interfaces. Next, phase-field simulations are used to generate digital representation of realistic microstructures of the materials, which are combined with the atomistic simulation results to parameterize mesoscale effective property calculations and to establish microstructure-property relationships for ion transport. Finally, these relationships inform a cell-level macroscopic electro-chemo-mechanical modeling framework, which can be used to optimize performance of ceramic 3D SSLBs based on LLZO SEs.

Out-Year Goals. Future activities will focus on applying potentials capable of scaling the atomistic interface diffusion models to longer timescales. The team will also work with collaboration partners to reconstruct microstructures of 3D-printed materials and apply them to determine effective stresses and ion transport through the polycrystalline materials. They will also further develop and validate the EIS models for connection to macroscale observables, including implementation of space-charge contributions near interfaces.

Collaborations. This project collaborates with N. Adelstein from San Francisco State University on atomistic diffusion modeling, and J. Ye from LLNL on 3D printing of SSB materials. They also partner with T. Danner and A. Latz from Deutsches Zentrum für Luft- und Raumfaurt (DLR) on impedance modeling and electro-chemo-mechanical interface models, with P. Zapol from ANL on modeling of interfaces in LLZO, and with D. Fattakhova-Rohlfing from Forschungszentrum Jülich (FZJ) and E. Wachsman from UMD on properties of LLZO with varying densities and microstructures as part of the U. S.–Germany partnership on SSB research.

Milestones

1. Demonstrate microstructural model of stress effect on ion transport. (Q1, FY 2021; Completed)
2. Compute barriers for ion transport across LCO/LLZO interface. (Q2, FY 2021; In progress)
3. Integrate polycrystalline diffusion model with EIS simulations. (Q3, FY 2021; In progress)
4. Demonstrate full multi-scale EIS model using ion transport simulations of CEIs. (Q4, FY 2021; On schedule)

Progress Report

Machine-Learning Interatomic Potentials for Accelerated Atomistic Simulations of Interfaces. Although quantum simulations of the cathode-electrolyte and internal electrolyte interfaces are continuing, obtaining transport information requires long and large simulations that are computationally demanding. As such, in this quarter, the team pursued a new effort to accelerate these simulations by developing interatomic potentials that can retain quantum accuracy with reduced computational expense. Specifically, they have been working on the improvement of ML interatomic potentials for pure and doped LLZO internal interfaces. Their ML model is based on artificial neural network (ANN) with a 20-10 hidden-layer architecture and the Chebyshev polynomial representations of local atomic environment. For pure crystalline LLZO, current ML model predicts the lattice constant of 13.034 Å (expt. 13.004 Å), lithium transport (see Figure 62) with an activation anergy of 0.33 eV (expt. ~ 0.3 eV) and diffusivity of 7.1×10^{-7} cm^2/s at 1000 K (comparable with previous simulations using classical potentials and *ab initio* methods). Based on a similar approach, the team is collecting training data for the Al-doped LLZO system to predict lithium diffusivity as a function of doping level and at different temperatures. The results will be used to parameterize the mesoscale models to predict microstructure-dependent Li-ion diffusivity. The prediction will then be directly compared with experiments through the ongoing U. S.–Germany collaboration on cathode/solid electrolyte interfaces.

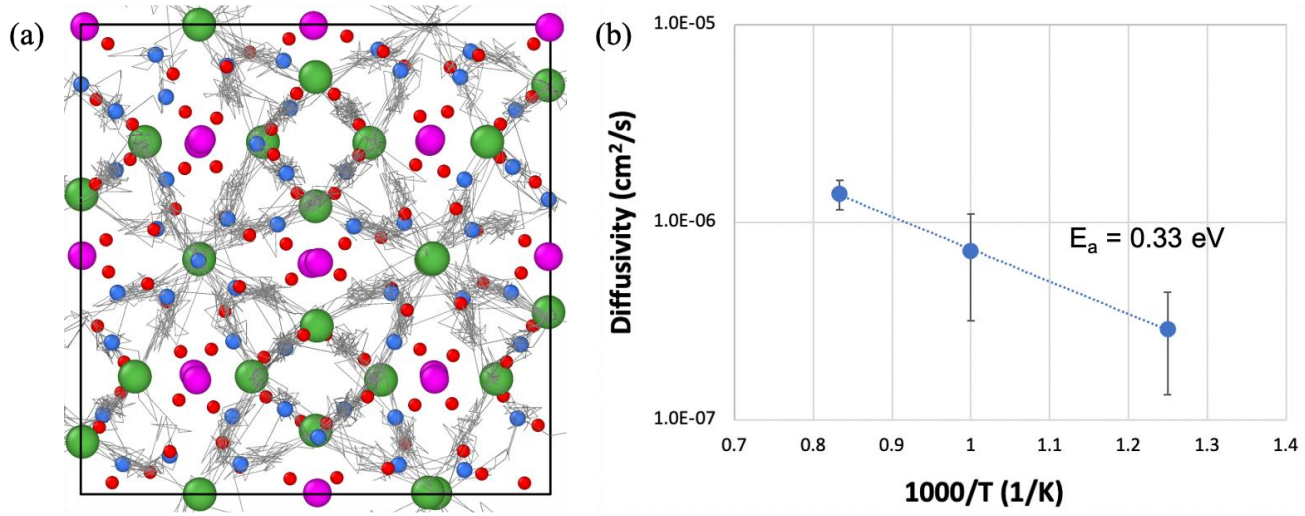

Figure 62. Li-ion diffusion predicted from machine-learning interatomic potentials for cubic LLZO. (a) Li-ion diffusion trajectory at 1200ºC. (b) Extracted Arrhenius plot.

Modeling of Microstructural Effects on Lithium Transport and EIS. In previous quarters, the team reported development of mesoscale models for predicting (1) microstructural impacts on Li-ionic transport, and (2) microstructural impacts on local mechanical stress concentrations in LLZO. This quarter, they completed integration of the two models within their simulation code framework, fulfilling the project's FY 2021 Q1 milestone. The team is performing simulations of mechanical stress effects on the Li-ionic transport in polycrystalline LLZO, the results of which will be reported next quarter.

The team is also progressing on the framework for EIS modeling, which more closely connects the experimental and simulation efforts. This framework will be used within the U. S.–Germany collaboration to aid analysis of grain and GB contributions to ionic conductivity as a function of processing conditions. Last quarter, they reported their mesoscale modeling efforts on lithium GB segregations and corresponding space charge and electrical potential distribution in polycrystalline SEs. This quarter, they extended the model to predict the EIS spectra of SEs that show GB space charge phenomena. The model was tested by considering initial Li^+ concentrations of 0.5 and 0.75 M for the grain and the GB, respectively, with Li^+ diffusivities (10^{-10} m^2/s)

that are twice as fast in the grain compared with the GB (0.5×10^{-10} m^2/s). Figure 63 shows the Li^+ ion concentration distribution and the corresponding voltage in a sample polycrystal. Two cases are compared in the figure: the model polycrystalline electrolyte in the top row has twice the GB diffusivity compared with the bottom row. Figure 63d thus shows higher segregation effects and larger potential gradients across the GB when compared to Figure 63a due to its lower GB diffusivity. The space charge density distribution follows the concentration distribution through the relation $\rho = zF(c_{Li^+} - c^{\circ}_{Li^+})$. Here, the inclusion of space charge segregation in the GB leads to an increase in the overall predicted impedance (specifically the imaginary component of the impedance). This ion transport and EIS prediction model has been developed with an in-house phase field modeling framework and is being further refined prior to full application.

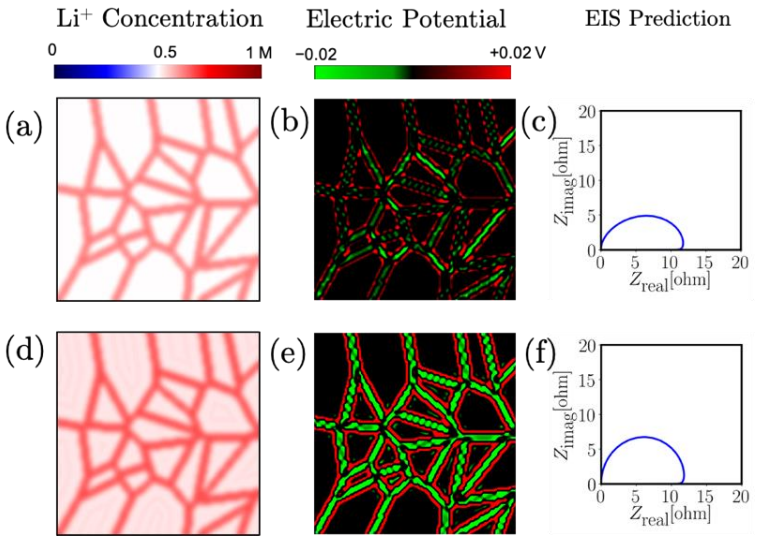

Figure 63. Effect of space charge on electrochemical impedance spectroscopy. The polycrystal considered in the top row has twice the grain boundary diffusivity compared to the one in the bottom row. The polycrystal in the bottom row thus shows higher Li-ion segregation in the grain boundary region [inset (d) compared to inset (a)], higher potential gradients across the grain boundary region [inset (e) compared to inset (b)], which leads to increased impedance [inset (f) compared to inset (c)].

Patents/Publications/Presentations

The project has no patents, publications, or presentations to report this quarter.

Task 3.8 – First-Principles Modeling of Cluster-Based Solid Electrolytes (Puru Jena, Virginia Commonwealth University)

Project Objective. The objective of the project is to use cluster-ions, which are stable atomic clusters that mimic the chemistry of individual atoms, as the building blocks of new SEs for Li-ion batteries and the corresponding battery system. The advantages of using cluster-ions to replace elemental ions is that the size, shape, and composition of the former can be tailored to achieve higher superionic conductivity, electrochemical stability, and charge transfer across the SSIs than the conventional materials. More specifically, the goal is to develop superior SEs based on cluster-ions and to model these SEs and their interfaces with electrodes, especially with the Li-metal anode, for successful integration into high-performance SSBs for EVs. The team will model and screen cluster-based SEs that, compared to conventional SEs, have low activation energies, practical room-temperature ionic conductivities, wide electrochemical stability windows, and desired mechanical properties that, for example, can inhibit the Li-metal anode dendrite growth. They will provide a fundamental understanding of the ionic conduction mechanism in the newly developed, cluster-based SEs and identify means to further improve property metrics via chemical and defect engineering. The team will model the interfacial properties, such as the structural, chemical, electrochemical, and ion/charge transfer properties, between the cluster-based SEs and electrodes at the atomic level, as well as find the interfacial coating materials with desired properties. Based on accumulated data from modeling, they will establish links between the basic parameters of the cluster-ions and the bulk/interface properties, which can directly guide experiments. Meanwhile, the team will work closely with experimentalists in the BMR Program to complement the project's theoretical efforts and to guide them in focused development of the predicted cluster-based SEs and the interfaces.

Project Impact. The proposed project will open a new avenue for guiding experiments in the synthesis of SSBs equipped with cluster-based SEs and capable of operating over a wide temperature range. Modeling and understanding of the ionic conduction of cluster-based electrolytes and their interfacial properties with electrodes, especially with Li-metal anode, will enrich current battery science and also train the future workforce in SSB development for next-generation EVs by supporting postdoctoral fellows.

Approach. This project will employ multi-scale theoretical methods and computational techniques.

Out-Year Goals. The out-year goals involve modeling development of new cluster-based SE materials and database.

Collaborations. The team is working with J. Nanda of ORNL on SEs.

Milestones

1. Complete development of new cluster-based SE materials with a database. (Q4, FY 2021; Completed)
2. Structural studies of the chemically mixed systems containing both cluster-ions and elemental ions. (Q2, FY 2021; Completed)
3. Characterizations of the chemically mixed systems. (Q3, FY 2021; In progress)
4. Cation doping in the cluster-based SE systems. (Q4, FY 2021)

Progress Report

Research toward this quarter's milestone is completed as planned. The structures of the cluster-based SE materials with different halogen-substitution concentrations have been identified based on the electrostatic model. Given a specified concentration of halogen in the supercell of a material, all possible substitutional configurations in the range of 0 to 100% with a 12.5% step size are considered. The total energy of each configuration is computed, and the lowest-energy structure is identified.

To demonstrate, Figure 64 shows the results of one typical case in the team's study. The charge states of different atomic species in the cell are calculated using the Bader charge analysis. The total CE of the periodic system is computed using the point charges and the Ewald method. The lowest CE is increasing with the increase of the halogen concentration in the system (Figure 64a). Figure 64b shows the density of states of all possible substitutional configurations for a halogen concentration of 50%. The configurations in the lowest-energy peak are of interest for further detailed studies. Figure 64c shows the lowest-energy structure containing both the cluster-ions and the halogens.

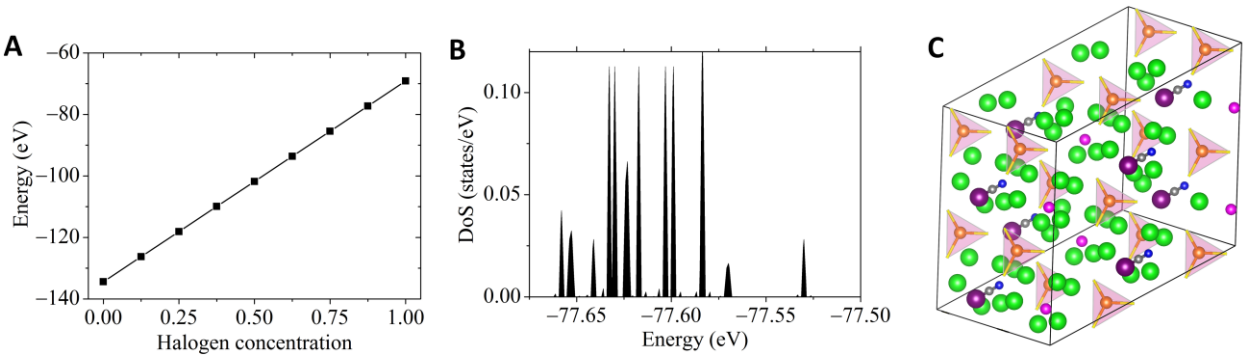

Figure 64. Demonstration of the chemically mixed systems in the study. (a) The calculated lowest Coulombic energies at different halogen substitution concentrations at 0, 12.5, 25, 37.5, 50, 62.5, 75, 87.5, and 100%. (b) Calculated density of states by considering all possible configurations with the halogen concentration of 50%. The structures in the lowest-energy peak are those of interest for further characterizations. (c) The identified crystal structure according to the electrostatic model. The structure contains two types of cluster-ions, with one in rod shape and the other in tetrahedron. Fifty percent of the rod-like cluster-ions are replaced by halogen (in magenta). Li-ions are in green.

A program is developed to automate the following procedure. First, for certain substitution concentration, possible combinations of different cluster sites in a 2 × 2 × 2 cell are identified. Second, the atoms in the cluster-ions in the cell are identified. Third, each combination of the cluster-ions is replaced by the halogen atoms. Fourth, the CE of the substituted periodic system is computed, and the lowest-energy structures are identified. Based on these results, further characterizations of the chemically-mixed structures, including the ionic conductivity, are in progress as planned.

Patents/Publications/Presentations

The project has no patents, publications, or presentations to report this quarter.

Task 3.9 – Predictive Engineering of Interfaces and Cathodes for High-Performance All-Solid-State Lithium-Sulfur Batteries
(Badri Narayanan, University of Louisville)

Project Objective. The primary goal of this project is to leverage data-driven methods and ML strategies to develop accurate multi-physics models for all-solid-state Li-S battery materials that can capture electrochemical and transport phenomena over atomic-to-mesoscopic length/timescales; these models will be rigorously validated by synthesis and advanced characterization experiments. The team will leverage the predictive power of these models, alongside synthesis/characterization experiments and battery fabrication to address longstanding issues at the electrode/electrolyte interfaces in all-solid-state Li-S batteries. The project's proposed technology involves the following: (1) halide-doped solid sulfide electrolytes that can concurrently provide high Li^+ ion conductivity and suppress dendrite growth; (2) novel mesoporous cathode composed of interconnected carbon nano-cages co-infiltrated with sulfur and sulfide electrolyte, which hold potential to allow high sulfur loading and optimal ion/electron pathways; and (3) functionalization of sulfide electrolyte with ILs to improve physical contact and minimize impedance at the CEI.

Project Impact. All-solid-state Li-S batteries remain far from commercialization due to poor understanding of fundamental electrochemical/chemical and transport processes that occur at the interfaces, especially at atomic to mesoscopic scales. Successful development of proposed predictive models (at multiple scales) will bridge this knowledge gap and will advance fundamental understanding of reaction chemistry, kinetics, charge transfer, and dendrite growth at electrified SSIs. This will enable predictive design of effective strategies to mitigate interfacial problems in all-solid-state Li-S batteries, including poor interfacial contact, interfacial impedance to Li^+ ion transport, and poor electron/ion conduction within cathodes. Ultimately, the fundamental knowledge gained will lead to development of high-performance all-solid-state Li-S batteries that meet DOE targets of specific energy (350 Wh/kg @C/3), sulfur loading (> 6 mg/cm^2), and high cycle life (1000).

Approach. The project brings together innovative solutions in multi-scale materials modeling, electrolyte synthesis, fabrication of cathode architecture, and electrolyte functionalization to overcome the issues at electrode/electrolyte interfaces in all-solid-state Li-S batteries. The central idea is to employ a data-driven and ML-based approach to develop accurate multi-physics battery models at atomic-to-mesoscopic scales. This approach overcomes critical problems with existing model development methods by foregoing the need for pre-defined functional forms, introducing deep-learning technique to describe reactivity, and employing optimization methods that do not require human intuition. Multi-scale simulations based on the newly developed models will provide insights into electrochemical phenomena at electrode/electrolyte interfaces.

Out-Year Goals. In Year 2, the goal is to gain atomic-scale understanding of interfacial reactions in solid-state Li-S batteries, and to assess the effectiveness of functionalizing CEIs with ILs.

Collaborations. The team collaborates with the groups under A. Ngo and L. A. Curtiss at ANL for quantum simulations of battery systems; they plan to collaborate with J. Nanda at ORNL for advanced spectroscopic *in situ* characterization of interfaces.

Milestones

1. Extend reactive interatomic potential models to include interfaces. (Q1, FY 2021; Completed)
2. Advance characterization of CEIs to understand their reactivity, stability, and structure; validate predictions of reactive interatomic potentials. (Q2, FY 2021; In progress)
3. Utilize reactive MD to gain insights into interfacial processes, and predictively design stable interface with good ion transport. (Q3, FY 2021; In progress)
4. Fabricate batteries that meet interim performance metrics. (Q4, FY 2021; In progress)

Progress Report

This quarter, the team made good progress on (1) gaining atomic-scale understanding of the effect of halide doping on the interfacial reactions between sulfide electrolytes and lithium anode, and (2) fabrication of coin-cell batteries with improved CEIs and spectroscopic characterization.

Atomic-Scale Understanding of Reactions between Halide-Doped Argyrodite SSE and Lithium Anode

To understand the effect of halide doping of argyrodite SSEs on their reactivity toward lithium metal, the team performed AIMD simulations for three electrolyte cases, namely Li_6PS_5F, $Li_6PS_5F_{0.5}Cl_{0.5}$, and Li_6PS_5Cl at 300 K for 20 ps. For all cases, they studied symmetric Li|SSE|Li systems, in which both lithium and SSE are placed such that crystallographic 001 directions are aligned normal to the interface (Figure 65). They employed $1 \times 1 \times 2$ supercell of SSE (001) and slabs of 3×3 lithium (001) slabs containing six layers on each side of the SSE (Figure 65a-c). Note that the as-formed hetero-structure was nearly epitaxial (< 1% strain) for all electrolyte cases. In all cases, the team found that there is extensive mixing of atomic species across the interface owing to the chemical reactions. In particular, regardless of type of halogen doping, ~ 13% of lithium atoms from anode move into the electrolyte; similarly, sulfur and phosphorus atoms from the electrolyte diffuse into the anode. They also observed formation of LiX species at the interface. The average atomic Bader charges on phosphorus and sulfur decrease with time during AIMD simulations, indicating that all three electrolytes undergo reductive decomposition (Figure 65e-f). Consistent with these results, direct observation of the project's AIMD trajectories indeed shows breakdown of PS_4^{3-} tetrahedra along with formation of new Li_xS and Li_xP species. Interestingly, Figure 65e-f shows the average atomic charges decrease the most for the electrolyte co-doped with fluorine and chlorine, that is, $Li_6PS_5F_{0.5}Cl_{0.5}$, followed by the argyrodites with single halogen dopant. This suggests that $Li_6PS_5F_{0.5}Cl_{0.5}$ undergoes the most reductive decomposition. Indeed, careful analysis of the AIMD trajectories indicates formation of ~ 2 times new Li-P, Li-S, and LiX (X = F, Cl) bonds at Li|$Li_6PS_5F_{0.5}Cl_{0.5}$|Li interface as compared to the electrolytes containing a single type of halogen dopant. To gain further understanding into the types of species that form at the interface, the team evaluated the extent of reduction of each phosphorus and sulfur atom in the electrolytes at the end of AIMD run. This is accomplished by comparing their atomic charges (q) with that in the fully reduced states (that is, P: Li_3P; S: Li_2S), and that in the pristine electrolyte (non-reduced state). If the charge on a particular P/S atom at the end of an AIMD run is similar to that in the fully reduced state (that is, P: $q_P < -2.25e$; $q_S < -1.55e$), it is deemed to be part of Li_3P or Li_2S. Similarly, if their charges are still close to those

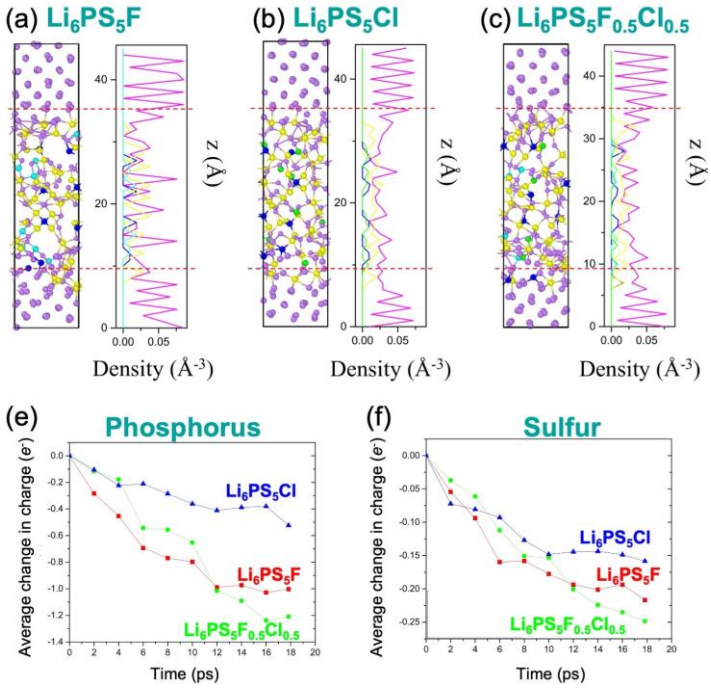

Figure 65. *Ab initio* molecular dynamics simulations of evolution of Li|SSE|Li interface at 300 K. The equilibrated atomic-scale structure of the interface between Li (001) and SSE (001) is shown for three electrolyte compositions, namely (a) Li_6PS_5F, (b) Li_6PS_5Cl, and (c) $Li_6PS_5F_{0.5}Cl_{0.5}$. In panels (a-c), the spatial distribution of lithium (purple), phosphorus (blue), sulfur (yellow), fluorine (cyan), and chlorine (green) atoms (in terms of number density) are shown in the direction normal to the interface. The edges of lithium slab are marked by the dotted red line. Temporal evolution of the average change (e-) in atomic charge on (e) phosphorus, and (f) sulfur is shown for the three electrolytes (red: Li_6PS_5F; blue: Li_6PS_5Cl; and green: $Li_6PS_5F_{0.5}Cl_{0.5}$).

in the pristine electrolyte (P: $q_P > 0.74e$; S: $q_S > -1.25e$), they are considered as unreduced. The team found that the unreduced phosphorus always constituted the PS_4^{3-} tetrahedra that remain intact, while unreduced sulfur atoms could be part of $LiPS_x$ species. All the phosphorus and sulfur atoms whose charges lie somewhere in between are considered as partially reduced. The partially reduced sulfur forms Li_xS, while the partially reduced phosphorus forms $LiPS_x$. The relative population of different reduced states of phosphorus and sulfur in the three electrolytes is shown in Figure 66. It is interesting to note that no Li_3P forms during reductive decomposition of Li_6PS_5Cl. The decomposition products are primarily Li_2S, Li_xS, and $LiPS_x$; these compounds have negligible Li-ion conductivity, suggesting that the $Li|Li_6PS_5Cl$ interface should exhibit high impedance. On the other hand, during decomposition of the F-containing electrolytes, ~ 25% of phosphorus reduces completely, forming Li_3P; additionally, the partially reduced phosphorus forms $LiPS_x$ with the unreduced sulfur, while fully reduced sulfur yields Li_2S (Figure 66). Note that Li_3P has a reasonable Li-ion conductivity of ~ 10 mS/cm, which could reduce the interfacial impedance with lithium anode. These findings are in excellent agreement with the project's EIS data, which shows a much higher impedance for $Li|Li_6PS_5Cl|Li$ (1250 ohm) than $Li|Li_6PS_5F_{0.5}Cl_{0.5}|Li$ (800 ohm) symmetric cells. The $Li|Li_6PS_5F|Li$ cell shows the highest measured impedance (2650 ohm), but this is likely due to the low bulk Li-ion conductivity of Li_6PS_5F, since EIS measures impedance of the whole cell including both interface and bulk components. Furthermore, the chemical reactions (and decomposition products) predicted by AIMD are in good agreement with the XPS results.

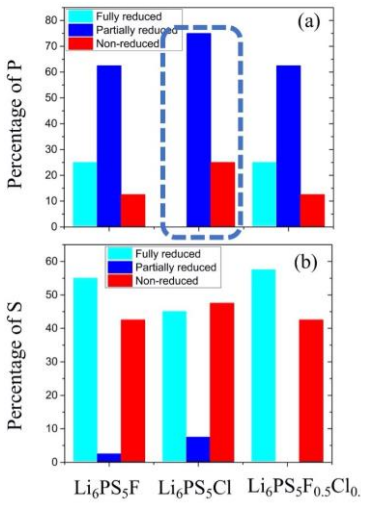

Figure 66. Comparison of the extent of reduction of (a) phosphorus and (b) sulfur atoms during the reductive decomposition of Li_6PS_5F, Li_6PS_5Cl, and $Li_6PS_5F_{0.5}Cl_{0.5}$ solid electrolytes with lithium, as obtained from *ab initio* molecular dynamics simulations.

Battery Fabrication and Spectroscopic Characterization of CEIs

Last quarter, the team showed that interfacial resistance on the cathode side can be reduced significantly by coating a mesoporous carbon cathode (super-P) hosting sulfur with a concentrated solution of LiTFSI salt in N-butyl-N-methyl pyrrolidinium (PYR-14) IL. However, they found that although the IL enhances cycle life of solid-state Li-S batteries (with $Li_6PS_5F_{0.5}Cl_{0.5}$ electrolyte, lithium anode, and Super-P cathode), the initial discharge capacity remains low (~ 600 mAh/g). This is possibly due to the high viscosity of LiTFSI-PYR14 IL, which inhibits reaction kinetics (Figure 67a). To mitigate this issue, the team diluted the LiTFSI-PYR14 with DOL. Indeed, the addition of DOL significantly increases initial discharge capacity to ~ 1100 mA/h (Figure 67b). They systematically analyzed the effect of (1) concentration of LiTFSI, (2) relative fractions of PYR-14 and DOL, and (3) volume of liquid for coating. They found that functionalizing the cathode with a 0.04-mL solution containing 2 M LiTFSI in 1:1 (volume) PYR:DOL gives the most optimal performance with $Li_6PS_5F_{0.5}Cl_{0.5}$ electrolyte, lithium anode, and Super-P cathode (note that they operated under low sulfur loading of ~ 0.7 mg/cm^2). Using half the volume of functionalizing liquid (that is, 0.02 mL) yields similar capacities [~ 1100 mAh/g (cycle 1); ~ 300 mAh/g (cycle 100)] but slightly lowers CE (~ 85% and ~ 90% at 0.02 mL and 0.04 mL liquid, respectively). They also

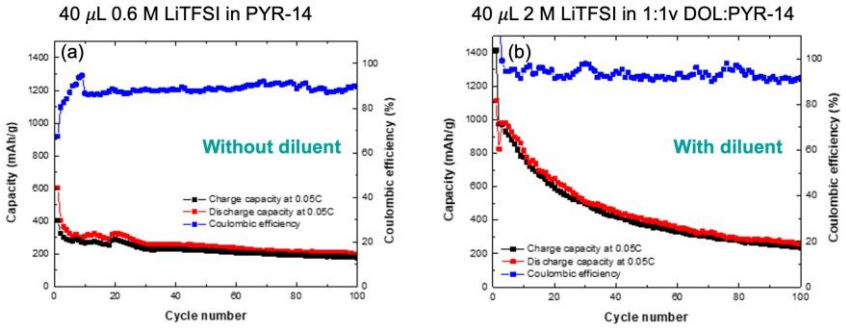

Figure 67. Electrochemical performance during cycling of Li-S batteries made up of super P/C-S cathode, $Li_6PS_5F_{0.5}Cl_{0.5}$ solid-state electrolyte, and lithium anode with 0.04 mL of functionalizing liquid containing (a) 0.6 M of LiTFSI in PYR and (b) 2 M LiTFSI in PYR:DOL (1:1). The left axis corresponds to discharge capacity, while the right axis shows the Coulombic efficiency. The batteries are cycled at a rate of C/20.

tested rate capability of the batteries. At both C/20 and C/10, initial discharge capacity is ~ 1100 mAh/g, which fades to ~ 300 mAh/g after 100 cycles. The charging profiles exhibit long plateaus ~ 2.1 V, indicative of formation of long-chain polysulfides. However, CE is better at C/10 (~ 100%) as opposed to 90% at C/20. To further enhance electrochemical performance of Li-S batteries, they incorporated SSE in the C-S cathode. $Li_6PS_5F_{0.5}Cl_{0.5}$ was dissolved in anhydrous ethanol (1 wt%) and drop casted onto the C-S cathode. Figure 68a compares battery performance with and without SSE in the C-S cathode. As shown in Figure 68a, the battery without SSE in the C-S shows initial discharge capacity of ~ 1100 mAh/g with retention of ~ 400 mAh/g after 50 cycles with excellent CE. However, after incorporation of $Li_6PS_5F_{0.5}Cl_{0.5}$ in the C-S cathode, initial capacity is slightly lower (~ 1000 mAh/g), but shows an improved retention of ~ 480 mAh/g after 50 cycles.

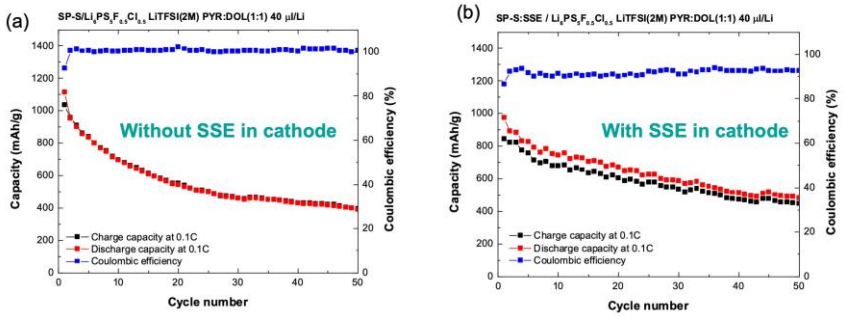

Figure 68. Electrochemical performance during cycling of Li-S batteries made up of super P/C-S cathode, $Li_6PS_5F_{0.5}Cl_{0.5}$ SSE, and lithium anode with 0.04 mL of functionalizing liquid containing 2 M LiTFSI in PYR:DOL (1:1) with (a) bare cathode and (b) cathode mixed with $Li_6PS_5F_{0.5}Cl_{0.5}$. The left axis corresponds to discharge capacity, while the right axis shows the Coulombic efficiency. The batteries are cycled at a rate of C/20.

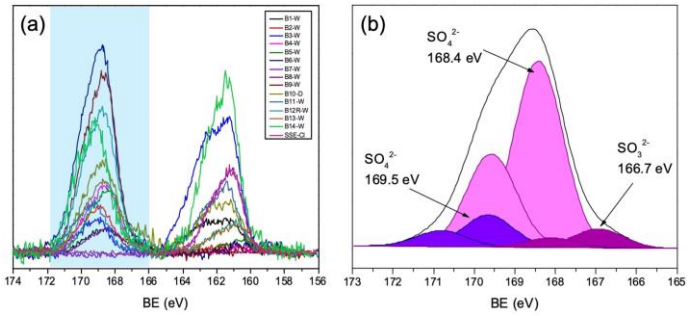

Figure 69. X-ray photoelectron spectra of the cathode – solid-state electrolyte interface of 14 representative batteries under various charge and discharge conditions. (a) S 2p spectra: all batteries with functionalizing liquid show similar feature in the high binding energy range (166 – 171 eV). (b) Further analysis of shaded region in panel (a) shows the peak at ~ 169 eV arises from the sulfonyl group in TFSI- anion.

Next, to gain a fundamental understanding of reactions at the CEIs, the team performed XPS experiments for the CEIs in a wide range of batteries. Before careful analysis, all spectra were calibrated with respect to the C-C (sp^2) binding energy (BE, 284.8 eV) of the C 1*s* peak. The low energy peak of the S 2p in Figure 69b spectra represents lithium polysulfides (Li_2S, bridging sulfur, terminal sulfur due to reduction of C-S cathode), PS_4 polyhedral compounds, and P_2S_5 structures (from the SSE). The high energy peak of Figure 69b could be fitted with three peaks, with each peak consisting of both S $2p_{1/2}$ and S $2p_{3/2}$ components due to spin-orbit splitting (energy spacing, Δ = 1.16eV, intensity ratio = 0.5). Each peak can be assigned to SO_4^{2-} and SO_3^{2-} species resulting from TFSI (present in the functionalizing liquid). Similar TFSI-related spectra showing SO_4^{2-} and SO_3^{2} species were observed at the interfaces of all batteries, except for the battery where no LE was added.

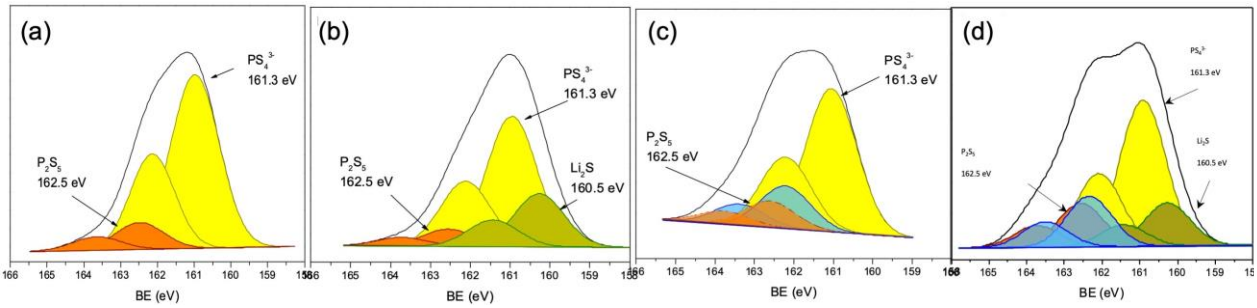

Figure 70. X-ray photoelectron spectroscopy S 2p low binding energy peak of the cathode – solid-state electrolyte interface of four representative batteries with (a) no TFSI; (b) containing TFSI- and after 2 discharge cycles, (c) containing TFSI and after 20 discharge cycles, and (d) containing TFSI and after 100 cycles.

Figure 70 shows the XPS S 2p low BE peak of the cathode-SSE interface of four batteries: one without functionalizing liquid and another three containing IL (with TFSI) and after discharge cycles of 2, 20, and 100. Again, each spectrum could be fitted with multiple peaks, with each peak consisting of both S $2p_{1/2}$ and S $2p_{3/2}$ components. The battery without the IL shows the characteristic peaks corresponding to PS_4 and P_2S_5 species of the SSE. The other three spectra all show additional peaks in addition to the SSE related peaks. Batteries after 2 and 100 cycles show doublet peaks corresponding to Li_2S (green). However, that feature is not present in the battery after 20 cycles, which could be the reason for its low capacity. Interestingly, that battery and the one after 100 cycles show an additional doublet (blue) that could be due to the presence of terminal/bridging from long-chain Li-polysulfides. Efforts are under way to modify the cathode architecture such that use of functionalizing liquid could be minimized, and sulfur loading can be increased to meet DOE targets (> 6 mg/cm^2)

Patents/Publications/Presentations

Presentations

- The Minerals, Metals and Materials Society (TMS) Annual Meeting & Exhibition, Virtual (March 2021): "Data Science Approaches to Develop Predictive Models for Energy-Relevant Materials"; B. Narayanan.
- Chemical Engineering Graduate Seminar Series, University of New Hampshire, Durham, New Hampshire, Virtual (March 2021): "Computationally Guided Design of Electrolytes for Lithium-Sulfur Batteries"; B. Narayanan.

Task 3.10 – Predicting the Nucleation and Evolution of Interphases in All-Solid-State Lithium Batteries
(Sabrina (Liwen) Wan, Lawrence Livermore National Laboratory)

Project Objective. The goal of this project is to develop and apply a suite of new computational tools to predict early-stage formation of metastable interphases in SSBs. To achieve this goal, this project focuses on meeting three primary objectives corresponding to different regimes within the early-stage interphase formation: (1) identify chemical motifs for pre-nucleation; (2) predict possible interphase structures; and (3) model the kinetics of interphase formation.

Project Impact. Degradation of SSE and formation of undesired secondary interphases at the solid electrolyte / electrode interfaces are some of the key issues that limit SSB technology from practical applications. The computational tools developed in this project will allow modeling of nucleation and formation of interphases with quantum-level accuracy and significantly improved efficiency compared to currently available methods. Completion of this project will also provide valuable insights into the correlation between local chemistry and interphase formation, which can be used to inform design of interfacial structures to lower interfacial resistance and to extend cycling life of SSBs.

Approach. The project approach centers on close integration of *ab initio* simulations, ML, and stochastic methods to probe chemistry and nucleation across broad ranges of time and length scales. First, the team will identify chemical motif, which acts as chemical precursor for pre-nucleation based on ML and large-scale AIMD simulations. Second, they will predict possible interphase structures based on stochastic minimizations of population-weighted chemical motifs identified from the MD simulations. Third, they will model the kinetics of interphase formation and evolution using KMC. To test the general applicability of the proposed computational methods, the team considers a variety of commercially viable SE and cathode materials, including cubic LLZO and LiPON SEs, and $LiCoO_2$ (LCO) and $LiFePO_4$ (LFP) cathodes. These materials also represent a range of degrees of stability arising from their intrinsic properties—in particular, LiPON|LCO, LLZO|LCO, and LLZO|LFP are expected to form stable, less stable, and reactive interfaces, respectively.

Out-Year Goals. The future goal is to predict practical strategies either to facilitate formation of the desired interphase that allows for fast Li^+ diffusion and is stable on cycling or to suppress the formation of undesired interphase to reduce interfacial impedance of ASSBs.

Collaborations. There are no collaborative activities this quarter.

Milestones

1. Identify chemical precursors for interphase formation. (Q1 FY 2021; In progress)
2. Construct initial interphase structures. (Q2, FY 2021; In progress)
3. Identify proper constraints for global optimization. (Q3, FY 2021; In progress)
4. Obtain possible interphase structures and compositions. (Q4, FY 2021; On schedule)

Progress Report

Development of ML Interatomic Potentials. This quarter, the team continued their effort to develop and refine ML interatomic potentials for the LLZO|LCO interfacial systems. They have added training data from AIMD simulations using various LLZO|LCO interfacial models at temperatures ranging from 2000 K to 6000 K (~ 23,000 structures) and LCO bulk system at 1000 K to 6000 K (~ 16,500 structures). Their current ML model, based on the ANN with a 20-20 architecture, predicts similar structures and energies as DFT relaxations at 0 K (for ~ 28,000 testing data). However, classical MD using the same set of ML potentials shows structural deviations at increased temperatures compared to AIMD simulations. They will continue to improve training of their ML models next quarter using the iterative refinement method previously introduced.

Large-Scale AIMD Simulations of Interfaces and Identifications of Potential Interphase Nucleation. The team has continued to sample the interfacial structures of LLZO|LCO from high-temperature AIMD simulations. In addition to the large supercells they ran in the past, they generated smaller supercell models (~ 300 atoms) to speed up sampling of possible structural degradation products at the interfaces. Note here that using these extremely small size models, they practically only probe the chemical reactions and processes initiated right at the LLZO|LCO interface; that is, there will be no bulk phase maintained. As shown in Figure 71, similar cobalt migration behavior is observed, initially into the lithium layers near the LCO surface and then across the interface into LLZO. As the interface continues to evolve, LCO gradually loses its layered bulk characteristics and the interfacial region constitutes predominately of the La-Co-O ions. Figure 72 shows the change of averaged local coordination number (CN) of cobalt with respect to oxygen, lanthanum, and cobalt ions during the course of AIMD simulations. It is observed that cobalt ions converge to a local tetrahedral environment at the interface, as compared to the octahedral environment originally possessed in bulk LCO. This decrease in averaged local CN is associated with LCO degradation at the interface, as shown in Figure 71c. In addition to cobalt migration, lanthanum interdiffusion is also observed, as indicated in Figure 72b, where the averaged local CN of lanthanum around cobalt is increased at the interface compared to in the bulk of LLZO. In summary, the interphase region is found to be predominantly comprised of La-Co-O clusters at various La/Co ratios with cobalt ions preferably residing in a tetrahedral coordination environment, where cobalt ion is partially reduced (from Bader charge analysis).

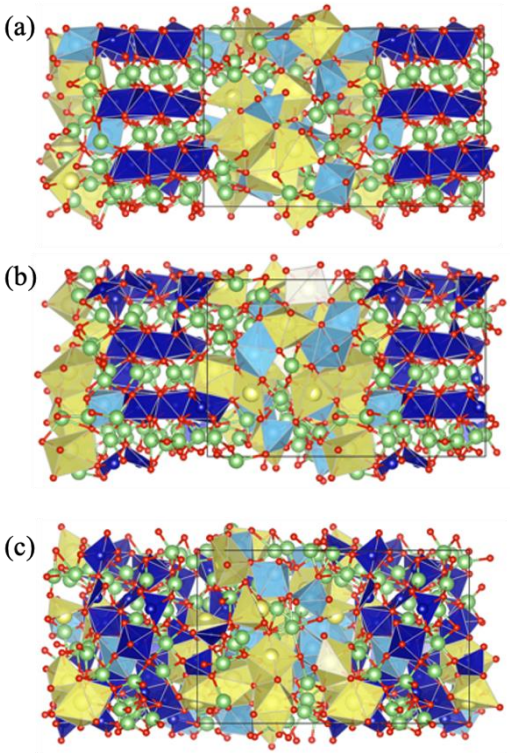

Figure 71. Snapshots of structural evolution of LLZO|LCO interface during *ab initio* molecular dynamics simulations. Lanthanum, zirconium, cobalt, lithium, and oxygen ions are represented as yellow, light-blue, dark-blue, green, and red spheres, respectively. Their corresponding local coordination is represented as polyhedral.

Based on the chemical precursors identified at the LLZO|LCO interfaces, including La-Co-O, Co-O, Li-O, and Li-Zr-O, the team constructed initial interphase nucleation structures, and they are performing energy minimization using a global optimization algorithm that has been tested previously as well as a melt-and-quench technique from AIMD. Figure 73 shows snapshots of example interphase nucleation structure during energy minimization using the abovementioned methods.

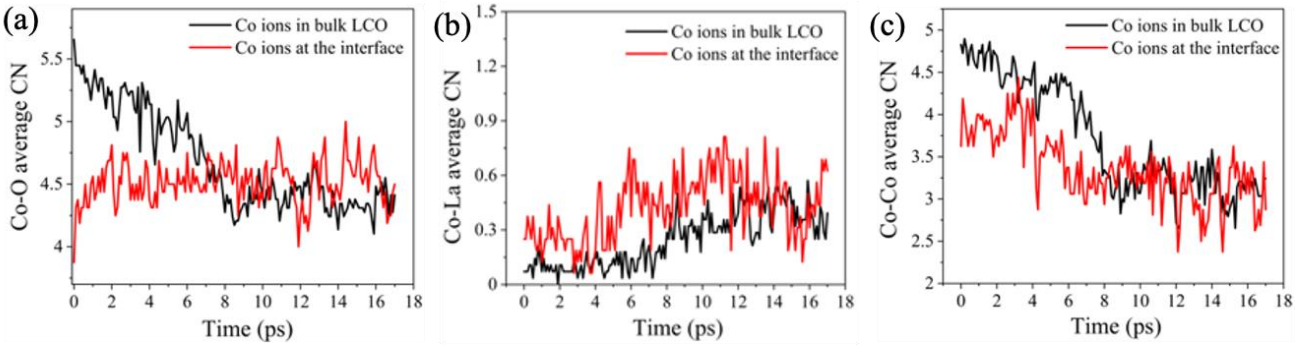

Figure 72. Changes of local coordination environment of cobalt during *ab initio* molecular dynamics simulations for cobalt ions in bulk LCO and at the LLZO|LCO interface.

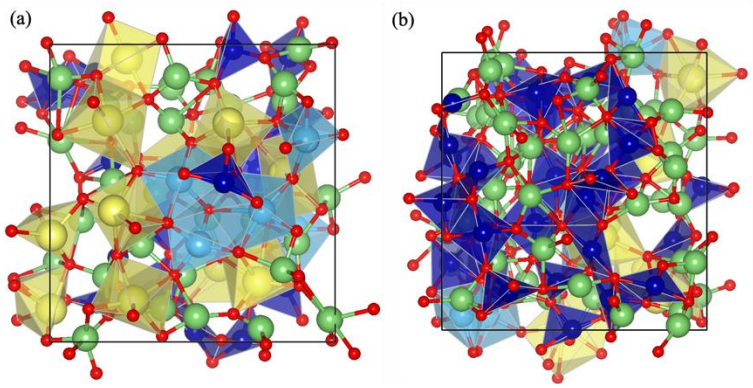

Figure 73. Example interphase formation nuclei constructed from chemical precursors identified from *ab initio* molecular dynamics simulations of LLZO|LCO interfaces. (a) $Li_{29}La_{11}Zr_5Co_{16}O_{65}$. (b) $Li_{57}La_6Zr_5Co_{31}O_{94}$.

Patents/Publications/Presentations

The project has no patents, publications, or presentations to report this quarter.

Task 3.11 – Design of Strain Free Cathode – Solid-State Electrolyte Interfaces Using Chemistry-Informed Deep Learning
(Hakim Iddir, Argonne National Laboratory)

Project Objective. The main objective of this project is to use state-of-the-art ML techniques and high-performance computing (HPC) to model complex oxide materials that will allow the team to develop cathode – SE interfaces that exhibit minimal or no strain as well as provide chemical stability at the interface between the cathode material and the SSE. A deep understanding and control of the cathode/SSE interface (including its chemical and mechanical stability) is needed to develop an effective SSB. The active cathode material changes volume during cycling, particularly at high SOC. This volume change leads to strained interfaces triggering loss of contact and delamination, and hence reduction/elimination of electron and ion transport pathways. The increased strain could also generate cracks within the SSE, creating new paths for lithium dendrite growth channels. These structural changes degrade the electrochemical performance of the battery. Several strategies have had limited success in alleviating these drawbacks, including mixed SSE, buffer layers between the cathode and the SSE, and dopants to improve chemical stability of the interface. These approaches, although promising, could not solve both the chemical and mechanical stability of the interface. In this project, the team proposes a new approach that takes advantage of well-established ML techniques and HPC to screen for candidate dopants of high-Ni-content NMC cathodes that would both reduce the volume expansion and the chemical reactivity (mixing) at the interface, with minimum impact on electrochemical performance and energy density of the cathode.

Project Impact. Structure-property relationships are at the heart of most fundamental scientific approaches. However, the link between structure and property remains a challenge in the materials science of complex systems, such as the oxides that form battery components. In particular, the chemical and mechanical stability of the cathode-SSE interface presents a challenge to development of SSBs. High-performance DFT calculations provide the necessary framework to understand such systems. Unfortunately, given the limited number of atoms and time scales accessible by the method, along with the myriad calculations required to achieve satisfactory results, the computational cost of simulating all the possible configurations of a multicomponent oxide is prohibitive. In this work, the team augments the DFT data with ML (especially deep learning) techniques that allow them to access the large system sizes and longer time scales necessary to build thermodynamic models. They focus on understanding the nature of benchmark $Li_{1-\alpha}Ni_{1-x-y-z}Mn_xCo_yM_zO_2$ structures (M dopant, α, x, y, z < 1), their volume change with lithium content, the nature and concentration of the dopants, and chemical stability of the SSE-cathode interface. The DFT and ML approach will provide new cathode compositions that will reduce the strain of the SSE-cathode interface and hence improve its mechanical and chemical stabilities.

In this project, the team aims at developing a methodology that will allow them to explore and expand the configurational space using HPC approaches in a systematic and efficient way. The methodology will encompass DFT, AIMD, MD, and ML. The methodology will also take advantage of various software already developed at ANL and at other DOE laboratories (for example, Balsam) to automate, manage, and control the large number of calculations needed to achieve the project goal.

Approach. All calculations will be performed by spin-polarized DFT as implemented in the Vienna *ab initio* simulation package (VASP). After geometry optimization within the DFT+U framework, electronic relaxation will be performed using a single-point calculation with the hybrid functional HSE06. For production calculations, they will use the message-passing interface (MPI) parallelized version of VASP.

Exploration of the potential energy surface (PES) is needed to predict the structure of solid materials and interfaces. Such calculations are infeasible using MD or DFT calculations alone. Thankfully, the PES of a system can be represented by the sum of the energies of the local neighborhoods surrounding each atom. This enables the use of ML surrogate models trained with DFT calculations to capture the energies in local neighborhoods. The input to the ML surrogate must be a unique representation of the system under study.

Consequently, the local environment of each ion is described using a local environment descriptor that renders the atomic configuration invariant to rotations, translations, and permutations of the atoms. In recent years, several different descriptors have come to prominence with advantages and disadvantages. Once the ML surrogate is trained, the total energy and forces over all the ions of any structural configuration can be determined. Such information can be used for atomistic simulations, namely, MD and MC.

In this project, the team proposes to use the open-source DeepMDkit python/C++ package to construct the ML PES and FFs. The promise of DeepMDkit in this work is to provide near-DFT accuracy at orders-of-magnitude lower computational expense, comparable to traditional MD simulations. Efficiency in training is facilitated through integration with TensorFlow and MPI/GPU support.

One of the challenges of developing ML PES is achieving accurate predicted forces and energies across the entire configurational space, while minimizing the total number of calculations required for training. In recent years, active learning has been highlighted for its ability to target training examples most likely to improve the model quality or to achieve some other objective (that is, maximizing a predicted material property). DP-GEN, an open source python package based on DeepMDkit, implements a similar active learning scheme with HPC support, and has been employed to construct ML PES with accuracy approaching DFT and sometimes exceeding embedded atom potential for experimentally measured properties of interest. In this work, the team proposes to leverage DeepMDkit and DP-GEN to efficiently generate ML-PESs for cathode-electrolyte systems including a variety of dopants.

Out-Year Goals. One out-year goal involves developing a DFT-trained ML model on NMC/LLZO interface, ready to use for large screening of new cathodes, SSE compositions, and cathodes/SSE interfaces. A second is to provide fundamental understanding on critical parameters limiting performance and stability of the cathode/SSE interface and hence of the SSB.

Collaborations. Project collaborators include J. Croy, C. Johnson, and E. Lee from ANL Chemical Sciences and Engineering Division for the synthesis phase of the project.

Milestones

1. Determine volume changes and phase transformation during charging for $LiNiO_2$ using the developed DFT-trained ML model. (Q1, FY 2021; Completed)
2. Determine elemental segregation, volume changes, and phase transformation during charging of $Li(Ni_{0.8}Mn_{0.1}Co_{0.1})O_2$ using the developed DFT-trained ML model. (Q2, FY 2021; In progress)
3. Extend solid bulk models to include surfaces and dopants. (Q3, FY 2021; In progress)
4. Apply ML model to understand mechanical and chemical interactions on CEIs. (Q4, FY 2021)

Progress Report

This quarter, the team has finalized the modeling and understanding of Li_xNiO_2 (LNO) volume change with delithiation (particularly at very low lithium content). It is important to highlight that the volume change is the fundamental variable that affects the mechanical properties of cathode SEIs. Hence, a detailed understanding of the physics behind the volume change is crucial for the design of new strategies to mitigate the deleterious processes that occur at the cathode-SSE interface during cycling. Furthermore, they continue to advance on accomplishing the next milestones: elemental segregation and volume changes in $Li(Ni_{0.8}Mn_{0.1}Co_{0.1})O_2$ and setting up Li_xNiO_2 - SSE interface models.

The team has shown before that the volume collapse at very low lithium content can be simulated using DFT, using the Hubbard *U* correction when taking into account the vdW interactions appropriately using the XC functional optB86b-vdW. However, they have come to the conclusion that at this level of theory it is not possible to discriminate between the O1 and O3 phases of NiO_2 because the energies (internal and free energies) are within the accuracy of the methods. Hence, they used the state-of-the-art Random Phase Approximation (RPA) to get a more accurate description of the system. Figure 74 shows the PES projections on the a-c plane, where a and c are the hexagonal unit cell lattice parameters of NiO_2 with space group R-3m. The blue basin in Figure 74a shows the minimum energy for the O3 oxygen stacking at a = 2.88 Å and c = 13.77 Å with an energy of -204.215 eV/cell, whereas Figure 74b shows it for the O1 oxygen stacking at a = 2.88 Å and c = 13.77 Å with an energy of -204.186 eV/cell. Therefore, unexpectedly, the O3 oxygen stacking at the RPA level of theory is found to be 29 meV/cell lower in energy than the O1 stacking. It is important to notice that the c lattice parameter is the same for both cases, indicating that the collapse of the volume at high SOC does not depend on the oxygen stacking sequence. This result is very important for the understanding of volume change of high-Ni cathodes at high SOCs and for the continuation of this project. However, any gliding could have consequences on the formation of cracks and possible changes in the properties of the top surface layers.

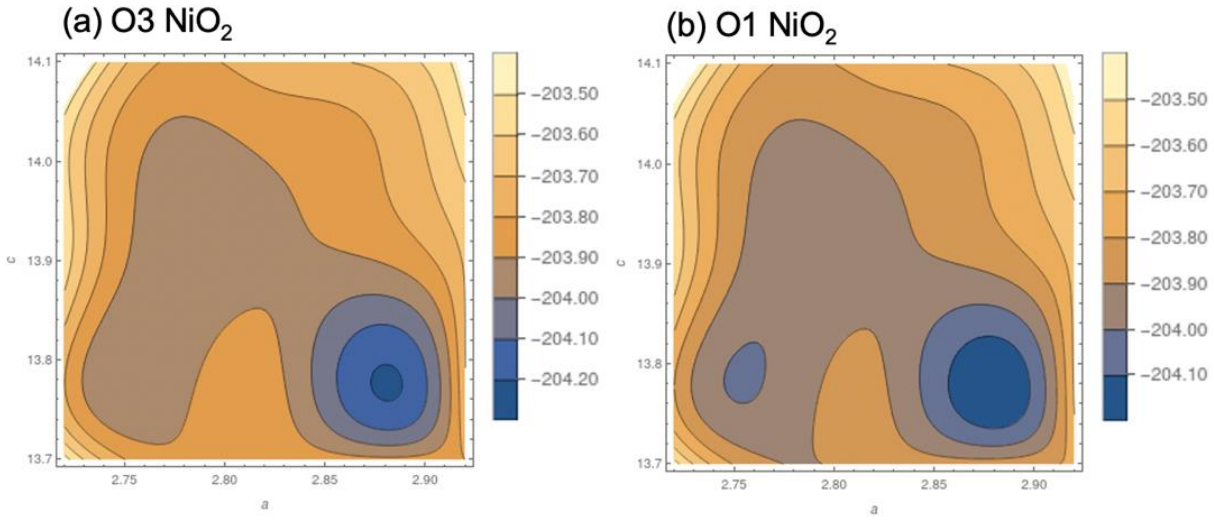

Figure 74. Potential energy surface of NiO_2 with the oxygen stacking (a) O3 and (b) O1.

Enthalpies were computed using ML-FF MD for NiO_2 phases over the temperature range 298.15 K to 350 K because of suspicion in the literature that the two phases can coexist in a fully delithiated LNO cathode. Results are shown in Figure 75. Further, Gibbs Free Energies (see Figure 76) are computed for the phases assuming a quadratic form for the enthalpy, and reference Gibbs Free Energy for nickel at 330 K taken from HSC Chemistry[1] and using an in-house thermodynamic integration code. The reference is chosen as nickel because the amount of nickel does not change in the composition space of interest for the thermodynamics study

of Li_xNiO_2 (x = 0.04, 0.08, 0.12, and 0.17). The difference between the Gibbs Free Energy between O1 and O3 stacking is shown in Figure 76b, as the discrepancy is not visible in Figure 76a. Calculations are in progress to compare the Gibbs Free Energy of the lithiated phases of mixed O1/O3 stacking.

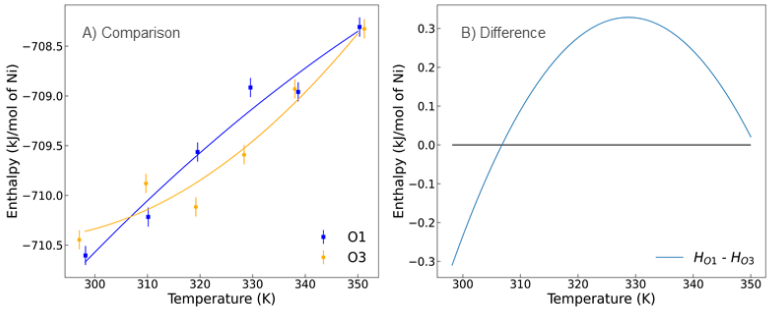

Figure 75. Enthalpy of O1 and O3 stacked NiO_2. (a) Comparison. (b) Differences are plotted showing that enthalpy difference between the two phases is within 1 kJ/mol of nickel.

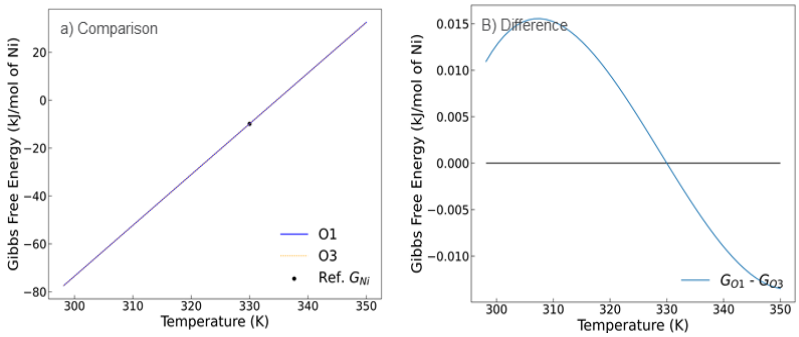

Figure 76. Gibbs Free Energy of O1 and O3 stacked NiO_2. (a) Comparison. (b) Differences show that the two phases are within 1 kJ/mol of energetic stability of each other over the temperature range 298.15 K to 350 K. The Gibbs Free Energy is calculated with respect to the reference Gibbs energy of nickel at 330 K, sourced from HSC Chemistry.

Slab model calculations were set up to understand elemental segregation in Ni-rich materials. A representative cell of $Li_x(Ni_{0.8}Mn_{0.1}Co_{0.1})O_2$ is shown in Figure 77. More than 200 calculations have been performed to compare the energies of randomly generated TM arrangements. The segregation to the most common surface has been studied as a first step to understand which ions would interact with the cathode SE at the interface. The team's results showed a trend where cobalt atoms preferentially segregate to the surfaces of the slab models for all the facets considered (104) and (012). This contrasts with the previous findings for NMC-111 where the segregation was only found for the (104) facet. These results are being incorporated in the team's SSE–NMC-811 interface models under study.

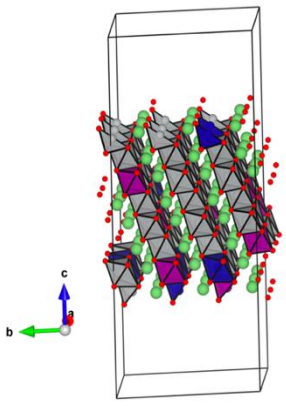

Figure 77. Slab model representing (012) facet of $Li_x(Ni_{0.8}Mn_{0.1}Co_{0.1})O_2$. Grey polyhedrons represent nickel sites, purple polyhedrons represent manganese sites, blue polyhedrons represent cobalt sites, and green spheres represent lithium ions.

To understand the effect of composition and dopants on the volume change in Ni-rich materials, a simulation cell was set up to model the delithiation process of $Li_x(Ni_{0.8}Mn_{0.1}Co_{0.1})O_2$ (NMC-811) (see Figure 78a). The supercell with a space group R-3m has 27 MO_2 units (M = Ni, Co, Mn) distributed in three layers. Each composition was generated randomly shuffling the lithium ions in all the available octahedral lithium sites. Symmetry equivalent structures were

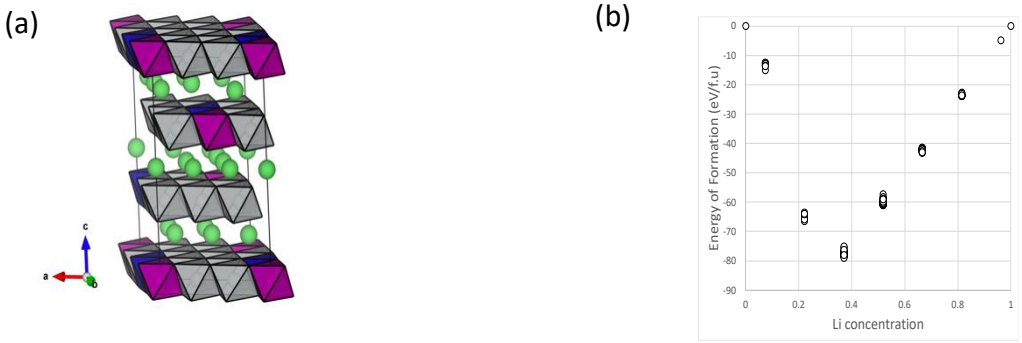

Figure 78. (a) Sample $Li_x(Ni_{0.8}Mn_{0.1}Co_{0.1})O_2$ supercell model for x = 0.33 with randomly distributed lithium ions in the lithium layer. Grey octahedrons represent nickel sites, purple octahedrons represent manganese sites, blue octahedrons represent cobalt sites, and green spheres represent lithium ions. (b) Density functional theory computed $Li_x(Ni_{0.8}Mn_{0.1}Co_{0.1})O_2$ energy of formation.

discarded using the recipe from Lonie et al.[2] So far the team has tested 138 configurations at different lithium compositions, and more simulations are being conducted. Preliminary results are shown in Figure 78b.

Additionally, interfacial models have been developed to understand chemical reactivity, reconstruction, and mixing at the cathode-LLZO interface. Figure 79 shows the interfacial model between the lithium terminated (001) facet of LLZO and the (104) facet of $LiNiO_2$. The goal is to understand the chemical and mechanical stability of the interfacial region at high SOC. Several terminations (Li, La, Zr, O) are being tested with $LiNiO_2$ facets. It is important to highlight that the main goal of these sets of simulations is to generate training data to add into the ML-FF that the team is developing. The supercells needed for a full representation of an interface are beyond the size that is tractable by DFT. Hence, the ML-FF will be trained on non-stoichiometric structures, but ultimately it will be able to predict the structure and stability of many-atom stoichiometric interface structures.

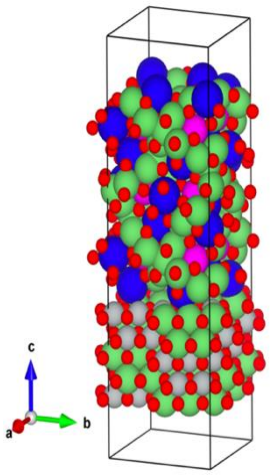

Figure 79. Supercell interfacial model between lithium terminated (001) facet of LLZO and the (104) facet of $LiNiO_2$. Blue spheres represent lanthanum, magenta spheres represent zirconium, green spheres represent lithium, grey spheres represent nickel, and red spheres represent oxygen.

References

[1] Metso Outotec's chemical reaction and equilibrium software HSC Chemistry (https://www.hsc-chemistry.com/hscchemistry).

[2] Lonie, D. C., and E. Zurek. "Identifying Duplicate Crystal Structures: XtalComp, an Open-Source Solution." *Computer Physics Communication* 183, No. 3 (2012): 690–697. doi: 10.1016/j.cpc.2011.11.007.

Patents/Publications/Presentations

Presentations

- American Institute of Chemical Engineers Midwest Regional Conference, Virtual (March 17–18, 2021): "Machine Learning Force Fields for High Nickel Li Ion Cathodes"; J. Gabriel, J. Garcia, N. H. Paulson, J. Low, M. Stan, and H. Iddir. Abstract of presentation.
- National Renewable Energy Laboratory, Machine Learning for Batteries Workshop, Virtual (March 23, 2021): "Deep-Learned Interatomic Potentials to Simulate Volume Change in Cathode Materials"; N. H. Paulson.

Task 3.12 – Tackling Solid-State Electrochemical Interfaces from Structure to Function Utilizing High-Performance Computing and Machine-Learning Tools

(Shinjae Yoo, Feng Wang, and Deyu Lu, Brookhaven National Laboratory; Nongnuch Artrith and Alexander Urban, Columbia University)

Project Objective. This project aims at elucidating the structural evolution and other dynamic properties of the interphases at the SSIs in SSBs under processing and electrochemical cycling conditions that strongly impact cell performance. By leveraging synergies of first-principles theory, HPC, ML, and computational/experimental spectroscopy, this project involves a comprehensive investigation of SE systems and SSIs that may enable the practical use of lithium anodes and high-nickel NMC cathodes in SSBs. Specific project objectives are as follows: (1) develop realistic atomic-scale structure models of the heterostructural SSIs, (2) determine the impact of structural evolution on the stability and transport properties of the SSIs, and (3) identify the coating/doping chemistry that may stabilize SSIs during formation and electrochemical cycling.

Project Impact. Interfacial properties and the dynamical evolution of interphase structures are crucial for the stability and performance of SSBs. This project will lead to fundamental understanding of current materials limits and will identify key materials parameters for optimizing the performance of SSBs. By corroborating atomic-scale theory with experiment, the project will identify structure–property relationships of the heterostructural SSIs in SSB systems that are relevant for EVs. The outcomes of this project will therefore accelerate development of high-energy-density, safe SSBs for EVs.

Approach. Accurate ML potentials will be trained on an extensive database from DFT calculations to simulate the structure evolution and electrochemical properties of the SSIs. Using a second ML model, key physical descriptors will be extracted from EELS and XAS measurements. This spectral fingerprinting will enable the automated interpretation of spectroscopy measurements, thereby bridging between atomistic modeling and experiment. An experimental platform will be developed to integrate experimental/computational spectroscopy and modeling of SSIs. In combination, the two ML models and the spectroscopic data will facilitate the construction of a physics-based model to unravel the structure-property relationships of the SSIs.

Out-Year Goals. The project will progress toward establishing dynamic composition-structure-property relationships for interface stability and transport within and across the electrochemical SSIs in SSBs. The ML approach will be further developed to a general model for thermodynamic and transport properties of dynamic heterostructural electrochemical interfaces and will eventually be applied to the practical SSB systems.

Collaborations. The project is collaborating with Y. Du at BNL.

Milestones

1. Complete mapping of the phase diagram and structure-stability-conductivity relationships in the glass/ceramic (*gc*) Li_2S–P_2S_5 (LPS) system. (Q1, FY 2021; Completed)
2. Characterize initial stages of the interfacial reaction of *gc*-LPS with lithium metal using ML-augmented DFT and XAS spectroscopy. (Q2, FY 2021; Completed)
3. Correlate characteristic structural motifs of *gc*-LPS and the *gc*-LPS/Li interface with XAS spectral features using ML. (Q3, FY 2021; In progress).
4. Determine formation and evolution mechanisms of *gc*-LPS/Li interphases using XAS measurements and ML models. (Q4, FY 2021; On track)

Progress Report

Following last quarter's report on a DFT database for mapping the structure-stability-conductivity relationship in *gc*-LPS, this quarter the team benchmarked simulated XAS spectra with experiments and established a workflow for constructing a database of XAS simulations. The two databases, including both structure and XAS on the same system, allow the team to explore the correlation between local structural motifs and spectral fingerprints in characterizing the interfacial reaction of *gc*-LPS with lithium metal as well as high-Ni NMC cathodes.

Benchmark of XAS Simulations. The *gc*-LPS electrolytes of varying composition $(Li_2S)_x(P_2S_5)_{1-x}$ are promising for use in SSBs, with the desired superionic conductivity at room temperature (> 10^{-3} Scm^{-1}), soft mechanical properties, and low GB resistance.[1] Although *gc*-LPS lacks long-range atomic ordering, characteristic short-ranged structural P–S motifs are present and vary with the LPS composition. To understand how the short-range ordering impacts the energy landscape for ion migration and thereby affects the lithium conductivity, tender energy XAS spectroscopy is employed here to probe the local geometric and electronic structures in *gc*-LPS. With increasing content of Li_2S in *gc*-LPS, the density of lithium atoms surrounding sulfur atoms increases, which in turn increases the electron density and gives rise to a shielding effect around sulfur atoms. This leads to a red shift of the sulfur K-edge, as observed in previous literature.[2] In practice, sulfur K-edge spectroscopy is of great interest because sulfur is more involved in the interfacial reactions on cycling than phosphorus, forming Li_2S or metal sulfides (for example, NiS) at SSIs. In comparison, phosphorus is mostly located in the center of PS_4^{3-} tetrahedra (as P^{5+} species), except for the direct P–P bonding in $P_2S_6^{4-}$ motifs (as P^{4+} species). There is no direct Li–P bonding in *gc*-LPS, and hence no significant change in the phosphorus K-edge is expected in different compositions. Here, the team conducts first-principles simulations of sulfur K-edge XAS with the core-hole potential method as implemented in VASP 6.1.1 and with measured experimental XAS reference data for LPS at NSLS-II (Figure 80), toward establishing a correlation between atomic structural motifs and XAS spectra.

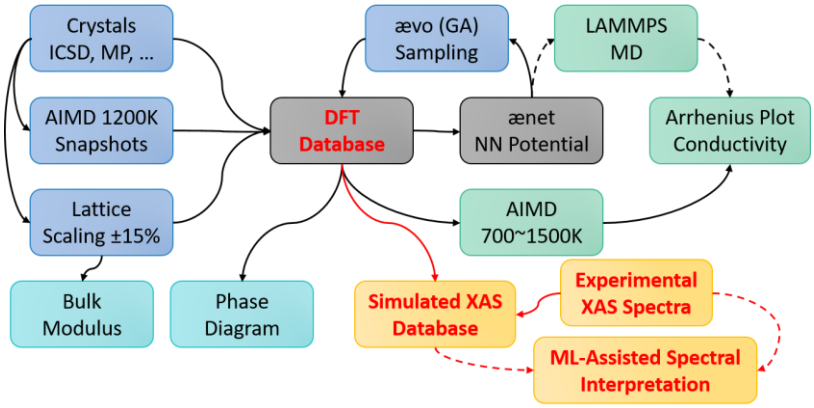

Figure 80. Flowchart of the methodology for studying interfacial reactions between gas/ceramic LPS and lithium metal using machine learning augmented density functional theory and X-ray absorption spectroscopy (dashed lines indicate future work).

The team's calculations started with the benchmark of the XAS simulations using reference sulfur compounds. Some of the most relevant compounds from *gc*-LPS/electrode interfacial degradation (including Li_2S,[3-4] P_2S_5,[5] and NiS[6]) were selected as validation systems. In the XAS simulations, the final state is treated self-consistently under the presence of the core-hole in the S 1s state.[7-8] The team has carefully tested the simulation parameters to ensure the numerical convergence, including energy cutoff for the plane-wave basis set, supercell size, k-point mesh, and the number of unoccupied bands. In addition, different functionals and pseudopotentials as well as the charge of the core-hole were tested to determine the optimal VASP inputs for XAS simulations. Based on a series of convergence tests, the parameters for VASP XAS simulations were determined. The simulated XAS spectra were convoluted by combining a 0.5 eV Gaussian broadening, a 0.59 eV core-hole life time broadening, and an energy-dependent Lorentzian broadening. The absorption edge was aligned using the excitation onset determined from the total energy difference between the final state and the initial state, following a previously reported procedure.[9]

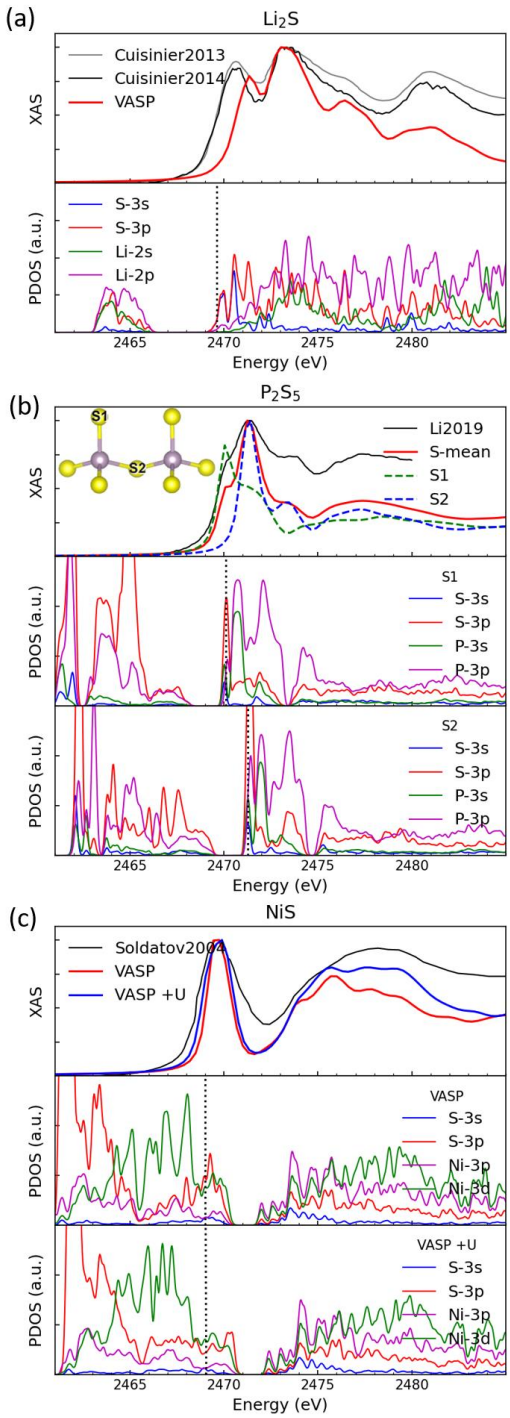

Figure 81. Comparison of VASP calculated and experimentally measured sulfur K-edge X-ray absorption spectra in Li_2S, P_2S_5, and NiS.

To validate the VASP XAS simulations, the simulated spectra were compared against reported experimental measurements for three benchmark systems (Li_2S, P_2S_5, and NiS), as shown in Figure 81. The simulated spectra successfully reproduce the main features in reference systems. It is known that Kohn-Sham DFT underestimates band gaps and concomitantly band widths, due to inaccurate estimates of quasiparticle (excitation) energies based solely on the Kohn-Sham eigenspectrum.[10] Therefore, the calculated XAS spectra may underestimate peak separations compared to experiments, as seen in Li_2S and NiS. A comparison between two DFT functionals (LDA and HSE) confirms that the hybrid functional HSE can describe the band widths more accurately and therefore yields a wider peak splitting that agrees better with experiments. However, the HSE calculation takes about 20 times longer in computational time than the LDA calculation, which is impractical to be implemented in the construction of a large database that contains thousands of spectra. Instead, it will be more efficient to compute the XAS spectra with a simple functional such as LDA and apply an empirical correction to the peak splitting afterward.

The spectrum of P_2S_5 exhibits a pronounced pre-edge feature. The structure of $(P_2S_5)_2$ is composed of two types of sulfur atoms: 4 terminal sulfur and 6 bridging sulfur, denoted as S1 and S2, respectively (Figure 81b). The terminal sulfur atom is coordinated with one phosphorus atom, and the P-S bond length is ~ 1.9 Å. In comparison, the bridging sulfur atom is coordinated with two phosphorus atoms; the charge distribution over the bridging sulfur is less negative than the terminal sulfur, leading to a longer P-S bond length of 2.1 Å and redshift of the absorption onset, as shown in the Figure. *These results are the first demonstration that the pre-edge and main edge of the sulfur K-edge in P_2S_5 can be attributed to two types of differently coordinated sulfur atoms.* This also proves the capability of VASP XAS simulations to distinguish the inequivalent absorption sites.

To study the interfacial reaction between LPS and high-Ni cathodes, the team also computed sulfur K-edge XAS for NiS, the most likely formed interphase, including a Hubbard *U* correction to account for the correlation of the nickel *d*-band electrons. As shown in Figure 81c, the Hubbard *U* correction did not change the main absorption edge, but leads to a broadened absorption edge and increased intensity in the post-edge region. Nevertheless, the *U* value is dependent on the species and materials and must be tested carefully. The capability to describe the spectra in this and other systems demonstrates the robustness of the team's approach.[11]

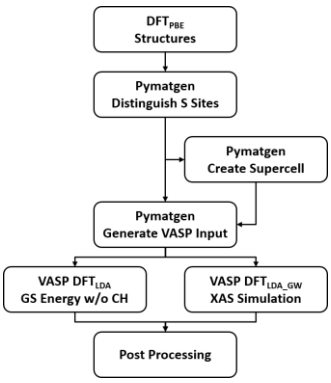

Figure 82. Workflow to construct the computed X-ray absorption spectroscopy database.

Automated DFT Workflow for Constructing XAS Database. On the basis of the determined parameters from the benchmark systems, the team devised a workflow for automated core-hole potential calculations for generating an XAS database (Figure 82). The structures of *gc*-LPS were previously sampled combining DFT, AIMD simulations, and ANN potential based genetic-algorithm (GA) sampling (ANN-GA); they were further optimized with DFT calculations using the PBE functional (see also the FY 2021 Q1 report). In terms of the structural parameters, the PBE functional outperforms the LDA functional in reference systems. For each optimized LPS structure, the workflow automatically determines the inequivalent sulfur sites for absorption and their respective weights. This implementation makes use of the symmetry tools from the Pymatgen package.[12] Pymatgen features are further used to create supercells and generate VASP input files for single-point LDA calculations to obtain the ground state energy without and with core-hole, and for core-hole potential calculations for all symmetrically distinct sulfur atoms in the supercell. Raw data from completed DFT calculations will be post processed, which mainly involves two steps: (1) apply the peak alignment to distinct sulfur atoms, and (2) average the aligned spectra with the correct weights to compute the XAS spectrum. Note that the data without averaging contain information about the XAS features of local atomic structures, which will be used for constructing XAS ML models in the remaining two quarters this fiscal year. The workflow was established, and construction of the XAS database is under way. Preliminary results of sulfur K-edge spectra of ~ 300 non-equivalent sulfur sites in the LPS XAS database, prior to energy alignment, are shown in Figure 83. A detailed analysis using ML-assisted approaches will be conducted in the team's future research.

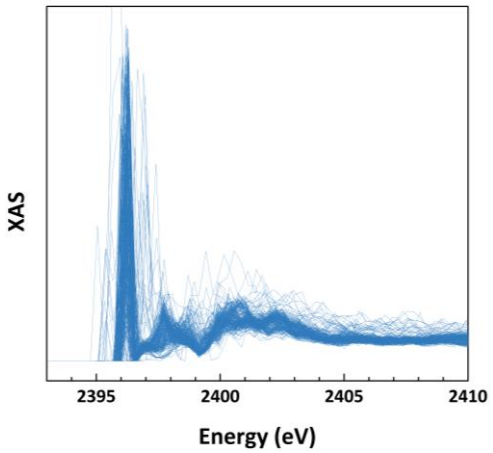

Figure 83. Raw simulation data for sulfur K-edge in LPS X-ray absorption spectroscopy database (without energy alignment).

Validation of DFT-Calculated Sulfur K-Edge in Crystalline β-Li_3PS_4. To better understand XAS spectra of the sampled *gc*-LPS phases, the team also conducted experimental measurements of XAS reference data for LPS crystal structures. The sulfur K-edge in crystalline β-Li_3PS_4 was measured under fluorescence mode from NSLS-II. The computed XAS spectra are in excellent agreement with the experimental data, As shown in Figure 84. The absorption edge is ~ 2471.0 eV, which is likely due to the S 1s to sulfur 3p σ* transition (dumbbell-shaped S_2^{2-}).[2] The simulated XAS not only reproduces most features, but also yields a comparable peak splitting for the sulfur K-edge in β-Li_3PS_4 crystal. In β-Li_3PS_4, there are three inequivalent sulfur sites (denoted as S1, S2, and S3 in Figure 84). While their charge distribution is comparable, the P-S and Li-S bond lengths exhibit sizable variation. In this case, the core level chemical shift cannot be simply explained by bond length and Bader charge. The team will develop optimal structural and chemical descriptors to interpret XAS spectral features in *gc*-LPS and interphases at SSIs with Li-metal and NMC cathodes.

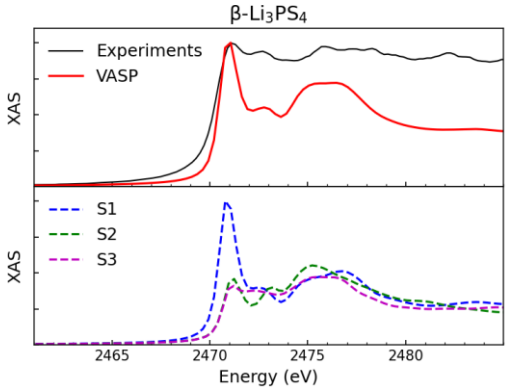

	Site	ΔΔ*E* (eV)	Coordination	P-S (Å)	Li-S (Å)	Bader
S1	4b	-0.085	P-S-Li3	2.06	2.40	-1.1
S2	2a	0.153	P-S-Li3	1.98	2.52	-1.1
S3	2a	0.017	P-S-Li3	2.02	2.44	-1.1

Figure 84. Comparison of calculated and experimentally measured sulfur K-edge X-ray absorption spectra in β-Li_3PS_4 crystal.

References

[1] Kudu, Ö. U., et al. *Journal of Power Sources* 407 (2018): 31.
[2] Dietrich, C., et al. *Physical Chemistry Chemical Physics* 20 (2018): 20088.
[3] Cuisinier, M., et al. *Journal of Physical Chemistry Letters* 4 (2013): 3227.
[4] Cuisinier, M., et al. *Energy & Environmental Science* 7 (2014): 2697.
[5] Li, X., et al. *ACS Energy Letters* 4 (2019): 2480.
[6] Soldatov, A. V., et al. *Journal of Physics: Condensed Matter* 16 (2003): 7545.
[7] Taillefumier, M., et al. *Physical Review B* 66 (2002): 195107.
[8] Gougoussis, C., et al. *Physical Review B* 79 (2009): 045118.
[9] England, A. H., et al. *Chemical Physics Letters* 4 **(**2011): 187.
[10] Pascal, T. A., et al. *Journal of Physical Chemistry Letters* 5 (2014): 1547.
[11] Yan, D., et al. *Nano Letters* 19 (2020): 3457.
[12] Ong, S. P., et al. *Computational Materials Science* 68 (2013): 314.

Patents/Publications/Presentations

Presentation

- American Physical Society Meeting, Virtual (March 2021): C22.00010 "Modeling the Dynamics of Complex Energy Materials with Machine Learning"; N. Artrith. Invited.

TASK 4 – METALLIC LITHIUM

Team Lead: Nancy Dudney, Oak Ridge National Laboratory

Summary and Highlights

The use of a metallic lithium anode is required for advanced battery chemistries like Li-ion, Li-air, and Li-S to realize dramatic improvements in energy density, vehicle range, cost requirements, and safety. However, use of metallic lithium with liquid and solid polymer or ceramic electrolytes has so far been limited due to parasitic SEI reactions and dendrite formation that eventually short circuit the battery. Adding excess lithium to compensate for such losses negates the high-energy-density advantage of a Li-metal anode and leads to further concern for battery safety. For a long lifetime and safe anode, it is essential that no lithium capacity is lost either (1) to physical isolation by roughening, dendrites, or delamination processes, or (2) to chemical isolation from side reactions. The key risk, and current limitation, for this technology is the gradual loss of lithium over the cycle life of the battery.

BMR, Battery500, and other DOE programs are addressing this challenge with many innovative and diverse approaches. Key to all is the need for a much deeper analysis of the degradation processes and new strategies to maintain a dense, fully connected lithium and a dendrite-free electrolyte so that materials can be engineered to fulfill the target performance metrics for EV application, namely 1000 cycles and a 15-year lifetime, with adequate pulse power. Projecting the performance required in terms of just the lithium anode, this requires a high rate of lithium deposition and stripping reactions, specifically about 30 µm of lithium per cycle, with pulse rates up to 10 and 20 nm/s (15 mA/cm^2) charge and discharge, respectively, with little or no excess lithium inventory. This is daunting in the total mass and rate of material transport that must be achieved without failures.

The efficient and safe use of metallic lithium for rechargeable batteries is then a great challenge, and one that has eluded R&D efforts for years. This project takes a broad look at this challenge for both SSBs and batteries continuing to use LEs. Electrolytes reported here include nonflammable liquid solutions, gel type polymer-in-a-salt, composites of ceramic polymer phases, common and novel PEs, and both oxide and sulfide ceramic electrolytes. In most studies, the electrolyte phases were modified by addition of plasticizers or interface coatings to improve transport, stability, and ease of manufacturing. Researchers are typically working toward cycling of full cells with relevant and balanced capacities for the lithium anode and cathode using measures of CE, interface resistance, and post-cycling observation of the disassembled cell components to assess stability of the Li-metal anode and chosen electrolyte.

Highlights

The highlights for this quarter are as follows:

- ORNL (J. Nanda's team) is casting doubt on a common strategy of using $LiNbO_3$ to stabilize the interface between a sulfide SE and Ni-rich oxide cathodes. The team observed that a 1 wt% $LiNbO_3$ coating on NMC-811 cathodes containing high surface-area carbon for enhanced electronic conductivity had little impact on cell capacity or cyclability.
- The X. C. Chen / N. Dudney team from ORNL published a paper entitled, "Gel Composite Electrolyte – An Effective Way to Utilize Ceramic Fillers in Lithium Batteries" in the *Journal of Materials A*. The paper describes a strategy to utilize discrete ceramic fillers to form a gel composite electrolyte with enhanced transport properties for Li-metal batteries.

Task 4.1 – Lithium Dendrite Prevention for Lithium Batteries (Wu Xu and Ji-Guang Zhang, Pacific Northwest National Laboratory)

Project Objective. The objective of this project is to enable lithium metal to be used as an effective anode in rechargeable Li-metal batteries with good stability and high safety. The investigation this fiscal year will focus on two aspects. First, develop nonflammable polymer composite electrolytes (NPCEs) and investigate effects of various flame-retardant solvents and polymers on ionic conductivity, lithium CE, Li-anode morphology, flammability, and battery performances in terms of long-term cycling stability and rate capability at various temperatures. Second, establish correlation of morphologies of SEI layer and deposited lithium with electrolyte formulation, current density, and lithium deposition/stripping cycling.

Project Impact. Lithium metal is an ideal anode material for high-energy-density rechargeable batteries; however, the application of Li-metal anode is hindered by safety concerns and short cycle life. The safety concerns of Li-metal batteries mainly arise from lithium dendrite growth and electrolyte flammability, while the short cycle life is related to low lithium CE. Although much progress has been achieved in suppressing lithium dendrites and increasing lithium CE in LEs, most LEs are flammable and may pose safety hazards in case of extreme conditions. Therefore, development of electrolytes with improved safety for advanced battery chemistry is imperative. An ideal electrolyte for Li-metal anode should not only suppress lithium dendrite growth and have high CE, but also be intrinsically nonflammable. This fiscal year, the team will develop NPCEs that have high lithium CE, suppress lithium dendrites, and are stable with high-voltage cathodes. The success of this project will increase safety of Li-metal and Li-ion batteries and accelerate market acceptance of EVs, as required by the EV Everywhere Grand Challenge.

Approach. The approach will encompass several areas: (1) develop NPCEs that can enable long-term cycling with significantly improved safety features of Li-metal batteries, (2) develop current collectors with 3D structure for Li-metal anode to suppress lithium dendrite growth, increase lithium utilization, and extend cycle life of Li-metal batteries, and (3) conduct mechanistic studies on lithium deposition behavior to lay groundwork for future improvement of electrolytes (salts, solvents, and additives) for Li-metal batteries.

Out-Year Goals. The long-term goal of the proposed work is to enable Li-metal and Li-ion batteries with a specific energy of > 350 Wh/kg (in cell level), 1000 deep-discharge cycles, 15-year calendar life, and less than 20% capacity fade over a 10-year span to meet the goal of EV Everywhere Grand Challenge.

Collaborations. This project collaborates with C. Wang of PNNL on characterization by TEM/SEM; K. Xu and M. Ding of U. S. Army Research Laboratory (ARL) on DSC measurements; and B. Polzin at ANL on coated electrode sampling.

Milestones

1. Evaluate properties of NPCEs and cycling performance of Li||NMC cells using the NPCE. (Q1, FY 2021; Completed, December 31, 2020)
2. Elucidate influencing factors on lithium deposition behavior by *in situ* AFM. (Q2, FY 2021; Completed)
3. Fabricate 3D-structured current collectors and characterize their physical properties. (Q3, FY 2021)
4. Evaluate influence of 3D-structured current collector on Li-metal deposition behavior and cycling performance of Li||NMC cells. (Q4, FY 2021)

Progress Report

Influences of Electrolyte Additives on the Deposition Behavior of Metallic Lithium via *In Situ* AFM

The deposition behaviors of lithium on copper substrate in conventional electrolytes with various additives were systematically studied by *in situ* AFM. Figure 85 reveals the morphology evolution of lithium deposited on copper over time. The team selected 1.0 M $LiPF_6$ in EC-EMC (3:7 by weight), hereinafter referred to as E257, as the benchmark electrolyte for evaluation (Figure 85a). On the basis of E257, three other electrolytes, E257 + 2 wt% VC (Figure 85b), E257 + 2 wt% $LiAsF_6$ (Figure 85c), and E257 + 2 wt% VC + 2 wt% $LiAsF_6$ (Figure 85d), were evaluated. As indicated by the *in situ* AFM results, the electrolyte additives have significant influence over the lithium deposition behavior. The introduction of VC postpones formation of lithium nuclei, while introduction of $LiAsF_6$ increases nucleation density. Quantitative analyses on the results obtained from *in situ* AFM were performed to better understand the mechanism of how electrolyte additives influence lithium deposition.

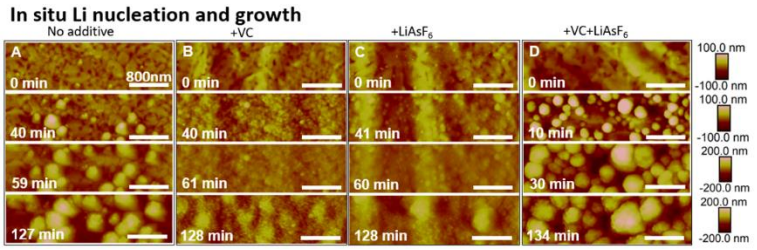

Figure 85. Morphology evolutions of copper electrodes on lithium deposition by *in situ* AFM. (a) In 1.0 M $LiPF_6$ in EC-EMC (3:7 by weight), hereinafter referred to as E257. (b) In E257 + 2 wt% VC. (c) In E257 + 2 wt% $LiAsF_6$. (d) In E257 + 2 wt% VC + 2 wt% $LiAsF_6$.

Safe Composite Separator Based on Polyimide (PI) and Polyethylene

The high service temperature of 221-241°C of PI makes possible maintaining its structural integrity on overheating. Moreover, PI is intrinsically nonflammable. Therefore, it is expected to protect the cell from internal short circuiting during thermal runaway. This quarter, the porous PI membrane was prepared by mixing the PI solution with Al_2O_3 nanoparticles of regular size. After obtaining the PI-Al_2O_3 composite membrane, the Al_2O_3 was removed by acid etching, leaving a PI membrane with highly regular pores arrays. The uniformity of the PI membrane is considered to regulate the Li^+ flux and achieve better lithium deposition morphology. Figure 86a-b shows the morphology of the PI separator. Regular pores with the diameter of 400-500 nm and the thickness of PI membranes can be controlled at 11-20 µm. These 3D porous PI membranes were evaluated as a separator in Li-metal batteries. However, it is found that the PI separator alone can easily lead to short circuit due to penetration by lithium dendrites. Therefore, the PI membrane was combined with a thin layer of polyolefin separator like polyethylene to construct the PI/polyethylene composite separator. Cycling performance of Li||NMC-622 cells using the PI/polyethylene composite separator and the mere polyethylene separator was evaluated and compared. As shown in Figure 86, cells using the PI/polyethylene

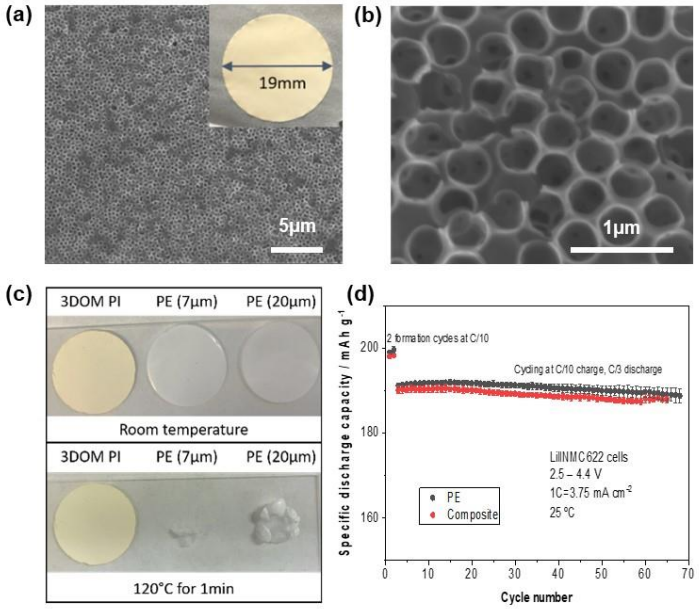

Figure 86. (a) Photograph and micrograph of functional polyimide (PI) separator with regular pore array. (b) Micrograph of PI separator at higher magnification. (c) Thermal stability test of PI (11 µm) and polyethylene (PE, 7 and 20 µm) separators before and after heating at 120°C for 1 minute. (d) Cycling performance of Li||NMC-622 cells using PE and PI/PE composite separators.

composite separator (total thickness of 18 μm) exhibit comparable cycling performance to those comprising polyethylene separator with similar thickness (20 μm). The long-term effectiveness of the composite separator is under evaluation.

Patents/Publications/Presentations

The project has no patents, publications, or presentations to report this quarter.

Task 4.2 – Composite Electrolytes to Stabilize Metallic Lithium Anodes (Nancy Dudney and X. Chelsea Chen, Oak Ridge National Laboratory)

Project Objective. The project has several objectives: (1) prepare novel polymer and ceramic electrolyte materials that can work together to achieve thin membranes that have the unique combination of electrochemical and mechanical properties required for practical manufacturing and to stabilize the metallic lithium anode for good power performance and long cycle life, (2) identify key features of the composite composition, architecture, and fabrication that optimize performance, and (3) fabricate thin electrolyte membranes to use with a thin metallic lithium anode that provides good power performance and long cycle life.

Project Impact. A stable lithium anode is critical to achieve high energy density with excellent safety, lifetime, and cycling efficiency. This study will identify key design strategies that should be used to prepare composite electrolytes to meet the challenging combination of physical, chemical, and manufacturing requirements to protect and stabilize the Li-metal anode for advanced batteries. By utilizing well characterized and controlled component phases, design rules developed for composite structures will be generally applicable toward substitution of alternative and improved SE component phases as they become available. Success will enable DOE technical targets: 500-700 Wh/kg, 3000-5000 deep discharge cycles, and robust operation.

Approach. This project seeks to develop practical SEs to provide stable, long-lived protection for Li-metal anode. Current electrolytes have serious challenges when used alone: oxide ceramics are brittle, sulfide ceramics are air sensitive, polymers are too resistive and soft, and many electrolytes react with lithium. Composites provide a clear route to address these issues. While work continues to emphasize study of ceramic electrolyte / PE interfaces, this effort has expanded to address the following: (1) practical processing routes to fabricate full batteries using better composite electrolytes with a composite cathode and thin Li-metal anode, and (2) introduction of alternative polymer and ceramic phases to replace well-known model materials and develop improved composite electrolytes. In addition to solid-state devices, hybrid batteries are investigated using a fluid or gel catholyte within the porous cathode. Coatings have also been employed to stabilize electrode interfaces. These directions increase complexity of the studies, but are needed to improve cycling stability and rate performance and to advance practical implementation of the SE and Li-anode technology.

Out-Year Goal. The goal is to use advanced manufacturing processes where the architecture of the composite membrane can be developed and tailored to maximize performance and cost-effective manufacturing.

Collaborations. Work is conducted by B. Armstrong, S. Kalnaus, A. Ullman, and X. C. Chen. Ceramic electrolyte powders (LICGC™) are obtained from Ohara Corporation. J. Libera from ANL provided a large quantity of LLZO powders.

Milestones

1. Sinter and characterize porous LLZO network by different processes. (Q1, FY 2021; 80% completed)
2. Compare polymer-LLZO ceramic composites with four different ceramic loadings. (Q2, FY 2021; 60% completed)
3. Elucidate the Li-ion path through at least two distinct polymer-ceramic composites. (Q3, FY 2021, Initiated)
4. Measure Li^+ transference number with at least two different anion receptors. (Q4, FY 2021; 30% completed)

Progress Report

This quarter, the team made progress on the first, second, and fourth quarter milestones.

Q1 Milestone: Sinter and Characterize Porous LLZO Network by Different Processes

The team received Al-doped lanthanum zirconia [LaZrAlO, $La_2Zr_2O_7$ (LZO), batch number RST-028] from the ANL Materials Engineering Research Facility (MERF). The first step is to determine a proper sintering temperature. A Netzsch dilatometer was used to measure the shrinkage of LZO and LLZO (batch number RST-020) uniaxially pressed bars over sintering temperature up to 1200°C in compressed air. The resulting shrinkage profiles of LZO and LLZO are shown in Figure 87a-b. Red arrows show the heating portion of the experiment, and blue arrows indicate cooling. The LZO bar exhibited a 5% decrease in weight and a linear shrinkage of 2.8%. The LLZO bar showed a 12.4 % linear shrinkage, approximately 4 times larger shrinkage than the LZO material. The mass loss was three times larger as well, at a 17.6% decrease in weight. A steep onset of sintering is seen at ~ 1000°C. A direct comparison of scale to highlight the shrinkage differences is given in Figure 88.

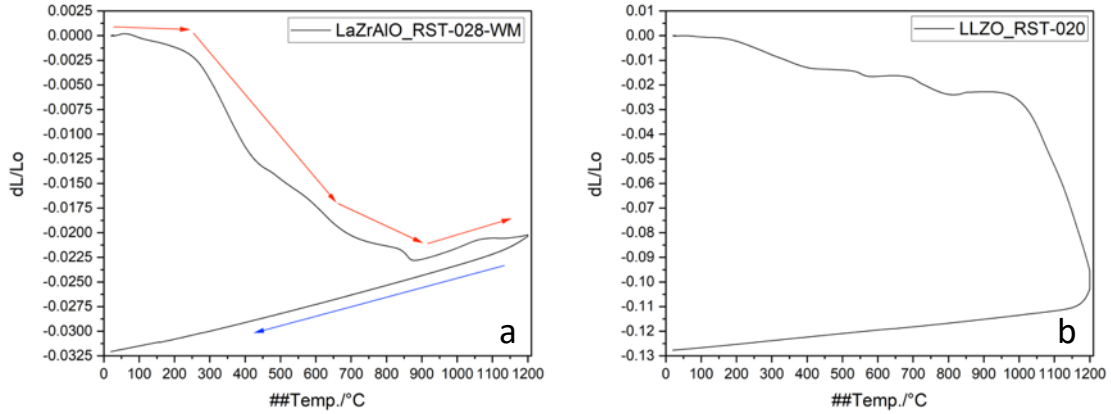

Figure 87. Shrinkage behavior of uniaxially pressed bars in compressed air over a temperature range from 0°C to 1200°C: (a) LZO and (b) LLZO.

The morphology of sintered LZO was investigated at different sintering conditions. To do this, 0.5 g of LZO powder was pressed into a .5-inch diameter pellet. Two pellets were sintered at 1100°C and 1400°C in dry air for two hours. The morphology of the cross-section of the pellets was examined by SEM, as shown in Figure 89. Compared to the as-pressed LZO pellet, the morphology after sintering at 1100°C did not show significant change. This is consistent with the shrinkage data shown in Figure 87. At temperatures below 1200°C, no significant shrinkage was observed. After sintering at 1400°C for 2 hours, clear morphology change is observed. The LZO particles formed necked structure. This is exactly the morphology that the team aimed to obtain. These data will support this milestone by identifying appropriate sintering conditions to achieve desired morphology in the sintered LZO network prior to lithiating.

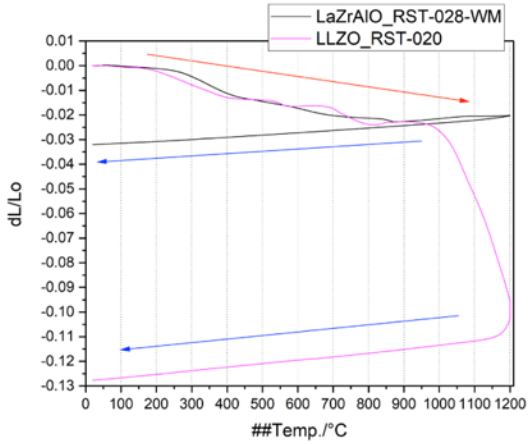

Figure 88. Shrinkage behavior of LZO and LLZO uniaxially pressed bars in compressed air over a temperature range from 0°C to 1200°C.

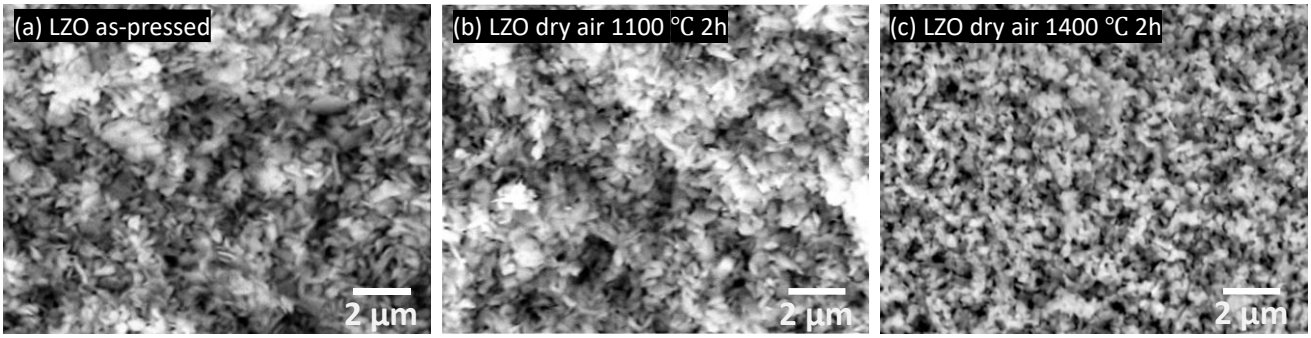

Figure 89. Cross-sectional scanning electron microscopy images of LZO pellets: (a) as-pressed, (b) sintered in dry air at 1100°C for 2 hours; and (c) sintered in dry air at 1400°C for 2 hours.

Q2 Milestone: Compare Polymer-LLZO Ceramic Composites with Four Ceramic Loadings

Last quarter, the team discovered that filling the sintered ceramic network with crosslinked PEO resulted in a large interfacial impedance with lithium metal, and the composite could not cycle well. This quarter, they compared filling the ceramic network with crosslinked PEO and linear PEO. The crosslinked PEO electrolyte (xPEO) consists of crosslinked PEO polymer, LiTFSI salt and tetraethylene glycol dimethyl ether (TEGDME) plasticizer. The linear PEO electrolyte consists of linear PEO polymer and LiTFSI salt. The xPEO was filled by immersing the partially sintered ceramic pellet in the liquid xPEO precursors and curing at 100°C in vacuum. After curing, the composite was soaked in dry TEGDME in an Ar-filled glovebox for an hour. Linear PEO electrolyte was filled by immersing the partially sintered ceramic pellet in dry acetonitrile containing PEO and LiTFSI. Acetonitrile was allowed to slowly evaporate at 60°C in a reactor inside an Ar-filled glovebox. After the evaporation of acetonitrile, the composite was further dried at 80°C before assembling into cells. After filling the ceramic network with polymers, there is a thin polymer surface layer on both sides of the composite.

A lithium symmetrical cell was assembled using 0.7-mm-thick lithium foil. Lithium foil was brushed to remove the surface layer and rolled out thin in a polypropylene bag in a glovebox. The composite electrolyte was sandwiched between two pieces of copper foil followed by two stainless-steel rods (both .5-inch diameter). The cell was sealed in two layers of heat shrink tubing and tested in an AA battery holder. Linear PEO based composites were tested at 70°C to avoid crystallization of the PEO. The results are shown in Figure 90. In the Nyquist plot, the semicircle (if there is only one semicircle) or the second semicircle (if there are two semicircles) represent the electrolyte's interfacial impedance with lithium. The interfacial impedance is tabulated in Table 5. Note that the interfacial impedance calculated from the Nyquist plot is the sum of two interfaces and needs to be divided by two. The interfacial impedance of composite xPEO + LICGC increased by more than four-fold compared to just the xPEO polymer (note that in both cases xPEO contains TEGDME plasticizer). In contrast, only slightly increased interfacial impedance was observed in linear PEO based composites. This is true for both lithium aluminum titanium phosphate (LATP) and LLTO ceramics, with similar necked structures. Since there is a surface polymer layer on all the composites, the interfacial resistance should be determined by the polymer and not the ceramic. This is the case for linear PEO, but not xPEO. This may suggest instability between the TEGDME plasticizer and lithium.

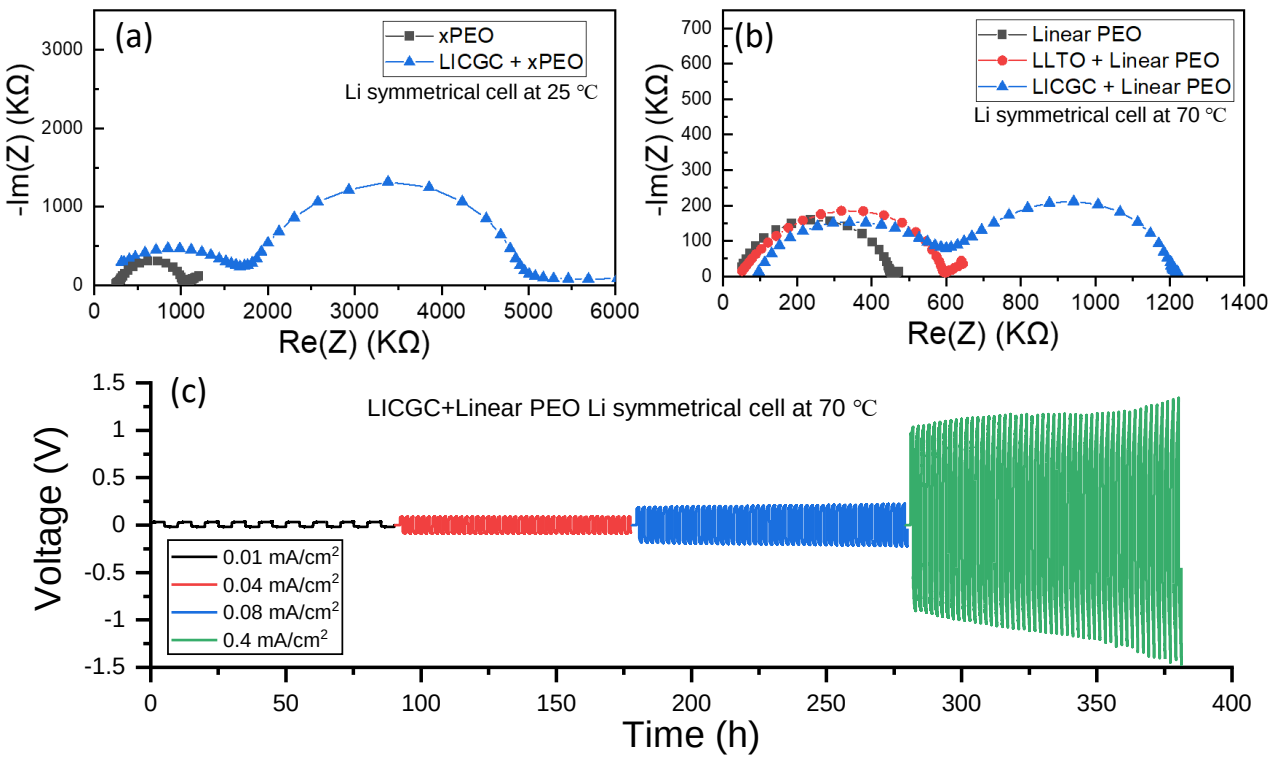

Figure 90. (a) Nyquist plots of lithium symmetrical cell with plasticized xPEO (red curve) and sintered LICGC™ ceramic filled with plasticized xPEO electrolyte (black curve); data collected at room temperature. (b) Nyquist plots of lithium symmetrical cell with linear PEO electrolyte (black curve), sintered LLTO filled with linear PEO electrolyte (red curve), and sintered LICGC ™ filled with linear PEO electrolyte (blue curve); data collected at 70°C. (c) Lithium symmetrical cell cycling using LICGC™/linear PEO composite electrolyte, at 70°C and a series of current densities. Each cycle lasted 10 hours at 0.01 mA/cm² and 2 hours at all the other current densities.

Table 5. Interfacial resistance with lithium for different polymer and composite electrolytes.

Electrolyte	Interfacial Impedance with Li (ohm·cm²)	Measuring Temperature (°C)
xPEO	485	25
LICGC™ + xPEO	2140	25
Linear PEO based PE	261	70
LICGC™ + linear PEO	386	70
LLTO + linear PEO	347	70

The LICGC™ + linear PEO composite symmetrical cell was cycled at 70°C between 0.01 mA/cm² and 0.4 mA/cm². The overpotential was 0.03 V, 0.09 V, 0.19 V, and 1.2 V at 0.01 mA/cm², 0.04 mA/cm², 0.08 mA/cm², and 0.4 mA/cm², respectively. The cell was able to cycle for nearly 400 hours before the test was stopped, indicating good interfacial stability between the composite and lithium. In contrast, LICGC™ with xPEO could only cycle for a few cycles (reported last quarter). However, the dramatic increase in overpotential at higher current densities limits the rate capability of this electrolyte. Next quarter, the team will continue improving the composite design.

Q4 Milestone: Measure Li^+ Transference Number with at Least Two Different Anion Receptors

The team has begun investigating novel PEs to include motifs that allow for dynamic bonds between polymer chains (invention disclosure in preparation). They expect that the dynamic bonds will affect the PEs in three beneficial ways: (1) enhance mechanical properties of membranes, (2) improve handleability of the membrane, and (3) increase the lithium transference number.

The enhanced mechanical properties come from an increase in elasticity, which has been predicted to be an important feature of a PE for inhibiting lithium dendrite growth during charging.[1] The initial polymer membranes synthesized indeed have markedly enhanced elasticity, being able to return to their initial length after being stretched to twice their size. Quantification of the elastic modulus is forthcoming. Importantly, the elastic properties of the membrane remain after the addition of lithium salt. The elasticity of the membranes is also good for ensuring that the membrane can easily withstand the pressure applied during coin-cell fabrication, rather than fracturing.

The dynamic bonding motifs along the polymer chains responsible for improving the mechanical properties are also postulated to interact with the anions of the lithium salt. The team hypothesizes that strengthening this interaction will decrease the diffusivity of the anion under applied voltage, thereby increasing the lithium transference number, which will also improve cycling performance. The conductivity and lithium transference number measurements for a membrane made with lithium perchlorate ($LiClO_4$) are shown below in Figure 91.

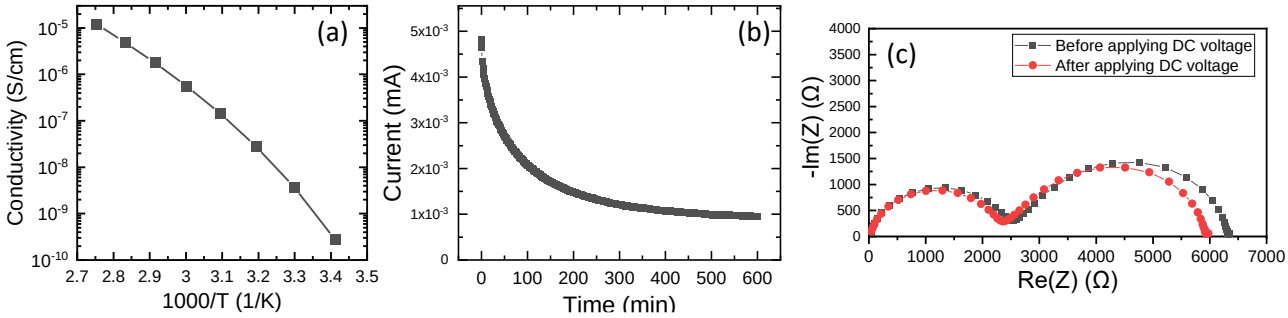

Figure 91. (a) Ionic conductivity of the polymer membrane as a function of inverse temperature. (b-c) Li^+ transference number measurement at 70°C: (b) chronoamperometry measurement with an applied DC voltage of 10 mV, and (c) Nyquist plots of the cell before and after applying the DC voltage.

The ionic conductivity of the polymer with $LiClO_4$ salt is shown in Figure 91a. Compared with standard PEO polymer with the same molar concentration of $LiClO_4$, the conductivity of this PE is one to two orders of magnitude lower. On the other hand, the Li^+ transference number was calculated to be 0.37, an approximately three-fold increase from the standard PEO electrolyte. These initial results are quite promising. The structure and chemistry of this PE will be optimized this fiscal year.

The numerical modeling efforts continued toward understanding of how addition of a SIC to a binary PE changes the cation concentration gradients in a composite. This quarter, the team investigated the influence of introducing SIC particles to PEO-LiTFSI binary electrolyte (PE standing for polymer electrolyte) with the inclusion of ceramic-PE interfacial resistance. The domain is 15-µm by 5-µm. The SIC is represented by the Ohara's LICGC (LATP) ceramic. Four scenarios are considered:

- The whole domain is represented by PE.
- The PE domain is divided by a 5-µm-thick plate of LICGC.
- A single LICGC particle in the middle of the PE domain.
- Composite of LICGC particles in the middle of the PE domain.

In all cases involving LICGC, the team has added an ultra-thin interface layer whose conductivity varied between 1.4e-03 S/cm (~ room-temperature conductivity of LATP) and 1e-07 S/cm (highly resistive). Other constants are arranged in Table 6.

Table 6. Transport properties of LATP and PEO-LiTFSI (with PE standing for polymer electrolyte).

	D_{Li}, m^2/s	D_{TFSI}, m^2/s	c_{Li}, mol/m^3
LATP	$5 \cdot 10^{-12}$ [2]	-	8310
PEO-LiTFSI	$3 \cdot 10^{-11}$	$7 \cdot 10^{-11}$ [3]	1329

The results are represented as the Li^+ concentration profiles normalized with respect to the initial concentration (according to Table 6) and taken along the mid-section of the domain. Normalizing the lithium content helps to visualize the gradients since the initial concentration of lithium ions in PE and LATP differs by a factor of ~ 6. In Figure 92, the different configurations of the simulated volume are shown together with the concentration profiles to help with interpretation of results. The concentrations are shown at 1000 s after application of 1 V polarizing potential. Each figure contains results for the PE alone, represented as a black dash-dotted line.

It can be seen that inserting a SIC and dividing the PE into two halves significantly improves the overall concentration polarization (Figure 92a). With increase of the interface resistance, the LICGC insert acts more like an insulator blocking the current, and therefore the concentration gradient decreases.

When the domain is not partitioned by a SIC wall, the concentrations in the binary electrolyte have to converge to a steady-state gradient (the current can flow through the particle as well as through the PE surrounding the particle). There appears to be no benefit in having the LICGC domain in the center of PE (Figure 92b), unless it blocks the transport of anions completely (that is, dividing layer in Figure 92a). Moreover, with increasing interfacial resistance, the particle is excluded from the transport of ions, forcing the flux to flow around it, which creates even higher concentration gradients. The same is true when the middle portion of the PE domain is occupied by a LICGC/PE particulate composite (Figure 92c).

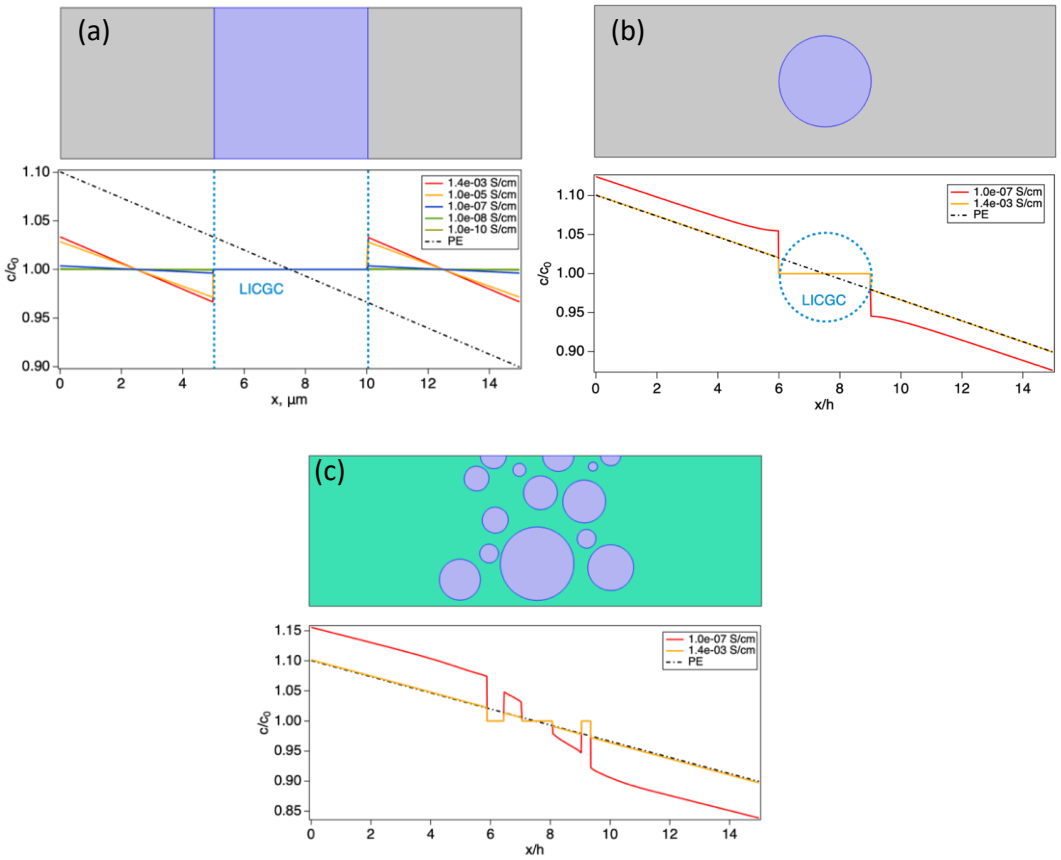

Figure 92. Concentration profiles in (a) polyethylene block divided by LICGC, (b) single LICGC particle in the center of PE block, and (c) LICGC/PE composite corresponding to 40% loading in the middle of PE block.

A separate case was considered (Figure 93) with the SIC layer acting as a coating on the composite layer in the mid-section of the cell. Here, this barrier blocks the transport of anions dividing the overall domain with PE into two smaller domains, each with reduced concentration gradients.

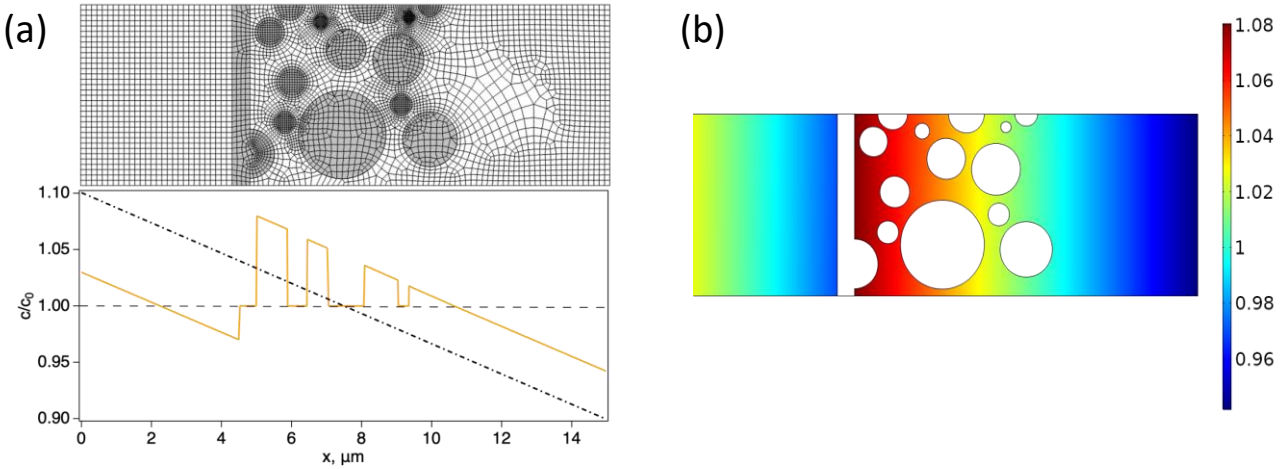

Figure 93. Composite electrolyte with a layer of LICGC blocking the transport of anions. (a) Normalized concentration profile through the midsection. (b) Overall normalized concentration of Li^+ in polymer electrolyte.

These simulation results are very different from those reported last quarter. The main reason is that in the model reported then, the simulation box size and the polarization voltage were both too small to induce large concentration gradients in the composite. In contrast, the concentration gradient of the neat polymer was simulated using a larger box size. The discrepancy in box size rendered the composite and the polymer not directly comparable then. This quarter, the team fixed this problem.

References

[1] Barai, P., K. Higa, and V. Srinivasan. *Physical Chemistry Chemical Physics* 19 (2017): 20493–20505.

[2] Epp, V., Q. Ma, E-M. Hammer, F. Tietz, and M. Wilkening. "Very Fast Bulk Li Ion Diffusivity in Crystalline $Li_{1.5}A_{l0.5}Ti_{1.5}(PO_4)_3$ as Seen Using NMR Relaxometry." *Physical Chemistry Chemical Physics* 48 (2015): 32115–32121.

[3] Timachova, K., H. Watanabe, and N. P. Balsara. "Effect of Molecular Weight and Salt Concentration on Ion Transport and the Transference Number in Polymer Electrolytes." *Macromolecules* 48, No. 21 (2015): 7882–7888.

Patents/Publications/Presentations

Publication

- Chen, X. C., Y. Zhang, L. C. Merrill, C. Soulen, M. L. Lehmann, J. L. Schaefer, Z. Du, T. Saito, and N. J. Dudney. *Journal of Materials Chemistry A* 9 (2021): 6555–6566.

Task 4.3 – Enabling Solid-State Batteries through Characterization and Modeling (Sanja Tepavcevic and Larry A. Curtiss, Argonne National Laboratory)

Project Objective. The project objectives are multi-faceted, including development of a new mechanically and chemically stable and Li-ion conductive ($\geq 2 \times 10^{-4}$ S/cm at 298 K) crystalline/amorphous SE for SSB. The anode and cathode are composed of lithium metal and a Li-based oxide, respectively, allowing operation at cathode potentials > 5 V (denoted as a S_{Li}-S_{EL}-S_C system).

Project Impact. Protective organic and inorganic compounds can enhance stability of the interface, improve Li-ion interfacial transport, minimize dendrite formation, and increase safety in Li-ion batteries.

Approach. The project proposes to develop and use interdisciplinary, atomic-/molecular-level insight obtained from integrating both experimental- and computational-based methodologies to define the landscape of parameters that control interfacial properties for a new generation of the Li-ion solid-solid battery systems. The strategy will involve transferring knowledge gained from well-characterized thin-film materials to real-world materials. This strategy forms a closed loop wherein the knowledge gained from model systems is used to design more complex, real-world materials, and vice versa. The work will focus on utilizing existing in-house synthesis and characterization methods to enable rapid transition from fundamental science to realistic cells.

Out-Year Goals. The out-year goals are to use and develop the physical and chemical synthesis methods for design of SSI with unique chemical/mechanical/conductivity properties. The proposed work will develop and exploit a variety of *ex situ* and *in situ* experimental optical and surface sensitive techniques and electrochemical methods to explore and explain bulk and interfacial properties of the selected materials. The results will serve to unravel many puzzling bulk and interfacial properties of S_{Li}-S_{EL}-S_C systems, including various types of ceramic and glass materials.

Collaborations. This project funds work at ANL and collaboration with J. Sakamoto at UM.

Milestones

1. Evaluating chemical stability and correlating with interfacial reactivity for vacuum-deposited Li/Al- doped LLZO interfaces. (Q1, FY 2021; Completed)
2. Understanding impact of different dopants in LLZO (aluminum versus gallium) on chemical and electrochemical reactivity with metallic lithium by surface and bulk sensitive techniques and computational tools. (Q2, FY 2021)
3. Modifying energy barrier for Li^+ transport in Al-doped LLZO by controlling the chemistry of the GBs via additives. (Q3, FY 2021)
4. Optimizing nanoLLZO+PEO composite and characterizing chemical and electrochemical reactivity with metallic lithium by surface and bulk sensitive techniques. (Q4, FY 2021)

Progress Report

LLZO garnet-based oxides are a promising class of SEs used as the separator in ASSBs. When synthesized, LLZO is commonly chemically modified by aliovalent doping on the lithium or zirconium sites, lowering the lithium concentration and stabilizing the high-conductivity cubic phase of garnet. While LLZO is considered to have a wide electrochemical stability window, its intrinsic stability in contact with lithium metal is not sufficiently well understood, and there is still a debate on the key question of whether LLZO does or does not form passivation layers before and during cycling. Understanding the role of lithium concentration modifying dopants, such as tantalum, niobium, aluminum, and gallium, is critical to understanding the phase and microstructural evolution of LLZO in ASSBs.

Cationic substitution with the species above (that is, Ta^{5+}, Nb^{5+}, Al^{3+}, and Ga^{3+}) works via a conservation of charge mechanism, where the addition of these more positively charged species requires a sufficient number of lithium to be removed to ensure charge neutrality for the whole electrolyte. Both Ta^{5+} and Nb^{5+} substitute on the Zr^{4+} site, resulting in the removal of one Li^{+} atom for every atom of dopant added. In the team's previous work,[1] they began investigating the change in electrochemical environment at a Li^{0}|LLZO interface as Ta^{5+} or Nb^{5+} were systematically placed at varying distances from the interface. As evidenced from their calculations and XPS experimental results, the species tantalum and niobium are chemically different as dopants. Tantalum shows no reduction near the surface or in the bulk, while niobium was more chemically active, reducing from its 5^{+} oxidation state down to its 1^{+} state. The reduction of niobium appears to propagate through the material, starting at partial reduction of niobium and zirconium, near the surface, with continual charge compensation accruing through the formation of an oxygen deficient layer (ODI). The ODI acts on the electrolyte, either drawing lithium from the metal into LLZO, or expelling oxygen from LLZO out to the metal. The resulting microstructural defects could be impeding performance of the device through formation of impurity phases, charge nucleation sites, or pore formation. Work continues to define what new phases could form after long exposure; what is known, however, is that these impurity phases appear to be less ionically conductive with respect to lithium, and possibly electronically conductive as evidenced by lowering of the bulk resistance in EIS measurements, and observation of a color change from white to black, after exposure to lithium and during cycling.

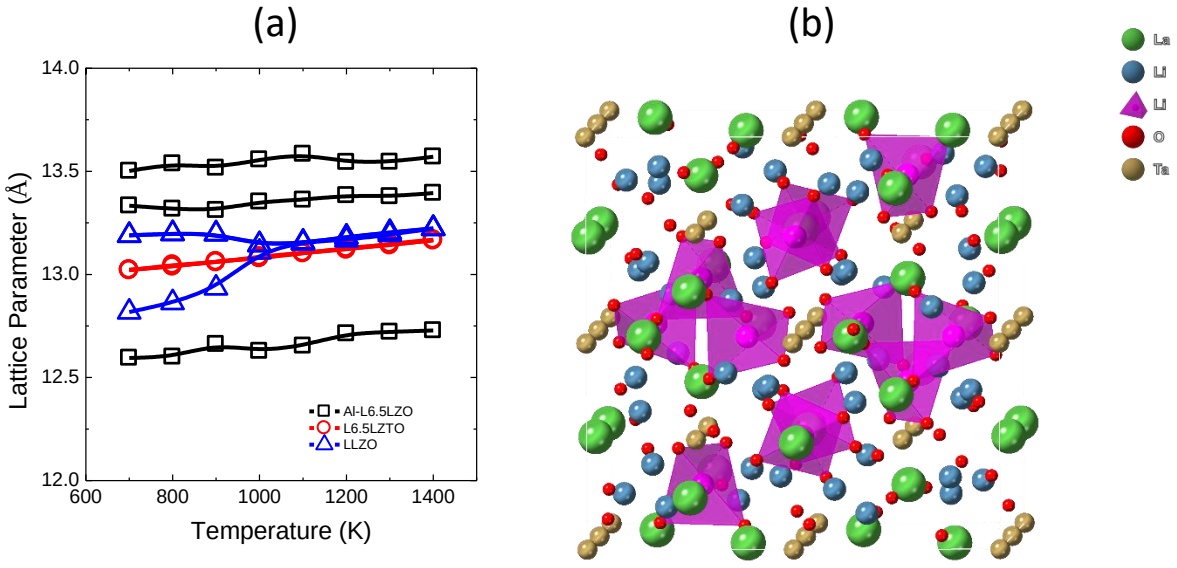

Figure 94. (a) Lattice transformation behavior of Al-doped LLZO and undoped LLZO as a function of temperature. (b) Unit cell of LLZO; pink polyhedra show ideal aluminum doping sites.

The second class of dopants, Al^{3+} and Ga^{3+}, work by directly substituting onto the lithium sublattice of interconnected tetrahedral and octahedral sites. Both dopants when inserted into bulk LLZO, absent lithium metal, show relatively little difference in formation energy with respect to defects on the lithium sublattice. This has led to the belief that both dopants are chemically similar in LLZO, making the choice of dopant a matter of personal preference and availability. An investigation into the phase transformation, dopant clustering, and diffusivity effects of Al^{3+} doping was initiated. At the onset, the team combined classical FFs as first implemented by Daza et al.[2] and Klenk et al.[3] to try and effectively study the Al^{3+} concentration dependance in LLZO. As noted by Daza, in their implementation the FF did not accurately describe the phase transformation behavior with increased doping or increased temperature. Figure 94a shows that the implementation attempted in this study also failed to accurately predict the phase transformation from tetragonal to cubic when the critical concentration of lithium was reduced to 6.5, or the temperature of the simulation was increased to 900 K. The model shows three unique lattice parameters for Al-doped LLZO ([Li] = 6.5) when heated from an initial structure at 300 K, giving the appearance of a tetragonal-like phase, but not cubic as to be expected given the lithium concentration. In contrast, the Ta^{5+}-doped LLZO has a consistently cubic phase, and undoped LLZO has both tetragonal and cubic phases present in agreement with experimental results. A second model with Ga^{3+} was also attempted, but it likewise failed to give compelling structural results. The failure of this model system to accurately predict the correct phase of LLZO led to abandonment of this model system. The model is intrinsically flawed in its inability to model off stoichiometric concentrations of lithium, so modeling the Li-metal interface is an impossibility; further, it is incapable of modeling oxidation/reduction due to fixing of ionic charge.

To address the flaws in the previous study, a series of modeling experiments was initiated using DFT calculations. DFT is uniquely suitable for modeling the oxidation/reduction of ionic species as they are moved closer to or further from the Li-metal interface. Example simulation cells of the Li^0|LLZO interface are shown in Figure 95Figurea. Single ions of Al^{3+}/Ga^{3+} dopants were inserted into the simulation cell and optimized with lowest energy configurations arising when the dopant is on tetrahedral sites. The oxidation/reduction potential of LLZO was assessed by looking for changes in the DOS for electrons in the structures shown in Figure 95b-c, respectively. Substitutions of Al^{3+}/Ga^{3+} in the bulk of LLZO, Figure 95d, show there is no change with respect to the location of the Fermi energy or width of the band gap, indicating that the substitution of Al^{3+}/Ga^{3+} does not form electronically conducting states. However, when interfaced with lithium metal, Figure 95Figuree, the metallic-lithium states fall between the valance and conduction bands of LLZO, shifting the DOS to the left, raising the Fermi energy closer to the conduction band of LLZO. Assessment of the profile in the interface system is under way, but appears consistent with an electronically conductive metallic state, overlapping with the conduction band of the insulator. There are no discernable features identified uniquely with Al^{3+}/Ga^{3+} ions, so any change in band structure appears to be purely from the metallic lithium when the dopant is not directly on the surface. The depth and propagation of the electronic states into the bulk of the cell are of interest and could be indicative of the ODI formation previously observed.

In line with the team's previous experimental studies, a thin layer of lithium metal was deposited on the Ga-LLZO surface by E-beam evaporation, which limits the additional energy input to the surface (< 0.1 eV). Reduction with Li^0 does not perturb the structure of Ga-doped LLZO. Raman measurements in Figure 96a show that the cubic phase of pristine Ga-LLZO is maintained (within the ~1-μm space probed by the laser), and no tetragonal or impurity phases, which might result from continuous reaction with Li^0, are detected. With the reduction of Ga^{3+} to Ga^0, there is the possibility of having a mixed conducting interphase (MCI) due to electronic and ionic conduction. Tunneling AFM of the reacted Ga-LLZO interface shows no evidence of electronic conductivity, Figure 96b, with resistivity in the TΩ regime. Therefore, while Ga-LLZO does react at the Li-electrolyte interface, there seem to be no complications arising from disruption of the Li^+-conducting cubic phase or an MCI.

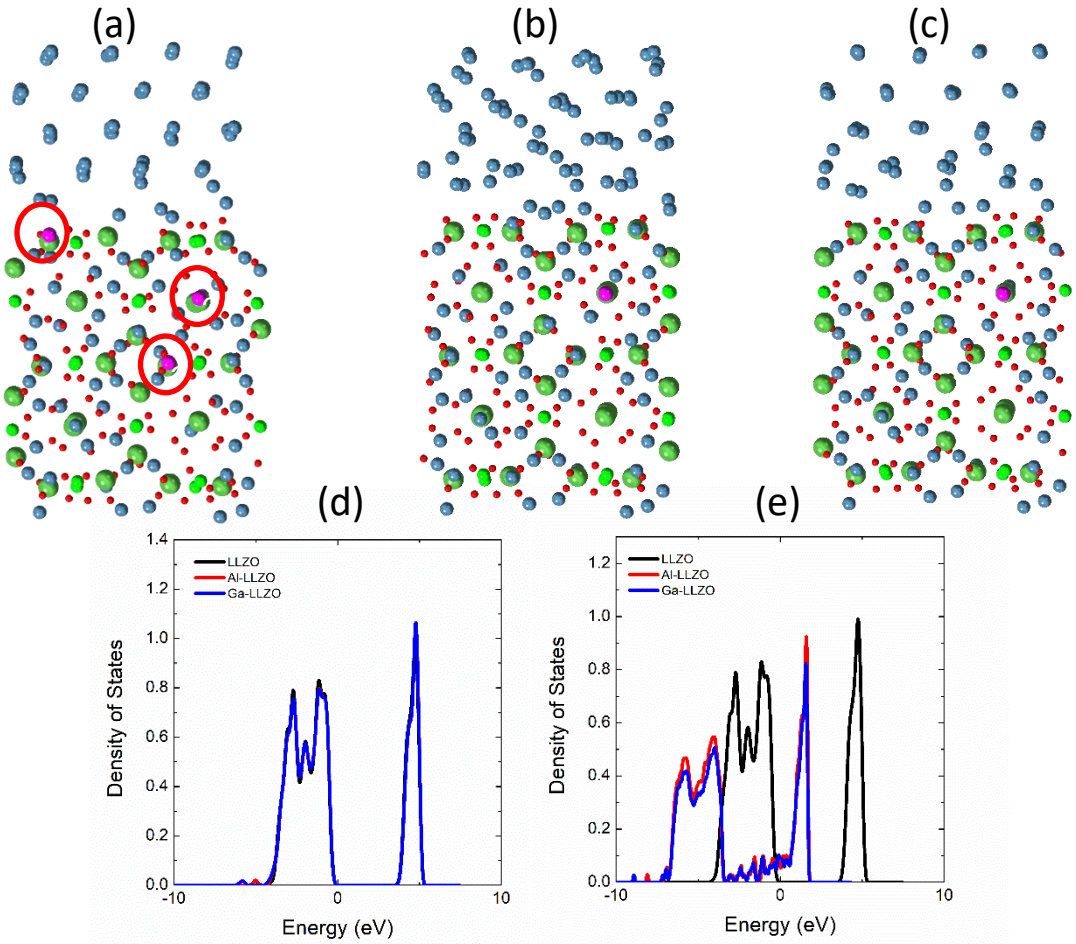

Figure 95. Density functional theory simulation cells of Li^0 and doped LLZO. (a) Simulation cell showing three possible dopant locations in the LLZO: at the surface, one layer down, and two layers down. (b-c) Geometry optimized structures of doped LLZO with Al^{3+} (b) and Ga^{3+} (c). Density of states for both doped and undoped bulk LLZO (d) and Li^0|LLZO interface (e) shifted to the Fermi level at zero.

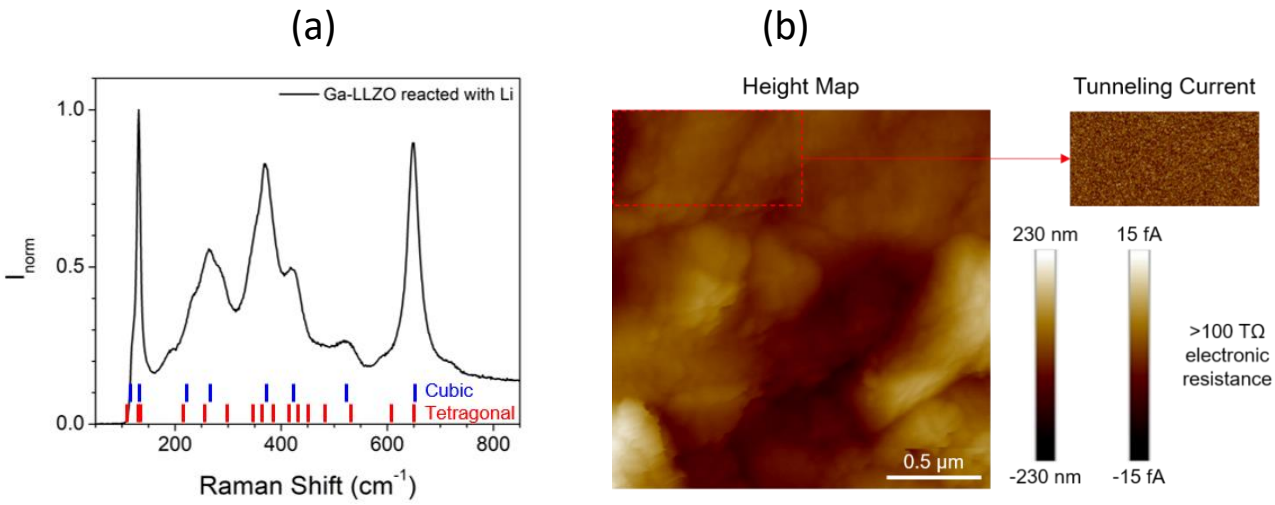

Figure 96. (a) Raman spectrum of Ga-LLZO reacted with lithium metal; peak positions for the cubic and tetragonal phases of undoped LLZO are marked in blue and red, respectively. (b) AFM images showing (left) height map of Li^0-reacted Ga-LLZO and (right) tunneling current measured while applying 5 V DC between the AFM tip and Ga-LLZO pellet. Images in (b) share the same scale bar.

References

[1] Zhu, Y., J. G. Connell, S. Tepavcevic, P. Zapol, R. Garcia-Mendez, N. J. Taylor, J. Sakamoto, B. J. Ingram, L. A. Curtiss, J. W. Freeland, D. D. Fong, and N. M. Markovic." *Advanced Energy Materials* 9 (2019): 1803440.

[2] García Daza, F. A., M. R. Bonilla, A. Llordés, J. Carrasco, and E. Akhmatskaya. *ACS Applied Materials & Interfaces* 11 (2019): 753–765.

[3] Klenk, M. J., and W. Lai. *Solid State Ionics* 289 (2016): 143–149.

Patents/Publications/Presentations

The project has no patents, publications, or presentations to report this quarter.

Task 4.4 – 3D Printing of All-Solid-State Lithium Batteries (Jianchao Ye, Lawrence Livermore National Laboratory)

Project Objective. This project has three objectives: (1) tuning microstructures of 3D-printed SSE separators, (2) determining material and processing compatibilities with cathode printing, and (3) 3D printing of sintering-free SSE separators.

Project Impact. All-solid-state lithium batteries are difficult to process due to the brittleness of ceramic materials, poor solid-solid contact, and electrolyte-electrode stability issues. As a result, the energy and power density and also cycling stability are far from satisfying. This project will address fabrication difficulties by using state-of-the-art 3D-printing techniques that can introduce 3D interfaces and architectures to enhance solid-solid contact and reduce charge transfer resistance. Success will benefit the DOE by establishing the best manufacturing methods for ASSBs to achieve VTO goals on the performance of beyond Li-ion batteries.

Approach. The project employs 3D-printing techniques to manufacture SSEs and related components for ASSBs. The team starts with direct ink writing (DIW) to develop ink recipes with desired rheological properties and to explore post-sintering approaches to achieve high densification. In parallel with DIW 3D printing, the team also explores other 3D printing options, such as projection microstereolithography (PuSL). Both sintering and sintering-free approaches can gain benefit from 3D printing and therefore will be investigated.

Out-Year Goals. The team will determine the co-sintering stability of printed NMC/LLZTO films and compare with that of hydraulic-pressed NMC/LLZTO pellets. They will print SSE/cathode bilayer structures with controlled interfaces and determine their electrochemical performance with or without post sintering process.

Collaborations. Microstructures, ionic conductivities, and mechanical properties will be provided to the LLNL simulation team, led by the PI, B. Wood, for establishing and validating phase-field modeling methods.

Milestones

1. Evaluate new commercial LLZTO powder sources. (Q1, FY 2021; Completed)
2. Determine performance of ASSBs based on 3D-architected LLZTO structure. (Q2, FY 2021; Completed)
3. Determine performance of ASSBs based on composite PE. (Q3, FY 2021; In progress)
4. Evaluate ASSBs based on co-sintering approach. (Q4, FY 2021; In progress)

Progress Report

DIW and Post Sintering of LLZTO Structures. Inks based on LLZTO powders (Vendor 2: NEI) and polyethylene glycol diacrylate (PEGDA) binders were prepared for 3D printing. To improve the ink homogeneity and facilitate sintering densification, the purchased LLZTO raw powders were further high-energy wet milled together with various sintering agents [Al_2O_3, SiO_2, Li_3BO_3 (LBO)]. After ball milling, PEGDA was directly added without drying procedure. After removing the solvent (acetonitrile), the obtained ink can easily pass 30-μm mesh. In Figure 97, the top panel shows some examples of DIW-printed bilayer structures: first, a dense film, and then one to two layers of zig-zag patterns. The whole structure is used as ion conductive separator for ASSB fabrication. The dense layer is to prevent short circuit; the patterned layer is to increase the contact area with cathode. After printing, the structures were UV cured for 1 minute to form the solid green body for post sintering.

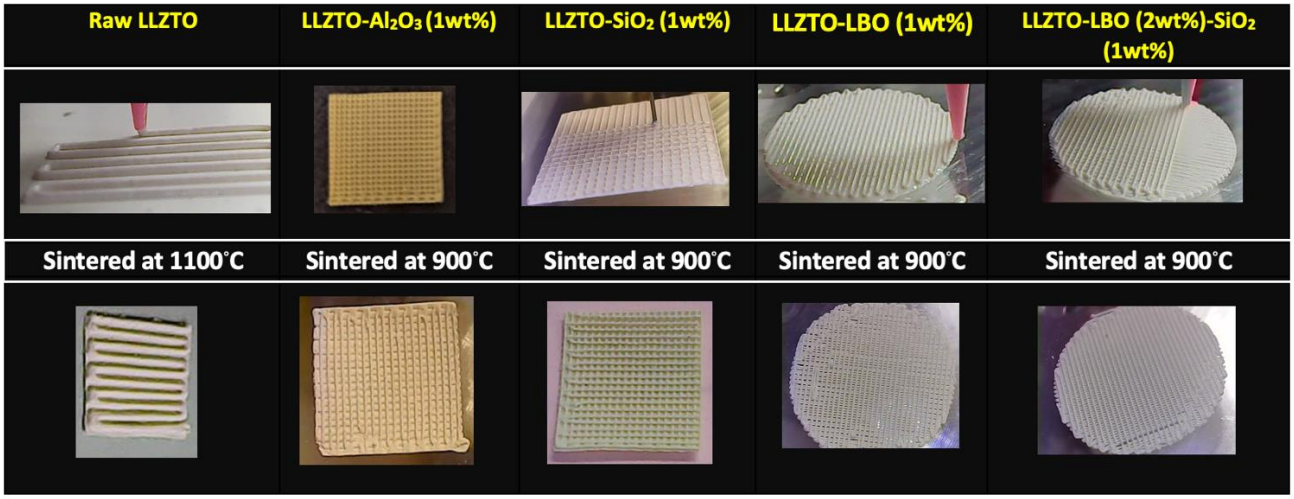

Figure 97. Optical images of the different 3D-printed LLZTO structures before and after sintering.

The bottom panel of Figure 97 shows the corresponding photos of two-step sintered structures, with very nicely maintained shapes. Shrinkage after sintering at 900°C is summarized in Table 7. Raw LLZTO with micrometer-sized particles has little driving force for densification at 900°C, and thus only shrank ~ 2%. The others made from ball-milled powders shrank from 30% (with Al_2O_3) to 38% (with LBO/SiO_2). Interestingly, the shrinkage difference among those ball-milled powder samples is not considerably large, despite the variation of sintering agent and solid content. This suggests the densification is dominated by size-dependent translational motion of particles. Higher sintering agent content may be needed to increase surface tension and facilitate surface diffusivity for further densification.

Table 7. Shrinkage of the 3D-printed LLZTO structures sintered at 900°C for 2 hours.

Solid Content of 3D-Printed LLZTO Structures	Shrinkage (%) after Sintering at 900°C
LLZTO raw (75 wt%)	2
LLZTO (60 wt%)-Al_2O_3 (1 wt%)	30
LLZTO (55 wt%)-SiO_2 (1 wt%)	35
LLZTO (38 wt%)-LBO (1 wt%)	32
LLZTO (38 wt%)-LBO (2 wt%)-SiO_2 (1 wt%)	38
LLZTO (60 wt%)-LBO (3 wt%)-Al_2O_3 (1 wt%)	33

Although none of the current LLZTO structures are fully densified, the LLZTO-LBO/SiO_2 sample demonstrated good mechanical robustness compared with others due to better sintering of LLZTO grains, which is revealed from cross-sectional observations (Figure 98). XRD results (Figure 99) reveal formation of LZO phase in the samples with LBO and/or SiO_2 sintering agents, suggesting lithium loss in LLZTO structure. Note the lithium loss could be compensated by adding additional lithium source in the milling process. The open porous structure and LZO impurity phase lead to high resistivity and low fracture toughness that prevents them from being directly used as conductive separator for ASSB assembly. Before optimizing the ink compositions to achieve high densification and purity, the team decided to use the porous LLZTO as backbone and infill PE to make LLZTO – solid polymer electrolyte (SPE) composite structure, which can increase both ionic conductivity and mechanical robustness.

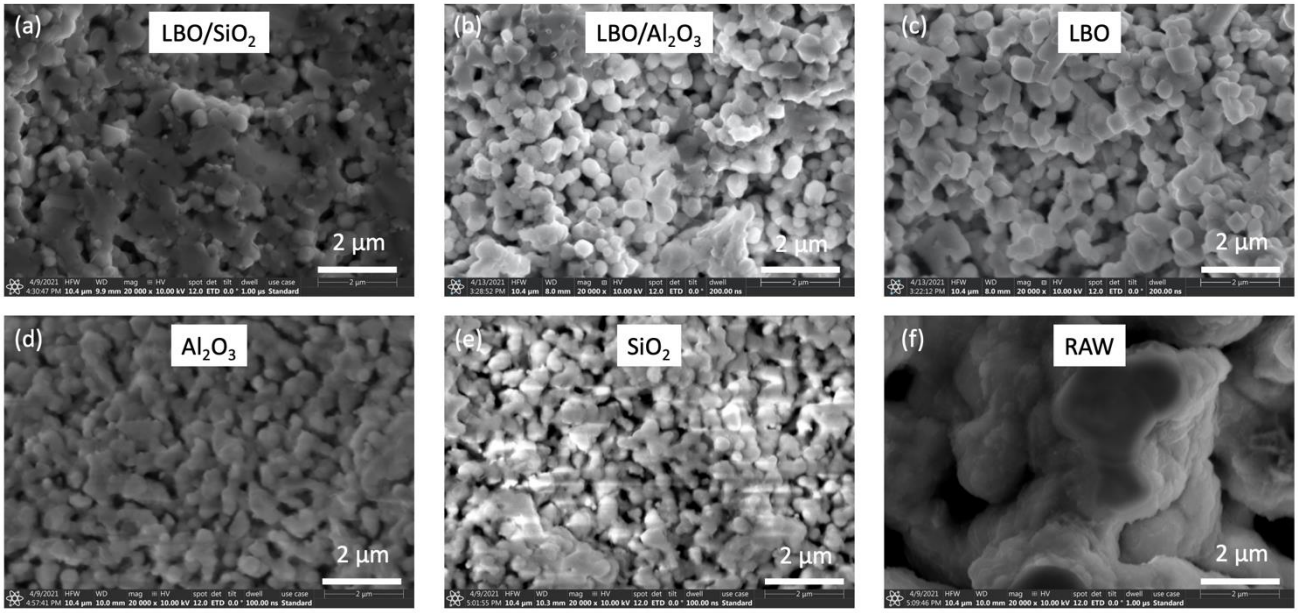

Figure 98. Cross-sectional scanning electron microscopy of LLZTO films with different sintering agents after argon pyrolysis and air burning at 900°C.

Infilling with Solid PEs. UV-curable SPEs were developed for the infilling purpose. The SPEs are composed of PEGDA / polyethylene glycol methacrylate (PEGMA) / LiTFSI with or without PEO addition. PEGDA provides mechanical stiffness and strength; PEGMA increases flexibility and conductivity; and PEO increases elasticity and ductility. Figure 100 shows an example of a PEGDA/PEGMA/PEO/LiTFSI infilled LLZTO-1 wt% Al_2O_3 film sample.

It is mainly composed of three layers: bottom, thick SPE layer (~ 100 µm); middle, LLZTO-SPE composite (~ 50 µm); and top, thin SPE layer (~ 3 µm, Figure 100b). The additional SPE layer serves as a cushion against mechanical failure. Even though cracks are formed in the LLZTO layer (Figure 100c), the SPE layer is still intact, which helps prevent shorting. The room-temperature ionic conductivity of the SPE (PEGDA-PEGMA-PEO)/LiTFSI) was measured to be 1.06 x 10^{-4} S/cm (EIS shown in Figure 100d), much higher than PEO/LiTFSI system (10^{-5} to 10^{-6} S/cm). When this SPE was infilled into the porous LLZTO-1wt% Al_2O_3 film, similar ionic conductivity was obtained for the composite (1.00 x 10^{-4} S/cm); the team expects that the composite may show higher transference number and resistance to lithium dendrite penetration. The SPE composition will be further optimized next quarter, and the effect of 3D-printed LLZTO backbone will be investigated.

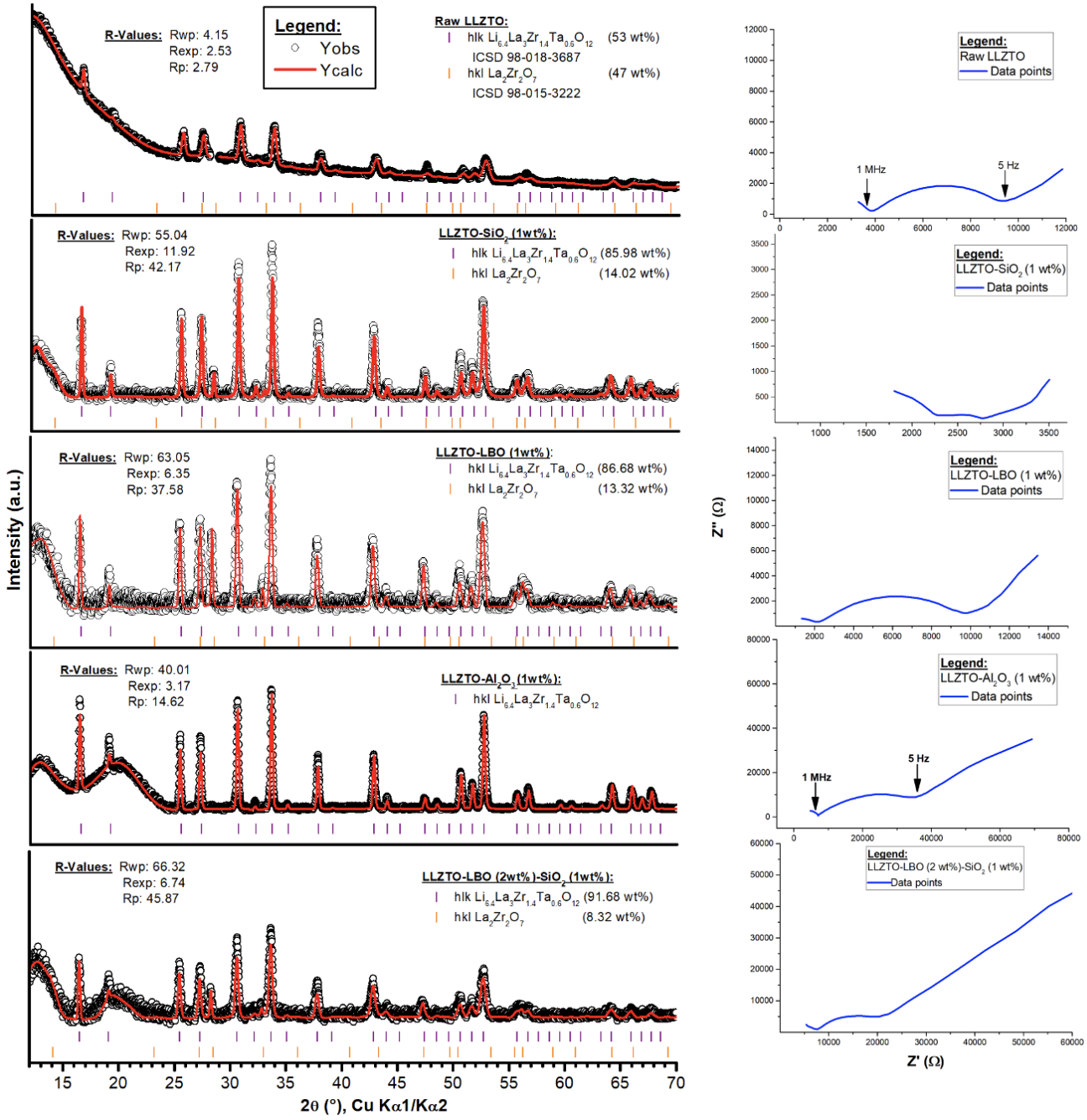

Figure 99. (left) Rietveld refinement fits of 3D-printed LLZTO structures. (right) Nyquist plots at room temperature of the assembled full cells using the 3D-printed LLZTO structures filled with solid polymer electrolyte (PEGDA-PEGMA/LiTFSI) as solid electrolytes and NMC as cathode.

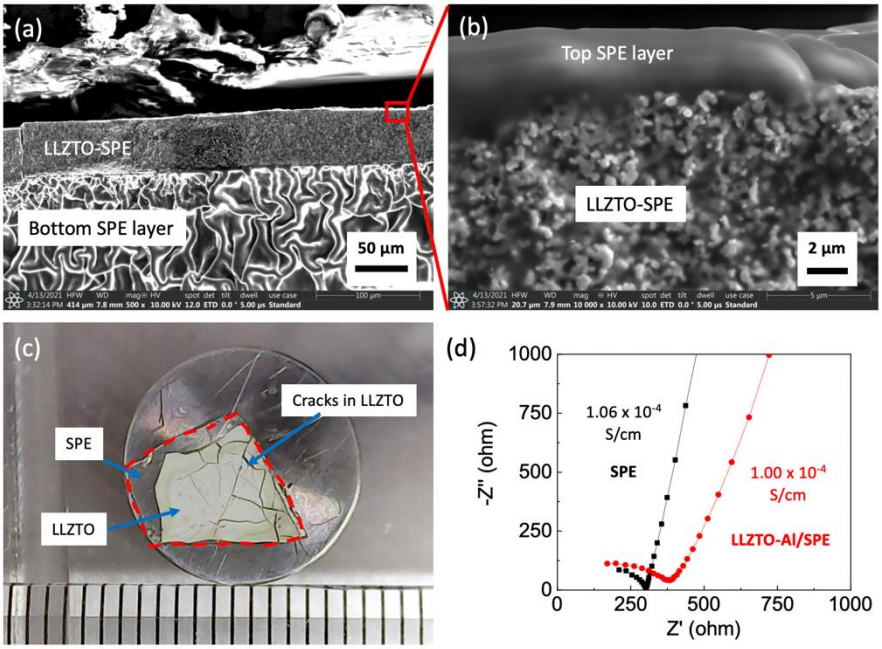

Figure 100. Sintered LLZTO film filled with solid polymer electrolyte (SPE) composed of UV cross-linked (PEGDA-PEGMA-PEO)/LiTFSI. (a-b) Scanning electron microscopy morphology. (c) Cracks formed in LLZTO during cell assembly. (d) Nyquist plots of SPE and LLZTO/SPE membranes sandwiched between stainless-steel electrodes.

Full Cell Integration. To demonstrate a full-cell battery using the 3D-printed LLZTO structure, a NMC-622 cathode ink with PVDF and carbon black additives was prepared and applied on the patterned side of porous LLZTO structure. After vacuum drying, SPE (PEGDA/PEGMA/LiTFSI) ink was infilled into both LLZTO separator and NMC cathode and then UV cured. A lithium chip was then pressed on the LLZTO side to make the full-cell battery for testing. Nyquist plots are shown in the right panel of Figure 99. The total resistances of the cells at room temperature vary from ~ 3000 ohm to 40000 ohm for a footprint area of 0.13 cm^2. Such a large internal resistance has to be further reduced to achieve good charging/discharge rate performance. Figure 101 shows preliminary galvanic charging/discharge curves of an NMC-622/LLZTO-SPE/Li all-solid-state cell run at 60°C. Performance could be improved by adding PEO in the SPE to enhance ionic conductivity and mechanical properties, and adding Li^+ conducting salts in the NMC cathode ink. Those activities will be carried out next quarter.

Summary and Future Efforts. To increase the contact area between cathode and SSE, 3D-printed LLZTO films with zig-zag patterns were prepared as the separator. For the partially sintered samples, UV-curable SPE was infiltrated into the open pores to make the composite separator to enhance both conductivity and mechanical properties. NMC/LLZTO-SPE/Li full cells were assembled, and battery performance was evaluated. In upcoming quarters, the tam will continue two research lines to improve full-cell performance: (1) increasing ionic conductivity of composite PEs with both polymer-in-ceramics and ceramics-in-polymer designs; and (2) optimizing ink recipes to densify the printed LLZTO structures for pure ceramic cells with co-sintered cathodes.

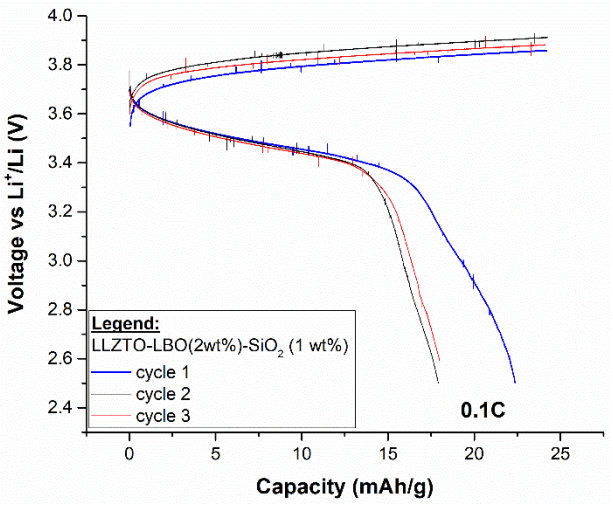

Figure 101. Charge-discharge capacity curves at 0.1 C-rate using the 3D-printed LLZTO-LBO (2 wt%)-SiO_2 (1 wt%) structure infilled with PEGDA/PEGMA/LiTFSI solid polymer electrolyte as solid electrolyte, and NMC-622/PVDF/CB as cathode.

Patents/Publications/Presentations

The project has no patents, publications, or presentations to report this quarter.

Task 4.5 – Interfacial Studies on Lithium Thiophosphate Based Solid Electrolytes and Cathodes (Jagjit Nanda, Oak Ridge National Laboratory)

Project Objective. Capacity fading and the underlying interfacial side reactions between thiophosphate SEs and cathode active materials are not well understood. A key project deliverable is to combine EIS measurements with complementary *in situ* and *ex situ* spectroscopy and microscopy to identify decomposition reaction products at the CEI. Ultimately, this work will enable a mechanistic understanding of factors that limit the rate performance and capacity loss of SSBs. The goal here is to combine the information from these techniques to provide a unified overview of the interfacial layer's composition, structure, and morphology. In this multi-year work, the team will investigate a number of SEs [Li_3PS_4 (LPS), $Li_{10}GeP_2S_{12}$ (LGPS), and $Li_{9.54}Si_{1.74}P_{1.44}S_{11.7}Cl_{0.3}$ (LSiPCl)] and cathode compositions belonging to different structural families [$LiFePO_4$ (olivine), FeS_2 (sulfide-based conversion cathode), and $LiNi_{0.6}Mn_{0.2}Co_{0.2}O_2$ (NMC-622, layered oxide)].

Project Impact. SSBs are poised to be the next-generation battery technology for meeting EV goals in terms of energy density, cycle life, and safety. Among other technical barriers, the success of this technology relies on design of stable electrode/electrolyte interfaces. Sulfide-based SEs have high ionic conductivity ($> 10^{-4}$ S/cm) and are mechanically soft, which simplifies processing compared to their oxide counterparts. Furthermore, sulfide SEs are comprised of earth abundant materials (for example, sulfur and phosphorus) and can be easily synthesized using scalable, low-temperature solution-based routes.

Approach. A low-temperature (< 350°C) solution-based synthesis method will be used to synthesize the LPS family of SEs. The structure of these materials is characterized using XRD, Raman spectroscopy, and neutron scattering. Standard AC/DC electrochemical methods are used to characterize ionic conductivity, electrochemical stability, and CCD. The work scope includes using various *in situ* and *ex situ* electrochemical, microscopic, and spectroscopic tools for characterizing the structure, morphology, and kinetics of the interfacial reaction layer formed between thiophosphate SEs and cathodes.

Out-Year Goals. Develop thiophosphate SEs – sulfide cathode interfaces with low ASR for ASSBs.

Collaborations. This project will collaborate with G. Ceder (UCB) and P. Jena (Virginia Commonwealth University) on modeling and synthesis guideline, as well as with S. Greenbaum on solid-state NMR to measure ion-diffusivity and local bonding.

Milestones

1. Demonstrate and test hot-sintering method to fabricate composite thiophosphate SE-NMC cathodes. (Q1, FY 2021; Completed)
2. Optimize synthesis and processing conditions (for example, interfacial coatings and stack pressure) to minimize the ASR between argyrodite SEs and NMC cathodes. (Q2, FY 2021; Completed)
3. Perform Raman microscopy, NMR, and electron microscopy to characterize bulk argyrodite SE and cathode SE-interfaces to investigate capacity loss and degradation mechanisms. (Q3, FY 2021; In progress)
4. Select and optimize a few solid-state cathode compositions to demonstrate room-temperature cycling with LPS and/or argyrodite SEs. Stretch Goal: 50 cycles with < 20% capacity fade. (Q4, FY 2021; In progress)

Progress Report

This quarter, activities focused on evaluating SSBs containing NMC-based cathodes. Pellet-type cells were prepared by pressing a thin lithium anode (~ 45 µm on copper foil), ß-Li_3PS_4 (LPS) separator, and composite cathode (NMC-811+C+LPS) at 500 MPa. All measurements were performed at room temperature using a stack pressure of 5 MPa. Figure 102a shows voltage profiles for NMC-811 cathodes with/without a 1 wt% $LiNbO_3$ (LNO) coating. While the cathodes exhibited high charge capacities of ~ 1.3 mAh/cm^2 (200 mAh/g) during the 1st cycle, the reversible capacity was low (~ 100 mAh/g). Interestingly, the LNO coating (a common strategy report in the literature to stabilize the cathode/Li_3PS_4 interface) had little impact on the cathode's capacity or cyclability (see Figure 102b). To investigate the redox properties of the SE phase in these composite cathodes, LPS was blended with carbon powder and characterized in Li|LPS|LPS+C cells. The LPS loading in this control experiment (3.3 mg/cm^2) was identical to that in the NMC-based cathodes. As shown in Figure 102a, the LPS exhibited a sloping voltage profile that matched the feature ~ 3.0-3.5 V in the NMC cathode tests. LPS oxidation was an irreversible process, and the SE had negligible redox activity during subsequent cycles. Overall, results in Figure 102 demonstrate that performance of NMC+LPS+C cathodes is significantly hindered by decomposition of LPS at high voltages. Furthermore, applying interfacial coatings directly on the active material does not address the poor oxidative stability of LPS, especially when the composite cathode contains high surface area carbon additives that exacerbate SE decomposition.

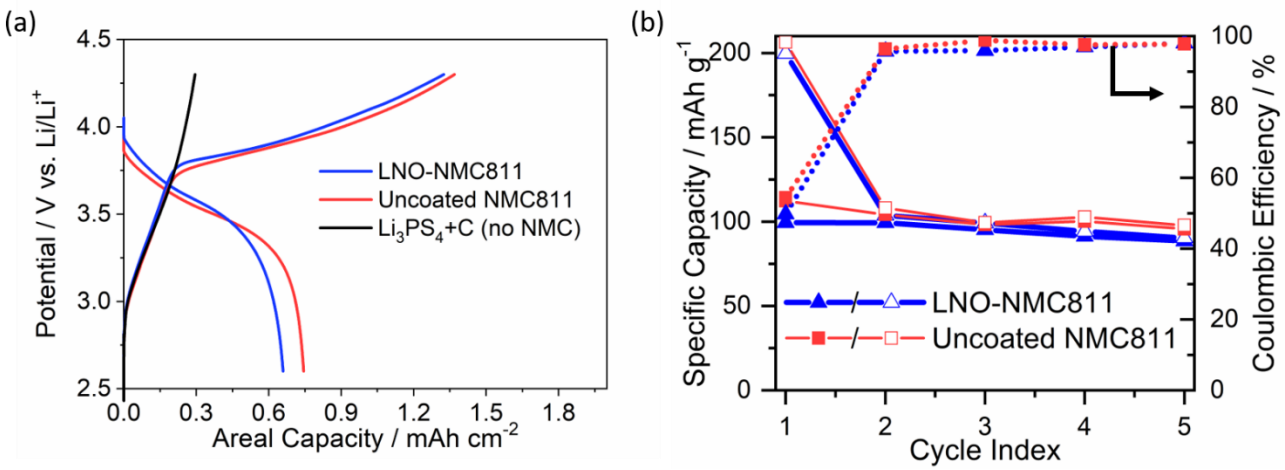

Figure 102. Electrochemical characterization of solid-state batteries containing a lithium anode, LPS separator, and NMC-811 cathodes with/without an LNO coating (1 wt%) showing (a) 1st cycle charge/discharge curves and (b) capacity and Coulombic efficiency over 5 cycles. In (b), open/closed symbols represent charge/discharge capacities, respectively. All cells were cycled at a current density of ±66 µA/cm^2 (10 mA/g$_{NMC}$)

Due to its high Li^+ conductivity (~ 1 x 10^{-4} S/cm at 25°C) and good oxidative stability, a phosphate-based SE powder from Ohara Corp. was investigated as a replacement for LPS in the composite NMC-based cathodes. These experiments used the same cell fabrication and testing protocols described above. As shown in Figure 103, the Li|LPS|NMC+C+Ohara cell exhibited negligible electrochemical activity with capacities < 5 mAh/g$_{NMC}$. The poor performance of this composite cathode is attributed to the lack of long-range connectivity among the Ohara particles. Unlike lithium thiophosphate SEs (for example, LPS), which can be compacted to > 90% relative density at room temperature, phosphate-based SEs likely require high-temperature sintering processes to ensure percolating Li^+ pathways throughout the composite cathode. In this regard, the hot-pressing setup developed in FY 2020 may be useful to improve performance of the Ohara-containing cathodes, but this topic was not explored this quarter.

Considering the poor oxidative stability of LPS, experiments next quarter will investigate new cathode formulations containing either: (1) active materials with high capacities and moderate operating voltages (< 3 V versus Li/Li^+) such as FeS_2, sulfur, and FeF_3, and/or (2) alternate sulfide SEs such as Li_6PS_5Cl or $Li_{10}SnP_2S_{12}$. Polymer buffer layers will also be explored to improve interfacial stability at Li/SE and cathode/SE interfaces.

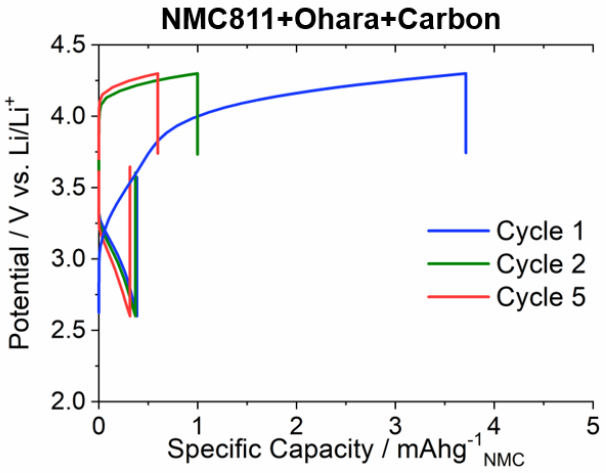

Figure 103. Galvanostatic charge/discharge profiles for a Li|LPS|NMC-811+C+Ohara solid-state battery cycled at ±66 µA/cm² (10 mA/g_{NMC}).

Patents/Publications/Presentations

The project has no patents, publications, or presentations to report this quarter.

Task 4.6 – Prelithiation of Silicon Anode for High-Energy Lithium-Ion Batteries (Yi Cui, Stanford University)

Project Objective. Prelithiation of high-capacity electrode materials is an important means to enable those materials in high-energy batteries. This study pursues three main directions: (1) developing facile and practical methods to increase 1st cycle CE of anodes, (2) synthesizing fully lithiated anode to pair with high-capacity Li-free cathode materials, and (3) prelithiation from the cathode side.

Project Impact. Prelithiation of high-capacity electrode materials will enable those materials in the next generation of high-energy-density Li-ion batteries. This project's success will make high-energy-density Li-ion batteries for EVs.

Approach. Silicon electrode film will be prepared by coating the slurry of silicon nanoparticles, carbon black, and binder mixture on copper foil through a doctor-blading method. The silicon electrode film will be prelithiated by pressing a Li-metal foil on top of it and heating it in an argon glovebox for a certain time. Then, Li_xSi electrode film can be obtained by removing the redundant lithium foil through a peeling-off approach. The redundant lithium foil is reusable for the next prelithiation. The structure, morphology, and other properties can be analyzed by SEM, TEM, XPS, Raman spectroscopy, XRD, etc. In the first year, the team aims to fabricate Li_xSi freestanding electrode film and improve its air stability. In the second year, the team aims to improve the electrochemical stability in full cells.

Out-Year Goals. Materials containing a large quantity of lithium will be synthesized for pre-storing lithium ions inside batteries. Materials and process will be developed to be compatible with battery electrode and cell fabrication. First-cycle CE of anodes will be improved and optimized by prelithiation materials. Develop materials for prelithiation from the cathode side.

Collaborations. This project engages in collaboration with the following: BMR PIs; SLAC: M. Toney *(in situ* X-ray); and Stanford: W. Nix (mechanics).

Milestones

1. Produce ultra-thin lithium foil as a new dry prelithiation reagent. Produce lithium foil of different thickness to match the varied anode capacity. (Q1, FY 2021; Completed)
2. Demonstrate controllable initial CE improvement by prelithiation with ultra-thin lithium foil of different thickness. (Q2, FY 2021; Completed)
3. Demonstrate the microstructural and chemical evolution of silicon anode during ultra-thin lithium foil prelithiation. (Q3, FY 2021; In progress)
4. Demonstrate the role of ultra-thin lithium foil prelithiation to improve good cycle capacity retention in full battery. (Q4, FY 2021)

Progress Report

Substantial improvements on energy density of Li-ion batteries require development of high-capacity electrodes. Silicon anodes that have high theoretical capacities (3579 mAh/g)—ten times higher than the conventional graphite anodes (372 mAh/g)—hold great potential for application in high-energy Li-ion batteries. However, silicon anodes exhibit a low initial CE of 50-80%, which means 20-50% of active lithium ions will be lost after the 1st cycle due to side reactions. This huge loss indicates inefficient usage of active materials and battery energy density degradation. Therefore, a strategy to compensate the initial active lithium loss and improve initial CE is urgently needed to prevent battery energy density degradation.

The report last quarter presented fabrication of rGO-hosted ultra-thin lithium (Li@eGF) foils as new prelithiation reagent. Through a tunable calendering process and an edge-contacting molten lithium infusion, Li@eGF foils with varied thickness of 0.5 µm to 20 µm were fabricated, breaking the thickness limit of the commercialized lithium foils. The project's Li@eGF foils have capacities of 0.1 mAh cm^{-2} to 4 mAh cm^{-2} (corresponding to 0.5- to 20-µm thickness), and these capacity amounts can promisingly compensate the irreversible capacity loss in the 1st cycle of various anode materials. Here, the team applies Li@eGF foil to silicon battery system and demonstrates its prelithiation effectiveness.

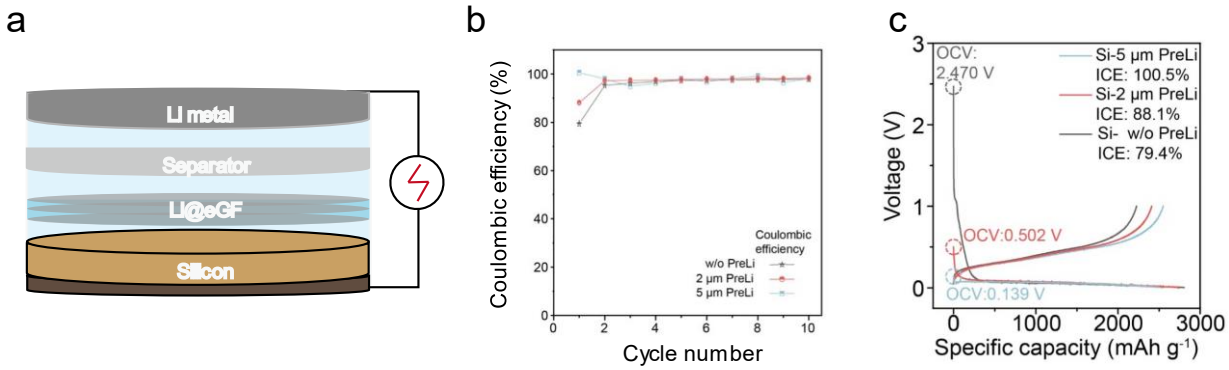

Figure 104. (a) Schematic of the prelithiation step using Li@eGF films. (b) Coulombic efficiencies of prelithiated silicon anodes using different thickness of Li@eGF films in the 1st cycle. (c) Voltage profiles of silicon electrodes using different thickness of Li@eGF films in the first cycle.

Prelithiation was carried out as the schematic shows in Figure 104a. Li@eGF foil was inserted between silicon anode and seperator in the cell assembly process. With electrolyte immersed, silicon was lithiated through electrochemical reaction between silicon and lithium. The mass loading of silicon electrodes was controlled ~ 1.2 mg cm^{-2}. Two different thicknesses of Li@eGF foils of 2 µm and 5 µm were applied for prelithiation, exhibiting capacities of 0.4 mAh cm^{-2} and 1 mAh cm^{-2}, respectively. Shown in Figure 104b, 2-µm-Li@eGF foil improves the initial CE of silicon from ~ 80% to 88.1%, and 5-µm-Li@eGF foil successfully improves the initial CE of silicon to the nearly ideal 100%. Noticeably, considering the initial CE of 80% of pristine silicon, the theoretical initial capacity loss in silicon anode is ~ 1 mAh cm^{-2}. Therefore, 5-µm-Li@eGF foil, exhibiting capacity of 1 mAh cm^{-2}, both theoretically and experimentally fully compensated the irreversible capacity loss in silicon. This result indicates that Li@eGF foil is promising for precise prelithiation through thickness tuning to match its stored capacity with the theoretically desired prelithiation capacity. Figure 104c further shows the delithiation capacity improvement after prelithiation. While the lithiation capacity remains similar, silicon without prelithiation has the lowest delithiation capacity, and 5-µm-Li@eGF lithiated silicon anode has the highest delithiation capacity. This increase further supports that Li@eGF prelithiation successfully compensates the initial capacity loss. The decreased open circuit voltage (OCV) indicates increased prelithiation level with more lithium applied for prelithiation. In sum, Li@eGF with its unique tunable thickness and ultra-thin properties was demonstrated to be an ideal prelithiation reagent. The tunable thickness makes Li@eGF facilely control the prelithiation amount, and the ultra-thin thickness provides Li@eGF appropriate capacity for prelithiation without the safety and stability concern of excessive lithium.

Patents/Publications/Presentations

The project has no patents, publications, or presentations to report this quarter.

TASK 5 – SULFUR ELECTRODES

Team Lead: Prashant Kumta, University of Pittsburgh

Summary

The collected work of the projects in this Task encompasses the following areas:

- Conducting focused fundamental research on the mechanism of "shuttle effect" inhibition for rechargeable Li-S batteries.
- Developing electrode and electrolyte systems that can mitigate the "shuttle effect" so the low self-discharge and long cycle life can be achieved.
- Synthesizing sulfur composite materials with an emphasis on polymer sulfur composite materials.
- Developing creative electrode-making processes to improve processability and aerial capacity; for example, polymeric sulfur composites may not be suitable for the traditional slurry casting process.
- Developing a novel S_xSe_y cathode material for rechargeable lithium batteries with high energy density and long life, as well as low cost and high safety.
- Delivering an electrochemically responsive self-formed hybrid LIC as a protective layer for Li-metal anodes, enabling Li-metal anodes to cycle with a high efficiency.
- Developing high-energy, low-cost Li-S batteries with long lifespan.

Highlights. The highlights for this quarter are as follows:

- Task 5.1 led by K. Amine's group at ANL focused this quarter on synthesizing a novel catalytic cathode host comprised of single atom catalyst (SAC) and double end binding (DEB) sites involving ZnS nanoparticles and Co-N-C, SAC serving as DEB sites all packaged into a highly oriented macroporous carbon conductive framework derived using polymeric polystyrene templates. The hypothesis for selecting and designing such a structure is based on the potential of the combined SAC system and the ZnS nanoparticle to effectively boost the electrochemical redox kinetics and also greatly eliminate the shuttle effect under high sulfur loadings. The Co-N-C SAC site and the polar ZnS nanoparticles can serve as effective combined anchors for effectively immobilizing the Li-containing polysulfides (LiPSs) by binding with the negatively charged S^{2-} and positively charged ends of Li^+, leading to almost zero shuttling effects and also eliminating Li-metal corrosion. They show by electron microscopy that the ordered macropores with a pore diameter of ~ 180 nm contain about 33.53 wt% of ZnS and 1.23 wt% of Co-N-C. Finally, they show by SAXS that ~ 85% of the macropores are filled by sulfur following encapsulation. The team plans to report the electrochemical response of this confinement architecture next quarter. The results demonstrate the influence of careful engineering of the confinement concept and incorporation of binding agents and catalysts serving to effectively mitigate shuttling of LiPSs and likely enhance the electrochemical performance of Li-S batteries.
- Task 5.2 led by D. Lu and J. Liu's group at PNNL this quarter continued to study the influence of particle size of the carbon in the sulfur cathode on electrolyte wettability and electrolyte uptake. They have shown that the large particle sized cathode (LPC) with > 90 μm size particles has larger open porosity, enabling better electrolyte infiltration than the small particle sized cathode (SPC) with particle size < 20 μm. Using the computational fluid dynamics (CFD) simulations of STAR-CCM+, they determined the volume of fluid (VOF) to study the electrolyte wetting and electrolyte uptake in both the LPC and SPC electrodes. By computing the wetted area of particles (A_w) and normalizing to the total area of the outer surfaces of the particles (A_p), they have determined the degree of surface wetting and the degree of electrolyte infiltration.

The calculations reveal that LPC displays rapid increase in wetting, resulting in 40% of the outer surfaces to be effectively wetted and leading to ~ 31% of the void spaces in the electrode to be filled with the electrolyte. By contrast, in the case of the SPC, the electrode displays a plateau at the outset, indicating barrier to infiltration of electrolyte due to capillary forces. As a result, at steady state, the SPC displays only 20% of the voids are filled with the electrolyte. These issues are, however, overcome in both cases under flooded electrolyte conditions, depicting the strong influence of particle size on electrode performance under lean electrolyte conditions. The results demonstrate the efficacy of CFD modeling to model the influence of particle size on electrolyte transport, which will likely have a strong bearing on the electrochemical performance of Li-S batteries particularly under lean electrolyte conditions.

- Task 5.3 led by Y. Cui's group at Stanford University reports this quarter on the continuing results of the homemade *in situ* optical cells to study the dissolution behavior of intermediate polysulfides in solid-polymer-based Li-S ASSBs. They have carefully created a coating of ~ 20 nm of TiS_2 on Li_2S as determined by electron microscopy via ion-exchange process of converting 20% of Li_2S on the surface to TiS_2 to form a $Li_2S@TiS_2$ composite of 1-5 μm size with an average size of 2 μm. Using sulfur K-edge XANES for the PEO/LiTFSI electrolytes after cycling, they have shown that the bare Li_2S electrodes show formation and dissolution of polysulfides into the electrolyte, while the $Li_2S@TiS_2$ electrodes effectively trap the polysulfides with a structurally intact layer of TiS_2 and avoiding dissolution of polysulfides into the solid PE. The result demonstrates the use of the TiS_2 coating to serve as effective traps of polysulfides, a key finding in the generation of Li-S ASSBs likely useful to demonstrate their potential.
- Task 5.4 led by D. Qu's group at the University of Wisconsin, Milwaukee (UWM) this quarter have conducted full atomistic MD simulation to unravel the binding effectiveness of tetra-sulfides of lithium with the polymer backbones to prove their experimental findings of certain polymers effectively showing better propensity to confining long-chain polysulfides within the cathode, thus enabling higher reversible capacity of Li-S batteries. They conducted MD simulations with several polymer backbones of various forms of polyaniline (PNB, LEB), poly (3, 4-ethyl-enedioxythiophene, or PEDOT) and polypyrrole (PPY) in the presence of 1:1 volume mixture of DOL/DME. They showed that the polymers are ineffective in binding the polysulfides via non-bonded interaction since the concentration of polysulfide/binder is low in the local domain of the cathode in the simulations. The simulations were also used to determine the interaction energy of the polymer, with S_4^{2-} and polymer-Li_2S_4 showing the propensity of MD simulations to shed more light into effect of solvation, side groups of polymer binders, and doped states. Results of these studies show how MD simulations could be used to study the interactions of polysulfides with various binder and polymer backbone structures and in turn advance understanding of Li-S batteries.
- Task 5.5 led by G. Liu's group at UCB this quarter have studied the solubility of polysulfides in their fluorinated micelle electrolyte by preparing the electrolyte saturated with sulfur and Li_2S at various polysulfide composition and measuring the overall concentration of sulfur species. They prepared various polysulfide solutions by adding and mixing Li_2S, sulfur in 1.0 M LiTFSI-F_3EO_2/TTE electrolyte, keeping the total concentration of sulfur added as fixed at 5 M and stirring at elevated temperature of 60°C to enhance the solubility followed by filtration. They calculated the weight percentages of carbon, hydrogen, nitrogen, and sulfur in the supernatant liquid to determine polysulfide concentration. The results showed that the F_3EO_2/TTE electrolyte exhibited limited solubility up to Li_2S_6 in the electrolyte. Even at a longer chain of Li_2S_8, the solubility of the polysulfides in the F_3EO_2/TTE electrolyte is much lower (< 0.25 M) than that of the DOL/DME based ether electrolytes displaying solubility of sulfur species exceeding 6 M. Results of their work show promise of the fluorinated ether electrolyte for use in high-density Li-S batteries.

Task 5.1 – Novel Chemistry: Lithium Selenium and Selenium Sulfur Couple (Khalil Amine, Argonne National Laboratory)

Project Objective. The project objective is to develop a novel S_xSe_y cathode material for rechargeable lithium batteries with high energy density and long life, as well as low cost and high safety.

Project Impact. Development of a new battery chemistry is promising to support the goal of PHEV and EV applications.

Approach. The dissolution of lithium polysulfides in nonaqueous electrolytes has been the major contribution to the low energy efficiency and short life of Li-S batteries. In addition, insulating characteristics of both end members during charge/discharge (sulfur and Li_2S) limit their rate capacity. To overcome this problem, sulfur or Li_2S is generally impregnated in a carbon-conducting matrix for better electronic conductivity. However, this makes it difficult to increase the loading density of practical electrodes. It is proposed to solve these barriers using the following approaches: (1) partially replace sulfur with selenium, (2) nano-confine the S_xSe_y in a nanoporous conductive matrix, and (3) explore advanced electrolytes with suppressed shuttle effect.

Out-Year Goals. This new cathode will be optimized with the following goals:

- A cell with nominal voltage of 2 V and energy density of 600 Wh/kg.
- A battery capable of operating for 500 cycles with low capacity fade.

Collaborations. This project engages in collaboration with the following: Y. Ren and C. Sun of APS at ANL, and L. A. Curtiss and L. Cheng at ANL.

Milestones

1. Build in-house Li-S pouch cell fabrication line, and demonstrate > 100 mAh pouch cell performance using Se-doped sulfur cathode and fluorinated ether-based electrolytes. (Q1, FY 2021; Completed)
2. Design and characterize novel cathode host for Li-S and Li-Se/S batteries. (Q2, FY 2021; Completed)
3. Validate electrochemical performance of new cathode host. (Q3, FY 2021; In progress)
4. Conduct *operando* and *ex situ* characterization on developed cathodes during charge/discharge. (Q4, FY 2021; In progress)

Progress Report

Introducing anchoring sites into the micro- or mesoporous host material is a common strategy to immobilize LiPSs; these sites can be divided into two main categories: polar materials and single-atom catalysts. Both host materials can be thought of as single-end binding sites and fail to completely eliminate the shuttle effect. This is because the interfacial redox kinetics of Li-S batteries is dominated by (1) a large binding energy, allowing adsorption with sufficient surface coverage, and (2) fast charge transfer at the triple-phase boundaries during the redox reaction of the adsorbates, requiring an optimal 'polysulfides confinement-catalysis' process. This quarter, the team proposed and synthesized a novel catalytic cathode host by embedding polar ZnS nanoparticles and Co-N-C SAC DEB sites into a highly oriented macroporous conductive framework.

Figure 105 shows the design rationale of the project's macroporous sulfur host with DEB sites. Such structure can significantly boost the electrochemical redox kinetics and greatly eliminate shuttle effect under high sulfur loading, thanks to the improved catalytic and enhanced confinement effect of DEB sites toward LiPSs. The Co-N-C SAC site and the ZnS polar site can effectively immobilize the LiPSs by binding with the negatively charged end Sn^{2-} and positively charged end Li^{+}, respectively, leading to almost zero shuttle effect and no Li-metal corrosion. The ordered macropores can attain both high sulfur accommodation (high specific energy) and fast ion transport, which can facilitate formation of triple-phase boundaries and avoid "dead sulfur." The sufficient triple-phase boundaries, combined with the excellent immobilization and catalytic effect of the DEB sites, can further boost the electrochemical sulfur redox kinetics.

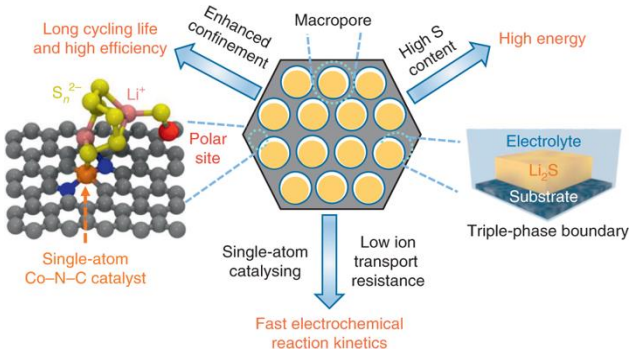

Figure 105. Design strategy of macroporous host with double-ending binding sites.

The 3D ordered macroporous sulfur host with ZnS and Co-N-C DEB sites (denoted as 3d-omsh/ZnS,Co-N-C) was synthesized by connecting Zn^{2+}/Co^{2+} ions with 2-methylimidazole linkers inside a 3D template. The team further characterized the structure of the host and sulfur-embedding materials via multiple tools. TEM images (Figure 106a-b) clearly confirmed the ordered and interconnected macroporous structure of 3d-omsh/ZnS,Co-N-C with a pore diameter of ~ 180 nm. Furthermore, single-atom spots were identified from a STEM HAADF image of 3d-omsh/ZnS,Co-N-C (highlighted by red circles in Figure 106c), indicating the existence of SAC inside the host material. EDX analysis showed that the weight percentages of ZnS and Co-N-C SAC in the host material are about 33.63 wt% and 1.23 wt%, respectively.

Moreover, the cobalt K-edge EXAFS of 3d-omsh/ZnS,Co-N-C (Figure 106e) shows a weaker peak with much lower radial distance than the reference cobalt foil, indicating that atoms such as carbon and nitrogen are distributed around the cobalt atom. The only one strong shell located at 1.35 Å in the 3d-omsh/ZnS,Co-N-C, which is slightly shorter than the Co-O (1.47 Å) in Co_3O_4, is assigned to the Co-N structure. The Co-Co peak (2.14 Å), which is evident for the standard cobalt foil, is undetectable in the 3d-omsh/ZnS,Co-N-C. The cobalt K-edge EXAFS of the 3d-omsh/ZnS,Co-N-C peak fits the model of two carbon and two nitrogen atoms surrounding the cobalt atom. In the case of the zinc K-edge EXAFS (Figure 106f), the team observed a stronger signal than that of the Zn-Zn (2.24 Å) in the zinc foil, which is assigned to Zn-S (3.65 Å). A good fit of the zinc K-edge EXAFS result using the ZnS model further confirmed existence of ZnS in the 3d-omsh/ZnS,Co-N-C host material. Therefore, the DEB sites configured as polar ZnS and Co-N-C SAC were successfully introduced into the 3d-omsh. The TEM EDX elemental mapping (Figure 106g) confirmed that sulfur was successfully encapsulated into the macroporous chambers of the 3d-omsh/ZnS,Co-N-C. Moreover, the homogeneous distribution of cobalt, nitrogen, carbon, and zinc confirms uniform distribution of DEB sites inside the cathode. SAXS characterization (Figure 106h) reveals that ~ 85% of the macropores was filled by sulfur after sulfur encapsulation.

Through these characterization results, the team confirmed synthesis of macroporous carbon with embedded polar ZnS and Co-N-C SAC. They will report electrochemical results next quarter.

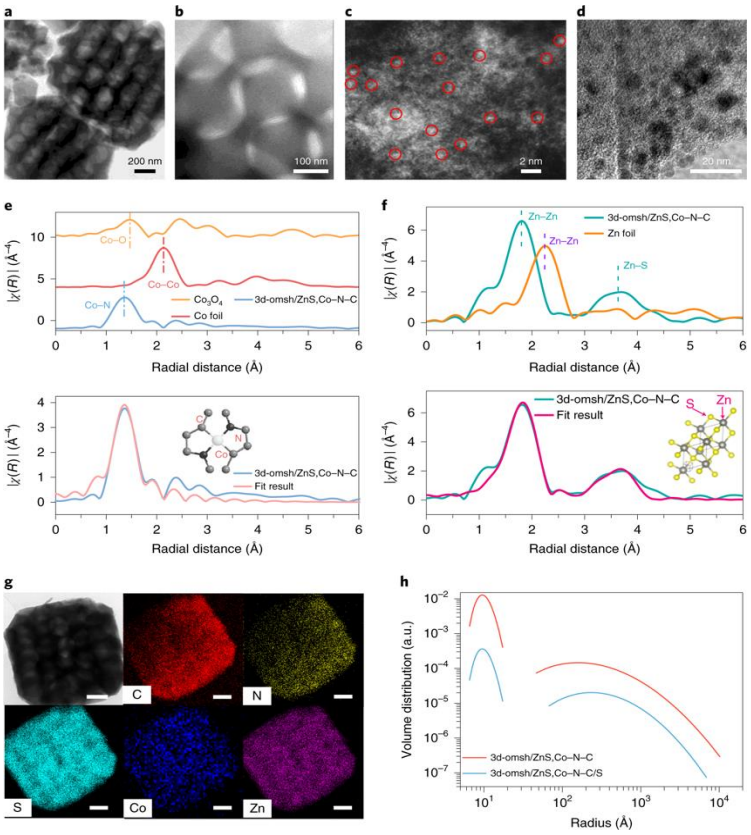

Figure 106. (a-b) Transmission electron microscopy (TEM) images of the 3d-omsh/ZnS,Co-N-C. (c) High-angle annular dark-field TEM image of the SAC sites (marked by red circles) inside the 3d-omsh/ZnS,Co-N-C. (d) TEM image of the polar binding sites inside the 3d-omsh/ZnS,Co-N-C. (e) Cobalt K-edge extended X-ray absorption fine structure (EXAFS) of the 3d-omsh/ZnS,Co-N-C with the reference cobalt foil and Co_3O_4 (top), and the fitting result using the Co-N-C model (bottom), as shown in the inset. χ, absorption coefficient; R, average distance of neighboring atoms from atoms emitting photoelectrons. (f) Zinc K-edge EXAFS of the 3d-omsh/ZnS,Co-N-C with the reference zinc foil (top), and the fitting result using the ZnS model (bottom), as shown in the inset. (g) TEM image of the 3d-omsh/ZnS,Co-N-C/S cathode and the corresponding energy dispersive X-ray spectroscopy element mapping of carbon, nitrogen, sulfur, cobalt, and zinc. The scale bars are 200 nm. (h) Small angle X-ray scattering simulation on the pore size distributions of 3d-omsh/ZnS,Co-N-C and 3d-omsh/ZnS,Co-N-C/S using spherical shape model.

Patents/Publications/Presentations

Presentation

- 239th ECS meeting with the 18th International Meeting on Chemical Sensors (IMCS), Virtual (May 30 – June 3, 2021): "New Cathode and Electrolytes Strategies to Enable High-Energy Li-S Batteries"; G. Xu and K. Amine.

Task 5.2 – Development of High-Energy Lithium-Sulfur Batteries (Dongping Lu and Jun Liu, Pacific Northwest National Laboratory)

Project Objective. The project objective is to develop high-energy, low-cost Li-S batteries with long lifespan. All proposed work will employ thick sulfur cathode (≥ 4 mg/cm^2 of sulfur) at a relevant scale for practical applications. The diffusion process of soluble polysulfide out of thick cathode will be revisited to investigate cell failure mechanism at different cycling. The fundamental reaction mechanism of polysulfide under the electrical field will be explored by applying advanced characterization techniques to accelerate development of Li-S battery technology.

Project Impact. The theoretical specific energy of Li-S batteries is ~ 2300 Wh/kg, which is almost three times higher than that of state-of-the-art Li-ion batteries. The proposed work will design novel approaches to enable Li-S battery technology and accelerate market acceptance of long-range EVs required by the EV Everywhere Grand Challenge.

Approach. The project proposes to (1) identify and address key issues of applying high-energy sulfur cathodes including materials, binders, electrode architectures, and functional electrode additives, (2) advance the mechanism study of sulfur cathode and electrolyte by using *in situ* / *ex situ* techniques and custom-designed hybrid cell setup, and (3) verify effectiveness of the new approaches with coin/pouch cells by using high-loading electrodes (> 4 mg/cm^2), limited lithium (< 200% lithium excess), and lean electrolyte (E/S < 4 µL/mg).

Out-Year Goals. This project has the following out-year goals:

- Fabricate Li-S pouch cells with thick electrodes to understand sulfur chemistry/electrochemistry in environments similar to real application.
- Leverage the Li-metal protection project funded by the DOE and PNNL advanced characterization facilities to accelerate development of Li-S battery technology.
- Develop Li-S batteries with a specific energy of 400 Wh/kg at cell level, 1000 deep-discharge cycles, improved abuse tolerance, and less than 20% capacity fade over a 10-year period to accelerate commercialization of EVs.

Collaborations. This project engages in collaboration with the following: X-Q. Yang (BNL), J. Bao (PNNL), P. Khalifah (BNL), and J. Tao (PNNL).

Milestones

1. Optimize electrode architecture to realize sulfur utilization of > 1000 mAh/g in high loading sulfur electrode (> 4 mg S/cm^2) at very low porosity (< 40%). (Q1, FY 2021; Completed)
2. Build an electrode model to understand the effects of electrode porosity and tortuosity on the electrolyte transport and sulfur reaction kinetics. (Q2, FY 2021; Completed)
3. Enable a quasi-solid electrolyte network by introducing polymer and/or solid electrolytes into the low porosity electrodes, and realize cell operation at an extremely low E/S. (Q3, FY 2021; In progress)
4. Identify compatible binder and solvent combinations to enable the scale-up preparation of the quasi-solid electrodes. (Q4, FY 2021; In progress)

Progress Report

The S/C composite holds the largest mass/volume ratio in the electrode, so its property dictates an electrode's architecture. Last quarter, the team demonstrated that use of small particles for dense sulfur electrode fabrication will lead to a high tortuosity architecture in which the tortuous or even disconnected pores between the particles will affect electrolyte permeability and mass transfer. By using large-sized particles, more open-throat pores are expected to form and facilitate electrolyte infiltration.

To identify key factors limiting electrode wetting, electrode models with different particle sizes were built, and CFD simulations were conducted using STAR-CCM+. The multiphase flow simulations using VOF are applied to study the electrolyte wetting process in a porous LPC and SPC. When adding electrolyte on the top of electrodes, gravity is the main driving force to initiate the electrolyte infiltration, and the wetting process can be dictated by the competing effect between gravity and pore scale capillary pressure. Figure 107a demonstrates the initial state of the LPC and SPC, in which the blue and black colors represent the electrolyte and void space in the electrode, respectively. By conducting a transient flow simulation, the temporal evolution of the LPC and SPC wetting can be monitored. The steady-state electrolyte distribution inside the electrode is illustrated in Figure 107b. It is clear that with the same electrolyte volume and electrode porosity in the initial state, LPC shows better wetting, and the electrolyte can be uniformly distributed in the deeper part of electrode. As for SPC, within the same simulation period, electrolyte can hardly penetrate the porous electrode, leaving most of the particles unwetted. The wetted area of particles (Aw) is computed and normalized by the total area of the particles' outer surfaces (Ap). When plotting the evolution of normalized wetted area with time, the Aw/Ap (%) not only quantifies the net degree of wetting, but also indicates the electrolyte infiltration speed in different electrodes. As shown in Figure 107c, in LPC, the Aw/Ap quickly increases once the electrolyte infiltration starts, and more than 40% of the outer surfaces can be wetted after achieving steady state, suggesting both faster infiltration speed and a high degree of wetting. In contrast, the Aw/Ap curve for SPC shows a plateau behavior at the beginning of infiltration process, which means the electrolyte infiltration experiences high capillary pressure developed in the small pores in SPC. Although the normalized wetted area reaches steady state, the wetting degree is significantly lower than that of LPC. As the result, when calculating the fraction of electrode wetted at the steady state, 31% of the void spaces in the electrode are filled with electrolyte in LPC, while only 20% of the void spaces are filled in SPC. It is also important to notice that the slow electrolyte infiltration can be improved by increasing electrolyte volume. As shown in Figure 107c-d, when the electrolyte volume is doubled (denoted as flooded electrolyte), the gravitational force overwhelms the pore scale capillary pressure; subsequently, the wetting degree and absorbed electrolyte are increased in both SPC and LPC electrodes. This clearly demonstrates how a flooded electrolyte condition obscures the wetting issues of sulfur cathodes under lean electrolyte conditions. The VOF flow simulations suggest the LPC composed of large particles has faster electrolyte infiltration and better wettability compared to the corresponding ones for SPC.

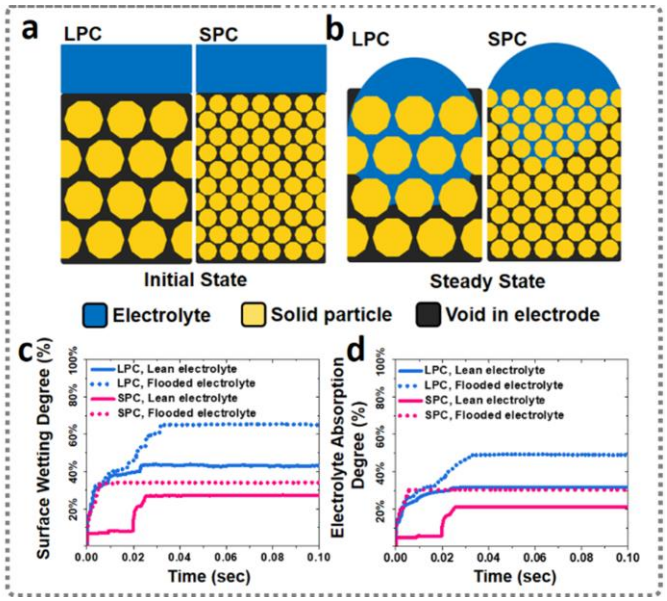

Figure 107. Simulations of electrolyte infiltration in different electrode structure: (a) initial state and (b) steady state of electrolyte infiltration in large particle cathode (LPC) and small particle cathode (SPC), (c) surface wetting degree, and (d) electrolyte absorption degree in LPC and SPC at steady state.

Patents/Publications/Presentations

The project has no patents, publications, or presentations to report this quarter.

Task 5.3 – Nanostructured Design of Sulfur Cathodes for High-Energy Lithium-Sulfur Batteries (Yi Cui, Stanford University)

Project Objective. The charge capacity limitations of conventional TM oxide cathodes are overcome by designing optimized nano-architectured sulfur cathodes. This study aims to enable sulfur cathodes with high capacity and long cycle life by developing sulfur cathodes from the perspective of nanostructured materials design, which will be used to combine with Li-metal anodes to generate high-energy Li-S batteries. Novel sulfur nanostructures as well as multi-functional coatings will be designed and fabricated to overcome issues related to volume expansion, polysulfide dissolution, and the insulating nature of sulfur.

Project Impact. The capacity and cycling stability of sulfur cathode will be dramatically increased. This project's success will make Li-S batteries to power EVs and decrease the high cost of batteries.

Approach. The approach involves three main efforts:

- Advanced nanostructured sulfur cathodes design and synthesis, including (1) engineer empty space into sulfur cathode to solve problem of electrode volume expansion, (2) develop novel sulfur nanostructures with multi-functional coatings for confinement of S/Li polysulfides to address issues of active materials loss and low conductivity, (3) develop/discover optimal nanostructured materials that can capture the polysulfide dissolved in the electrolyte, (4) develop space-efficiently-packed nanostructured sulfur cathode to increase volumetric energy density and rate capability, and (5) identify interaction mechanism between sulfur species and different types of oxides/sulfides, and find optimal material to improve capacity and cycling of sulfur cathode.
- Structure and property characterization, including *ex situ* SEM, XPS analysis, and *in operando* XRD and optical microscopy (OM).
- Electrochemical testing including coin cells and pouch cells as well as a set of electrochemical techniques.

Out-Year Goals. The cycle life, capacity retention, and capacity loading of sulfur cathodes will be greatly improved (200 cycles with 80% capacity retention, > 0.3 mAh/cm^2 capacity loading) by optimizing material design, synthesis, and electrode assembly.

Collaborations. This project collaborates with the following: BMR PIs; SLAC: M. Toney *(in situ* X-ray); and Stanford: W. Nix (mechanics) and Z. Bao (materials).

Milestones

1. Understanding polysulfides dissolution behavior in polymer-based Li-S all-solid-state batteries. (Q1, FY 2021; Completed)
2. Demonstrating nanoscale encapsulation concept from liquid to all-solid-state Li-S batteries. (Q2, FY 2021; Completed)
3. Exploring mechanism of nanoscale encapsulation in improving all-solid-state Li-S batteries experimentally and theoretically. (Q3, FY 2021; Ongoing)
4. Enabling all-solid-state Li-S batteries with high energy density, long-term cycling stability, and high safety. (Q4, FY 2021; Ongoing)

Progress Report

Last quarter, the team fabricated homemade *in situ* optical cells to study dissolution behavior of intermediate polysulfides in solid-polymer-based Li-S ASSBs. This quarter, to solve the polysulfide dissolution in SPEs, the team incorporated nanoscale encapsulation concept from liquid to all-solid-state Li-S batteries. $Li_2S@TiS_2$ particles were synthesized by converting 20% of the Li_2S on the surface into TiS_2 via an ion exchange process. SEM imaging of Li_2S after TiS_2 coating reveals that the typical particle size of as-prepared $Li_2S@TiS_2$ ranges between 1-5 µm, with an average size of 2 µm (Figure 108a). TEM imaging shows that Li_2S is encapsulated by a uniform polycrystalline TiS_2 layer with a thickness of ~ 20 nm (Figure 108b). The team measured sulfur K-edge XANES for PEO/LiTFSI electrolytes after cell cycling in the corresponding area marked as A in Figure 108c for bare Li_2S and area marked as B in Figure 108d for $Li_2S@TiS_2$ electrodes, respectively (Figure 108e). Both bare Li_2S and $Li_2S@TiS_2$ electrodes show absorption features at 2,481 and 2,486 eV, originating from LiTFSI in the electrolyte. The presence of a broadened peak around 2,472 eV in area A confirms generation of polysulfides in the PEO/LiTFSI electrolyte in the cell with bare Li_2S electrode (Figure 108e). Combining *in situ* OM and sulfur K-edge XANES measurement, the team concludes that polysulfides form and dissolve into PEO/LiTFSI electrolytes from bare Li_2S electrodes during cycling, while $Li_2S@TiS_2$ electrodes can effectively trap polysulfides by a structurally intact encapsulation layer, thereby avoiding polysulfides dissolution into SPEs.

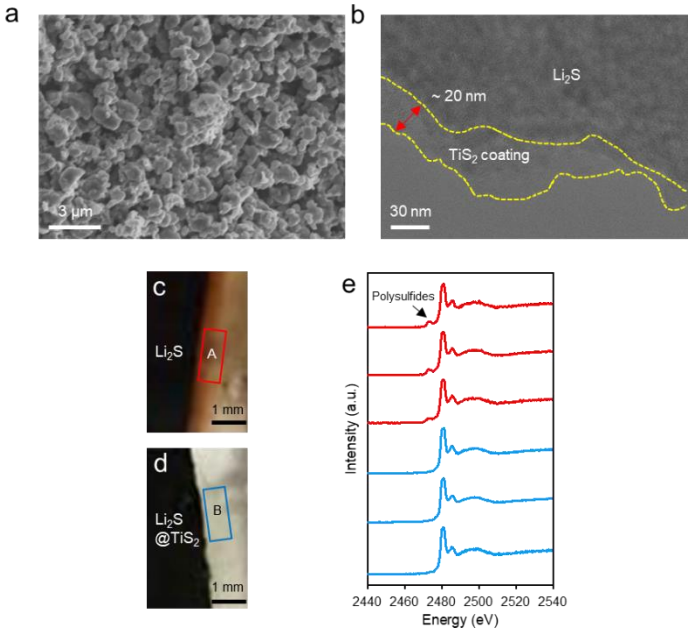

Figure 108. Polysulfides entrapment in $Li_2S@TiS_2$ cathodes. (a) Scanning electron microscopy and (b) transmission electron microscopy image of $Li_2S@TiS_2$ particles. The thickness of TiS_2 coating is ~ 20 nm. Photographs show the overall working electrode/electrolyte interface after cycling for optical cells with (c) bare Li_2S electrode and (d) $Li_2S@TiS_2$ electrode. For the optical cell with bare Li_2S working electrode, the color of the solid electrolyte near the working electrode side changes from transparent to red brown after cycling, indicating that polysulfides are dissolving into the PEO/LiTFSI electrolyte. For the optical cell with $Li_2S@TiS_2$ working electrode, no color change is observed, indicating that polysulfides are well trapped. (e) Sulfur K-edge X-ray absorption near-edge structure spectra of PEO/LiTFSI electrolytes in corresponding area A for bare Li_2S and area B for $Li_2S@TiS_2$ electrode. The presence of a broadened absorption peak around 2,472 eV in area A confirms generation of polysulfides in PEO/LiTFSI electrolytes for bare Li_2S electrode. The absorption features at 2,481 and 2,486 eV are from LiTFSI in the electrolyte.

Patents/Publications/Presentations

The project has no patents, publications, or presentations to report this quarter.

Task 5.4 –Investigation of Sulfur Reaction Mechanisms (Enyuan Hu, Brookhaven National Laboratory; Deyang Qu, University of Wisconsin, Milwaukee)

Project Objective. The primary objectives are as follows:

- To continue conducting fundamental research on the mechanism of the sulfur redox reaction, especially those on the interplay of the dissolved polysulfides in electrolyte and those in the solid phase in cathode during charging.
- To continue developing the polymeric sulfur electrode, adequate anode, and corresponding electrolyte to achieve high-energy-density, long-cycle-life Li-S batteries. The team will focus on the overall dissolution of polysulfide in an electrolyte and the effectiveness of polymeric sulfur electrodes.
- To develop the alternative anode materials having low reactivity with dissolved polysulfide ions.
- To continue to develop and optimize creative electrode making processes to improve processability and aerial capacity (for example, dry process and thick electrodes).

Project Impact. Further understanding of the mechanisms of all reactions in a Li-S cell will lead to mitigation of the "shuttle effect." The project results will thus guide development of sulfur cathode and Li-S designs with significant increase of energy density and of cycle life and with reduction of cost. This will greatly accelerate deployment of EVs and reduce carbon emission associated with fossil fuel consumption.

Approach. This collaborative project involves the following: (1) continue to synthesize cross-linked polymerized sulfur compounds, in which a sulfur is attached to the conductive backbone with covalent bonds; therefore, the polysulfides can be immobilized within the matrix, (2) investigate the sulfur redox reaction mechanism in the solid phase, (3) continue exploring the alternative anode materials that can cycle well and do not react with dissolved polysulfide and sulfur in the electrolyte to mitigate the "shuttle effect," and (4) develop an engineering process for high sulfur loading electrodes.

One-Year Goals. In FY 2021, the interim goal is to develop a Li-sulfur battery with sulfur containing cathode of 600-800 mAh/g capacity with mitigation of the "shuttle effect."

Collaborations. The PI works closely with beamline scientists at synchrotron facilities to develop novel Li-S characterization tools. The PI and co-PI collaborate closely with top scientists at ANL, LBNL, and PNNL, as well as U. S. industrial collaborators at GM, Duracell, Clarios, etc. The PI and co-PI also collaborate with scientists in China, Japan, and South Korea. These collaborations will be strengthened and expanded to give this project a vision on both today's state-of-the-art technology and tomorrow's technology in development, with feedback from the material designer and synthesizers upstream and from industrial end users downstream.

Milestones

1. Synthesize new polymeric sulfur compounds. Conduct preliminary electrochemical, optical, and synchrotron based testing of sulfur redox reaction in the solid phase (in cathode). (Q1, FY 2021; Completed)
2. Test alternative anode materials with both sulfur and polymeric sulfur electrodes and determine interaction with dissolved polysulfide ions and overall electrochemical performance. (Q2, FY 2021; Completed)
3. Investigate sulfur redox reaction in the solid phase in cathode. Test the newly synthesized polymeric sulfur materials. (Q3, FY 2021; In progress)
4. Test full cell in either coin or pouch cell format with polymeric sulfur cathode and alternative anode. (Q4, FY 2021; In progress)

5. Conduct preliminary investigations of sulfur redox reaction mechanism in the solid phase in cathode and the interplay between dissolved polysulfide ions in electrolyte and sulfide compounds in the solid. Complete and continue testing of polymeric sulfur cathode and alternative anode in full-cell format. (Annual Milestone; In progress)

Progress Report

This quarter, the team continued synthesizing and testing polymeric sulfur cathodes. In previous reports, they concluded the following: (1) the shuttle-effect can be mitigated by using alternative anodes that do not react with dissolved polysulfides; and (2) the shuttle-effect can be mitigated by forming short-chain polysulfide ions, which are much less reactive than longer chain polysulfide ions. They provided initial experimental evidence demonstrating that the polymeric sulfur compounds, which have better ability to restrain both elemental sulfur and long-chain polysulfides within the cathode, can retain the cycle capacity of a Li-S battery.

The team performed a full-atomistic MD simulation to unravel the binding effectiveness between tetra-sulfides and polymer backbones PNB, LEB, PEDOT, and PPY with the effect of a 1:1 (v/v) mixture of DOL/DME when considering the ratio between sulfur and binder in a real Li-S cell. The simulations in solvent demonstrate that the end group 2 of PNB can effectively bind one Li_2S_4 cluster or 2 out of 43 Li_2S_4 molecules with the effect of the solvent mixture through non-bonded interaction. Therefore, PNB, LEB, PEDOT, and PPY seem to be ineffective in binding polysulfides through non-bonded interaction, especially when the concentration of polysulfide/binder in a local domain of the cathode is as low as that in the simulations. Based on that, polymers with the functional group (that is, end group 2 of PNB) are suggested to be further studied to achieve effective backbones.

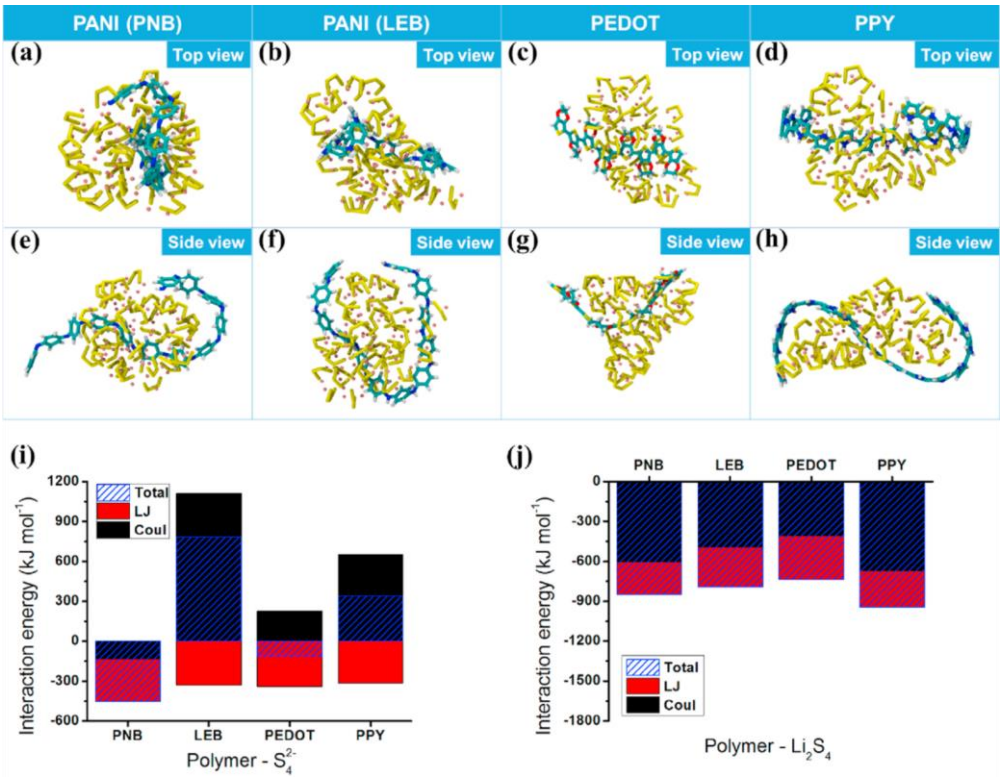

Figure 109. (a-h) Structure, (i) polymer-S_4^{2-} interaction energy, and (j) polymer-Li_2S_4 interaction energy of the self-assembled multiple S_4^{2-}, Li^+ and single polymer chain. Columns with heights equal to the value of the interaction energy components are stacked up, where the summation is total interaction energy corresponding to each polymer.

Figure 109a-h shows the structures of the simulation frames. It can be observed that Li^+ and S_4^{2-} form a cluster in each system, and the interaction between the cluster and each polymer results in a twisted and/or bended conformation of the polymer chain. In other words, the whole polymer chains are involved in the interaction, rather than only the involving three units. Figure 109i/j shows the polymer-S_4^{2-} and polymer-Li_2S_4 interaction energies, respectively. The Li^+ in the clusters contributes to the attractive interaction mainly through electrostatic interaction, while S_4^{2-} makes the contribution mainly by vdW interaction. Figure 109e shows that an end of the PNB chain is dangling, indicating that the end of PNB has weaker binding effect with Li_2S_4.

The constructed MD models have potential to be extended to study binding effectiveness between polysulfides and polymers under other influencing factors, such as side groups of polymer backbones and doped states of conductive polymers. Since the solvent environment has considerable impact on the binding effectiveness between tetra-sulfides and polymer backbones, it is suggested to use the explicit solvation models, similar to those built in this work, to predict how other influencing factors affect binding effectiveness between polysulfides and polymers, which will contribute to the existing demand for guiding binder design and rational experiments for Li-S technology, as well as propel the advancement of MD modeling methodology for understanding properties and performance of polymer materials in energy storage systems.

Patents/Publications/Presentations

The project has no patents, publications, or presentations to report this quarter.

Task 5.5 – New Electrolytes for Lithium-Sulfur Battery (Gao Liu, Lawrence Berkeley National Laboratory)

Project Objective. The project objective is to develop new electrolytes, additives, and electrode compositions for Li-S battery with high ion-conductivity, stable toward polysulfide and promoting the polysulfide affiliation with the electrode substrate to prevent polysulfide dissolution.

Project Impact. This work will address the high cost and low energy density of Li-ion rechargeable batteries. The emerging Li-S batteries could feature both high energy density and low cost. This project enables applications of the low-cost, abundant sulfur element as a major chemical component for electrical energy storage. This project will develop new approaches for electrolytes and electrode compositions of Li-S rechargeable batteries.

Approach. This project aims to develop new electrolytes and additives for Li-S battery. The properties of the ideal electrolyte for sulfur electrode would be high ion conductivity, stable toward polysulfide, and promoting the polysulfide affiliation with the electrode substrate to prevent polysulfide dissolution. The project is designed to first understand the electrode substrate interaction with the polysulfides in different electrolytes. This will lead to better understandings of the polysulfide nucleation and precipitation mechanisms in common electrolytes. The second stage of the project will focus on chemically modifying the structures of the solvent and salt electrolyte molecules to increase electrolyte stability and ionic conductivity, to prevent polysulfide dissolution, and to promote polysulfides precipitation.

Out-Year Goals. The team will also investigate the contribution of Li-metal electrodes to overall Li-S battery performance and will develop methods to stabilize Li-metal surface.

Collaborations. This project collaborates with J. Guo and W. Yang (ALS/LBNL), A. Minor (National Center for Electron Microscopy at LBNL/UCB), L-W. Wang (LBNL), and P. B. Balbuena, Texas A&M University.

Milestones

1. Measure polysulfide dissolution in the new amphiphilic electrolytes. (Q1, FY 2021; Completed)
2. Map out the Li-ion diffusion path in sulfur materials. (Q2, FY 2021; Completed)
3. Develop optimized sulfur electrodes according to the electrolyte properties and Li-ion transport in sulfur materials. (Q3, FY 2021; Not yet initiated)
4. Investigate the Li-metal electrode properties in the Li-S cell. (Q4, FY 2021; In progress)

Progress Report

Polysulfides are intermediate species formed from the lithiation and delithiation process of the sulfur electrode. The long-chain polysulfides (Li_2S_m, m = 4-8) are extremely soluble in the conventional ether-based electrolyte in Li-S battery. Thus, sulfur electrode experiences transformation of solid sulfur to solid Li_2S with the formation of polysulfides, which has only been observed in the liquid form during cycling. By preparing electrolyte saturated with sulfur and Li_2S at various polysulfide compositions and measuring the overall concentration of sulfur species, the team is able to quantify the solubility of polysulfides in the project's fluorinated micelle electrolyte.

The elements carbon, hydrogen, nitrogen, and sulfur (wt%) were detected by the Thermo Fisher FlashSmart Elemental Analyzer. Various polysulfide solutions were prepared by adding and mixing Li_2S, sulfur in 1.0 M LiTFSI F_3EO_2/TTE electrolyte (0.3 ml, accurately measured by micro-pipet) based on stoichiometric ratio. The total concentration of sulfur added is fixed at 5 M for all samples. To overcome the slow kinetic of dissolution process, the solution was stirred at elevated temperature (60°C) for two days, followed by continuous stirring at room temperature for another two days. The solution was syringe filtered (< 0.45 μm pore sizes) to remove undissolved solids. The clear supernatant sample was analyzed. The weight percentage of the carbon, hydrogen, nitrogen, and sulfur elements was measured and used to calculate polysulfide concentration in the electrolyte. The X-axis of molecular formula label of Li_nS_m is nominal based on the ratio of lithium and carbon, hydrogen, nitrogen, and sulfur element in the Li_2S and sulfur starting materials (Figure 110). The measurement shows very limited solubility of polysulfide up to Li_2S_6 in the electrolyte. Even at Li_2S_8, the solubility of polysulfide in the F_3EO_2/TTE electrolyte is significantly below the solubility of polysulfide in DOL-based electrolyte, noted that solubility of sulfur species is above 6 M for a typical ether solvent electrolyte [*Frontiers in Chemistry* (2020)]. The finding indicates that polysulfide dissolution was effectively suppressed in the fluorinated ether electrolyte, which agrees with electrochemical performance.

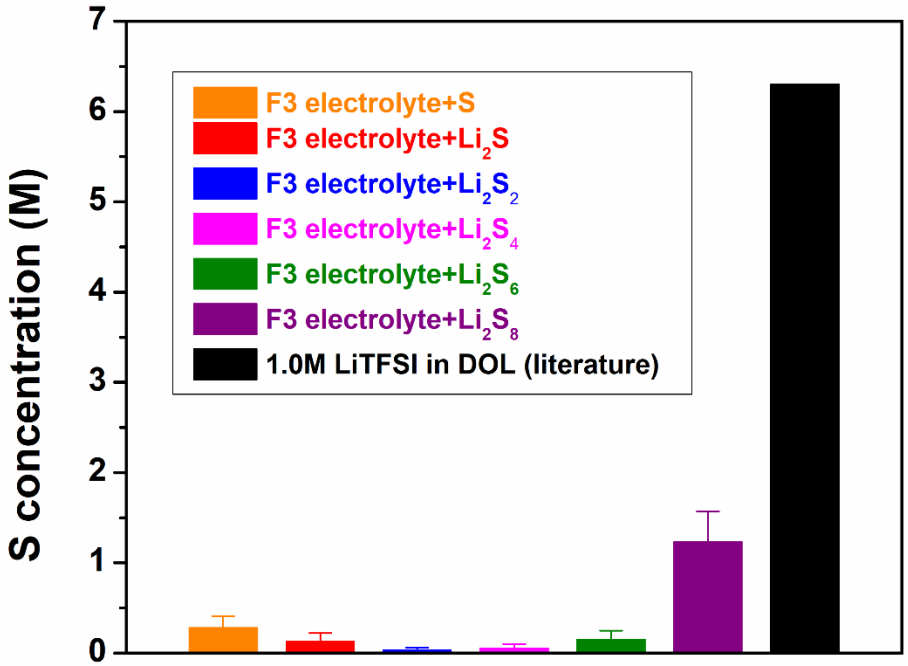

Figure 110. The sulfur concentration detected from the supernatant of the electrolyte solution saturated by Li_2S, sulfur, and all types of polysulfides (Li_2S_m, m = 2, 4, 6, 8), respectively. The error bar was calculated based on Gaussian distribution analysis. In comparison, the sulfur concentration of 1.0 M LiTFSI in DOL is 6.3 M based on the literature [*Frontiers in Chemistry* (2020)].

Patents/Publications/Presentations

The project has no patents, publications, or presentations to report this quarter.

TASK 6 – AIR ELECTRODES / ELECTROLYTES

Team Lead: Ji-Guang Zhang, Pacific Northwest National Laboratory

Summary and Highlights

High-density energy storage systems are critical for EVs required by the EV Everywhere Grand Challenge. Conventional Li-ion batteries still cannot fully satisfy the ever-increasing needs because of their limited energy density, high cost, and safety concerns. As an alternative, the rechargeable lithium-oxygen (Li-O_2) battery has potential to be used for long-range EVs. The practical energy density of a Li-O_2 battery is expected to be ~ 800 Wh kg^{-1}. The advantages of Li-O_2 batteries come from their open structure; that is, they can absorb the active cathode material (oxygen) from the surrounding environment instead of carrying it within the batteries. However, the open structure of Li-O_2 batteries also leads to several disadvantages. The energy density of Li-O_2 batteries will be much lower if oxygen must be provided by an onboard container. Although significant progress has been made in recent years on fundamental properties of Li-O_2 batteries, research in this field is still in an early stage, with many barriers to be overcome before practical applications. These barriers include:

- Instability of electrolytes—The superoxide species generated during discharge or O_2 reduction process is highly reactive with electrolyte and other components in the battery. Electrolyte decomposition during charge or O_2 evolution process is also significant due to high over-potentials.
- Instability of air electrode (dominated by carbonaceous materials) and other battery components (such as separators and binders) during charge/discharge processes in an O-rich environment.
- Corrosion of Li-metal anode in an electrolyte saturated with oxygen.
- Low energy efficiency associated with large over-potential and poor cyclability of Li-O_2 batteries.
- Low power rate capability due to electrode blocking by the reaction products.
- Absence of a low-cost, high-efficiency oxygen supply system (such as oxygen selective membrane).

The main goal of this Task is to provide a better understanding on the fundamental reaction mechanisms of Li-O_2 batteries and identify the required components (especially electrolytes and electrodes) for stable operation of Li-O_2 batteries. This task will investigate several new approaches to improve stability of Li-metal anode in Li-O_2 batteries:

- Li-metal anodes will be protected using two approaches: (1) *in situ* formation of a stable SEI layer before Li-O_2 cell operation through various electrolyte formulations and treatment protocols, and (2) *ex situ* formation of stable inorganic/polymeric hybrid electrolyte layers through dip-coating or tape-casting method to coat the inorganic/polymeric hybrid electrolyte layer on Li-metal surface.
- A joint theoretical/experimental approach for design and discovery of new cathode and electrolyte materials will act synergistically to reduce charge overpotentials and increase cycle life. Synthesis methods, in combination with design principles developed from computations, will be used to make new cathode architectures. Computational studies will be used to help understand decomposition mechanisms of electrolytes and how to design electrolytes with improved stability.
- A new cathode will be developed based on high-efficiency catalyst such as 2D TM dichalcogenides (TMDs). These cathode materials will be combined with new electrolyte blends and additives that work in synergy to reduce charge potentials and increase stability of the Li-air system.

State-of-the-art characterization techniques and computational methodologies will be used to understand charge and discharge chemistries. Success of this Task will establish a solid foundation for further development of Li-O_2 batteries toward practical applications for long-range EVs. The fundamental understanding and breakthrough in Li-O_2 batteries may also provide insight on improving performance of Li-S batteries and other energy storage systems based on chemical conversion process.

Highlights. The highlights for this quarter are as follows:

- The ANL / University of Illinois, Chicago (UIC) team identified evidence that fast charge and discharge rates are possible in Li-O_2 batteries using a new binary TMD alloy, $Nb_{0.5}Ta_{0.5}S_2$, for the cathode. Due to its low work function, effective electron transfer between the $Nb_{0.5}Ta_{0.5}S_2$ metal edge and O_2 facilitates both oxygen reduction and evolution reactions (ORR and OER) occurring during discharge and charge processes.
- The PNNL team optimized the concentration of redox mediator (2,2,6,6-tetramethyl-1-piperidinyloxy, or TEMPO) in a 1 M LiTFSI/G4 electrolyte and combined it with the polymer-supported solid electrolyte interphase (PS-SEI) generated by electrochemical pretreatment. This approach lowered charge voltage and increased cycle life of Li-O_2 batteries from 54 cycles to 123 cycles compared to the baseline cells.
- ANL team demonstrated a novel carbon nanosphere material with an open hierarchical pore structure with proper surface properties for enhancing the electrochemical performance of Li-O_2 cells. Particularly, benefiting from an open slit-shaped structure exposing a large portion of active sites to the surface, the porous carbon based Li-O_2 batteries deliver a super-high discharge capacity and long-cycle life.

Task 6.1 – Rechargeable Lithium-Air Batteries (Ji-Guang Zhang and Wu Xu, Pacific Northwest National Laboratory)

Project Objective. The objective of this project is to develop rechargeable Li-O_2 batteries with long-term cycling stability through in-depth research on more stable electrolytes and highly efficient catalysts for air electrodes, protection of Li-metal anodes, and deeper understanding on the ORR and OER mechanisms behind the electrochemical performance of Li-O_2 cells. In FY 2021, the team will further improve the cycle life and safety of Li-O_2 batteries using novel polymeric colloidal localized high concentration electrolytes (PC-LHCEs), binder-free catalysts with a robust artificial SEI layer, and synthesis of stable solvents. The fundamental mechanism behind the enhanced stability of Li-O_2 batteries using these new materials will also be investigated.

Project Impact. The project will develop rechargeable Li-O_2 batteries with long-term cycling stability through in-depth research on more stable electrolytes and highly efficient catalysts for air electrodes and protection of Li-metal anodes. This fiscal year, the team will further investigate stability of electrodes with different types of catalysts to keep the reversible reactions during the Li-O_2 battery operation and electrolytes to build more stable Li-O_2 batteries with long-term cycling capability.

Approach. Develop highly stable electrolytes, including novel PC-LHCEs with an optimization of Li-metal surface protection and effective catalysts to prevent the irreversible parasitic reactions at the electrodes (cathode and anode). The electrochemical test of Li||Li symmetric cell containing above stable electrolyte will be first measured comparatively with typical ether (TEGDME) based electrolytes to evaluate the stability of the electrolyte itself and the artificial SEI layer. Then, the stability of proposed electrolytes at the cathode side with reactive oxygen species during ORR/OER will be further characterized in the Li-O_2 cells. In addition, with new synthesis of solvents to stabilize the electrolyte system, the team will find the key parameters for suitable electrolyte in Li-O_2 batteries.

Out-Year-Goals. The long-term goal of the proposed work is to enable rechargeable Li-air batteries with a specific energy of 800 Wh/kg at cell level, 1000 deep-discharge cycles, improved abuse tolerance, and less than 20% capacity fade over a 10-year period to accelerate commercialization of long-range EVs.

Collaborations. This project collaborates with C. Wang of PNNL on characterization of cycled air electrodes by TEM/SEM, with P. Gao of PNNL on computational calculations and simulations, and with J. Read of ARL on oxygen solubility tests.

Milestones

1. Develop binder-free electrocatalysts on the surface of air electrode with polymer-supported SEI and redox mediators (RMs). (Q1, FY 2021; Completed)
2. Develop PC-LHCEs using osmosis effect. (Q2, FY 2021; Completed)
3. Understand the interphase properties of PC-LHCE/electrode. (Q3, FY 2021)
4. Develop new solvents that are stable against oxidation and singlet oxygen species for reversible Li-O_2 battery systems. (Q4, FY 2021)

Progress Report

Efforts this quarter involved concentration of RM (TEMPO) in 1 M lithium trifluoromethanesulfonate (LiTf) / tetraglyme (G4) electrolyte for long-term Li-O_2 battery operation in the cut-off voltage range of 2.0-4.5 V with the PS-SEI as a protection layer generated by electrochemical pretreatment. It is known that RM such as TEMPO can reduce the overvoltage during charge process. However, TEMPO added in electrolyte may also react with Li-metal anode and shorten the cycle life of Li-O_2 batteries. As shown in Figure 111a, Li-O_2 battery with pristine Li-metal anode can only last (54 cycles) when TEMPO is used. In contrast, Li-O_2 battery cells with lithium anode protected by PS-SEI layer show much better cycling stability at different TEMPO concentrations (105, 123, and 115 cycles at a TEMPO concentration of 0.1 M, 0.15 M, and 0.2 M, respectively). This is because the PS-SEI layer can protect Li-metal anode against side reactions (Figure 111b). Increasing TEMPO concentration leads to lower cell resistance after 10 cycles (Figure 111c), but too much TEMPO may lead to solubility issue in 1 M LiTf/G4 electrolyte. Through the formation of a robust PS-SEI layer on Li-metal anode, cycling stability of Li-O_2 batteries has been significantly improved. It is also found that Li-O_2 batteries using LiTFSI-based electrolytes lead to better cycling stability (123 cycles) compared to those using LiTf-based electrolyte (106 cycles), as seen in Figure 111d. To further improve performance of Li-O_2 batteries, solid catalyst (ruthenium oxide, RuO_2) was also added on air electrode in addition to solvable catalyst (TEMPO) added in electrolyte. The dual-catalyst system can further reduce the resistance of fresh cell (Figure 111e) with LiTFSI/G4 electrolyte and PS-SEI layer. In addition, it affects the pre-charging process (Figure 111f) due to oxidation of two different catalysts at ~ 3.7 V. The synergic effect of dual-catalyst system with PS-SEI layer and LiTFSI-based electrolyte is expected to further extend the lifespan of Li-O_2 batteries.

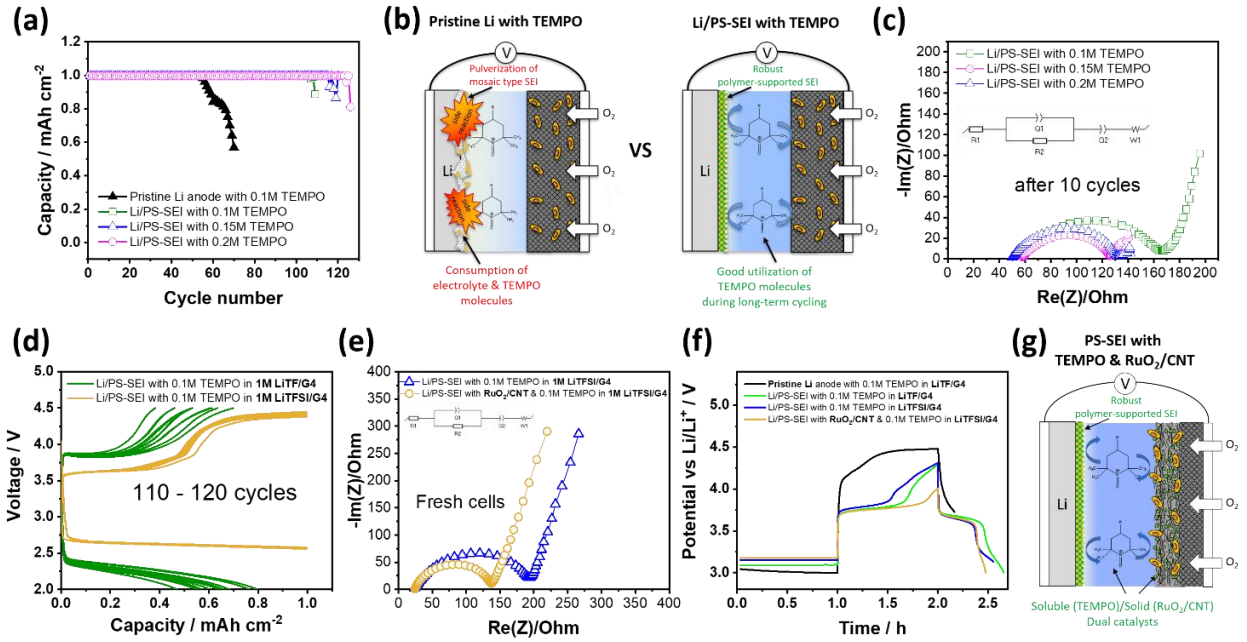

Figure 111. (a) Cycling stability of pristine lithium anode with 0.1 M TEMPO and Li/PS-SEI anodes with different TEMPO concentrations (0.1, 0.15, and 0.2 M) in 1 M LiTf/G4 and (b) schematic illustration of the effect of PS-SEI layer operating with TEMPO as redox mediator. (c) Electrochemical impedance spectroscopy (EIS) Nyquist plots of the corresponding cells after 10th cycle at a current density of 0.2 mA cm-2 under a capacity limited protocol of 1.0 mAh cm-2 in the operation voltage range of 2.0-4.5 V operated at 25°C. (d) Charge/discharge curves (110th – 120th) of Li-O_2 batteries with two different lithium salts (LiTf or LiTFSI) in G4 solvent with PS-SEI layer and 0.1 M TEMPO. (e) EIS of fresh Li-O_2 batteries with 0.1 M TEMPO in the LiTFSI-based electrolytes and GDL carbon or RuO_2 / carbon nanotube (CNT) electrodes. (f) Charge profiles of pristine lithium anode in 1 M LiTf/G4 with 0.1 M TEMPO, Li/PS-SEI in 1 M LiTf/G4 with 0.1 M TEMPO, Li/PS-SEI in 1 M LiTFSI/G4 with 0.1 M TEMPO, and Li/PS-SEI with RuO_2/CNT electrode in 1 M LiTFSI/G4 with 0.1 M TEMPO, respectively. (g) Schematic illustration of the synergic effect of dual-catalysis with PS-SEI layer in Li-O_2 battery cell.

Patents/Publications/Presentations

The project has no patents, publications, or presentations to report this quarter.

Task 6.2 – Lithium-Air Batteries
(Khalil Amine, Larry A. Curtiss, and Jun Lu; Argonne National Laboratory)

Project Objective. This project will develop new cathode materials and electrolytes for Li-air batteries for long cycle life, high capacity, and high efficiency. The goal is to obtain critical insight that will provide information on the charge and discharge processes in Li-air batteries to enable new advances to be made in their performance. This will be done using state-of-the-art characterization techniques combined with state-of-the-art computational methodologies to understand and design new materials and electrolytes for Li-air batteries.

Project Impact. The instability of current nonaqueous electrolytes and degradation of cathode materials limits performance of Li-air batteries. The project impact will be to develop new electrolytes and cathode materials that are stable and can increase energy density of electrical energy storage systems based on lithium.

Approach. The project is using a joint theoretical/experimental approach for design and discovery of new cathode and electrolyte materials that act synergistically to reduce charge overpotentials and increase cycle life. Synthesis methods, in combination with design principles developed from computations, are used to make new cathode architectures. Computational studies are used to help understand decomposition mechanisms of electrolytes and how to design electrolytes with improved stability. The new cathodes and electrolytes are tested in Li-O_2 cells. Characterization, along with theory, is used to understand the performance of materials used in the cell and to make improved materials.

Out-Year Goals. The out-year goals are to find catalysts that promote discharge product morphologies that reduce charge potentials and to find electrolytes for long cycle life through testing and design.

Collaborations. This project engages in collaboration with K. C. Lau (UC at Norridge), Y. Wu (Ohio State University), D. Zhai (China), and R. Shahbazian-Yassar (UIC).

Milestones

1. Design functionalized cathodes to achieve high electrochemical performance of Li-O_2 batteries. (Q1, FY 2021; Completed)
2. Characterize cathode materials and investigate electrochemical behaviors. (Q2, FY 2021; In progress)
3. Gain understanding of the processes of ORR and OER of these materials, and reveal the possible parasitic reactions. (Q3, FY 2021)
4. By understanding the effects, engineer new catalysts with improved catalytic performance and suppressed side reactions. (Q4, FY 2021)

Progress Report

Li-O_2 batteries have attracted extensive research interest due to their high energy density. Unfortunately, although the electrolyte stability and the basic cathode reactions in non-aqueous Li-O_2 battery have been extensively studied, the current system is plagued by porous cathode materials that are easily blocked by solid discharge product, Li_2O_2, during discharge process, which degrades the reaction kinetics with shortened cycle life. A reasonable pore architectonic design and a good catalytic capacity of the cathode are considered to be key to solving this problem.

Last quarter, the team reported a series of nanocarbon materials with unique pore structures, which were prepared via a low-cost, facile, and nanoscale controllable method (lignin, xylan, cellulose, and pomelo peel derived products are defined as C_L, C_X, C_C, and C_P, respectively). Among the nanocarbon materials, C_P exhibits the highest catalytic activity and the largest discharge capacity, while C_L shows the worst performance. To understand the correlation between electrochemical reaction and unique pore structure, further studies have been carried out.

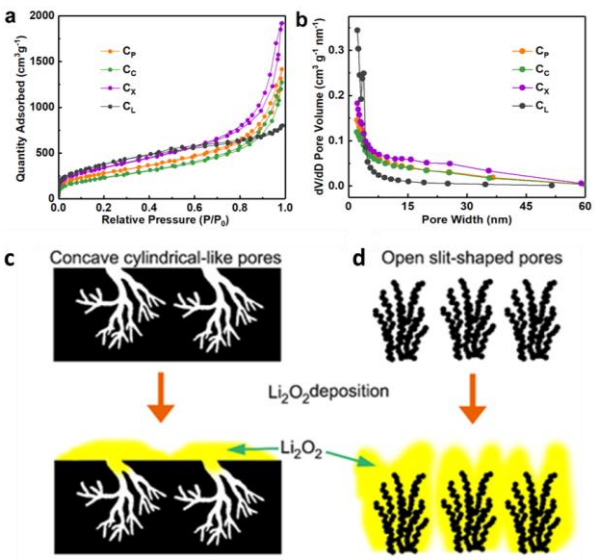

Figure 112. (a) Nitrogen adsorption-desorption isotherms. (b) Pore-size distributions of C_L, C_X, C_C, and C_P. Schematic representation of the Li_2O_2 deposition on (c) concave cylindrical pores and (d) open slit-shaped pores: the black and yellow parts in the figure represent the porous carbon matrix and the discharge product Li_2O_2, respectively.

As seen in Figure 112a-b, C_P, C_C, and C_X have a hierarchical pore structure where the pore size distribution contains micropores and mesopores, while the pore type of C_L is mainly microporous. C_L shows the highest specific surface area, but its pore volume and average pore diameter are significantly smaller than those of the other three carbons. Physisorption isotherms of C_P, C_C, and C_X are classified into a type H3 hysteresis loop, indicating that their pores are assemblage of non-rigid slit-shaped pore structures. The hysteresis curve of C_L belongs to the H4 type. This material contains concave cylindrical-like micropores and mesopores. In the case of concave cylindrical-like pores, discharge products would close the openings on the surface, block the mass transfer inside the pore, and deactivate the inner surface reactive sites (Figure 112c). Conversely, with an open slit-shaped pore structure, porous carbon can fully expose the reactive sites, and the non-rigid open pore can transport reactive ions and gases quickly (Figure 112d). Besides the pore structure, surface properties were also investigated. C_L, C_X, C_C, and C_P all have a fairly high C/O ratio of 14.7, 19.4, 16.5, and 17.94, respectively (Figure 113a). With a relatively low concentration of oxygenic groups and structure defects on the surface, the side reactions associated with carbon decomposition can be minimized, and the electric conductivity can also be enhanced (Figure 113b). Therefore, fast reaction kinetics and ultra-high specific capacity are achieved.

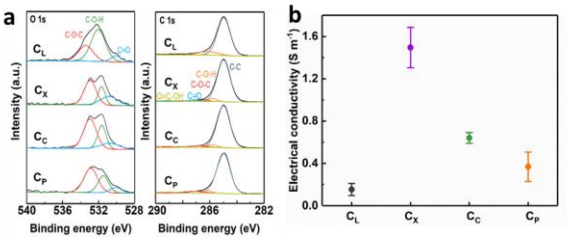

Figure 113. (a) O 1s and C 1s X-ray photoelectron scan and (b) electric conductivity of C_L, C_X, C_C, and C_P, respectively.

In conclusion, a novel carbon nanosphere material with an open hierarchical pore structure has been synthesized through a hydrolysis and carbonization process. The relationship between pore structure/surface properties and electrochemical performance in Li-O_2 batteries has been clearly revealed. Particularly, benefiting from an open slit-shaped structure exposing a large portion of active sites to the surface, the porous carbon based Li-O_2 batteries deliver a super-high discharge capacity and long-cycle life.

Patents/Publications/Presentations

Publication

- Zhao, T., Y. Yao, Y. F. Yuan, M. L. Wang, F. Wu, K. Amine, and J. Lu. "A Universal Method to Fabricating Porous Carbon for Li-O_2 Battery." *Nano Energy* 82 (2021): 105782.

Task 6.3 – Lithium Oxygen Battery Design and Predictions
(Larry A. Curtiss / Anh Ngo, Argonne National Laboratory; Amin Salehi-Khojin, University of Illinois, Chicago)

Project Objective. The objective of this work is to develop new materials for Li-O_2 batteries that give longer cycle life and improved efficiencies in an air environment. New electrolyte blends and additives will be investigated that can reduce clogging and at the same time promote the cathode functionality needed to reduce charge overpotentials. New cathode and anode materials will be investigated that can work in conjunction with the electrolytes to improve cycle life in the presence of air components.

Project Impact. Li-air batteries are considered as a potential alternative to Li-ion batteries for transportation applications due to their high theoretical specific energy. The major issues with the existing Li-O_2 systems include degradation of the anode electrode, reactions with air components, clogging of the cathode, and electrolyte instability. Thus, this project is using a comprehensive approach to improve cycle life and efficiency through developing new materials for electrodes, anodes, and electrolytes that work in synergy.

Approach. The experimental strategy is to use cathode materials based on 2D TMDs that the team has found to be among the best oxygen reduction and evolution catalysts. These cathode materials will be combined with new electrolyte blends and additives that work in synergy to reduce charge potentials and increase stability of the Li-air system. DFT and AIMD simulations are used to gain insight at the electronic structure level of theory of the electrolyte structure, and function both in bulk and at interfaces with the cathode, anode, and discharge product. Classical MD is used to obtain understanding at longer length and time scales of processes occurring in the electrolyte and growth mechanisms of discharge products. The team will also utilize a HT screening strategy based on experiment and theory to develop a large database of properties and outcomes of electrolyte combinations that can be analyzed using ML to predict electrolytes and additives with the best performance.

Out-Year Goals. The out-year goals are to find electrolytes that give high capacities and long cycle life in an air atmosphere using HT screening.

Collaborations. This project engages in collaboration with R. Assary and J. G. Wen of ANL, B. Narayanan of University of Louisville, T. Li of Northern Illinois University, and F. Khalili-Araghi and R. Klie of UIC.

Milestones

1. Use a conductive MOF for Li-O_2 battery to increase the number of active sites in cathode materials based on MOFs as well as localize them in pores. (Q1, FY 2021; Completed)
2. Utilize new TMD alloy catalyst for Li-O_2 batteries to increase charge/discharging rates. (Q2, FY 2021; Completed)
3. Investigate new concepts in electrolyte additives that work with the new alloy catalyst to increase charge/discharge rates and give anode protection. (Q3, FY 2021; Initiated)
4. Perform computational studies of new electrolyte additives and alloy catalyst to increase charge/discharge rates and give anode protection. (Q4, FY 2021; Initiated)

Progress Report

Li-O_2 batteries are considered as an advanced energy storage system that could provide a much higher specific energy than Li-ion batteries for electrical transportation. However, there are major issues with the existing Li-O_2 systems, including degradation of the anode electrode, poor volumetric energy density, poor charge/discharge rates, electrolyte instability, and high charge overpotential. This work is focused on finding a combination of electrolytes, additives, and cathode catalysts to enable a Li-O_2 battery that can operate in an air atmosphere with a low charge potential while maintaining a long cycle life.

Work this quarter has focused on increasing charge and discharge rates by using a more active catalyst. Thus far, research in the field has mostly resulted in batteries with low capacities (1000 $mAhg^{-1}$ or less) and current densities (0.1 $mAcm^{-2}$ or less). However, for electrified transportation, the battery must operate at much higher current rates in an air-like atmosphere. This requires overcoming inherent limitations (for example, sluggish kinetics) of currently utilized electrochemical processes during discharge and charge.

In this study, the team has used a new binary TMD alloy, $Nb_{0.5}Ta_{0.5}S_2$, as a cathode. They used this alloy because it has a work function (3.8 eV) much lower than most noble metals (for example, 5.4 eV for gold nanoparticles) as well as MoS_2 (4.5 eV), which they previously used. Due to its low work function, effective electron transfer between the $Nb_{0.5}Ta_{0.5}S_2$ metal edge and O_2 facilitates both ORR and OER occurring during discharge and charge processes. This material also shows excellent structural stability when operated at high current densities. The $Nb_{0.5}Ta_{0.5}S_2$ alloy was synthesized with the desired stoichiometry of x = 0.5 through a chemical vapor transport (CVT) method followed by a liquid phase exfoliation technique to produce nanoflakes with an average size of ~ 220 nm.

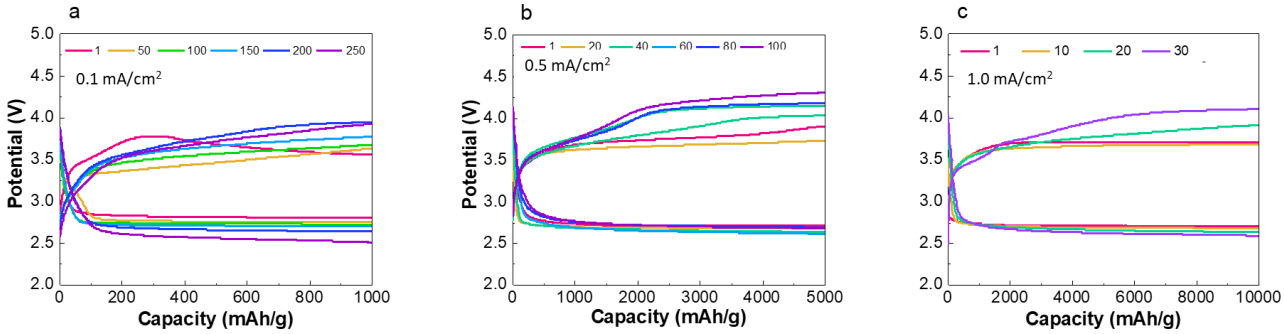

Figure 114. Discharge-Charge voltage profile of Li-O_2 battery with $Nb_{0.5}Ta_{0.5}S_2$ as the cathode catalyst and with (a-c) current density of 0.1, 0.5, and 1 mA cm^{-2}, respectively.

The $Nb_{0.5}Ta_{0.5}S_2$ cathode was used with an electrolyte based on a 9:1 ratio of dimethyl sulfoxide (DMSO) / IL solvents with three salts (LiCl, $LiClO_4$, and $KMnO_4$) in the Li-O_2 cell with dry air. Figure 114a-b shows the discharge and charge profiles of the battery operating in a dry air environment tested up to 250 and 100 cycles, with the cut-off potential of 2.5-4.5 V and the current density of 0.1 (1000 mA/g) and 0.5 $mAcm^{-2}$ (5000 mA/g), respectively. The discharge plateaus are stable without any evidence of capacity loss of Li_2O_2. At 0.5 $mAcm^{-2}$ and 5000 $mAhg^{-1}$ specific capacity, the battery did not fail until 130 cycles before a sudden drop in the discharge potential was observed. Figure 114c demonstrates the battery results with the current density of 1 $mAcm^{-2}$ (5000 mA/g) and a specific capacity of 10,000 $mAhg^{-1}$ that ran up to 34 cycles.

To characterize the battery cathode after discharge and charge, the team performed HRTEM, EELS, Raman spectroscopy, XPS, DEMS, SEM, and EDX. HRTEM image micrographs and diffraction patterns of the cathode after the 20th cycle indicate a stable $Nb_{0.5}Ta_{0.5}S_2$ cathode with a highly crystalline structure. The TEM results also show that the Li_2O_2 product attached to the $Nb_{0.5}Ta_{0.5}S_2$ catalyst is the nanocrystalline with grains and GBs. The grains are crystalline particles, and the GBs are amorphous. XPS analysis was carried out

to study the elemental composition of the product after 20 discharge cycles. In the Li 1s region, the main peak was located at 55.1 eV. The O 1s major peak appeared at 531.9 eV, confirming formation of Li_2O_2. Raman spectroscopy was performed to further confirm the presence of Li_2O_2. After the 20th discharge cycle, there are two distinctive Raman peaks at 250 cm^{-1} and 788 cm^{-1} corresponding to Li_2O_2. The first peak is attributed to the stretching of the Li-O bond, while the second peak is for the vibration of O-O bond.

In summary, the team has provided evidence that fast charge and discharge rates are possible in Li-O_2 batteries accomplished using a new binary TMD alloy, $Nb_{0.5}Ta_{0.5}S_2$, for the cathode. They used this TMD alloy because it has a work function (3.8 eV) much lower than most noble metals (for example, 5.4 eV for gold nanoparticles) as well as MoS_2 (4.5 eV) that the team previously used. Due to its low work function, effective electron transfer between the $Nb_{0.5}Ta_{0.5}S_2$ metal edge and O_2 facilitates both ORR and OER occurring during discharge and charge processes.

Patents/Publications/Presentations

Publications

- Ahmadiparidari, A., S. Fuladi, L. Majidi, S. Plunkett, E. Sarnello, Z. Hemmat, S. Rastegar, S. Misal, P. C. Redfern, J. Wen, T. Li, A. T. Ngo, F. Khalili-Araghi, L. A. Curtiss, and A. Salehi-Kojin. "Lowering Charge Potentials with Negligible Capacity Loss in High Rate Lithium Oxygen Batteries." *Journal of Power Sources* 491 (2021): 229506.
- Rastegar, S., Z. Hemmat, C. Zhang, S. Plunkett, J. G. Wen, N. Dandu, T. Rojas, L. Majidi, S. Misal, A. T. Ngo, L. A. Curtiss, and A. Salehi-Khojin. "A Lithium-Oxygen Battery that Operates in Dry Air with a Bifunctional InX_3 (X = Br, I) Electrolyte Additive." *ACS Applied Materials and Interfaces* 13, No. 4 (2021): 4915–4922.

TASK 7 – SODIUM-ION BATTERIES

Team Lead: Xiao-Qing Yang, Brookhaven National Laboratory

Summary

The Na-ion battery will require investigations to identify optimal electrode materials, electrolytes, separators, and binders to reach full potential. The BMR program will therefore have a limited effort directed toward identifying Na-ion battery materials that have potential value for vehicle applications. During FY 2019, the BMR added several new projects in the area of Na-ion batteries, four of which have been continuously funded. Progress on these projects is described in this report.

Highlights. The highlights for this quarter are as follows:

- The ANL team conducted experiments to evaluate stability of the Na-ion battery canonical layered oxide cathode, $NaFeO_2$, in different electrolytes. The type of electrolyte used can drastically affect electrochemical performance, possibly related to the chemical stability of tetravalent iron in the cathode. It was found that FEC helps to stabilize the material at high SOC, leading to improved electrochemical performance.
- The BNL team carried out synchrotron-based spectroscopy studies on two new P2 types of layered cathode materials for Na-ion batteries: $Na_{0.67}[Mn_{0.66}Ni_{0.33}]O_2$ (MN) and Sb-substituted MN, $Na_{0.67}[Mn_{0.61}Ni_{0.28}Sb_{0.11}]O_2$ (MNS). The XANES evolutions for the K-edge of manganese and nickel in MNS during the first charge, first discharge, and second charge were studied. In the second charge, the valence states of manganese and nickel undergo reversed changes to the first discharge process, suggesting highly reversible valence state changes of manganese and nickel in MNS.
- The LBNL team carried out laboratory XRD and Raman studies on $Na_{0.74}Ti_{1.815}O_4$ electrodes at differing SOC, confirming that redox proceeds via a solid-solution process, which is highly reversible. Gradual impedance build-up on cycling appears to be responsible for capacity fade.
- The PNNL team developed a nonflammable high-concentration electrolyte (HCE) using triethylphosphate (TEP) as solvent and tailored for high-voltage cathode. The Na||NaNMC cell using this electrolyte exhibits CE near 100% at a high voltage of 4.2 V. After 500 cycles, these cells still retain 78%, 85%, and 81% capacity at a rate of 0.2 C, 0.33 C, and 0.5 C, respectively.

Task 7.1 – Exploratory Studies of Novel Sodium-Ion Battery Systems (Xiao-Qing Yang and Zulipiya Shadike, Brookhaven National Laboratory)

Project Objective. To meet the challenges of powering PHEVs and BEVs, new rechargeable battery systems with high energy and power density, low cost, good abuse tolerance, and long calendar and cycle life need to be developed. The primary objective of this project is to develop new advanced synchrotron-based material characterization techniques and apply these techniques to study the new rechargeable battery systems beyond the Li-ion batteries, namely the Na-ion battery systems for electrified vehicles.

Project Impact. The results of this project will be used for developing technologies that will significantly increase the energy density and cycle life and reduce the cost of beyond Li-ion battery systems. This will greatly accelerate deployment of EVs and reduce carbon emission associated with fossil fuel consumption and will help in the direction of building U. S. based energy storage manufacture chains.

Approach. This project will use the synchrotron-based *in situ* X-ray diagnostic such as *in situ* XRD and *in situ* XAS tools, combined with TEM, STEM, and TXM imaging techniques developed at BNL to evaluate the new materials and redox couples to obtain in-depth understanding of the reaction mechanisms of these materials, aiming to improve existing materials and to provide guidance for new materials and new technology development for Na-ion battery systems.

Out-Year Goals. The out-year goal is to complete the synchrotron-based XRD, XAS, and XANES mapping studies of new cathode materials P2-$Na_{0.66}[Mn_{0.61}Ni_{0.28}Sb_{0.11}]O_2$ and P2-$Na_{0.7}Mg_{0.2}[Mn_{0.6}Fe_{0.2}\square_{0.2}]O_2$ (□ here representing TM vacancy) and a high-capacity, high-C rate, multi-component cathode material.

Collaborations. The BNL team has been closely working with top scientists on new material synthesis at ANL, LBNL, and PNNL, with U. S. industrial collaborators at GM and Johnson Controls, and with international collaborators.

Milestones

1. Complete XAS (including XANES and EXAFS) and 2D XANES mapping of the pristine P2-$Na_{0.66}[Mn_{0.61}Ni_{0.28}Sb_{0.11}]O_2$ cathode material at nickel and manganese K-edge. (Q1, FY 2021; Completed)
2. Complete nickel and manganese K-edge XAS (including XANES and EXAFS) of P2-$Na_{0.66}[Mn_{0.61}Ni_{0.28}Sb_{0.11}]O_2$ cathode material at different SOCs. (Q2, FY 2021; Completed)
3. Complete *ex situ* TEM, XRD study, and 2D XANES mapping of high-capacity high-C rate multi-component sodium cathode material with P2 type at different SOCs. (Q3, FY 2021; In progress)
4. Complete iron and manganese K-edge XAS of P2-$Na_{0.7}Mg_{0.2}[Mn_{0.6}Fe_{0.2}\square_{0.2}]O_2$ cathode material at different SOCs. (Q4, FY 2021; In progress)

Progress Report

This quarter, the team completed the second milestone for FY 2021 and made progress on other milestones. BNL has been focused on developing new diagnostic techniques to study and improve performance of Na-ion batteries. These techniques have been applied to the study of a new P2 type layered cathode material for Na-ion battery: Sb-substituted MN, MNS. Figure 115a-f shows the XANES evolutions for the K-edge of manganese and nickel in MNS during the 1st charge, 1st discharge, and 2nd charge, respectively, while Figure 115g-h presents the change of the edge energy. The charge compensation of MNS during cycling is summarized in Figure 115i. Manganese and nickel ions in MNS dominate different voltage regions for charge compensation. In the first charge process, the specific capacity of 99 mAh g^{-1} is mainly contributed by Ni^{2+}/Ni^{3+} and $Mn^{3.7+}/Mn^{4+}$. During discharge, nickel ions are reduced in the voltage from 4.2 V to 2.3 V. Afterward, manganese ions are reduced in the voltage range from 2.3 V to 1.8 V. Correspondingly, a total number of 0.58 Na^+ per MNS is intercalated during discharge process, accompanying manganese and nickel redox reactions. In the second charge process, the valence states of manganese and nickel undergo reversed changes to the 1st discharge process, suggesting highly reversible valence state changes of manganese and nickel in MNS.

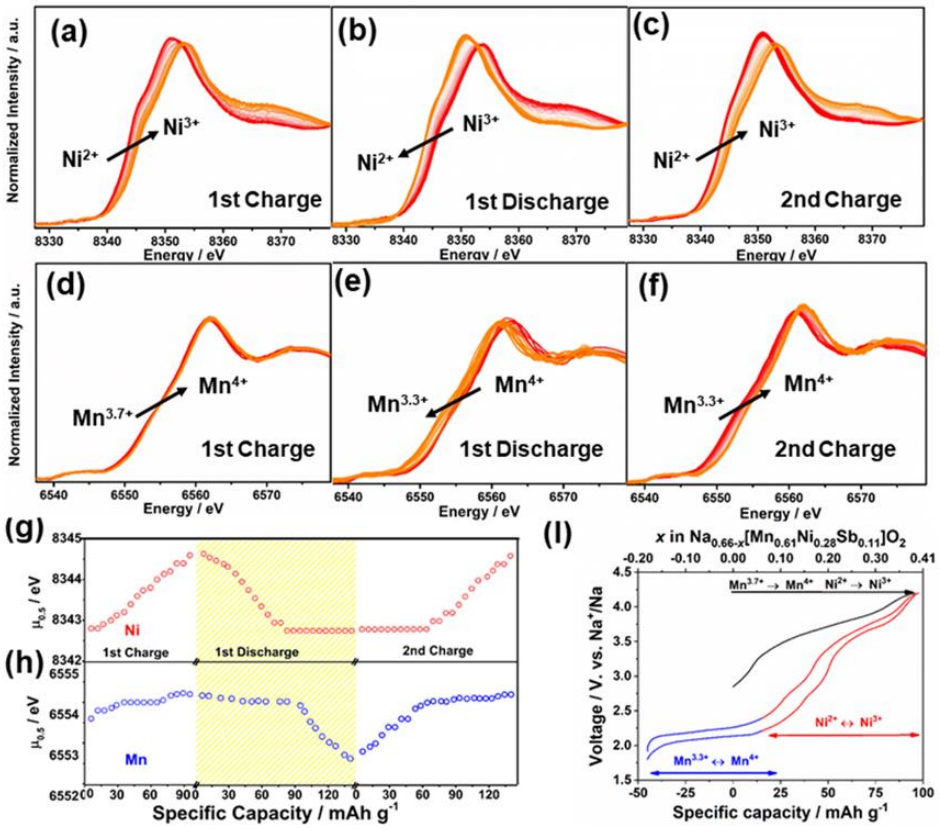

Figure 115. ***In situ*** **X-ray absorption spectra for MNS. (a-c) Nickel and (d-f) manganese K-edge X-ray absorption near-edge structure (XANES) of MNS at various stages during the 1st charge, 1st discharge, and 2nd charge processes, respectively. The edge energy evolution at half edge-step ($E_{0.5}$) for (g) nickel and (h) manganese in $Na_{0.67}[Mn_{0.61}Ni_{0.28}Sb_{0.11}]O_2$ at different states. (i) Charge compensation of different element contributions during charge and discharge.**

Patents/Publications/Presentations

Publications

- Xiao, B., Y. Wang, S. Tan, M. Song, X. Li, Y. Zhang, F. Lin, K. S. Han, F. Omenya, K. Amine, X-Q. Yang, D. Reed, Y. Hu, G-L. Xu, E. Hu,* X. Li,* and X. Li.* "Vacancy-Enabled O3 Phase Stabilization for Manganese-Rich Layered Sodium Cathodes." *Angewandte Chemie*. doi: 10.1002/anie.202016334; Publication Date (Web): January 21, 2021.
- Cui, J., H. Zheng, Z. Zhang, S. Hwang, X-Q. Yang, and K. He. "Origin of Anomalous High-Rate Na-Ion Electrochemistry in Layered Bismuth Telluride Anodes." *Matter* (2021). doi: 10.1016/j.matt.2021.01.005; Publication Date (Web): February 1, 2021.
- Shi, D-R., T. Wang, Z. Shadike, L. Ma, X-Q. Yang, S-F. Chu, Z-W. Zhao, Z-Q. Peng, and Z-W. Fu.* "Anionic Redox Reaction Triggered by Trivalent Al^{3+} in P3-$Na_{0.65}Mn_{0.5}Al_{0.5}O_2$." *Chemical Communications* (2021). doi: 0.1039/D1CC00373A; Publication Date (Web): February 17, 2021.
- Wang, Q-C.,* Z. Shadike, X-L. Li, J. Bao, Q-Q. Qiu, E. Hu, S-M. Bak, X. Xiao, L. Ma, X-J. Wu, X-Q. Yang,* and Y-N. Zhou.* "Tuning Sodium Occupancy Sites in P2-Layered Cathode Material for Enhancing Electrochemical Performance." *Advanced Energy Materials* (2021). doi: 10.1002/aenm.202003455; Publication Date (Web): February 24, 2021.
- Li, X-L., T. Wang, Y. Yuan, X-Y. Yue, Q-C. Wang, J-Y. Wang, J. Zhong, R-Q. Lin, Y. Yao, X-J. Wu, X-Q. Yu, Z-W. Fu, Y-Y. Xia, X-Q. Yang, T. Liu, K. Amine, Z. Shadike,* Y-N. Zhou,* and J. Lu.* "Whole-Voltage-Range Oxygen Redox in P2-Layered Cathode Materials for Sodium-Ion Batteries." *Advanced Materials* (2021). doi: 10.1002/adma.202008194; Publication Date (Web): March 1, 2021.

Task 7.2 – Development of a High-Energy Sodium-Ion Battery with Long Life (Chris Johnson and Khalil Amine, Argonne National Laboratory)

Project Objective. The project objective is to develop a high-energy Na-ion battery with long life. Moreover, the battery chemistry should utilize low-cost materials. The energy density target is 200 Wh/kg and/or 500 Wh/L, wherein the anode and cathode capacity targets are 600 $mAhg^{-1}$ and 200 $mAhg^{-1}$, respectively.

Project Impact. A Na-ion battery on par with the energy density of a Li-ion battery can have a high impact in the transportation sector with the assumption that the cost is significantly below $85/kWh and that the battery pack provides a 300-mile range. The consumer is not concerned about the battery chemistry employed if these metrics can be met. Development of these battery chemistries will situate the United States in a strong position as relates to new low-cost energy storage systems beyond lithium ion.

Approach. In a team approach, the Na-ion battery group will create a versatile Na-ion battery chemistry with beneficial advantages such as low cost, safety, recycling, and sustainability of materials used. The team will work synergistically so that the final design is the culmination of advances in phosphorus carbon composites mated with optimized lead or other highly dense metalloids, such as tin and/or antimony and derivatives thereof, for the recyclable anode. Synthesis and optimization of such blended composite anodes will be conducted in parallel to diagnostic characterization of structures, phase formation, and cycling stability. Cathode work will begin at the end of the first year and will involve gradient cathodes consisting of Fe-Mn compositions, as well as intergrowths of layer stacking sequenced oxides. If resources allow, the team also will attempt to stabilize cathode surfaces using ALD methods, particularly for the benefit of staving off dissolution of manganese and iron/electrolyte reactivity. Electrolytes will be partly procured from H. Li at PNNL.

Out-Year Goals. The state-of-the-art Na-ion battery in the literature has now been surpassed by this team, but performance is still too low for commercialization. Thus, the goal is to move forward and continually invent the most superior Na-ion battery chemistry that can compete worldwide through work output from this project.

Collaborations. Researchers from PNNL who are developing electrolytes for Na-ion batteries will provide this project with formulations to test with the various electrode combinations investigated at ANL.

Milestones

1. Doped red phosphorus (RP) anode with high specific capacity and stable cycle life. (Q1, FY 2021; Completed)
2. *In situ* characterization of layered cathodes during synthesis; synthesize Ni-based, Fe-based, and Mn-based sodium layered cathodes. (Q2, FY 2021; Completed)
3. Advanced characterization on developed cathodes and anodes during charge/discharge. (Q3, FY 2021; In progress)
4. Performance optimization of synthesized layered cathodes and demonstration of full-cell development using optimal phosphorus anode and developed/commercial cathodes. (Q4, FY 2021; In progress)

Progress Report

Irons have been one of the most attractive TM constituents in Li-ion battery cathode compounds, as they are abundant, non-toxic, environmentally benign, and light in weight. For example, olivine structured $LiFePO_4$ has been developed as a long-life and low-cost cathode option for EVs and large-scale energy storage systems. However, compared with that of the layered NMC oxides, the theoretical energy density of $LiFePO_4$ is limited by the low-voltage redox reaction of the Fe^{2+}/Fe^{3+} couple. The reversible operation of Fe^{3+}/Fe^{4+} redox, which would provide a higher operating voltage and subsequently a higher specific energy density, has not yet been successful in Li-ion batteries. For example, delithiation of layered $LiFeO_2$ only degrades the cathode without oxidizing Fe^{3+}. In subsequent discharge, Fe^{3+} reduces to Fe^{2+}. The inactivity of Fe^{3+}/Fe^{4+} redox in layered lithium TM oxides has been largely attributed to the structural instability where Fe^{3+} readily migrates to lithium sites during cycling, resulting in a significant cation disorder in the layered structure. In contrast, layer structured $NaFe_{1-x}M_xO_2$ supports reversible Fe^{3+}/Fe^{4+} redox reaction because the large size difference between sodium and iron effectively suppresses Na/Fe cation mixing, stabilizing the layered structure. Nevertheless, the reversibility of the Fe^{3+}/Fe^{4+} operation in layered oxides is still unsatisfactory and requires further improvement. The team has previously shown that, besides the structural irreversibility, the chemical instability of the Fe^{4+} species in contact with battery electrolytes (1 M $NaClO_4$/PC) also causes performance degradation. This quarter, they have revisited the layered $NaFeO_2$ model system to investigate the effect of different electrolytes on the chemical stability of Fe^{4+} species in charged $Na_{1-x}FeO_2$ cathode.

A $NaFeO_2$ powder sample was synthesized by solid-state synthesis of Na_2O_2 and Fe_3O_4 at 650°C for 12 hours in air. The XRD pattern in Figure 116a shows a single phase layered R-3m structure without any apparent impurity phases. Figure 116b compares the initial charge-discharge profiles of the $NaFeO_2$ half cells cycled with different electrolyte compositions. The cell cycled with 1 M $NaClO_4$/PC electrolyte shows the highest charge capacity, but the lowest discharge capacity, among the tested electrolytes; the initial CE (1st CE) is only 64%. The 1st CE was improved by replacing $NaClO_4$ with $NaPF_6$. The 1 M $NaPF_6$/PC with 2% FEC additive shows the highest 1st CE (91%).

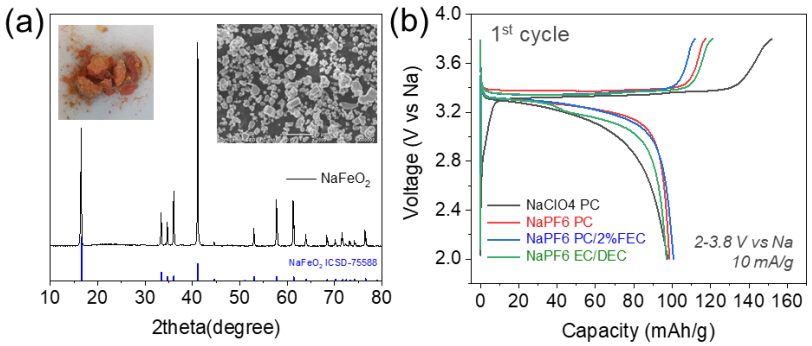

Initial Coulombic eff. (%)	
1M $NaClO_4$ / PC	64
1M $NaPF_6$ / PC	84
1M $NaPF_6$ / PC +2%FEC	91
1M $NaPF_6$ / EC-DEC	80

Figure 116. (a) Scanning electron microscopy morphology and X-ray diffraction pattern of layered $NaFeO_2$. (b) Initial charge and discharge curves Na/$NaFeO_2$ cell in various electrolytes.

Figure 117 displays the performance degradation after aging the charged $Na_{1-x}FeO_2$ electrodes in different electrolytes. The aging cycle was performed applying a series of charge (C1) – aging for 10 days at OCV (aging@SOC) – discharge (D'1) – charge (C'2) – discharge (D'2) steps. In Figure 117a, the discharge capacity for the 1 M $NaClO_4$/PC cell significantly decreases after the aging@SOC step (D1 = ~ 90 mAh/g versus D'1 = ~ 40 mAh/g). The subsequent C'2 and D'2 capacities show even lower values, indicating an irrecoverable degradation to the cell. In Figure 117b, the 1 M $NaPF_6$/PC cell shows similar degradation after the aging@SOC step (D1 = ~ 90 mAh/g versus D'1 = ~ 40 mAh/g). However, the average discharge voltage of the D'1 curve is higher than that for the 1 M $NaClO_4$/PC cell. Furthermore, the cell performance partially recovers in the subsequent C'2-D'2 steps (D'2 = 60 mAh/g). The aging stability significantly improves when 2% FEC is added to 1 M $NaPF_6$/PC electrolyte (Figure 117c; D1 = 90 mAh/g versus D'1 = ~ 85 mAh/g).

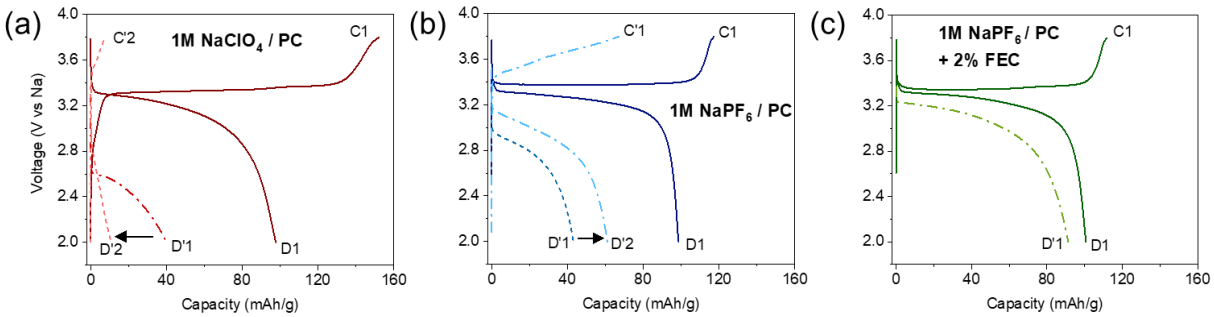

Figure 117. Comparison of performance degradation of Na/$NaFeO_2$ cell after resting at the end of 1st charge for 10 days in (a) 1 M $NaClO_4$/PC, (b) 1 M $NaPF_6$/PC, and (c) 1 M $NaPF_6$/PC with 2% FEC electrolytes. Continuous cycle (C1 – D1) versus Aging cycle (C1 – OCV storage for 10 days – D'1 – C'2 – D'2).

Although the potential benefit of FEC to Na-metal anode cannot be ruled out, the team has performed further evaluation focused on the effect of FEC on cathodes. Figure 118a compares the SEM morphology of the $Na_{1-x}FeO_2$ electrodes. The electrode aged with FEC shows a more uniform surface morphology. The electrode surface aged without FEC appears to have built up thicker surface layers. The inset images display the separators (interfaced against the cathode) harvested from the aged cells. The clean separator collected from the FEC-containing cell contrasts with the significantly discolored separator harvested from the FEC-free cell. Figure 118b also shows that the FEC-containing cell has a lower leakage current during the constant voltage hold at 3.8 V versus sodium. The cathode impedance build-up during the aging@SOC step was also measured using three-electrode cells. In Figure 118c, the cathode impedance of the FEC-free cell continuously increases during the aging period, whereas FEC effectively suppresses the impedance rise. In Figure 118d, *ex situ* XRD shows that the lattice parameters and peak intensities of the $Na_{1-x}FeO_2$ electrode aged in the FEC-free cell gradually recover the values for pristine $NaFeO_2$. This observation suggests that degradation during the aging@SOC step is associated with self-discharge of the $Na_{1-x}FeO_2$ (spontaneous reduction of Fe^{4+} to Fe^{3+} and associated sodium insertion). FEC suppresses the spontaneous parasitic reaction at the $Na_{1-x}FeO_2$ surface, stabilizing the Fe^{4+} oxidation state and the layered structure.

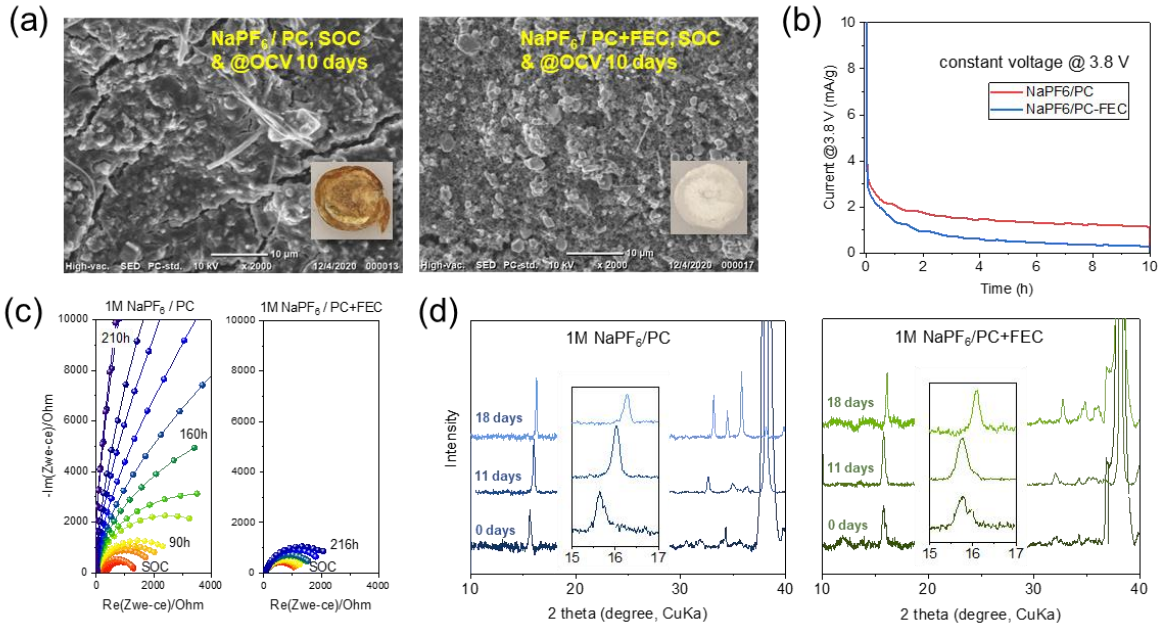

Figure 118. The effect of FEC additive on stabilizing the charged $Na_{1-x}FeO_2$ electrode in 1 M $NaPF_6$/PC electrolyte. (a) Scanning electron microscopy morphology (inset image showing the surface of harvested separator). (b) Leakage current at 3.8 V. (c) Cathode electrochemical impedance spectroscopy as a function of state of charge resting time. (d) *Ex situ* X-ray diffraction of harvested $Na_{1-x}FeO_2$ electrodes.

Patents/Publications/Presentations

Publications

- Liu, X.; B. Xiao, A. Daali, X. Zhou, Z. Yu, X. Li, Y. Liu, L. Yin, Z. Yang, C. Zhao, L. Zhu, Y. Ren, L. Cheng, S. Ahmed, Z. Chen, X. Li,* G. L. Xu,* and K. Amine.* "A Stress/Interface-Compatible Red Phosphorus Anode for High-Energy and Durable Sodium-Ion Batteries." ACS *Energy Letters* 6, No. 2 (2021): 547–556. Publication Date (Web): January 15, 2021.
- Xiao, B., Y. Wang, S. Tan, X. Li, Y. Zhang, F. Lin, K. S. Han, F. Omenya, K. Amine, D. Reed, Y. Hu, G. L. Xu,* E. Hu,* X. Li,* and X. Li.* "Vacancy-Enabled O3 Phase Stabilization for Manganese-Rich Layered Sodium Cathodes." *Angewandte Chemie International Edition* 60 (2021): 8258–8267. Publication Date (Web): January 21, 2021.

Task 7.3 – High-Capacity, Low-Voltage Titanate Anodes for Sodium-Ion Batteries (Marca Doeff, Lawrence Berkeley National Laboratory)

Project Objective. The objectives are to understand differences in the sodium intercalation mechanism of various sodium titanate anodes through an array of synthetic, electrochemical, and structural characterization techniques, and to overcome practical impediments to their use, such as the high 1st cycle Coulombic inefficiencies that are currently observed. The ultimate goal is to produce a 200-250 mAh/g anode that cycles reversibly.

Project Impact. Although several suitable cathode materials for Na-ion batteries exist, there are few suitable anode materials due to low potential instabilities. Therefore, sodium titanate variations will be synthesized through different routes to develop materials with various morphologies and dopants. Decreasing the 1st cycle inefficiencies and improving cycling performance will allow enabling technology for a practical high-energy Na-ion battery.

Approach. Candidate stepped layered titanates will be synthesized by appropriate routes (hydrothermal, solid-state, etc.). Materials will then be characterized electrochemically and physically. Structure-function relationships will be built to correlate the effect of changing structure (for example, step size) on electrochemical properties.

Out-Year Goals. A series of synchrotron characterization techniques will be used to further develop sodium titanate anode materials with stable cycling while delivering high capacities.

Collaborations. TXM is done in collaboration with Y. Liu (SSRL). Synchrotron hard, soft XAS, and X-ray Raman efforts are in collaboration with D. Nordlund and D. Sokaras (SSRL). Electrolyte design is done in collaboration with K. Xu (ARL).

Milestones

1. Characterize lepidocrocite titanates. (Q1, FY 2021; Completed)
2. Optimize electrode. (Q2, FY 2021; Completed)
3. Assemble, test, and study full cells. (Q3, FY 2021; In progress)
4. *Go/No-Go Decision*: On lepidocrocite titanate, stop if problems are not solved. (Q4, FY 2021)

Progress Report

The team performed HRTEM analysis this quarter. The SAED patterns confirm that the lepidocrocite titanate $Na_{0.74}Ti_{1.815}O_4$ crystallizes in the I*mmm* structure (Figure 119a-c), as also deduced from Rietveld refinement of the synchrotron XRD pattern (Figure 119m). The $[1\bar{1}\bar{1}]$ HRTEM image shows the lamellar features of lepidocrocite titanate $Na_{0.74}Ti_{1.815}O_4$ (Figure 119d). TEM-EDX mappings reveal uniform elemental distribution of sodium, titanium, and oxygen at both the particle- and bulk-level (Figure 119e-l).

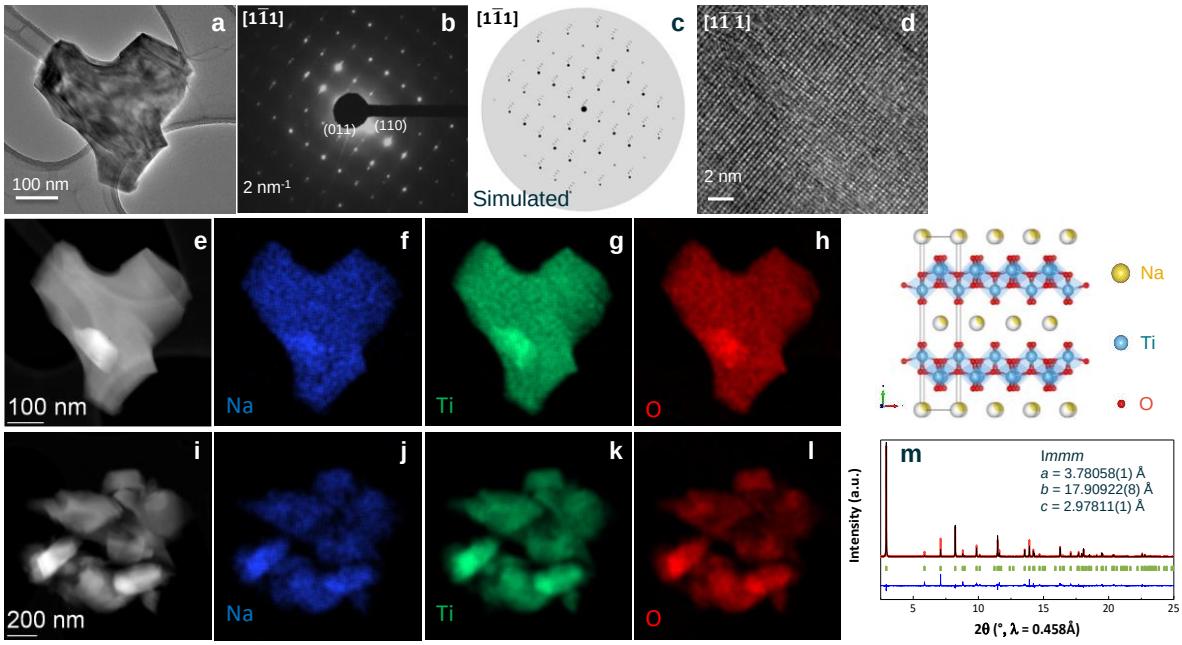

Figure 119. (a) High-resolution transmission electron microscopy (HRTEM) image of a single $Na_{0.74}Ti_{1.815}O_4$ particle, and the corresponding experimental (b) and simulated (c) selected area electron diffraction (SAED) patterns. Crystal structure model derived from Rietveld refinement of the synchrotron X-ray diffraction pattern of $Na_{0.74}Ti_{1.815}O_4$ was used in the SAED simulations. (d) HRTEM image showing the lattice fringes directing along the zone axis $[1\bar{1}\bar{1}]$. TEM image (e) and element mapping images for sodium (f), titanium (g), and oxygen (h) of a single $Na_{0.74}Ti_{1.815}O_4$ particle. TEM image (i) and element mapping images for sodium (j), titanium (k), and oxygen (i) of $Na_{0.74}Ti_{1.815}O_4$ particles.

Ex situ laboratory XRD patterns of $Na_{0.74}Ti_{1.815}O_4$ electrodes collected at various SOCs in the first electrochemical cycle (Figure 120a-b) and in the fully discharged state in selected cycles (Figure 121a) indicate that (1) the lepidocrocite structure of $Na_{0.74}Ti_{1.815}O_4$ electrodes is largely maintained on battery cycling, and (2) Na^+ insertion into/removal from $Na_{0.74}Ti_{1.815}O_4$ electrodes proceeds through a solid-solution reaction. *Ex situ* Raman spectra of $Na_{0.74}Ti_{1.815}O_4$ electrodes collected at various SOCs in the 1st electrochemical cycle also indicate the structural reversibility of $Na_{0.74}Ti_{1.815}O_4$ electrodes. Electrochemical impedance spectra collected at the fully charged state in selected cycles show gradual impedance build-up on cycling (Figure 121b), which may be responsible for the capacity fading observed during battery cycling.

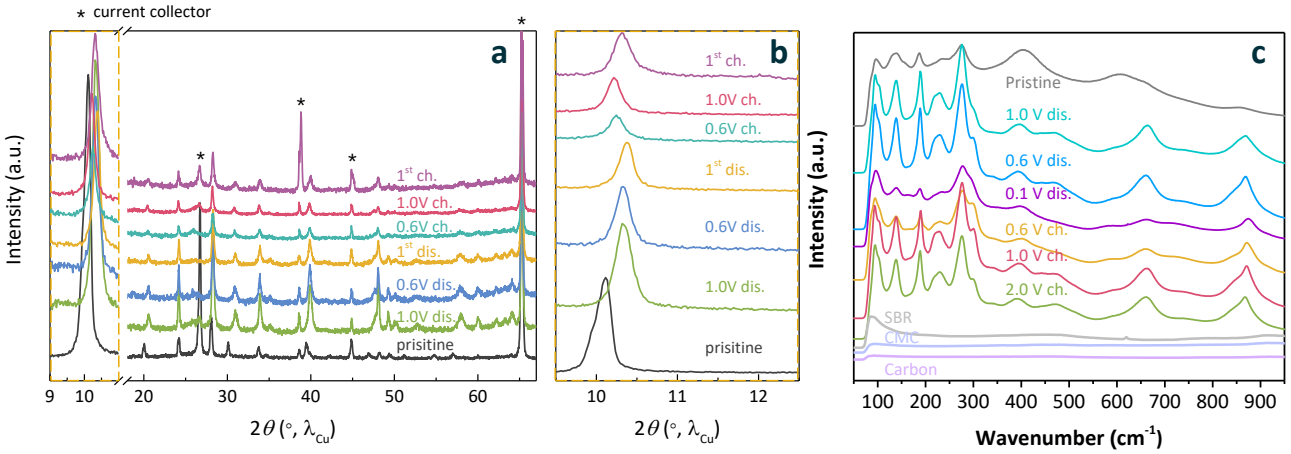

Figure 120. (a) Laboratory X-ray diffraction patterns of $Na_{0.74}Ti_{1.815}O_4$ electrodes in pristine state and cycled to the annotated voltages in the 1st electrochemical cycle. (b) Magnified plot of the dashed rectangle area in (a). (c) *Ex situ* Raman spectra of $Na_{0.74}Ti_{1.815}O4$ electrodes in pristine state and cycled to the annotated voltages in the 1st electrochemical cycle.

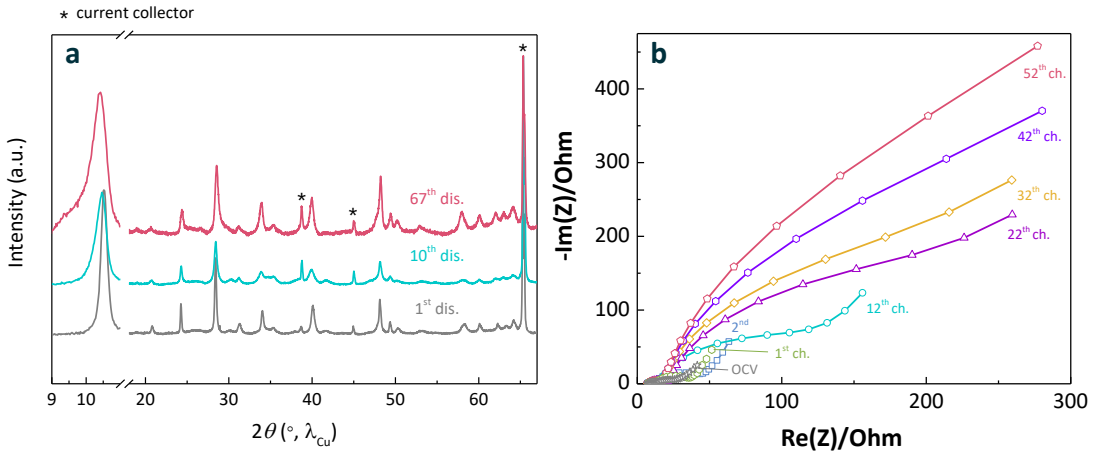

Figure 121. (a) Laboratory X-ray diffraction patterns of $Na_{0.74}Ti_{1.815}O_4$ electrodes collected at the end of discharge for annotated cycles. (b) Nyquist plots of a Na/ $Na_{0.74}Ti_{1.815}O_4$ cell showing impedance data at the open circuit voltage and at the end of charge for annotated cycles.

Patents/Publications/Presentations

The project has no patents, publications, or presentations to report this quarter.

Task 7.4 – Electrolytes and Interfaces for Stable High-Energy Sodium-Ion Batteries (Ji-Guang Zhang, Pacific Northwest National Laboratory)

Project Objective. The Na-ion battery is a potential alternative energy source for EVs and grid applications due to the low cost and the natural abundance of sodium. The performance of Na-ion batteries largely depends on development of electrode materials and electrolytes. In recent years, a series of potential electrode materials has been developed. However, a fundamental understanding of the electrochemistry of Na-ion batteries, especially the stability of the electrode-electrolyte interface in these batteries, is still not well established. This project will develop innovative electrolytes to enable fundamental understanding on the interface between electrode and electrolyte for stable operation of high-energy Na-ion batteries. A high-capacity anode will also be developed. The proposed research will enhance the achievable capacities of both anode and cathode for Na-ion battery and improve the stability of electrodes/electrolyte interface, establish correlation (electrolyte design rule) between electrochemical performances of Na-ion batteries and the electrolyte/interface properties, and enable long cycle life and safe operation of high-energy Na-ion batteries.

Project Impact. Success of this project will provide a solid understanding on the electrolyte/electrode interphase of Na-ion batteries and significantly improve their energy density, cycle life, and safety. It will also accelerate the practical application of Na-ion batteries in both EV and stationary energy storage.

Approach. This project will optimize the electrolyte components and concentrations to develop innovative electrolytes and additives with improved electrochemical and physical properties. Ether-based electrolytes with different salt will be optimized toward both anode (sodium metal and hard carbon) and cathode. Phosphate-based LHCE will be optimized to improve cycling performance of Na-ion batteries. SEI/CEI components of Na-ion battery in ether and phosphate electrolytes will be studied using XPS and SEM/TEM techniques to reveal the fundamental mechanism behind the improved stable performance of Na-ion batteries. Electrolyte additives in carbonate electrolyte will also be investigated to improve the electrochemical cathode performance. These approaches will unravel the origin of the SEI at the dynamic interface, providing guidance for the electrolyte and interface design and enabling high capacity and long life of Na-ion batteries.

Out-Year Goals. This project will select the electrolyte compounds and identify the formation of interfacial SEI layer on hard carbon and CEI layer-on-layer oxide cathode and its effect on the electrode materials. It will also provide guidance on electrolyte optimization and to improve CE of sodium deposition/stripping to be more than 99%.

Collaborations. This project will collaborate with ANL, LBNL, and other leading scientists in the field of cathode and anode materials for Na-ion batteries. It will also collaborate with C. Wang and M. Engelhard of PNNL for TEM and XPS characterization.

Milestones

1. Develop high-capacity carbon anodes in Na-ion batteries with optimized electrolytes. (Q1, FY 2021; Completed)
2. Develop high-voltage electrolytes (≥ 4.2 V) to increase energy density of Na-ion batteries. (Q2, FY 2021; Completed)
3. Characterize CEI/SEI interphase properties in optimized electrolyte to probe the mechanism of high-voltage cycling stability of Na-ion batteries. (Q3, FY 2021)
4. Develop electrolytes that are compatible with conventional polymer separators. (Q4, FY 2021)

Progress Report

To realize high energy density of Na-ion batteries, their electrolytes need to be stable at high voltage so a high-voltage cathode can be fully utilized. Ideally, these electrolytes should also be nonflammable to ensure the safe operation of Na-ion batteries. Last quarter, a nonflammable HCE using TEP as solvent was developed. This electrolyte is compatible with high-voltage cathode $NaNi_{0.68}Co_{0.1}Mn_{0.22}O_2$ (NaNMC). Figure 122a-b shows long-term cycling performance and CE of Na||NaNMC half-cell with HCE electrolyte (NaFSI: TEP = 1: 1.5 in mole ratio). The similar cells with a 1 M $NaPF_6$/PC electrolyte were used as a reference. The cell with HCE electrolyte exhibits excellent CE (near 100%) at a high voltage of 4.2 V. After 500 cycles, these cells still retain 78%, 85%, and 81% capacity at a rate of 0.2 C, 0.33 C, and 0.5 C, respectively. In contrast, the cell with conventional electrolyte retains only ~ 50% in 100 cycles. Its CE also shows significant fluctuation, which indicates an unstable interphase. Figure 122c shows the voltage profiles of these cells in selected cycles. At 0.33 C rate, the initial and 500th cycle discharge capacity were 181.2 and 146.9 mAh g^{-1} for the HCE-based cell compared to 161.9 and 30 mAh g^{-1} for the conventional electrolyte based cell. The superior performance of Na-ion batteries using HCEs could be attributed to the highly stable CEI that prevents further electrolyte oxidation at high potential when in contact with NaNMC electrode.

The performance of the new electrolyte developed in this work is also evaluated in full cells using hard carbon anode coupled with NaNMC cathode and cycled in both HCE and baseline electrolyte. The full cell using HCE electrolyte shows stable performance in 100 cycles, with initial discharge capacity of 183.5 mAh g^{-1} and capacity retention of 86% at 0.2 C compared to 168.8 mAh g^{-1} and 68% capacity retention when baseline electrolyte is used (Figure 123a-b). In addition, the rate capability of full cells using HCE is also much better than that when using baseline electrolyte (Figure 123c). The excellent compatibility between HCE electrolyte versus cathode and anode material will be further studied by advanced characterization tools to have a better understanding on the role of interphase in cycling performance of Na-ion batteries.

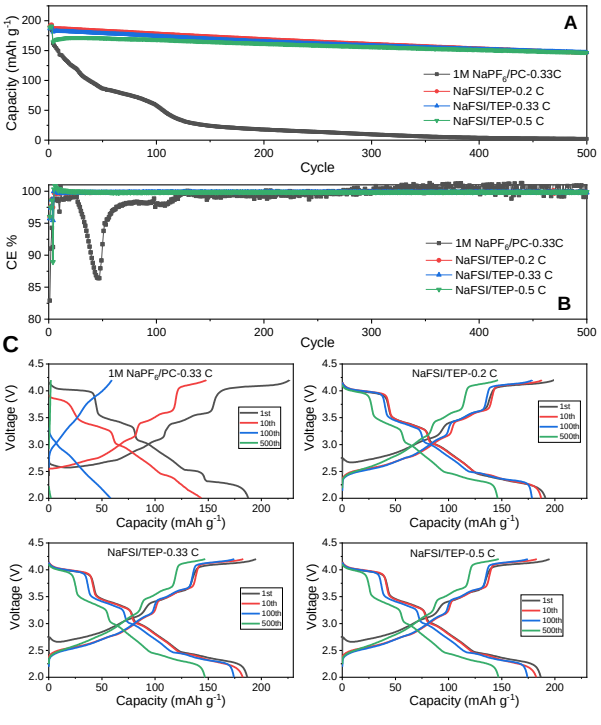

Figure 122. Performance of Na||NaNMC half cells using HCE and baseline electrolyte: (a) cycling capacity, (b) Coulombic efficiency, and (c) voltage profiles.

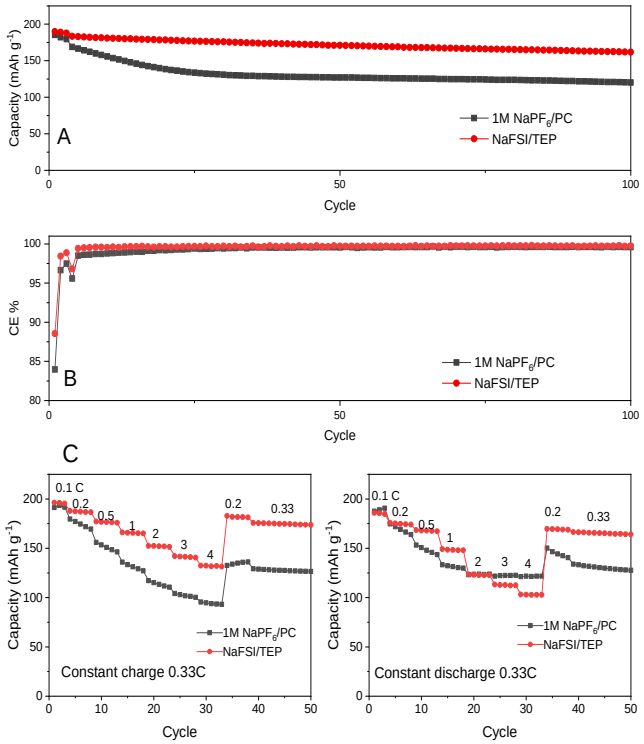

Figure 123. Performance of HC||NaNMC full cell using HCE and baseline electrolyte: (a) cycling stability at 0.2 C, (b) Coulombic efficiency, and (c) rate capability.

Patents/Publications/Presentations

The project has no patents, publications, or presentations to report.

Innovation Center for Battery500
(Jun Liu, Pacific Northwest National Laboratory; Yi Cui, Stanford University)

Project Objective. The project aims to develop commercially viable lithium battery technologies with a cell-level specific energy of 500 Wh/kg through innovative electrode and cell designs that enable the extraction of the maximum capacity from advanced electrode materials. In addition to achieving high specific energy, the project aims to be able to achieve 1,000 cycles for the developed technologies.

Project Impact. The Battery500 Consortium will develop next-generation lithium battery technologies that will significantly increase energy density, improve cycle life, and reduce cost. This will greatly accelerate deployment of EVs and reduce carbon emission associated with fossil fuel consumption. The consortium will utilize first-class expertise and capabilities in battery research in the United States and develop an integrated and multi-disciplinary approach to accelerate development and deployment of advanced electrode materials in commercially viable high-energy batteries. The advances made in this consortium will also benefit the improvement of current Li-ion battery technologies.

Approach. This project will utilize an assortment of national resources located at the national laboratory level and university level. The lithium anode combined with a compatible electrolyte system and two cathodes—one high-Ni $LiNi_xMn_yCo_zO_2$ and another sulfur—will be studied and developed to reach high energy density. The project focus is to design novel electrode and cell architectures to meet the 500 Wh/kg goal. The consortium will work closely with R&D companies, battery/materials manufacturers, and end users / OEMs to ensure that the developed technologies are aligned with industry needs and can be transitioned to production.

Out-Year Goals. This project aims for the following out-year goals. First, fabricate and test a pouch cell capable of 350 Wh/kg and 350 cycles. Second, fabricate and test a pouch cell capable of 400 Wh/kg and 100 cycles.

Collaborations. Collaboration among consortium team members will be well coordinated by the leadership team, which includes the keystone project leads and co-leads along with PIs at all member institutions. Collaboration with the community outside of this consortium and with industry will be facilitated by the executive committee, the advisory board, and the industry committee.

Milestones

1. Benchmark Li-anode architecture with 50-µm lithium anode using protocols for 350 Wh/kg cells, and achieve over 200 cycles in coins. (Q1, FY 2021; Completed)
2. Optimize pressure effect for Li-S from coin cells. (Q2, FY 2021; Completed)
3. Provide new electrolyte formulation for Li-S (PNNL). (Q3, FY 2021; In progress)
4. Demonstrate 350 Wh/kg pouch cell with > 450 cycles; 400 Wh/kg > 100 cycles; and > 450 Wh/kg pouch cell. Demonstrate good cycling of Li-S pouch cell 300 Wh/kg. (Q4, FY 2021; In progress)

Progress Report

Keystone Project 1: Materials and Interfaces

The goal of Keystone 1 is to provide the materials and chemistry support for Keystone projects 2 and 3. The Binghamton team found that niobium substitution can greatly reduce heat evolution and shift the peak to higher temperature for high-Ni NMC. The UT Austin group synthesized four ultrahigh-Ni cathodes with high capacities of > 220 mAh g^{-1} and superior cyclability in LHCE compared to those in carbonate electrolyte. The UW team used sputter coating to coat LATP on Al-doped NMC-811 electrodes and improved their electrochemical performance in terms of cycling performance and polarization. UW also developed a robust 2D model and code for modeling and simulating Li-metal deposition and stripping in real-time. The PNNL group developed a new solvent with low-polysulfide-solubility and good Li-metal stability to improve the overall performance of Li||S cells in terms of cycling stability, CE, and self-discharge.

The Binghamton team used Nb-based coating and substitution to stabilize high-Ni NMC by reducing its reactivity. It is found that a Nb-based coating assists in removing surface impurities, such as Li_2CO_3, and reduces the 1st cycle loss, whereas substitution in the lattice enhances capacity retention. The latter occurs with the substitution of part of the lattice manganese by niobium, formation of a mixed $Li_x[NbMn]O_y$ on the surface. This stabilization of the lattice was demonstrated by a DSC study that showed a remarkably reduced heat evolution from the Nb-treated material, and a shift to higher temperature, as shown in Figure 124. The peak of heat evolution increased from 199.4°C for the untreated NMC-811 to 203.7°C to 204.3°C for surface modified (sintered at 500°C) and bulk substituted (sintered at 700°C), as shown in Figure 124; the associated heat evolution decreased from 204 J/g to 175 J/g to 162 J/g, respectively (Figure 124b). Consistent with this increased stability, cell impedance drops on niobium modification, as shown in Figure 124c.

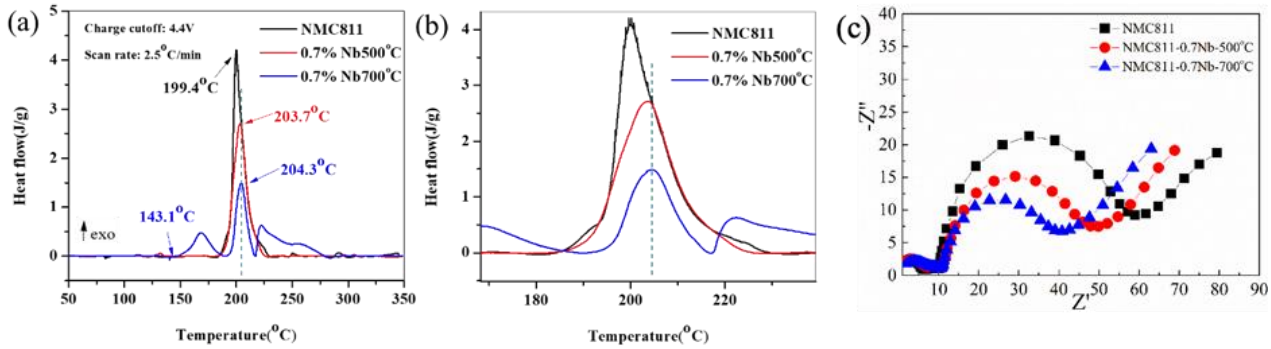

Figure 124. (a-b) Differential scanning calorimetry profiles of NMC-811 and Nb-modified NMC-811 heated at 500°C and 700°C charged to 4.4 V versus Li/Li+, and (c) reduction of impedance of Nb-modified NMC-811.

The Binghamton team also worked with the groups at Stanford and PNNL to determine the electrochemical and thermal stabilities of the advanced next-generation electrolytes, which are much more effective in Li-metal cells compared to carbonate-based electrolytes. In these initial experiments, the electrolytes were pushed to their limits to determine those limits to optimize the testing regimes for future in-depth studies. As shown in Figure 125, all electrolytes are stable up to ~ 4.4 V and up to 60°C. The 1 M LiFSI/FDMB was as stable as the baseline carbonate electrolyte, only showing side reactions at 60°C above 4.4 V. The M47 LHCE showed side reactions at both 45°C and 60°C above 4.5 V, and at 30°C above 4.6 V as expected. Longer term testing is now under way within the stability ranges at 4.4 V and 30°C, which is within the stability limits of these next-generation electrolytes.

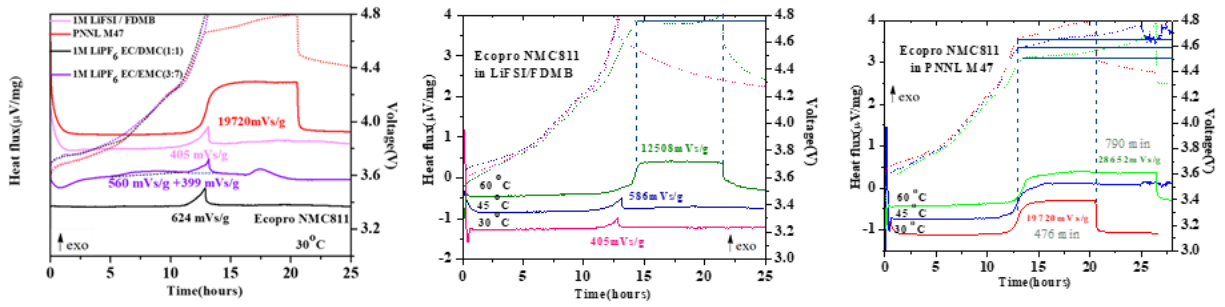

Figure 125. *Operando* differential scanning calorimetry studies comparing the 2020 carbonate electrolyte with the next-generation LiFSI ether-based FDMB and M47 electrolytes.

With an aim to obtain cathodes with specific capacities of > 220 mAh g^{-1} and benchmark with NMC-811 cathodes, the UT Austin team synthesized three high-Ni layered-oxide cathodes [$LiNiO_2$ (LNO), $LiNi_{0.94}Co_{0.06}O_2$ (NC9406), and $LiNi_{0.95}Co_{0.02}Mn_{0.015}Al_{0.01}Mg_{0.005}O_2$ (NCMAM)] and assessed their performances in the 1st and 2nd baseline electrolytes [carbonate electrolyte of LP57 with 2 wt% VC, and LHCE composed of LiFSI-1.2DME-3TTE (by mol)]. The cathodes with and without multiple dopants were synthesized by a coprecipitation of the corresponding hydroxide precursors, followed by calcining with LiOH in a flowing oxygen atmosphere. Figure 126 shows the 5th cycle charge-discharge profiles and cyclabilities of the Li-metal cells in both carbonate electrolyte and LHCE. All three cathodes exhibit high capacities of > 220 mAh g^{-1} with superior cyclability in LHCE compared to that in carbonate electrolyte. The NCMAM cathode was supplied to PNNL to benchmark with NMC-811.

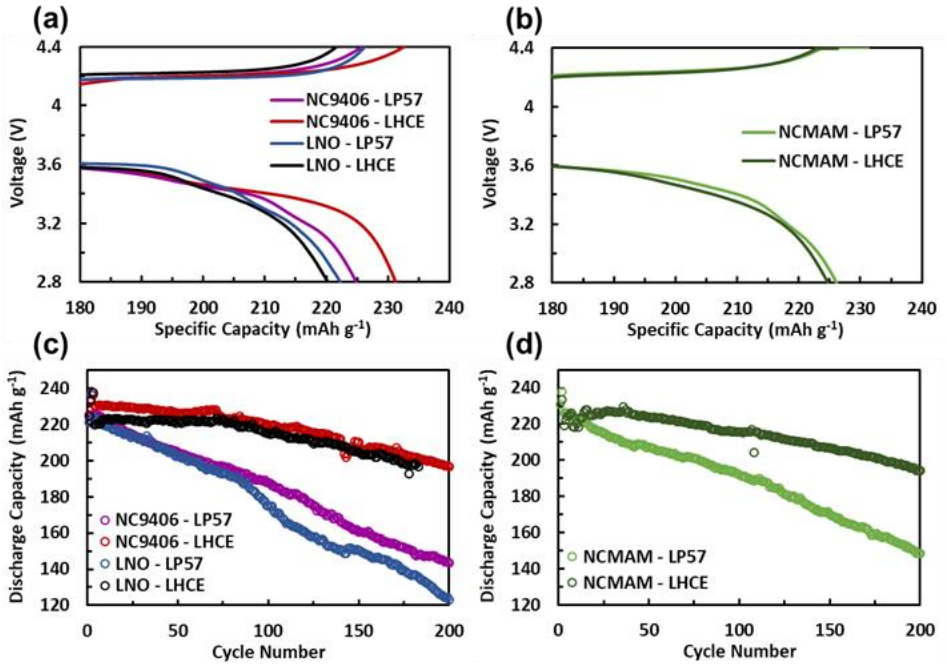

Figure 126. Fifth-cycle charge-discharge curves of (a) NC9406 and LNO and (b) NCMAM, and cycling performances of (c) NC9406 and LNO and of (d) NCMAM in carbonate electrolyte and localized high-concentration electrolyte.

The UT Austin team also synthesized another layered oxide cathode $LiNi_{0.94}Co_{0.04}Zn_{0.02}O_2$ (NCZ) with 94% nickel by directly incorporating zinc during the coprecipitation of the hydroxide precursor. The performance of the NCZ in carbonate electrolyte was compared with that of LiNi0.94Co0.06O2 (NC), as shown in Figure 127. Although zinc doping caused a small reduction in the C/3 capacity by ~ 7 mAh g^{-1} compared to that of NC, it provided a drastic improvement in capacity retention, especially voltage retention, which is attributed largely to a smoother H2 → H3 phase transition and a reduction in particle cracking and surface reactivity.

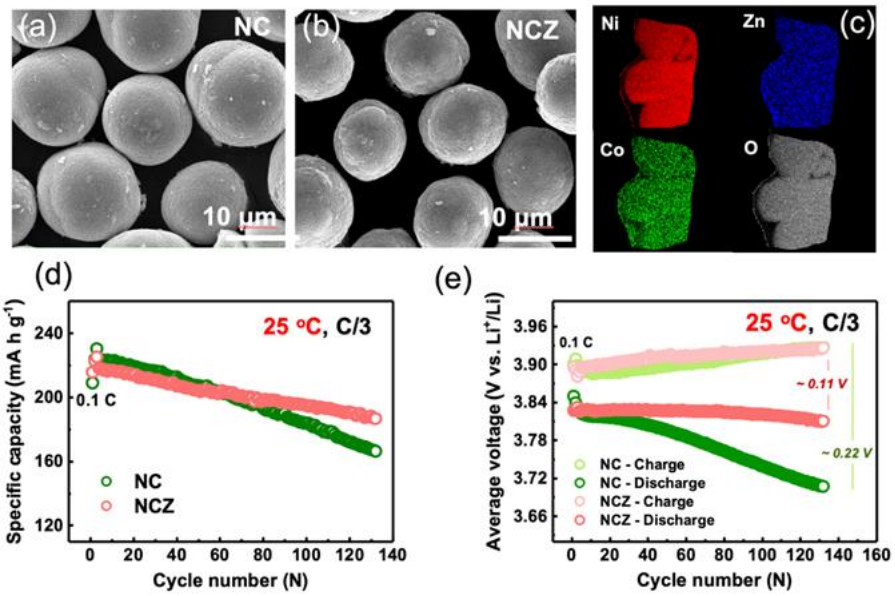

Figure 127. Scanning electron microscopy images of the calcined (a) NC and (b) NCZ samples. (c) Energy dispersive X-ray spectroscopy mapping of the primary particles in NCZ. (d) Cycling performances and (e) average charge/discharge voltages of NC and NCZ cathodes paired with Li-metal anode in coin cells.

The UW team employed the SE LATP as the coating material for Al-NMC-811 cathode by radio-frequency magnetron sputtering approach. The direct coating on the cathode surface effectively reduces the side reaction without disrupting the interparticle electronic/ionic pathways and hence improves electrochemical performance of Al-NMC-811. After sputtering for 8 hours, the grey surface of the Al-NMC-811 turns blue (Figure 128a) and the surface morphology of the Al-NMC811 becomes smoother (Figure 128b-c). These results suggest that a thin film has been smoothly coated on the surface of the Al-NMC-811 electrode. Figure 128d-g exhibits the initial charge–discharge curves at 0.1C (1 C = 1.4 mAh cm^{-2}) between 2.8 V and 4.4 V for Li-metal cells. The LATP-coated Al-NMC-811 shows a similar initial capacity and CE to those of pristine Al-NMC-811 cathode (Figure 128d). After 320 cycles at C/3, the LATP-coated Al-NMC-811 shows higher reversible capacity (163.2 mAh g^{-1}) and capacity retention (81.0%) than those of the pristine Al-NMC-811 (151.8 mAh g^{-1} and 75.3%). Figure 128e-f displays the dQ/dV curves of pristine and LATP-coated Al-NMC-811 electrodes at selected cycles. At the 150th cycle, the voltage hysteresis of pristine Al-NMC-811 in the high-voltage region is 87 mV, larger than that for the LATP-coated Al-NMC-811 (75 mV). At the 250th cycle, the voltage hysteresis of pristine Al-NMC-811 increases by 107 mV, while only a 76-mV increase in hysteresis is found for the LATP-coated Al-NMC-811. This result indicates that LATP direct coating on Al-NMC-811 electrode helps reduce polarization increase and enhances electrochemical performance.

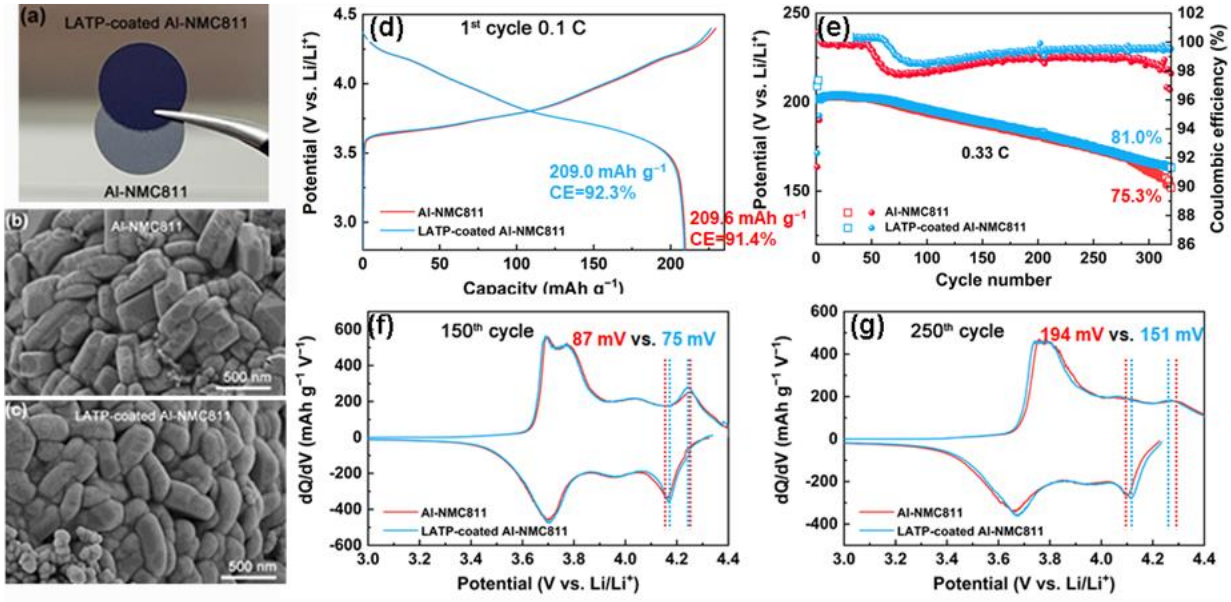

Figure 128. (a) Photo images of Al-NMC-811 and LATP-coated Al-NMC-811 electrodes. Scanning electron microscopy images of (b) Al-NMC-811 and (c) LATP-coated Al-NMC-811 electrodes. (d) Initial charge–discharge curves and (e) cycling performance of pristine and LATP-coated Al-NMC-811 electrodes. The dQ/dV curves of (f) the 150th cycle and (g) the 250th cycle of pristine and LATP-coated Al-NMC-811 electrodes.

The UW and UT Austin groups also developed efficient models and algorithms for 2D lithium deposition growth. A geometry representing the separator region in a Li-metal battery filled with LE was considered, as shown in Figure 129. The governing equations for liquid phase potential and concentration are solved using dilute solution theory coupled with nonlinear kinetics at the metal/liquid interface. The change in the overpotential with time over multiple charge/discharge cycles is shown in Figure 130. Case 1 (100 cycles) corresponds to the base case, and the diffusivity has been reduced by an order of 10 for Case 2 (30 cycles). A significant difference can be observed in the voltage-time curves for the two cases in Figure 130a, where the overpotential shows an increased reduction over cycles. This effect is further substantiated by comparing the moving boundary profiles for the two cases at the end of 30 cycles, as shown in Figure 130b.

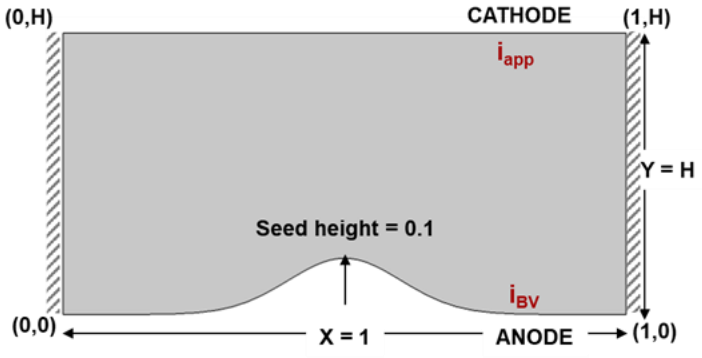

Figure 129. Schematic for model simulation of Li-metal deposition and dissolution at the anode surface. The dimensions are indicated in scaled form.

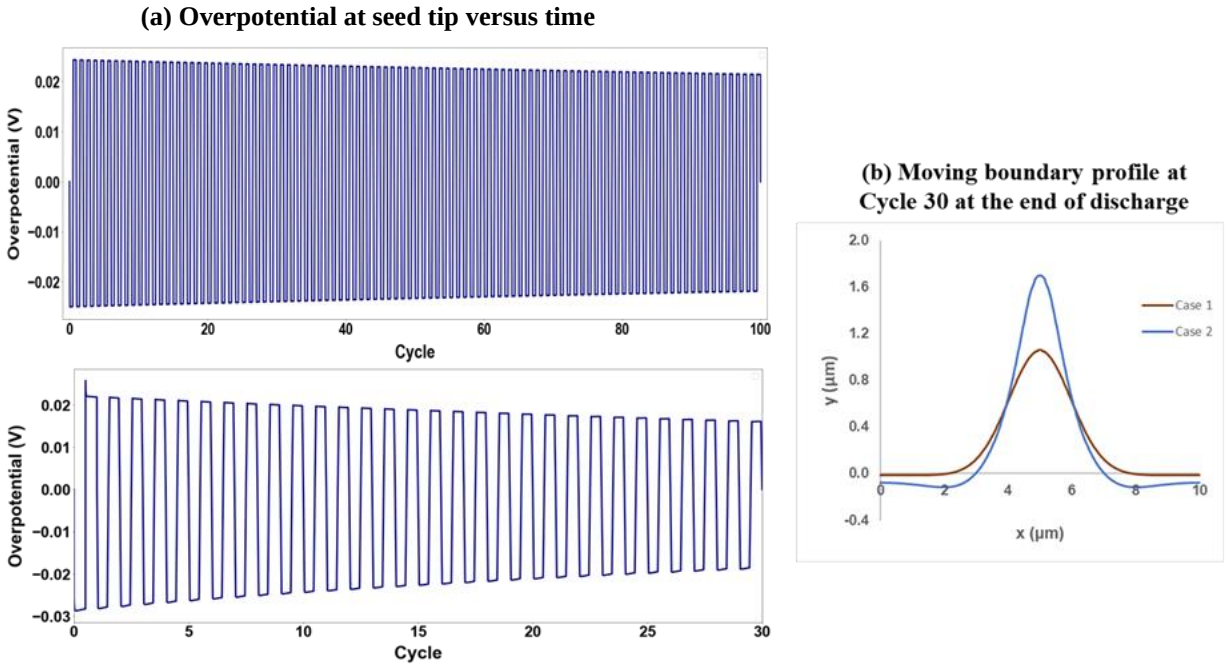

Figure 130. (a) Voltage-time curves for two test cases to study the effect of electrolyte diffusivity. (b) Comparison of the moving interface (solid/liquid interface) at the end of 30 cycles for two test cases.

The PNNL team investigated low-polysulfide-soluble electrolytes (LPSEs) for Li||S batteries. New solvents with low polysulfide solubility and good Li-metal stability were used to improve overall performance of Li||S cells. The electrochemical performances of Li||S cells with different electrolytes are shown in Figure 131. The conventional electrolyte for Li||S batteries, 1 M LiTFSI in DME-DOL + 0.3 M $LiNO_3$, was used as the baseline electrolyte, which shows a relatively stable cycling performance in the Li||S cell, as shown in Figure 131a. However, as shown in Figure 131b, the CE of the cell using this baseline electrolyte is still not bad, where the initial CE of 95% slightly increased to 97%, but then showed a fast CE decay after 40 cycles. LPSE-1 shows poor cycling performance and low CE. By using LPSE-2, although the initial capacity of the Li||S cell is slightly lower than baseline, the capacity retention and CE of the cell is greatly improved compared to the cell using the baseline electrolyte. After 270 cycles, the cell using LPSE-2 still retains 88% capacity, which is much higher than that using baseline electrolyte (~ 72%). The capacity of the cell using LPSE-2 turned higher than that using baseline electrolyte after 200 cycles. In addition, the self-discharge performance was also investigated. The Li||S cells were charged to 2.8 V first, and then rested for 48 hours before discharging. As shown in Figure 131c, the cell with LPSE-2 is almost consistent during the 48-hour resting time, while the cell with the baseline electrolyte shows a continuous voltage decay with time. This indicates that the cell with LPSE-2 is much more stable at the charged state. The cells were then discharged to see how this storage affects capacity. As shown in Figure 131d, the Li||S cell using baseline electrolyte shows 313.9 mAh g^{-1} difference between the charge capacity and the discharge capacity after resting for 48 hours, which means a 39.5% capacity (794.6 mAh g^{-1}) loss during the 48-hour resting time. As for the cell with LPSE-2, the capacity loss is only 12.5% (86.6 mAh g^{-1}). These results clearly demonstrate that the LPSE-2 significantly reduces self-discharge compared to the baseline electrolyte.

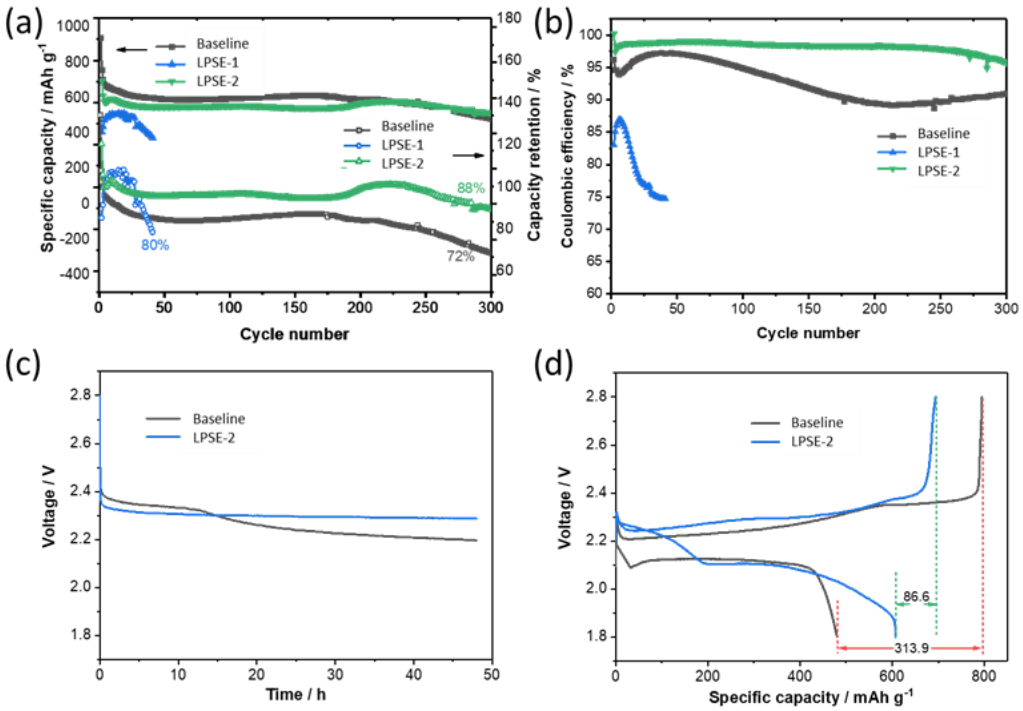

Figure 131. (a) Specific capacity, capacity retention, and (b) Coulombic efficiency of Li||S batteries with different electrolytes. (c) Voltage loss of Li||S batteries during rest period after fully charged to 2.8 V. (d) Charge/discharge profiles of Li||S batteries before and after 48-hour rest period. For cycling test, the cells were cycled in 1.8-2.8 V at C/10 after two formation cycles at C/20. Li||S cells were prepared with a cathode loading of 3.5 mAh cm^{-2} S, 250 µm lithium, and 75 µL electrolyte.

Highlights of Keystone Project 1

The highlights for this quarter are as follows:

- Niobium substitution has been found to remarkably reduce heat evolution and shift the peak to higher temperature range for high-Ni NMC during DSC test, demonstrating great advantage in improving thermal stability. (Binghamton)
- Four ultrahigh-Ni cathodes were synthesized: [$LiNiO_2$ (LNO), $LiNi_{0.94}Co_{0.06}O_2$ (NC9406), $LiNi_{0.95}Co_{0.02}Mn_{0.015}Al_{0.01}Mg_{0.005}O_2$ (NCMAM), and $LiNi_{0.94}Co_{0.04}Zn_{0.02}O_2$ (NCZ). All exhibit high capacities of > 220 mAh g^{-1} with superior cyclability, especially when LHCEs are used. (UT Austin)
- A new electrolyte using solvent with low polysulfide solubility and good Li-metal stability was developed. This new electrolyte demonstrated greatly improved overall performance of Li||S cells in terms of cycling stability, CE, and self-discharge. (PNNL)

Keystone Project 2: Electrode Architecture

The goal of Keystone 2 is to design, model, fabricate, and characterize the effect of electrode architecture on electrode and cell performance in support of reaching the project goal of 500 Wh/kg cell specific energy. Included in this report for Keystone 2 are Li-metal interphase characterization (BNL) and pressure-tailored Li-metal deposition and polymeric sulfur characterization (UCSD). Highlighted results of this quarter are identification and quantification of key components of the Li-metal interphase such as LiH and LiF and using pressure to tailor the Li-metal deposition.

Identification of LiH and Crystalline LiF in the SEI on Li-Metal Anode

In collaboration with the PNNL group, the BNL team applied synchrotron XRD to understand the chemical composition of Li-metal anode interphase. Two particular goals are (1) to resolve the controversy about whether LiH is a significant component in SEI, and (2) to understand why LiF, an ionic insulator in bulk phase, could be a favored SEI component. SEI samples are collected from Li-metal anodes that are cycled in a series of electrolytes using the same salt of LiFSI but different solvents, including propylene carbonate (PC), DMC, and DME. As Figure 132a shows, LiH is detected in all the SEI samples, regardless of the solvents used or the salt concentration employed. The identity of LiH is confirmed based on the fact that this phase has a face-centered-cubic structure with lattice parameter of 4.084 Å (Figure 132b), in full agreement with the literature report about the LiH phase. A larger amount of LiF was detected in the SEI of HCEs, regardless of the solvents used. This is consistent with the current understanding that anion decomposition dominates in HCE, with LiF being the major decomposition products. Interestingly, a detailed fitting of the XRD patterns indicates that the LiF in SEI differs from the bulk LiF in two aspects: the former has a larger lattice parameter and a much smaller grain size (< 3 nm); both of these features are favorable for Li-ion transport. To emphasize this discovery, LiF in SEI is denoted as $LiF_{(SEI)}$ in Figure 132. The unique properties of $LiF_{(SEI)}$ may explain why it is a favored component in Li-metal anode SEI.

Pressure Tailored Li-Metal Deposition

It is qualitatively believed that increased uniaxial stack pressure can help to alleviate Li-dendrite formation and improve CE and cycling performance of Li-metal batteries. Quantitatively understanding the role of stack pressure on lithium nucleation, growth, and dissolution, along with the pressure-morphology-performance relationship, will open new opportunities in efforts to solve problems regarding Li-metal anodes in high-energy Li-metal batteries. The UCSD team used a customized split cell with a load cell (Figure 133a) to precisely control the uniaxial stack pressure applied to the battery during cycling. The pressure was set as the on-set value for the electrochemical performance testing. Figure 133b shows the 1st cycle CE of Li-Cu cells as a function of applied stack pressure under different current densities from 1 mA/cm^2 to 1.5 mA/cm^2 to 2 mA/cm^2, using an ether-based electrolyte. At 0 kPa, the CE was the lowest among all current densities. When the stack pressure slightly increased to ~ 35 kPa, CE increased for all current densities, while the CE at 2 mA/cm^2 jumped to 92%. At 350 kPa, CE was boosted to 98%, 97%, and 96% at 1 mA/cm^2, 1.5 mA/cm^2, and 2 mA/cm^2, respectively. Increasing the stack pressure above 350 kPa did not further improve CE. Figure 133c shows the electrochemically deposited lithium at a high current density of 2 mA/cm^2 after high loading of 4 mAh/cm^2 deposition exhibits metallic silver color.

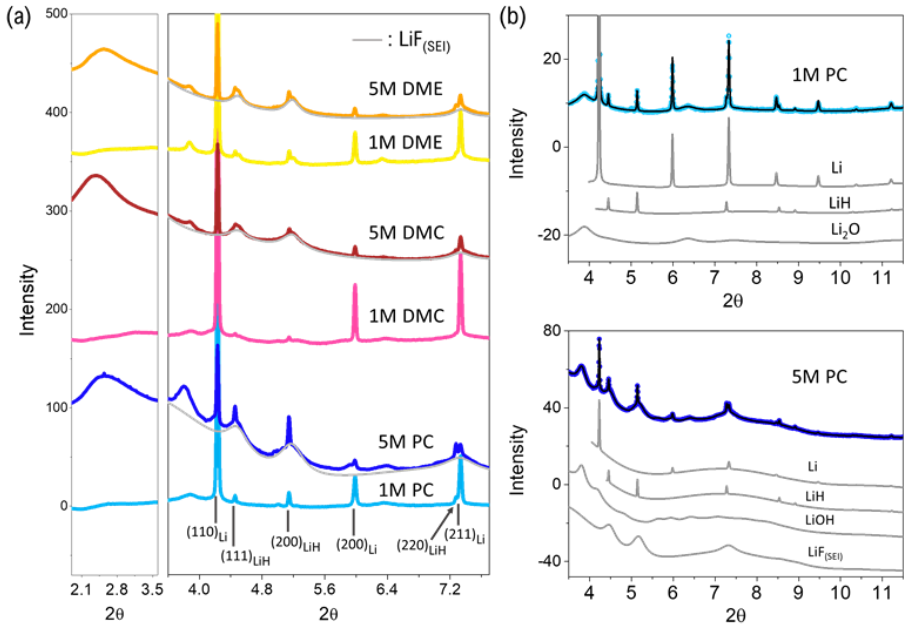

Figure 132. (a) SEI X-ray diffraction (XRD) of low and high concentration electrolytes using LiFSI as salt and PC, DMC, and DME as solvents. The light grey pattern belongs to SEI-LiF (denoted as $LiF_{(SEI)}$). The wavelength used is 0.18323 Å. (b) Rietveld refinement of SEI XRD data of low and high concentration LiFSI in PC. Contributions of individual phase to the XRD pattern are also shown. Open circles, experimental data; black lines, calculated data.

The team then used cryo-FIB-SEM to examine the deposited lithium morphology under four representative pressures: 70 kPa, 140 kPa, 210 kPa, and 350 kPa. A high current density of 2 mA/cm^2 was applied for the one-hour lithium deposition (2 mAh/cm^2) morphological study. The lithium deposits become notably close-packed with increased pressure from 70 kPa to 350 kPa (Figure 133d-g). The cross-section evolution is even more noticeable. As shown in Figure 133h-k, along with the increased stack pressure, the electrode thickness obviously decreased. In particular, the cross-section morphology at 350 kPa (Figure 133k) shows that the lithium deposits form perfect columnar structures with large granular diameter of ~ 4 µm, near-theoretical thickness (9.64 µm, 2 mAh/cm^2) of ~ 10 µm, and minimum electrode-level porosity; this indicates that stack pressure can be used to precisely control the lithium deposition morphology.

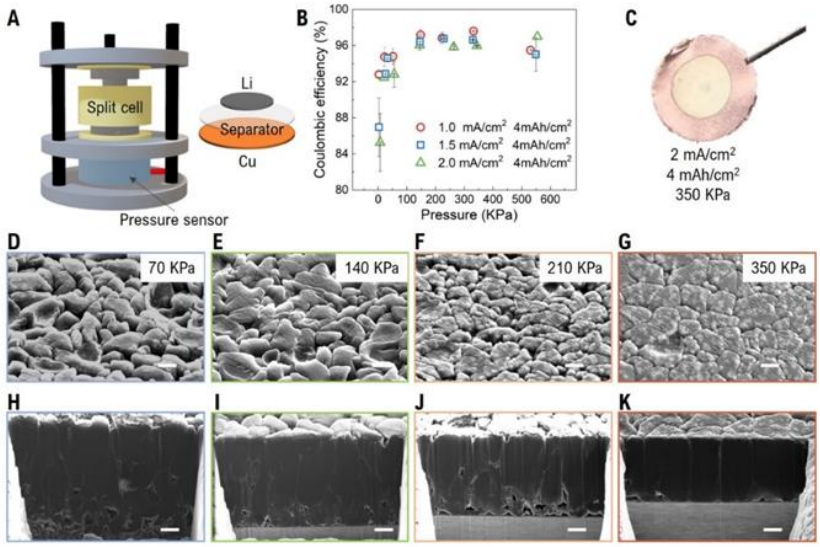

Figure 133. (a) The pressure experiment set-up. (b) Pressure versus Coulombic efficiency under various current densities. (c) Optical image of deposited lithium under high current density (2 mA/cm^2), high loading (4 mAh/cm^2), and optimized pressure conditions (350 kPa). (d-g) Top view and (h-k) cross section of lithium deposited under various pressure at 2 mA/cm^2 for 1 hour. (d/h) 70 kPa, (e/i) 140 kPa, (f/j) 210 kPa, and (g/k) 350 kPa. Scale bar is 2 µm.

STEM Analysis of Sulfurized Polyacrylonitrile (SPAN)

Last quarter, the UCSD team used STEM EDX to see whether long-term cycling would affect the structure and elemental distribution in SPAN particles. It was found that there was no large-scale elemental redistribution in the SPAN cathode after 10 cycles, meaning that sulfur was mostly immobilized in the SPAN particles. This quarter, the team used STEM EELS to probe the bonding environment evolution of nitrogen, sulfur, and carbon in SPAN cathode after 10 cycles.

Carbon K-edge. Figure 134a shows the carbon K-edge of SPAN in pristine state and after 10 cycles. In the pristine state, the carbon K-edge shows two peaks that are associated with 1s to π* and 1s to σ* transitions, which suggests that the carbon is in a sp^2-hybridization state. The carbon K-edge and nitrogen K-edge (Figure 134c) show similar near-edge structures at the pristine state, which indicates that carbon and nitrogen are in similar electronic environment and form an aromatic ring structure, which is consistent with existing literature. After discharge and charge, the most noticeable change happens in the relative peak intensity of the π* bonding peak. The ratio changed from 0.9135 at pristine state to 0.6828 after 10^{th} cycle at discharge, and then decreased even further to 0.6101 at charge state. This peak intensity change shows that there is some degree of irreversibility in the carbon bonding environment during cycling after the 10 cycles.

Sulfur L-edge. At the sulfur L-edge in Figure 134b, the peaks at 165.7 eV and 228.7 eV corresponding to the sulfur $L_{2,3}$ edge and sulfur L_1 edge confirm the presence of sulfur in the pristine SPAN. There is no clear change in the sulfur L-edge after discharge and charge. Although the low signal-to-noise ratio in spectrums of the cycled sample made it hard to decipher, the sulfur $L_{2,3}$ and sulfur L_1 edge can still be found after 10 cycles, which shows possible high reversibility of sulfur in SPAN.

Nitrogen K-edge. Figure 134c shows the nitrogen K-edge at three different states. In the pristine state, two peaks that are associated to 1s to π* and 1s to σ* transitions are seen, which suggests that nitrogen also exists in mostly the sp^2-hybridization state, which is same as the carbon. The most interesting finding is in the nitrogen K-edge after cycling. After discharge, the nitrogen K-edge shows a decrease in the σ* peak intensity compared to the π* peak. This change potentially indicates that nitrogen is actively participating in the electrochemical reaction between lithium and SPAN, which is not generally discussed in existing literature. After charging, the σ* peak was recovered to a higher intensity. The reversibility of the σ* peak intensity in nitrogen K-edge suggests that nitrogen plays an active reversible role in the electrochemical reaction. More characterization and analysis such as FTIR and XPS are in progress to further decipher the reaction mechanism between lithium and SPAN.

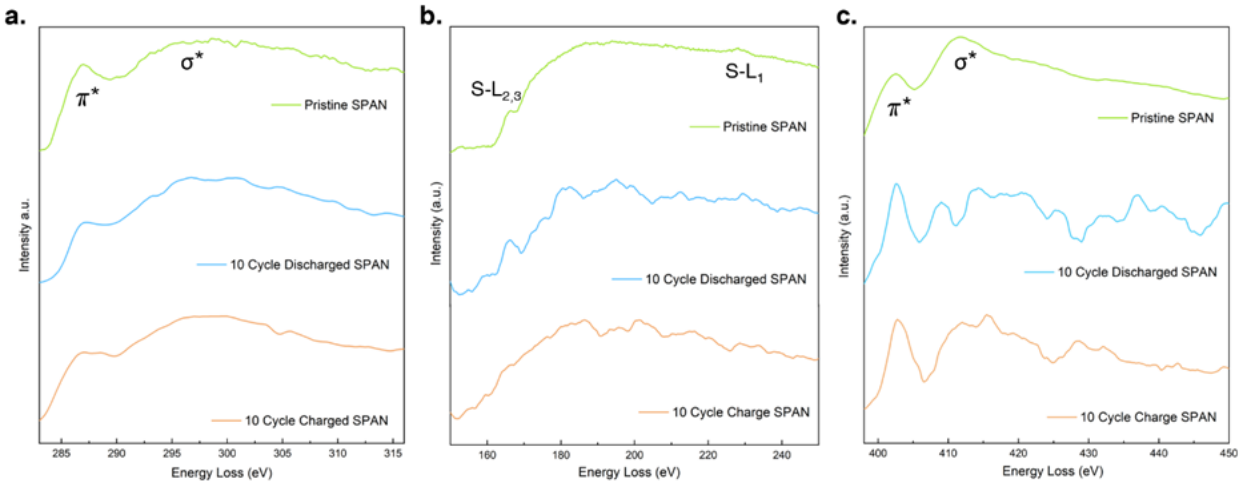

Figure 134. Scanning transmission electron microscopy – electron energy loss spectrum of (a) carbon K-edge; (b) sulfur L-edge; and (c) nitrogen K-edge; in pristine, 10 cycle discharged, and 10 cycle charged sulfurized polyacrylonitrile.

Highlights of Keystone Project 2

The highlights for this quarter are as follows:

- LiH was identified as a significant component, and nano-crystalline LiF with smaller lattice parameter was discovered and named LiF_{SEI} in SEI on Li-metal anode (BNL). This LiF_{SEI} may hold the key to answer the question about why LiF is a critically important component of SEI. Results were published in *Nature Nanotechnologies* in 2021.
- Quantitative studies of pressure-morphology-performance relationship were carried out to understand the role of stack pressure on lithium nucleation, growth, and dissolution (UCSD). It was found that at 350 kPa, CE was boosted to 98%, 97%, and 96% at 1 mA/cm^2, 1.5 mA/cm^2, and 2 mA/cm^2, respectively. This study may open new opportunities in the efforts to solve problems regarding Li-metal anodes.

Keystone Project 3: Cell Fabrication, Testing, and Diagnosis

This quarter, activities in Keystone 3 focused on understanding the impact of early cycling conditions on cycling life (Idaho National Laboratory, INL), the role of different porous host designs on lithium plating (INL), and on enhancing modeling tools for Li-S batteries (UW / UT Austin). It was observed that the cycling performance of Li||NMC-811 cells, operating at 25°C during aging, varied when the temperature during formation cycles was changed from 10°C, to 25°C, and to 45°C. It is suspected that the external temperature can be utilized to alter the composition and structure of early-formed SEI during the formation cycles. Three electrolytes were used, as shown in Figure 135a, each with different formation cycle temperature as the superior performer. With a carbonate-based electrolyte (1.6 M $LiPF_6$ in 3:7 wt% EC:EMC + 10 wt% VC), high-temperature (45°C) formation cycles benefit extended cycling before rapid capacity fade, maintaining over 175 mAh/g for 58 cycles. However, HCE (4 M LiFSI in DME) operated best when low temperature (10°C) was

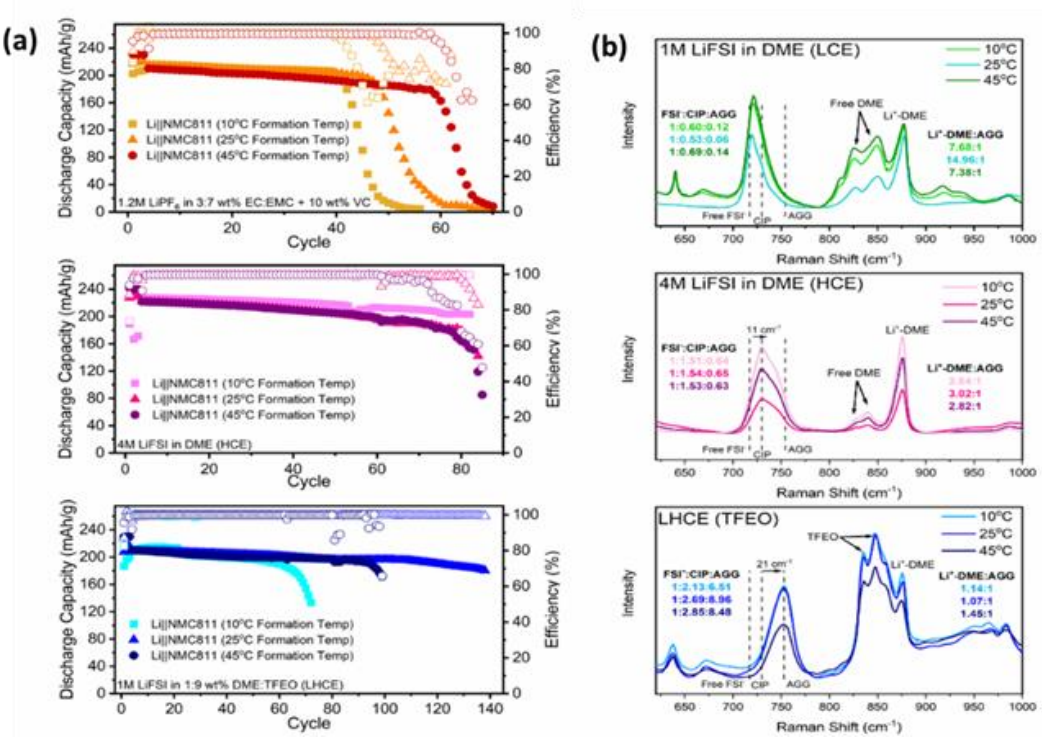

Figure 135. (a) Cycling performances of Li||NMC-811 cells for different electrolytes, operating at 25°C during aging, varied when the temperature during formation cycles was changed from 10°C to 25°C to 45°C. (b) Raman spectra of ether-based electrolytes (LCE, HCE, and LHCE) at different temperatures.

used for formation cycles, maintaining over 200 mAh/g for over 80 cycles. LHCE (1:1.2:2 mol% LiFSI:DME:TFEO) performed best in the middle temperature (25°C), maintaining over 180 mAh/g for over 135 cycles with CE above 99%. Capacity during the formation cycles was lower for 10°C cells, followed by 25°C and 45°C, respectively, among all the electrolytes. It appears that the difference in performance during aging cycles is based on the composition and morphology of the SEI and is not dependent on cycling behavior during those formation cycles. Raman spectra of ether-based electrolytes were observed at different temperatures (Figure 135b). It was seen that as the concentration of LiFSI in DME was increased, the amount of contact-ion pairs (CIPs, single Li^+-FSI^- coordination) and aggregate clusters (AGGs, multiple Li^+ coordinating to one FSI^-) increased, evidenced by an 11-cm^{-1} blue shift. At the low concentration (LCE, 1 M LiFSI in DME), solvent separated ion pairs (SSIPs, free FSI^-) are much more prevalent. When the TFEO diluent is incorporated to produce the LHCE, an even greater blue shift is seen (22 cm^{-1} from HCE peak), thus showing that AGG concentration is much higher. Comparing Li^+ coordination with the FSI^- anion (CIPs and AGGs) and coordination with the solvent (Li^+-DME), shifts in increased aggregates for HCE and LHCE also demonstrated reduced coordination between Li^+ and DME. Therefore, the utility of the LHCE electrolyte is shown to make a salt-derived SEI more viable than in LCE or even HCE. Looking at differences in Raman spectra as a function of temperature for both HCE and LHCE, there is a direct correlation between AGG concentration and cell performance, where less Li^+-DME coordination and an increase in AGG presence led to longer cycle life. For HCE, the amount of solvent coordination was reduced at 10°C, while it was reduced at 25°C for LHCE.

Effects of Pore Size Distribution on Li-Metal Plating into a Scalable 3D Host

The UCSD group has recently developed a scalable 3D host for Li-metal anode and investigated how the pore size distribution inside the host influences lithium plating. The 3D host is fabricated by coating a slurry of well-mixed $RbNO_3$, conductive carbon, and PVDF on a copper foil. After optimizing the fabrication process, the porosity of the 3D host is > 80%, and the Li/3D host composite anode achieves high specific capacity of > 2000 mAh/g. Moreover, it is found that the pore sizes and their distribution are tunable by controlling the ratio between different conductive carbons in the host. In this regard, pure Super P (a carbon black), 50 wt% Super P with 50 wt% VGCF, and pure VGCF hosts were made to examine the lithium deposition behavior in these hosts. As shown in Figure 136a-c, the VGCF host possesses larger pores than the Super P host. The inset figures display pore size distribution of each host obtained by image analysis of SEM results. Pore sizes of pure Super P, Super P + VGCF, and pure VGCF hosts are less than 1 µm, 1-2 µm, and 2-5 µm, respectively. The cross-sectional images confirm that those host thicknesses are all ~ 32 µm, as shown in Figure 136d-f. These hosts were paired with lithium metal to perform a lithium plating study in 1 M LiFSI EC/DMC electrolyte. In the case of the Super P host (Figure 136g),

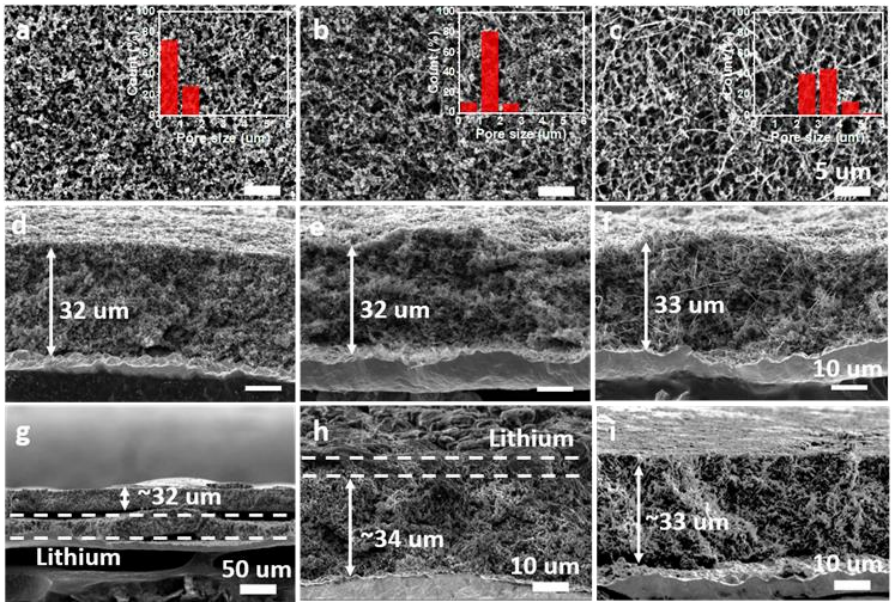

Figure 136. Effects of pore size distribution on lithium plating in 3D lithium host. Scanning electron microscopy images of (a/d/g) Super P (a carbon black) based high porosity host, (b/e/h) Super P + vapor grown carbon fiber (VGCF) based high porosity host, and (c/f/i) VGCF based high porosity host, respectively. Embedded images are the corresponding pore size distribution of each host. (a-c) and (d-f) are the top view and the cross-sectional view images of the hosts, respectively. (g-i) are the cross-sectional view images of the hosts after lithium plating at a current density of 1 mA cm^{-2} in 1 M LiFSI EC/DMC electrolyte.

after plating 5 mAh/cm^2 of lithium at 1 mA/cm^2, a layer of lithium was plated underneath the host instead of growing into it. The thickness of the lithium layer is ~ 30 µm, indicating that little or no lithium goes into the host. On the contrary, there is a ~ 6-µm lithium layer on the top of the Super P + VGCF host after plating 5 mAh/cm^2 of lithium, suggesting most of the lithium grows into the host (Figure 136h). The pure VGCF host is the best among the three hosts, Figure 136i shows that all of the 5 mAh/cm^2 of lithium is deposited into the host. In addition, the thickness of the electrode remains unchanged at 33 µm. The pure VGCF host with pore sizes ranging from 2 µm to 5 µm was selected for further electrochemical performance tests.

Coulombic Efficiency and Full Cell Performance of the 3D Host

Figure 137a-b systematically compares CE of copper foil and 3D_VGCF host at various current densities in 2 M LiFSI DME/BTFE electrolyte, a LCHE with high CE. Figure 137a exhibits the CE at 1 mA/cm^2 for 1 mAh/cm^2. Under this condition, the copper foil and 3D_VGCF host show good stability for 605 cycles and 860 cycles, respectively. In addition to the longer cycle life, the 3D_VGCF host delivers a high average CE of 99.36%. The benefits of 3D_VGCF host become more evident than the copper foil under more demanding testing conditions. As shown in Figure 137b, the cell using a copper foil lasts only 116 cycles at 3 mA/cm^2, while the 3D_VGCF host boosts cell life to > 180 cycles. Even at 3 mA/cm^2, the 3D_VGCF host possesses a high average CE of 99.2%. The 3D_VGCF host is further evaluated in the full cell with the NCM-811 cathode. The areal capacity of the cathode is 3.5 mAh/cm^2. There is only 1.5 mAh/cm^2 of lithium on the anode side, which corresponds to 0.4-fold excess of lithium. The cells are charged at C/5 and discharged at C/3 between 2.8 V and 4.3 V. Figure 137c-d presents cycling performance and voltage profiles of the full cells. The 3D_VGCF host cell shows much higher CE and better capacity retention than the copper cell. The copper cell exhibits an average CE of 98.4% for 120 cycles, which leads to low capacity retention of 23.1% at the 120th cycle. The 3D_VGCF host cell maintains 57.0% capacity at its 120th cycle with an average CE of 99.2%.

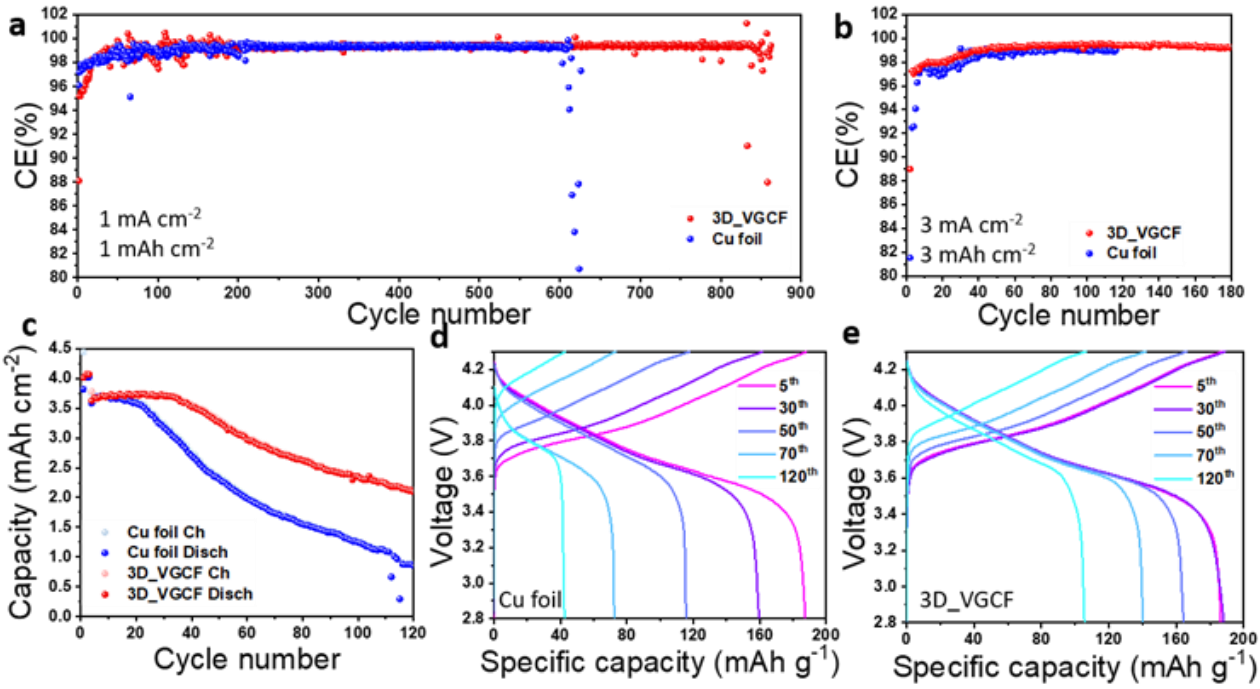

Figure 137. (a) The half-cell tests of 3D_VGCF host and copper foil at a current density of 1 mA cm^{-2} for 1 mAh cm^{-2}. (b) The half-cell tests of 3D_VGCF host and copper foil at a current density of 3 mA cm^{-2} for 3 mAh cm^{-2}. (c) The full-cell tests of 3D_VGCF host and copper foil with NCM-811 as cathode charged at C/5 and discharged at C/3, np ratio is 0.4. (d-e) Voltage profiles of Cu||NCM-811 and 3D_VGCF host || NCM-811 cells, respectively. The voltage range is 2.8−4.3 V.

This work provides a facile and scalable method to fabricate high-capacity 3D electrodes for dendrite-free, high-CE Li-metal anodes. The electrode is readily fabricated by slurry casting from readily available materials; use of carbon materials with different shapes and sizes offers controls of the pore size and location of lithium

deposition. A uniform pore size on the order of micrometers is highly beneficial for dimensionally stable, high-capacity 3D anodes.

Lithium Sulfur Modeling Work

Physics-Based Impedance Model for Lithium Sulfur

Continuum physics-based models for lithium sulfur systems are able to simulate voltage-time discharge curves during discharge with good agreement with experiments. However, these models do not exhibit macro-reversibility and are unable to reproduce charging curves from fundamentally derived equations. The team aims to explore micro-reversibility of existing models using impedance by investigating if the governing equations are valid for small changes in SOC in both directions during a small sinusoidal perturbation for an EIS experiment. Being able to successfully simulate an EIS measurement will also help them with parameter identification for the models, as EIS separates the timescale of different physical processes (that is, transport, ohmic, kinetic, etc.) compared to a typical slower timescale of a battery discharge (order of an hour). Also, since EIS is sensitive to a wide range of timescales of physical processes, it can be used as a distinguishing metric for experiments that are carried out to modify certain physical processes, for example, an additive to improve conductivity or a coating to slow down the kinetics of deleterious side reactions.

Model Development

Using the governing equations for a Li-S cell proposed in the work by Kumaresan et al.,[1] the team transformed them to the frequency domain by writing all variables as the sum of a steady-state DC component and a small perturbation term. They perform a Taylor expansion on all nonlinear expressions and gather all first-order terms in the governing equations for linear impedance. The system being modeled consists of the sulfur cathode and separator. The anode is modeled as a sheet of lithium foil that is fully protected and supplies lithium ions. Li_2S is the only solid product. A double layer capacitance charging term is also added at the SEI in the overall current balance equation.

The impedance model takes the mean steady-state concentrations, porosities, and potentials as inputs to simulate EIS spectra at different SOCs. To obtain these values to simulate EIS that is carried out at a truly equilibrated state, the team also developed an equilibrium model with no time-evolution aspect. This equilibrium model describes only the thermodynamics of the system, and the governing equations are simply the Nernst equations for each of the reduction reactions, overall charge balance, sulfur balance, electroneutrality, and ionic product expressions for solubility of solid S_8 and Li_2S. Development of this equilibrium model allows the team to understand the thermodynamics of the system, which they will continue to explore in greater depth.

Initial Results

The team has initial results of EIS spectra (Figure 138) at various SOCs based on parameters published by Kamyab et al.[2] They observe the relatively larger impedance at the start and end of discharge where solid S_8 and Li_2S are insulating. The charge transfer resistance in the 80% SOC region is small (small semicircle), where solid S_8 is dissolving and quickly reducing to lower-order polysulfides.

The next step is to conduct a convergence study, validation, and parameter sensitivity analysis to fully understand and explain the impedance behavior.

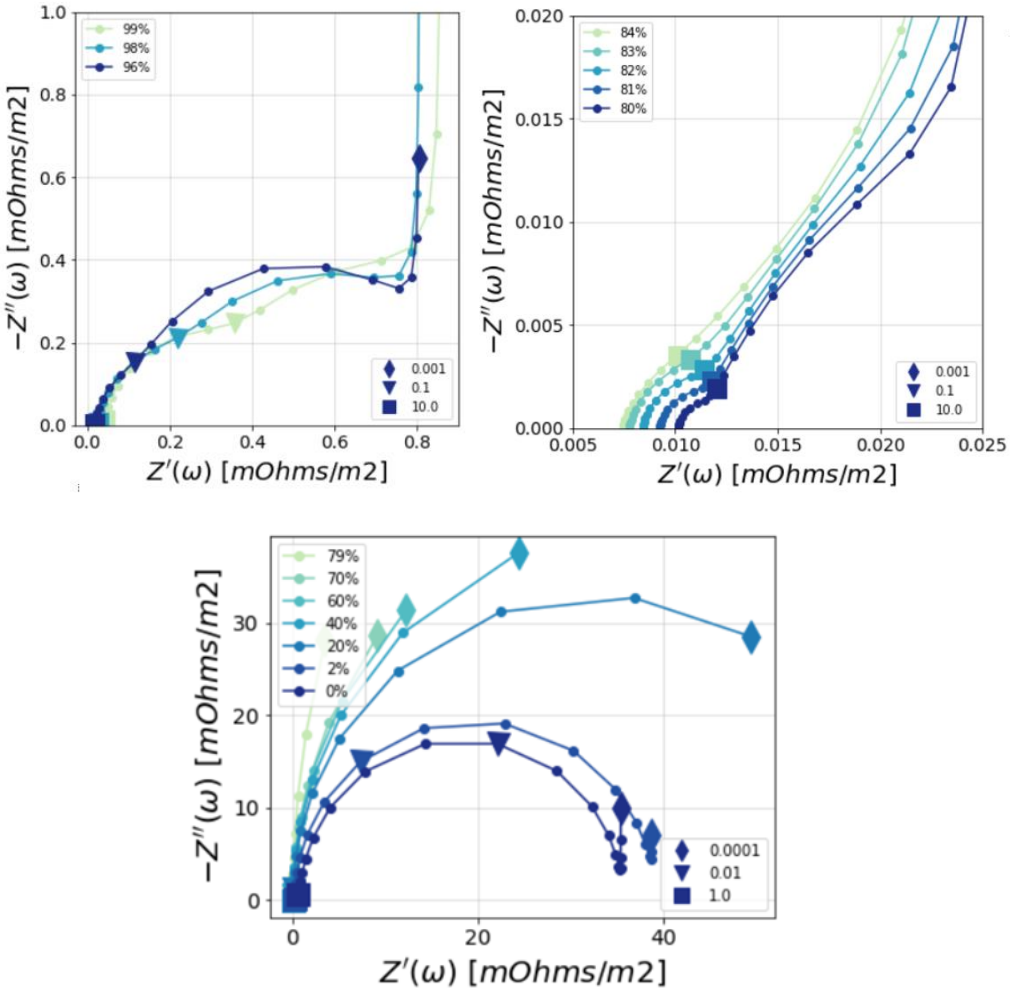

Figure 138. Predicted impedance spectra of Li-S batteries at different states of charge based on parameters published in the literature.

References

[1] Kumaresan, K., Y. Mikhaylik, and R. E. White. *Journal of the Electrochemical Society* 155 (2008): A576.

[2] Kamyab, N., P. T. Coman, S. K. Madi Reddy, S. Santhanagopalan, and R. E. White. *Journal of the Electrochemical Society* 167 (2020): 130532.

Highlights of Keystone Project 3

The highlights for this quarter are as follows:

- Discovery of a direct correlation between AGG concentration and cell performance, where less Li^+-DME coordination and an increase in AGG presence when LHCE was used led to longer cycle life. (INL)
- Developed and characterized performance of 3D lithium host materials that can achieve 2000 mAh/g specific capacity using a slurry making process. (UCSD)
- Developed initial models to predict EIS spectra for Li-S cells. (UW / UT Austin)

Patents/Publications/Presentations

Award

- Z. Bao has been selected by the Material Research Society (MRS) for their Mid-Career Award, "For pioneering contributions and conceptual developments to organic electronics and skin-inspired electronics." The award will be presented in the upcoming Spring MRS meeting on April 19th.

Patent

- Provisional patent filed on niobium oxide treatment of NMC materials. Filed by University of Binghamton.

Publications

- Xin, F., H. Zhou, Y. Zong, M. Zuba, Y. Chen, N. A. Chernova, J. Bai, B. Pei, A. Goel, J. Rana, F. Wang, K. An, L. F. J. Piper, G. Zhou, and M. S. Whittingham. "What is the Role of Nb in Nickel-Rich Layered Oxide Cathodes for Lithium-Ion Batteries?" *ACS Energy Letters* 6 (2021): 1377–1382. doi: 10.1021/acsenergylett.1c00190; Publication Date (Web): March 18, 2021.
- Whittingham, M. S. "Solid-State Ionics: The key to the Discovery and Domination of Lithium Batteries: Some Learnings from β-Alumina and Titanium Disulfide." *MRS Bulletin* 6 (2021): 168–173. doi: 10.1557/s43577-021-00034-2; Publication Date (Web): February 12, 2021.
- Hu, J., Q. Wang, B. Wu, S. Tan, Z. Shadike, Y. Bi, M. S. Whittingham, J. Xiao, X-Q. Yang, and E. Hu. "Fundamental Linkage Between Structure, Electrochemical Properties, and Chemical Compositions of $LiNi_{1-x-y}Mn_xCo_yO_2$ Cathode Materials." *ACS Applied Materials & Interfaces* 13 (2021): 2622–2629. doi: 10.1021/acsami.0c18942; Publication Date (Web): January 7, 2021.
- Liu, Y., X. Wu, C. Niu, W. Xu, X. Cao, J-G. Zhang, X. Jiang, J. Xiao, J. Yang, M. S. Whittingham, and J. Liu.* "Systematic Evaluation of Carbon Hosts for High-Energy Rechargeable Lithium-Metal Batteries." *ACS Energy Letters* 6 (2021): 1550–1559. doi: 10.1021/acsenergylett.1c00186; Publication Date (Web): March 29, 2021.
- Shadike, Z., H. Lee, O. Borodin, X. Cao, X. Fan, X. Wang, R. Lin, S-M. Bak, S. Ghose, K. Xu, C. Wang, J. Liu, J. Xiao,* X-Q. Yang,* and E. Hu.* "Identification of LiH and Nanocrystalline LiF in the Solid–Electrolyte Interphase of Lithium Metal Anodes." *Nature Nanotechnology* (2021). doi: 10.1038/s41565-020-00845-5; Publication Date (Web): January 28, 2021.
- Cao, X., P. Gao, X. Ren, L. Zou, M. H. Engelhard, B. E. Matthews, J. Hu, C. Niu, D. Liu, B. W. Arey, C. Wang, J. Xiao, J. Liu, W. Xu,* and J-G. Zhang.* "Designing Rules of Diluents in Localized High-Concentration Electrolytes for High-Voltage Lithium Metal Batteries." *Proceedings of the National Academy of Sciences of the United States of America* 118, No. 9 (2021): e2020357118. doi: 10.1073/pnas.2020357118; Publication Date (Web): March 2, 2021.
- Kim, J-M., X. Zhang, J-G. Zhang, A. Manthiram, Y. S. Meng, and W. Xu.* "A Review on the Stability and Surface Modification of Layered Transition-Metal Oxide Cathodes." *Materials Today* (2021): 138203. doi: 10.1016/j.mattod.2020.12.017; Publication Date (Web): February 27, 2021.
- Zhang, X., L. Zou, Z. Cui, H. Jia, M. H. Engelhard, B. E. Matthews, X. Cao, Q. Xie, C. Wang, A. Manthiram, J-G. Zhang, and W. Xu.* "Stabilizing Ultrahigh-Nickel Layered Oxide Cathodes for High-Voltage Lithium Metal Batteries." *Materials Today* (2021). doi: 10.1016/j.mattod.2021.01.013; Publication Date (Web): February 27, 2021.
- Cao, X., H. Jia, W. Xu, and J-G. Zhang.* "Localized High-Concentration Electrolytes for Lithium Batteries." *Journal of the Electrochemical Society* 168, No. 1 (2021): 010522. doi: 10.1149/1945-7111/abd60e; Publication Date (Web): January 14, 2021.

- Langdon, J., and A. Manthiram. "A Perspective on Single-Crystal Layered Oxide Cathodes for Lithium-Ion Batteries." *Energy Storage Materials* 37 (2021): 143-160. doi: 10.1016/j.ensm.2021.02.003; Publication Date (Web): February 4, 2021.
- Langdon, J., and A. Manthiram. "Crossover Effects in Batteries with High-Nickel Cathodes and Lithium-Metal Anodes." *Advanced Functional Materials* (2021): 2010267. doi: 10.1002/adfm.202010267; Publication Date (Web): February 17, 2021.
- Cui, Z., Q. Xie, and A. Manthiram. "Zinc-Doped High-Nickel, Low-Cobalt Layered Oxide Cathodes for High-Energy-Density Lithium-Ion Batteries." *Applied Materials and Interface* 13 (2021): 15324–15332. doi: 10.1021/acsami.1c01824; Publication Date (Web): March 24, 2021.
- Parke, C. D., A. Subramaniam, V. R. Subramanian,* and D. T. Schwartz. "Realigning the Chemistry and Parameterization of Lithium-Sulfur Battery Models to Accommodate Emerging Experimental Evidence and Cell Configurations." *ChemElectroChem* 8, No. 6 (2021): 1098–1106. doi: 10.1002/celc.202001575; Publication Date (Web): February 26, 2021.
- Teo, L., V. R. Subramanian,* and D. T. Schwartz. "Dynamic Electrochemical Impedance Spectroscopy of Lithium-ion Batteries: Revealing Underlying Physics through Efficient Joint Time-Frequency Modeling." *Journal of The Electrochemical Society* 168, No. 1 (2021): 010526. doi: 10.1149/1945-7111/abda04; Publication Date (Web): January 18, 2021.
- Mattei, G. S., Z. Li, A. A. Corrao, C. Niu, Y. Zhang, B. Liaw, C. C. Dickerson, J. Xiao, E. J. Dufek, and P. G. Khalifah. "High-Energy Lateral Mapping (HELM) Studies of Inhomogeneity and Failure Mechanisms in NMC-622/Li Pouch Cells." *Chemistry of Materials* (2021). doi: 10.1021/acs.chemmater.0c04537; Publication Date (Web): February 21, 2021.
- Zhang, Y., R. Nguyen, and B. Liaw. "Status and Gaps in Li-ion Battery Supply Chain: Importance of Quantitative Failure Analysis." *Proceedings of the IEEE*, Special Issue on Electric and Hybrid Vehicles (Invited). doi: 10.1109/JPROC.2020.3047880; Publication Date (Web): January 21, 2021.
- Holoubek, J., H. Liu, Z. Wu, Y. Yin, X. Xing, G. Cai, S. Yu, H. Zhou, T. A. Pascal, Z. Chen, and P. Liu. "Tailoring Electrolyte Solvation for Li Metal Batteries Cycled at Ultra-Low Temperature." *Nature Energy* 6 (2021): 303–313. doi: 10.1038/s41560-021-00783-z; Publication Date (Web): February 25, 2021.
- Boyle, D. T., W. Huang, H. Wang, Y. Li, H. Chen, Z. Yu, W. Zhang, Z. Bao, and Y. Cui. "Corrosion of Lithium Metal Anodes during Calendar Ageing and its Microscopic Origins." *Nature Energy* (2021). doi: 10.1038/s41560-021-00787-9; Publication Date (Web): March 22, 2021.
- Wang, H., W. Huang, Z. Yu, W. Huang, R. Xu, Z. Zhang, Z. Bao,* and Y. Cui.* "Efficient Lithium Metal Cycling over a Wide Range of Pressures from an Anion-Derived Solid-Electrolyte Interphase Framework." *ACS Energy Letters* 6 (2021): 816–825. doi: 10.1021/acsenergylett.0c02533; Publication Date (Web): February 3, 2021.

Presentations

- Global Young Scientists Summit, Singapore (January 13, 2021): "The Origins of the Lithium Battery and Future Challenges/Opportunities"; M. S. Whittingham.
- Clarkson University, ECS Student Chapter / Department of Chemistry and Biomolecular Science, Virtual Seminar (January 29, 2021): "The Lithium Battery: From a Dream to Domination of Energy Storage"; M. S. Whittingham.
- Paul Scherrer Institut Swiss Battery Days, Switzerland (February 16, 2021): "The Lithium Battery: From a Dream to Readiness to Take on Climate Change—Opportunities and Challenges"; M. S. Whittingham.
- Chey Institute, Seoul (February 18, 2021): "The Lithium Battery: From a Dream to Readiness to Take on Climate Change—Opportunities and Challenges"; M. S. Whittingham.

- North Carolina State University (February 19, 2021): "The Lithium Battery: From a Dream to Readiness to Take on Climate Change—Opportunities and Challenges"; M. S. Whittingham.
- ANL 75th Anniversary: Energy Storage for a Changing World, Director's Lecture (February 23, 2021): "Li-Ion Batteries: From an Idea to Readiness to Take on Climate Change—Opportunities and Challenges"; M. S. Whittingham.
- Brazilian Chemical Society (February 24, 2021): "The Lithium Battery: From a Dream to Domination of Energy Storage"; M. S. Whittingham.
- Netherlands Student Meeting, Utrecht (March 4, 2021): "The Lithium Battery: From a Dream to Domination of Energy Storage"; M. S. Whittingham.
- Forum on Clean Energy, Hong Kong (March 10, 2021): "Li-Ion Batteries: From an Idea to Readiness to Take on Climate Change—Opportunities and Challenges"; M. S. Whittingham.
- Commonwealth Scientific and Industrial Research Organisation, Sir Jerry Price Lecture, Melbourne, Australia (March 10, 2021): "Li-Ion Batteries: From an Idea to Readiness to Take on Climate Change—Opportunities and Challenges"; M. S. Whittingham.
- International Centre for Diffraction Data, Philadelphia, Pennsylvania (March 12, 2021): "Li-Ion Batteries: From an Idea to Readiness to Take on Climate Change—Opportunities and Challenges"; M. S. Whittingham.
- Binghamton University – Indian Institute of Technology Ropar, Webinar Series (March 16, 2021): "Li-Ion Batteries: From an Idea to Readiness to Take on Climate Change—Opportunities and Challenges"; M. S. Whittingham.
- Instituto Superior Técnico of the University of Lisbon, Chemical Engineering (March 18, 2021): "The Lithium Battery: From a Dream to Domination of Energy Storage"; M. S. Whittingham.
- China International Battery Fair, Shenzhen, China (March 19, 2021): "Li-Ion Batteries: From an Idea to Readiness to Take on Climate Change—Opportunities and Challenges"; M. S. Whittingham.
- Cambridge, England (March 22, 2021): "Li-Ion Batteries: From an Idea to Readiness to Take on Climate Change—Opportunities and Challenges"; M. S. Whittingham.
- International Workshop on Nanocatalysts and Green Energy, Chinese Academy of Sciences (March 27, 2021): "Li-Ion Batteries: From an Idea to Readiness to Take on Climate Change—Opportunities and Challenges"; M. S. Whittingham.
- Materials Engineering Program, Virtual Seminar, Department of Electrical and Computer Engineering, University of Houston, Houston, Texas (February 12, 2021): "Developing New Electrolytes for Lithium Metal Batteries"; W. Xu.
- Center for Research in Extreme Batteries Biannual Winter Meeting, ARL and University of Maryland, College Park, Maryland (January 15, 2021): "Next Generation Battery Technologies"; A. Manthiram. Invited.
- Columbia University, New York, New York (February 5, 2021): "Next Generation Battery Technologies"; A. Manthiram. Invited.
- Tata Institute of Fundamental Research, Mumbai, India (February 15, 2021): "Battery Technologies for Renewable Energy Storage and Vehicle Electrification"; A. Manthiram. Invited.
- NanoBioLab Symposium 2021 Webinar, Agency for Science, Technology, and Research (A*STAR), Singapore (February 23, 2021): "Sustainable Battery Chemistries for Electrical Energy Storage"; A. Manthiram. Invited.
- SRM Institute of Science and Technology, Chennai, India (March 25–27, 2021): "Sustainable Battery Chemistries for E-Mobility"; A. Manthiram. Invited keynote talk.

- Materials Science and Engineering Seminar, Virtual, University of Houston (March 26, 2021): "Electrochemical Energy Storage: From Materials Science to Prototype Batteries and Manufacturing"; J. Xiao.
- GM Warren Technical Center, Special Seminar (March 2, 2021): "First Cycle Capacity Loss of Li-NMC 811 Cells—A Close Look from Electrochemical Diagnostic Analysis"; Y. Zhang, B. Liaw,* E. J. Dufek, and B. Li.
- 2021 Interagency Advanced Power Group, Chemical Working Group, Safety Panel, Virtual Meetings (February 19, 2021): "Tracking Rechargeable Li Battery Cell Degradation through Quantifiable Capacity Fade Modes from Formation to Cycle Aging"; Y. Zhang, B. Liaw,* E. J. Dufek, and B. Li.
- American Physical Society Meeting, Virtual (March 18, 2021): "Quantifying Capacity Losses Due to Solid-Electrolyte Interface Formation"; M. Toney.
- Bright Future for *In Situ* and *Operando* Structural Science at APS (-U) Workshop, Advanced Photon Source (January 15, 2021): "Advances in *Operando* X-Ray Characterization of Batteries"; M. Toney.